# Quantification of Building Seismic Performance Factors

ATC-63 Project Report - 90% Draft

*FEMA P695 / April 2008*

FEMA

nehrp

# Quantification of Building Seismic Performance Factors

## ATC-63 Project Report - 90% Draft

Prepared by

APPLIED TECHNOLOGY COUNCIL
201 Redwood Shores Parkway, Suite 240
Redwood City, California 94065
www.ATCouncil.org

Prepared for

FEDERAL EMERGENCY MANAGEMENT AGENCY
Michael Mahoney, Project Officer
Robert D. Hanson, Technical Monitor
Washington, D.C.



April 22, 2008

FEMA

## Notice

Any opinions, findings, conclusions, or recommendations expressed in this publication do not necessarily reflect the views of the Department of Homeland Security's Federal Emergency Management Agency (FEMA) or the Applied Technology Council (ATC). Additionally, neither ATC, DHS, FEMA, nor any of their employees makes any warranty, expressed or implied, nor assumes any legal liability or responsibility for the accuracy, completeness, or usefulness of any information, product, or process included in this publication. Users of information from this publication assume all liability arising from such use.

# Preface

In September 2004 the Applied Technology Council (ATC) was awarded a "Seismic and Multi-Hazard Technical Guidance Development and Support" contract (HSFEHQ-04-D-0641) by the Federal Emergency Management Agency (FEMA) to conduct a variety of tasks, including one entitled "Quantification of Building System Performance and Response Parameters" (ATC-63 Project). The purpose of this project is to establish and document a recommended methodology for reliably quantifying building system performance and response parameters for use in seismic design. A key parameter to be addressed is the response modification coefficient (*R* factor), but related design parameters such as the system overstrength factor ($\Omega_0$) and deflection amplification factor ($C_d$) are also addressed. Collectively these factors are referred to as "Seismic Performance Factors".

*R* factors are used to estimate strength demands on systems that are designed using linear methods but are responding in the nonlinear range. Their values are fundamentally critical in the specification of seismic loading. *R* factors were initially introduced in the ATC-3-06 report, *Tentative Provisions for the Development of Seismic Regulations for Buildings*, published in 1978, and subsequently replaced by the *NEHRP Recommended Provisions for Seismic Regulations for New Buildings and Other Structures*, published by FEMA. Original *R* factors were based largely on judgment and on qualitative comparisons with the known response capabilities of relatively few lateral-force resisting systems in use at the time. Since then, the number of systems addressed in current seismic codes and the most recent edition of the *NEHRP Recommended Provisions* has increased substantially. The potential response characteristics of these recently defined systems, and their ability to meet seismic design performance objectives, are both untested and unknown.

The recommended methodology described in this report is a refinement of an earlier preliminary version of the methodology. It is based on a review of relevant research on nonlinear response and collapse simulation, benchmarking studies of selected structural systems, feedback from an expanded group of experts and potential users, and evaluations of additional structural systems to verify the technical soundness and applicability of the approach.

ATC is indebted to the members of the ATC-63 Project Team for their efforts in the technical development of the recommended methodology, and to the leadership of Charlie Kircher, Project Technical Director. The Project Management Committee, consisting of Michael Constantinou, Greg Deierlein, Jim Harris, John Hooper, and Allan Porush monitored and guided the technical efforts of the Project Working Groups, which included Andre Filiatrault, Helmut Krawinkler, Kelly Cobeen, Curt Haselton, Abbie Liel, Jianis Christovasilis, Jason Chou, Stephen Cranford, Brian Dean, Kevin Haas, Jiro Takagi, Assawin Wanitkorkul, and Farzin Zareian. The affiliations of these individuals are provided in the list of Project Participants.

ATC also gratefully acknowledges Michael Mahoney (FEMA Project Officer), Robert Hanson (FEMA Technical Monitor), and William Holmes (ATC Project Technical Monitor) for their input and guidance in the preparation of this report, Peter N. Mork for ATC report production services, and Ramon Gilsanz as ATC Board Contact.

Jon A. Heintz
ATC Director of Projects

Christopher Rojahn
ATC Executive Director

# Table of Contents

# List of Figures

# List of Tables

# Chapter 1
# Introduction

This report describes a recommended methodology for reliably quantifying building system performance and response parameters for use in seismic design. The recommended methodology (referred to herein as the Methodology) provides a rational basis for establishing global seismic performance factors (SPFs), including the response modification coefficient (*R* factor), the system over-strength factor ($\Omega_0$), and deflection amplification factor ($C_d$), of new seismic-force-resisting systems proposed for inclusion in model building codes.

The Methodology was developed by the Applied Technology Council (ATC) under its ATC-63 Project, with funding provided by the Federal Emergency Management Agency (FEMA).

## 1.1 Background and Purpose

*R* factors are used in current building codes to estimate strength demands for seismic-force-resisting systems designed using linear methods but responding beyond the linear range. Their values are fundamentally critical in the specification of design seismic loading. *R* factors were initially introduced in the ATC-3-06 report, *Tentative Provisions for the Development of Seismic Regulations for Buildings* (ATC, 1978). Original *R* factors were based largely on judgment and qualitative comparisons with the known response capabilities of relatively few seismic-force-resisting systems in widespread use at the time.

Since then, the number of structural systems addressed in seismic codes has increased dramatically. The most recent edition of the National Earthquake Hazards Reduction Program (NEHRP) *Recommended Provisions for Seismic Regulations for New Buildings and Other Structures*, published as FEMA 450 (FEMA, 2004a), includes more than 75 individual systems, each having a somewhat arbitrarily assigned *R* factor. Many of these recently defined seismic-force-resisting systems have never been subjected to any significant level of earthquake ground shaking. Their seismic response characteristics, and their ability to meet seismic design performance objectives, are both untested and unknown.

The purpose of this Methodology is to provide a rational basis for determining building system performance and response parameters that, when properly implemented in the seismic design process, will result in:

- *Equivalent safety against collapse in an earthquake, comparable to the inherent safety against collapse intended by current seismic codes, for buildings with different seismic-force-resisting systems.*

The Methodology is recommended for use with model building codes and resource documents to set minimum acceptable design criteria for standard code-approved seismic-force-resisting systems, and to provide guidance in the selection of appropriate design criteria for other systems when linear design methods are applied. It also provides a basis for evaluation of current code-approved systems for their ability to achieve intended seismic performance objectives. It is possible that results of future work based on this Methodology could be used to modify or eliminate those systems or requirements that cannot reliably meet these objectives.

## 1.2 Scope and Basis of the Methodology

The following key principles outline the scope and basis of the recommended Methodology.

### *1.2.1 New Building Structures*

The Methodology applies to the determination of seismic performance factors appropriate for the design of seismic-force-resisting systems in new building structures. While the Methodology is conceptually applicable (with some limitations) to design of non-building structures, and to retrofit of seismic-force-resisting systems in existing buildings, such systems were not explicitly considered. The Methodology is not intended to apply to the design of nonstructural systems.

### *1.2.2 NEHRP Recommended Provisions and ASCE/SEI 7-05*

The Methodology is based on, and intended for use with, applicable design criteria and requirements of the *NEHRP Recommended Provisions for Seismic Regulations for New Buildings and Other Structures (NEHRP Recommended Provisions)*, (FEMA, 2004a), and the seismic provisions of ASCE/SEI 7-05, *Minimum Design Loads for Buildings and Other Structures*, (ASCE, 2006a). The *NEHRP Recommended Provisions* recently adopted ASCE/SEI 7-05 as the "starting point" for future updates and development. At this time, ASCE/SEI 7-05 is the most current, published source of seismic regulations of model building codes in the United States.

ASCE/SEI 7-05 provides the basis for ground motion criteria and "generic" structural design requirements applicable to currently accepted and future (proposed) seismic-force-resisting systems. ASCE/SEI 7-05 provisions include detailing requirements for currently approved systems that may also apply to new systems. By reference, other standards, such as *Building Code Requirements for Structural Concrete*, *ACI 318-05*, (ACI, 2005), *Seismic Provisions for Structural Steel Buildings*, ANSI/AISC 341 (AISC, 2005) and *National Design Specifications for Wood Construction*, *AF&PA NDS-05* (AF&PA, 2005) apply to currently approved systems, and may also apply to new systems.

The Methodology requires the seismic-force-resisting system of interest to comply with all applicable design requirements in ASCE/SEI 7-05, including limits on system irregularity, drift, and height, except when such requirements are specifically excluded and explicitly evaluated in the application of the Methodology. For new (proposed) systems, the Methodology requires identification and use of applicable structural design and detailing requirements in ASCE/SEI 7-05, and development and use of new requirements as necessary to adequately describe system limitations and ensure predictable seismic behavior of components. The latest edition of the *NEHRP Recommended Provisions*, containing modifications and commentary to ASCE/SEI 7-05, may be a possible source for additional design requirements.

### *1.2.3 Life Safety*

The recommended Methodology is consistent with the primary "life safety" performance objective of seismic regulations of model building codes. As stated in the *Part 2: Commentary* to the *NEHRP Recommended Provisions for Seismic Regulations for New Buildings and Other Structures* (Commentary to the *NEHRP Recommended Provisions*), (FEMA, 2004b), "the *Provisions* provides the minimum criteria considered prudent for protection of life safety in structures subject to earthquakes."

Design for performance other than life safety was not explicitly considered in the development of the Methodology. Accordingly, the Methodology does not address special performance or functionality objectives of ASCE/SEI 7-05 for Occupancy III and IV structures.

### *1.2.4 Structure Collapse*

The Methodology achieves the primary life safety performance objective by requiring an acceptably low probability of collapse of the seismic-force-

resisting system when subjected to Maximum Considered Earthquake (MCE) ground motions.

In general, life safety risk (i.e., probability of death or life-threatening injury) is difficult to calculate accurately, due to uncertainty in casualty rates given collapse, and even greater uncertainty in assessing the effects of falling hazards in the absence of collapse. Collapse of a structure can lead to very different numbers of fatalities, depending on variations in construction or occupancy, including structural system type and the number of building occupants. Rather than attempting to quantify uniform protection of "life safety", the Methodology provides approximate uniform protection against collapse of the structural system.

Collapse includes both partial (e.g., single story collapse) and global instability of the seismic-force-resisting system, but does not include local failure of components not governed by the global seismic performance factors (e.g., localized, out-of-plane failure of wall anchorage and potential life-threatening failure of non-structural systems).

The Methodology does not explicitly address components that are not included in the seismic-force-resisting system (e.g., gravity system components and nonstructural components). It assumes that deformation compatibility and related requirements of ASCE/SEI 7-05 adequately protect such components against premature failure. Components that are not designated as part of the seismic-force-resisting system are not controlled by seismic-force-resisting system design requirements. Accordingly, they are not considered in evaluating the overall resistance to collapse.

### *1.2.5 MCE Ground Motions*

The Methodology evaluates collapse under Maximum Considered Earthquake (MCE) ground motions for various levels of ground motion hazard, as defined by the coefficients and mapped acceleration parameters of the general procedure of ASCE/SEI 7-05, which is based on the maps and procedures contained in the *NEHRP Recommended Provisions*.

While seismic performance factors apply to the design response spectrum, taken as two-thirds of the MCE spectrum, code-defined MCE ground motions are considered the appropriate basis for evaluating structural collapse. As noted in the Commentary to the *NEHRP Recommended Provisions*, "if a structure experiences a level of ground motion 1.5 times the design level, the structure should have a low likelihood of collapse."

### *1.2.6 Seismic Performance Factors*

The Methodology remains true to the definitions of seismic performance factors given in ASCE/SEI 7-05, and the underlying pushover concepts described in the Commentary to the *NEHRP Recommended Provisions*. Global seismic performance factors include the response modification coefficient ($R$ factor), the system over-strength factor ($\Omega_O$ factor) and the deflection amplification factor ($C_d$ factor). Values for currently approved seismic-force-resisting systems are specified in Table 12.2-1 of ASCE/SEI 7-05. Section 4.2 of the Commentary to the *NEHRP Recommended Provisions* provides background on seismic performance factors.

Figures 1-1 and 1-2 are used to explain and illustrate seismic performance factors, and how they are used in the Methodology. Parameters are defined in terms of equations, which in all cases are dimensionless *ratios* of force, acceleration or displacement. However, in attempting to utilize the figures to clarify and to illustrate the meanings of these ratios, graphical license is taken in two ways. First, seismic performance factors are depicted in the figures as incremental differences between two related parameters, rather than as ratios of the parameters. Second, as a consequence of being depicted as incremental differences, seismic performance factors are shown plotted on an axis having units, when, in fact, they are dimensionless.

Figure 1-1, an adaptation of Figures C4.2-1 and C4.2-3 from the Commentary to the *NEHRP Recommended Provisions*, defines seismic performance factors in terms of the global inelastic response (idealized pushover curve) of the seismic-force-resisting system. In this figure, the horizontal axis is lateral displacement (i.e., roof drift) and the vertical axis is lateral force at the base of the base of the system (i.e., base shear).

In Figure 1-1, the term, $V_E$, represents the force level that would be developed in the seismic-force-resisting system, if the system remained entirely linearly elastic for design earthquake ground motions. The term, $V_{max}$, represents the actual, maximum strength of the fully-yielded system, and the term, $V$, is the seismic base shear required for design. As illustrated in the figure and defined in Equation 1-1, the $R$ factor is the ratio of the force level that would be developed in the system for design earthquake ground motions (if the system remained entirely linearly elastic), to the base shear prescribed for design:

$$R = \frac{V_E}{V} \qquad (1\text{-}1)$$

and the $\Omega_O$ factor is the ratio of the maximum strength of the fully-yielded system to the design base shear, as defined in Equation 1-2,

$$\Omega_O = \frac{V_{max}}{V} \tag{1-2}$$

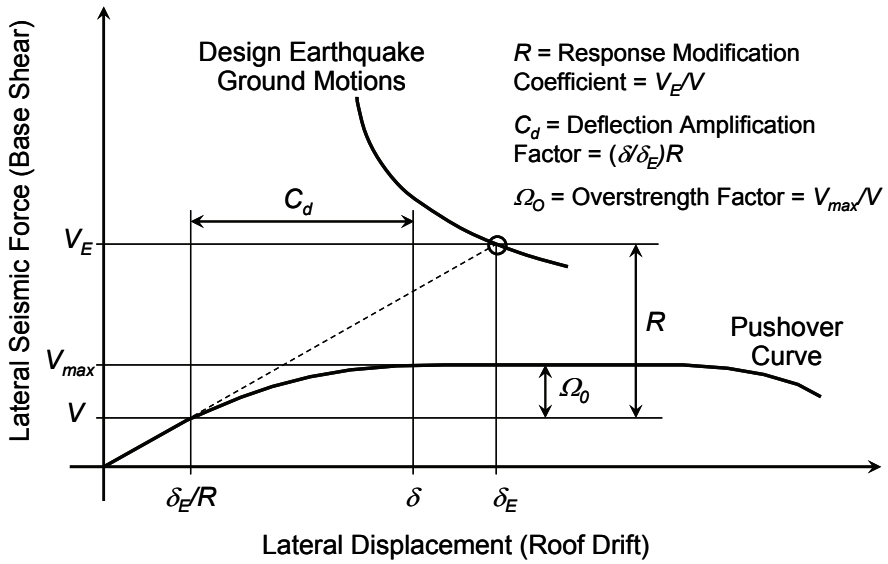


Figure 1-1 Illustration of seismic performance factors ($R$, $\Omega_O$ and $C_d$) as defined by the Commentary to the *NEHRP Recommended Provisions* (FEMA, 2004b).

In Figure 1-1, the term, $\delta_E/R$, represents roof drift of the seismic-force-resisting system corresponding to design base shear, $V$, assuming that the system remains essentially elastic for this level of force, and the term, $\delta$, represents the assumed roof drift of the yielded system corresponding to design earthquake ground motions. As illustrated in the figure and defined by Equation 1-3, the $C_d$ factor is some fraction of the $R$ factor (typically less than 1.0):

$$C_d = \frac{\delta}{\delta_E} R \tag{1-3}$$

The Methodology develops seismic performance factors consistent with the underlying pushover concept and definitions of the Commentary to the *NEHRP Recommended Provisions*, as described above. Figure 1-2 illustrates the seismic performance factors defined by the Methodology and their relationship to MCE ground motions.

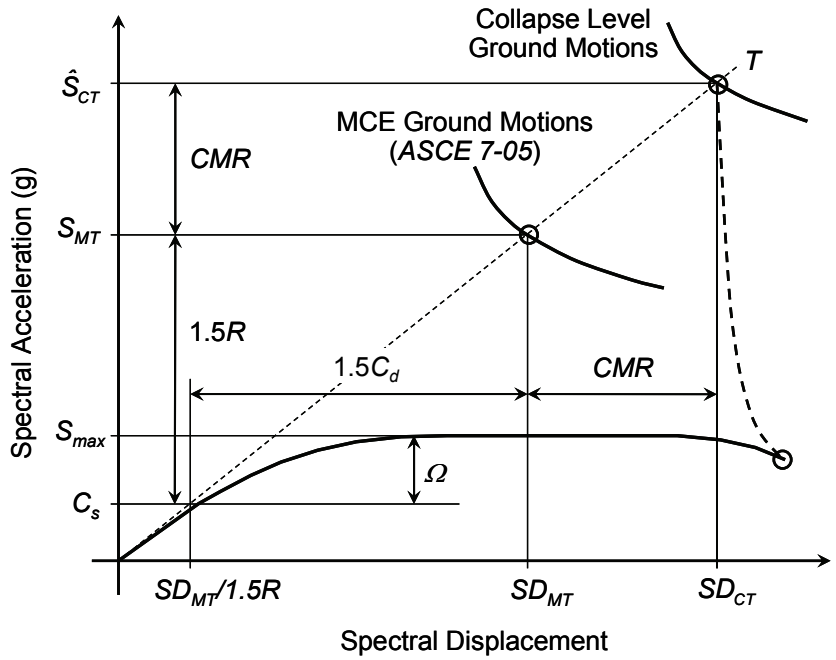


Figure 1-2 Illustration of seismic performance factors ($R$, $\Omega$ and $C_d$) as defined by the Methodology.

Figure 1-2 parallels the "pushover" concept shown in Figure 1-1 using spectral coordinates rather than lateral force (base shear) and lateral displacement (roof drift) coordinates. Conversion to spectral coordinates is based on the assumption that 100% of the effective seismic weight of the structure, $W$, participates in fundamental mode at period, $T$, consistent with Equation (12.8-1) of ASCE/SEI 7-05:

$$V = C_s W \tag{1-4}$$

In Figure 1-2, the term $S_{MT}$ is the Maximum Considered Earthquake (MCE) spectral acceleration at the period of the system, $T$; the term $S_{max}$ represents the maximum strength of the fully-yielded system (normalized by the effective seismic weight, $W$, of the structure); and the term $C_s$ is the seismic response coefficient. As shown in the figure and defined in Equation 1-5, 1.5 times the $R$ factor is the ratio of the MCE spectral acceleration to the seismic response coefficient, which is the design-level acceleration:

$$1.5R = \frac{S_{MT}}{C_s} \tag{1-5}$$

The 1.5 factor in Equation (1-5) accounts for the ASCE/SEI 7-05 definition of design earthquake ground motions as two-thirds of MCE ground motions.

In Figure 1-2, the overstrength parameter, $\Omega$, is defined as the ratio of the maximum strength (normalized by $W$), $S_{max}$, to the seismic response coefficient, $C_s$:

$$\Omega = \frac{S_{max}}{C_s} \tag{1-6}$$

The Methodology calculates the overstrength parameter, $\Omega$, based on pushover analysis. Calculated values of overstrength are different from the overstrength factor, $\Omega_O$, of ASCE/SEI 7-05, which is required for design of non-ductile elements. In general, different designs of the same system will have different calculated values of the overstrength parameter, $\Omega$. The value of $\Omega$ that is considered to be most appropriate for use in design of the system of interest, is the value used for $\Omega_O$.

In Figure 1-2, inelastic system displacement at the MCE level is defined as $1.5C_d$ times $\delta_E/R$, and set equal to the MCE elastic system displacement, $SD_{MT}$ (based on the "Newmark rule"), effectively redefining the $C_d$ factor to be equal to the $R$ factor:

$$C_d = R \tag{1-7}$$

The equal displacement assumption is reasonable for most conventional systems with effective damping approximately equal to the nominal 5% level used to define response spectral acceleration and displacement. Systems with substantially higher (or lower) levels of damping would have significantly smaller (or larger) displacements than those with 5%-damped elastic response. As one example, systems with viscous dampers have significantly higher damping than 5%. For these systems, the response modification methods of Chapter 18 of ASCE/SEI 7-05 are used to determine an appropriate value of the $C_d$ factor, as a fraction of the $R$ factor.

### *1.2.7 Collapse Margin Ratio*

The Methodology defines collapse level ground motions as the intensity that would result in median collapse of the seismic-force-resisting system. Median collapse occurs when one-half of the structures exposed to this intensity of ground motion would have some form of life-threatening collapse. As shown in Figure 1-2, collapse level ground motions are higher than MCE ground motions. As such, MCE ground motions would result in a comparatively smaller probability of collapse. As defined in Equation 1-8, the collapse margin ratio, $CMR$, is the ratio of the median 5%-damped spectral acceleration (or displacement) of the collapse level ground motions

to the 5%-damped spectral acceleration (or displacement) of the MCE ground motions, at the fundamental period of the seismic-force-resisting system:

$$CMR = \frac{\hat{S}_{CT}}{S_{MT}} = \frac{SD_{CT}}{SD_{MT}} \quad (1\text{-}8)$$

Collapse of the seismic-force-resisting system, and hence the collapse margin ratio, *CMR*, is influenced by many factors, including ground motion variability and uncertainty in design, analysis, and construction of the structure. These factors are considered collectively in a collapse fragility curve that describes the probability of collapse of the seismic-force-resisting system as a function of the intensity of ground motions.

### *1.2.8 Archetypes and Nonlinear Analyses*

The Methodology determines the response modification coefficient (*R* factor) and evaluates the system over-strength factor ($\Omega$) using nonlinear models of seismic-force-resisting system "archetypes." Archetypes capture the essence and variability of the performance characteristics of the system of interest. The Methodology requires nonlinear analysis of a sufficient number of archetype models, with parametric variations in design parameters, to broadly represent the system of interest.

The Methodology requires archetype models to meet the applicable design requirements of ASCE/SEI 7-05 and related standards, and additional criteria developed for the system of interest. Archetype design assumes a trial value of the *R* factor to determine the seismic response coefficient, $C_s$. The Methodology requires detailed modeling of nonlinear behavior of archetypes, based on representative test data sufficient to capture collapse failure modes. Collapse failure modes that cannot be explicitly modeled are evaluated using appropriate limits on the controlling response parameter.

### *1.2.9 Performance Evaluation*

The Methodology defines acceptable values of the collapse margin ratio in terms of an acceptably low probability of collapse for MCE ground motions given uncertainty in collapse fragility. Systems that have more robust design requirements, more comprehensive test data, and more detailed nonlinear analysis models, have less collapse uncertainty, and can achieve the same level of life safety with smaller collapse margin ratios.

Calculated values of collapse margin ratio are compared with acceptable values that reflect collapse uncertainty. If the calculated collapse margin is large enough to meet performance objective (i.e., an acceptably small probability of collapse at the MCE), then the trial value of the *R* factor used

to design the archetype is acceptable. If not, a new (lower) trial value of the *R* factor must be re-evaluated using the Methodology.

## 1.3 Content and Organization

This report is written and organized to facilitate potential use and adoption by the *NEHRP Recommended Provisions*. Chapter 2 provides an overview of the Methodology, introducing the basic theory and concepts that are described in more detail in the chapters that follow.

Chapters 3 through 7 step through the elements of the Methodology, including required system information, structure archetype development, nonlinear modeling, criteria for collapse assessment, nonlinear analysis, and evaluation of seismic performance factors.

Chapter 8 defines documentation and peer review requirements, and describes recommended qualifications, expertise, and responsibilities for personnel involved with implementing the Methodology in the development and review of a proposed system.

Chapter 9 provides example applications intended to assist users in implementing the Methodology, and to validate the technical approach. Example systems include special and ordinary reinforced concrete moment frame systems, and wood light-frame systems.

Chapter 10 includes supporting studies on non-simulated collapse failure modes for steel moment frame systems, and on dynamic response characteristics, performance properties, and collapse failure modes unique to seismically-isolated structures.

Chapter 11 provides summary conclusions, recommendations, and limitations on the use of the Methodology.

Appendices A through F provide background information supporting the development of the Methodology, and expanded guidance on key aspects of the Methodology.

A glossary of definitions and notations used throughout this report, and a list of references, are provided at the end of this report.

# Chapter 2
# Overview of Methodology

This chapter outlines the general framework of the Methodology and describes the overall process. It introduces the key elements of the Methodology, including required system information, development of structural system archetypes, archetype models, nonlinear analysis of archetypes, performance evaluation, and documentation and peer review requirements. These elements are specified in more detail in the chapters that follow.

## 2.1 General Framework

The Methodology consists of a framework for establishing seismic performance factors (SPFs) that involves development of detailed system design information and probabilistic assessment of collapse risk. It utilizes nonlinear analysis techniques, and explicitly considers uncertainties in ground motion, modeling, design, and test data. The technical approach is a combination of traditional code concepts, advanced nonlinear dynamic analyses, and risk-based assessment techniques.

Reliable analysis requires valid ground motions and representative nonlinear models of the seismic-force-resisting system. Development of representative models requires both detailed design information and comprehensive nonlinear test data on structural components and assemblies that make up the system of interest. Figure 2-1 illustrates the key elements of the Methodology.

The Methodology includes fully defined characterizations of ground motion and methods of analysis that are generically applicable to all seismic-force-resisting systems. Design information and test data will be different for each system, and may not yet exist for new systems. The Methodology includes requirements for defining the type of design information and test data that are needed for developing representative analytical models of the seismic-force-resisting system of interest.

Rather than establishing minimum requirements for design information and test data, the use of better quality information is encouraged by rewarding systems that have "done their homework." Systems that are based on well-defined design requirements and comprehensive test data will have inherently less uncertainty in their seismic performance. Such systems will

need a lower margin against collapse to achieve an equivalent level of safety, as compared to systems with less robust data.

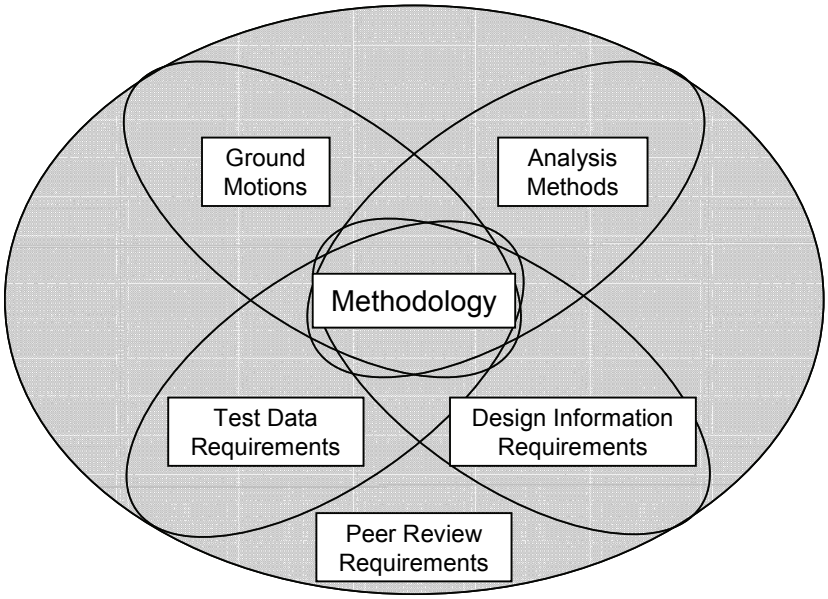


Figure 2-1 Key elements of the Methodology

Considering the complexity of nonlinear dynamic analysis, the difficulty in modeling inelastic behavior, and the need to verify the adequacy and quality of design information and test data, the Methodology requires peer review of the entire process.

## 2.2 Description of Process

The steps comprising the Methodology are shown in Figure 2-2. These steps outline a process for developing system design information with enough detail and specificity to identify the permissible range of application for the proposed system, adequately simulate nonlinear response, and reliably assess the collapse risk over the proposed range of applications. Each step is linked to a corresponding chapter in this report, and described in the sections that follow.

## 2.3 Develop System Concept

The process begins with the development of a well-defined concept for the seismic-force-resisting system, including type of construction materials, system configuration, inelastic dissipation mechanisms, and intended range of application. The amount of documentation necessary to describe the system and characterize system components will vary, depending on the

novelty and uniqueness of the proposed system relative to other well-established structural systems.

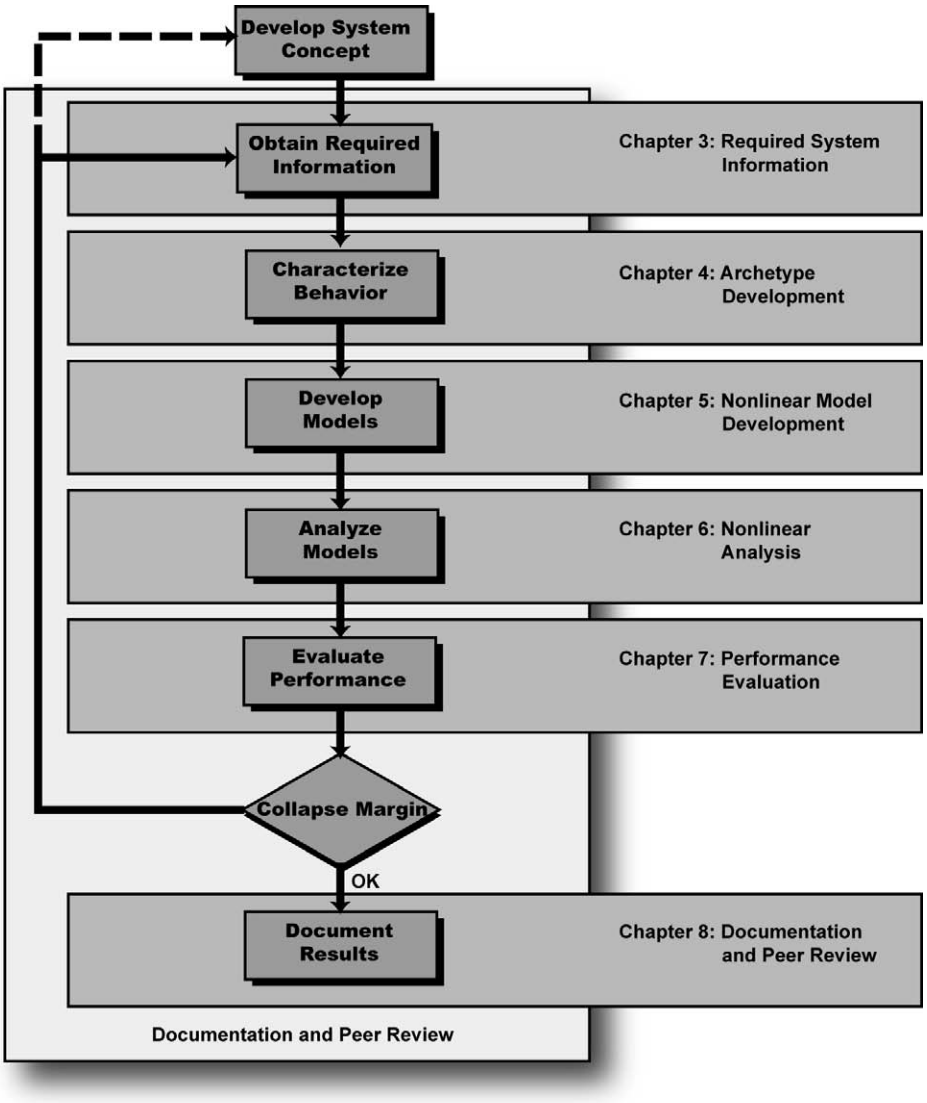


Figure 2-2 Process for establishing and documenting seismic performance factors (SPFs)

## 2.4 Obtain Required Information

Required system information is specified in Chapter 3. Required information includes detailed design requirements and results from material, component, and system testing. Design requirements include the rules that engineers will use to proportion and detail structural components of the system, and limits in the application of the system. Test results include information on component material properties, force-deformation behavior, and nonlinear response.

Comprehensive design provisions are developed within the context of the seismic provisions of ASCE 7-05, *Minimum Design Loads for Buildings and Other Structures*, (ASCE, 2005) and other applicable standards. The provisions should address all significant aspects of the design and detailing of the seismic resisting system and its components. Important exceptions and deviations from established building code requirements should be clearly stipulated. Design provisions should address criteria for determining minimum strength and ensuring inelastic deformation capacity through a combination of system design requirements, component design and detailing requirements, and project-specific testing requirements. Design provisions should also specify the seismic performance factors ($R$ , $\Omega_0$, $C_d$) and other criteria (e.g., drift limits, height limits, and seismic usage restrictions) that are proposed as part of the design basis for the new system.

Test data are necessary for characterizing the strength, stiffness and ductility of the materials, members, and connections of the proposed system. Test data are also necessary for establishing properties of the nonlinear analysis models used to assess collapse risk. Test data and other substantiating evidence should be acquired as the basis of the design provisions and for calibrating analysis models. Design requirements should be documented with supporting evidence to ensure sufficient strength, stiffness and ductility of the proposed system, across the intended range of application of the system.

## 2.5 Characterize Behavior

System behavior is characterized through the use of structural system archetypes. The concept of an archetype is described in Chapter 4. Establishment of archetypes begins with identifying the range of features and behavioral characteristic that describe the bounds of a proposed seismic-force-resisting system.

Archetypes provide a systematic means for characterizing permissible configurations and other significant features of the proposed system. Like building code provisions, archetypical systems are intended to represent typical applications of a seismic-force-resisting system, recognizing that it is practically impossible to envision or attempt to quantify performance of all possible applications. They should, however, reflect the degree of irregularity permitted within standard building code provisions.

The challenge in defining and assessing structural system archetypes is in narrowing the range of parameters and attributes to the fewest and simplest possible, while still being reasonably representative of the variations that

would be permitted in actual structures. In addition to ground motion intensity (Seismic Design Category), the following characteristics are considered in defining structural system archetypes: (1) building heights; (2) structural framing configurations; (3) framing bay sizes or wall lengths; (4) magnitude of gravity loads; and (5) member and connection design and detailing requirements. Structural system archetypes are assembled into bins called performance groups, which reflect major divisions, or changes in behavior, within the archetype design space. The collapse safety of the proposed system is then evaluated for each performance group.

In the collapse assessment process, only framing components that are specifically designated as part of the seismic-force-resisting system are included in the Index Archetype Configurations. While it is recognized that other portions of the building (e.g., components of the gravity system or certain nonstructural components) can significantly affect collapse behavior, such components are not controlled by seismic-force-resisting system design requirements, and cannot be relied upon for reducing collapse risk.

## 2.6 Develop Models

Development of structural models for collapse assessment is discussed in Chapter 5. Structural system archetypes provide the basis for preparing a finite number of trial designs and developing a corresponding number of idealized nonlinear models that sufficiently represent the range of intended applications for a proposed system. Index archetype models provide the most basic (generic) idealization of an index archetype configuration that is still capable of capturing significant behavioral modes and key design features of a proposed seismic-force-resisting system.

Designs consider the range of maximum and minimum seismic criteria for each applicable Seismic Design Category, variations in gravity loads, and other distinguishing features including alternative geometric configurations, varying heights, and different tributary areas that impact seismic design or system performance.

To the extent possible, nonlinear models include explicit simulation of all significant deterioration mechanisms that could lead to structural collapse. Recognizing that it is not always possible (or practical) to simulate all possible collapse modes, the Methodology includes provisions for assessing the effects of behaviors that are not explicitly simulated in the model, but could trigger collapse.

Nonlinear models must account for the seismic mass that is stabilized by the seismic-force-resisting system, including the destabilizing P-Delta effects

associated with the seismic mass. In most cases, elements are idealized with phenomenological models to simulate complicated component behavior. In some cases, however, two-dimensional or three-dimensional continuum finite element models may be required to properly characterize behavior. Models are calibrated using material, component, or assembly test data and other substantiating evidence to verify their ability to simulate expected nonlinear behavior.

## 2.7 Analyze Models

Collapse assessment is performed using nonlinear static (pushover) and nonlinear dynamic (response history) analysis procedures described in Chapter 6. Nonlinear static analyses are used to help validate the behavior nonlinear models and to provide statistical data on system overstrength and ductility capacity. Nonlinear dynamic analyses are used to assess median collapse capacities, and collapse margin ratios.

Nonlinear response is evaluated for a set of pre-defined ground motions that are used for collapse assessment of all systems. Two sets of ground motion records are provided for nonlinear dynamic analysis. One set includes twenty-two ground motion record pairs from sites located greater than or equal to 10 km from fault rupture, referred to as the "Far-Field" record set. The other set includes twenty-eight pairs of ground motions recorded at sites less than 10 km from fault rupture, referred to as the "Near-Field" record set. While both Far-Field and Near-Field record sets are provided, only the Far-Field record set is required for collapse assessment. This is done for reasons of practicality, and in recognition of the fact that there are many unresolved issues concerning the characterization of near-fault hazard and ground motion effects. The Near-Field record set is provided as supplemental information to examine issues that arise due to near-fault directivity effects, if needed.

The record sets include records from all large-magnitude events in the PEER NGA database (PEER, 2006). Records were selected to meet a number of sometimes conflicting objectives. To avoid event bias, no more than two of the strongest records are taken from each earthquake, yet the record sets have a sufficient number of motions to permit statistical evaluation of record-to-record (RTR) variability and collapse fragility. Strong ground motions were not distinguished based on either site condition or source mechanism. The record sets, and background information on their selection, are included in Appendix A.

For collapse evaluation, ground motions are systematically scaled to increasing earthquake intensities until median collapse is established. Median collapse is the ground motion intensity in which half of the records in the set cause collapse of an index archetype model. This process is similar to, but distinct from the concept of incremental dynamic analysis (IDA), as proposed by Vamvatsikos and Cornell (2002).

Shown in Figure 2-3 is an example of IDA results for a single structure subjected to a suite of ground motions of varying intensities. In this illustration, sidesway collapse is the governing mechanism, and collapse prediction is based on dynamic instability or excessive lateral displacements. Using collapse data obtained from IDA results, a collapse fragility can be defined through a cumulative distribution function (CDF), which relates the ground motion intensity to the probability of collapse (Ibarra et al. 2002). Figure 2-4 shows an example of a cumulative distribution plot obtained by fitting a lognormal distribution to the collapse data from Figure 2-3.

While the IDA concept is useful to illustrate the collapse assessment procedure, the Methodology only requires calculation of the median collapse point, which can be calculated with fewer nonlinear analyses than would otherwise be required to calculate the full IDA curve.

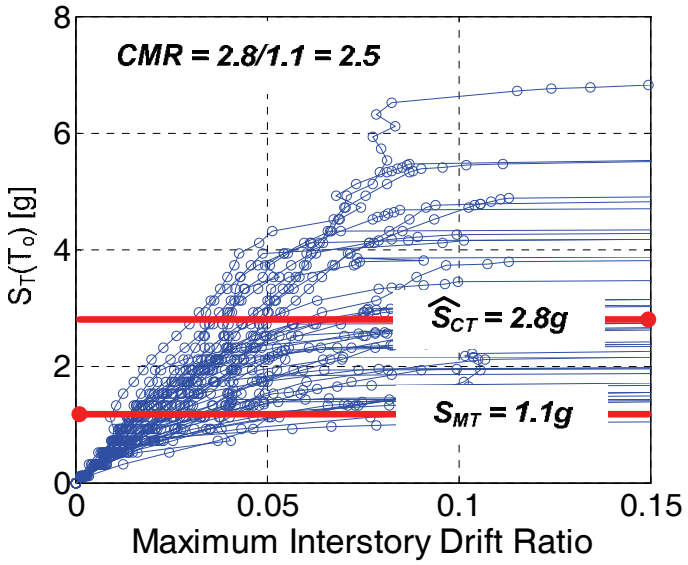


Figure 2-3 Incremental dynamic analysis response plot of spectral acceleration versus maximum interstory drift

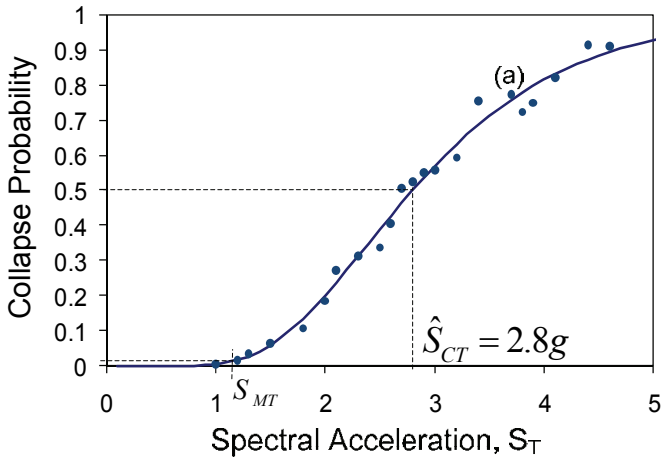


Figure 2-4 Collapse fragility curve, or cumulative distribution function

## 2.8 Evaluate Performance

The performance evaluation process is described in Chapter 7. It utilizes results from nonlinear static analyses to determine an appropriate value of the system overstrength factor, $\Omega_O$, and results from nonlinear dynamic analyses to evaluate the acceptability of a trial value of the response modification coefficient, $R$. The deflection amplification factor, $C_d$, is derived from an acceptable value of $R$, with consideration of the effective damping of the system of interest.

The trial value of the response modification coefficient, $R$, is evaluated in terms of the acceptability of a calculated collapse margin ratio, which is the ratio of the ground motion intensity that causes median collapse, to the MCE ground motion intensity defined by the building code. Acceptability is measured by comparing the collapse margin ratio, after some adjustment, to acceptable values that depend on the quality of information used to define the system, total system uncertainty, and established limits on acceptable probabilities of collapse.

To account for unique characteristics of extreme ground motions that lead to building collapse, the collapse margin ratio is converted to an adjusted collapse margin ratio. The adjustment is based on the shape of the spectrum of rare ground motions, and is a function of the structure ductility and period of vibration. Systems with larger ductility and longer periods benefit by larger adjustments. The background and development of this adjustment to account for the effects of spectral shape are provided in Appendix B.

Acceptable values of the collapse margin ratio are defined in terms of an acceptably low probability of collapse for MCE ground motions, considering

uncertainty in collapse fragility. Systems that have more robust design requirements, more comprehensive test data, and more detailed nonlinear analysis models, have less collapse uncertainty, and can achieve the same level of life safety with smaller collapse margin ratios. The following sources of uncertainty are explicitly considered: (1) record-to-record uncertainty; (2) design requirements-related uncertainty; (3) test data-related uncertainty; and (4) modeling uncertainty.

The probability of collapse due to MCE ground motions is limited to 10%. Each performance group is required to meet this collapse probability limit, on average, recognizing that some individual archetypes could have collapse probabilities that exceed this value. A limit of twice that value, or 20%, is used as a criterion for evaluating the acceptability of potential "outliers" within a performance group. It should be noted that theses limits were selected based on judgment. Within the performance evaluation process, these values can be adjusted to reflect different values of acceptable probabilities of collapse that are deemed appropriate by governing jurisdictions or other authorities employing this Methodology to establish seismic design requirements for a proposed system.

If the adjusted collapse margin ratio is large enough to result in an acceptably small probability of collapse at the MCE, then the trial value of $R$ is acceptable. If not, the system must be redefined by adjusting the design requirements (Chapter 3), re-characterizing behavior (Chapter 4), or redesigning with new trial values (Chapter 5), and then re-evaluated using the Methodology. In some cases, inadequate performance could require extensive revisions to the overall system concept.

## 2.9 Document Results

Documentation requirements are described in Chapter 8. The results of system development efforts must be thoroughly documented for review and approval by the peer review panel, review and approval by an authority having jurisdiction over its use, and eventual use in design and construction.

Documentation is required at each step of the process. It should describe seismic design rules, range of applicability of the system, testing protocols and results, rationale for the selection of structural system archetypes, results of analytical investigations, evaluation of quality of information, quantification of uncertainties, results of performance evaluations, and proposed seismic performance factors.

Documentation should be of sufficient detail and clarity to allow an unfamiliar structural engineer to properly implement the design, and an

unfamiliar reviewer to evaluate compliance with design requirements. Documentation should also provide sufficient information to allow peer reviewers, code authorities, or material standard organizations to assess the viability of the proposed system and the reasonableness of the proposed seismic performance factors.

## 2.10 Peer Review

Peer review by a qualified team of experts is a requirement of the Methodology and should be an integral part of the process at each step. Implementation of this Methodology involves much uncertainty, judgment and potential for variation. Deciding on an appropriate level of detail to adequately characterize performance of a proposed system should be performed in collaboration with a peer review panel on an ongoing basis during developmental efforts.

The peer review panel is responsible for reviewing and commenting on the approach taken by the development team including the extent of the experimental program, testing procedures, design requirements, development of structural system archetypes, analytical approaches, extent of the nonlinear analysis investigation, and the final selection of the proposed seismic performance factors. Members of the peer review panel must be qualified to critically evaluate the development of the proposed system including testing, design, and analysis.

The peer review panel, and their involvement, should be established early to clarify expectations for the collapse assessment. The peer review team is expected to exercise considerable judgment in evaluating all aspects of the process, from definition of the proposed system, to establishment of design criteria, scope of testing, and extent of analysis deemed necessary to adequately evaluate collapse safety.

Details on the required peer review process, and guidance on the selection of peer review panel members, are provided in Chapter 8.

# Chapter 3
# Required System Information

This chapter identifies information that is necessary for establishing seismic performance factors as part of the development, documentation, and review of a proposed seismic-force-resisting system. It describes the type of information that is required, and provides guidance on how it should be developed.

This information is used in the development of structural system archetypes in Chapter 4, and nonlinear analysis models in Chapter 5. It is subject to peer review as it is developed, and is an integral part of the reporting requirements in Chapter 8.

## 3.1 General

Seismic performance factors for a proposed system are established through nonlinear simulation of response to earthquake ground motion, and probabilistic assessment of collapse risk. Detailed system information is necessary for reliable prediction of structural response, and for development and validation of standardized engineering criteria that will lead to structures that perform as expected.

Required system information includes: (1) a comprehensive description of the proposed system, including its intended applications, physical and behavioral characteristics, and construction methods; (2) a clear and complete set of design requirements and specifications for the system that provide information to quantify strength limit states, proportion and detail components, analyze predicted response, and confirm satisfactory behavior; and (3) test data and other supporting evidence from an experimental investigation program to validate material properties and component behavior, calibrate nonlinear analysis models, and establish performance acceptance criteria. The process for obtaining required system information is shown in Figure 3-1.

## 3.2 Intended Applications and Performance

A description of the intended applications and expected performance of a proposed seismic-force-resisting system is required. This description should include: (1) the anticipated function and occupancy; (2) physical and

behavioral characteristics of the system; (3) typical geometric configurations; and (4) any similarities or differences between the proposed system and current code-conforming systems. The description should also indicate how the structural system and its key components are expected to perform in an earthquake.

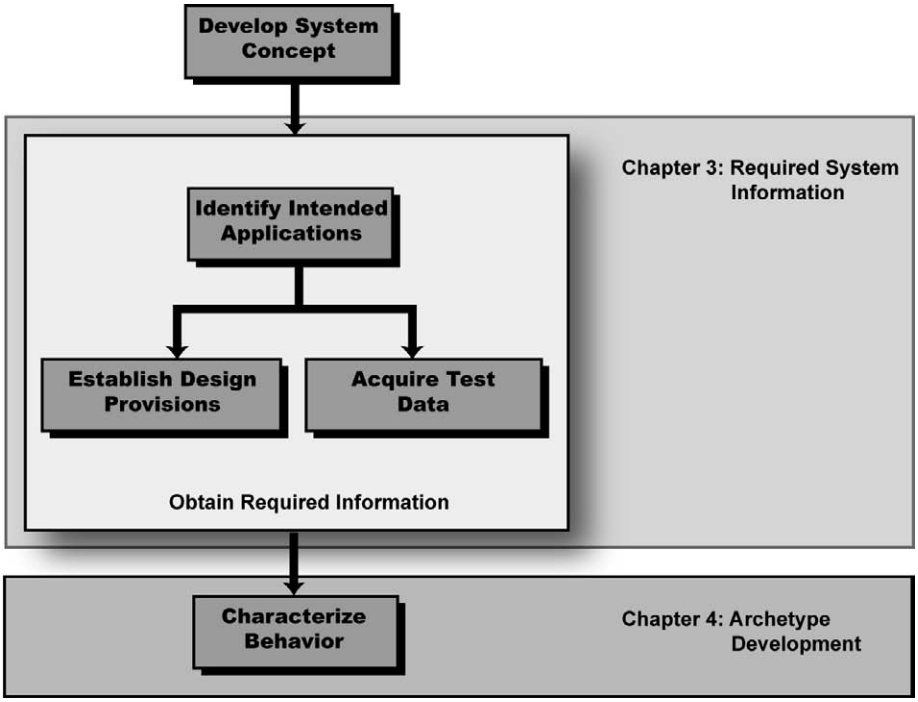


Figure 3-1 Process for obtaining required system information

The following information should be used a guide for describing the intended applications of a proposed seismic-force-resisting system:

- intended occupancies and use of facilities to be constructed using the proposed system
- horizontal and vertical configurations (e.g., framing layout, spans, story heights, overall heights) of typical facilities to be constructed using the proposed system
- structural gravity framing systems to be used in combination with the proposed system, including typical dead and live loads
- geometric configurations of the proposed seismic-force-resisting system
- expected inelastic behavior under seismic loading of varying intensity
- methods of construction

## 3.3 Design Requirements

Design requirements establish the fundamental information that will be used to proportion and detail components, analyze the predicted response, and confirm the behavior of a proposed system. They also set boundaries in the application of the system. Design requirements are an essential input to the development of structural system archetypes in Chapter 4. Information needed to define and document system design requirements is specified in the sections that follow.

### *3.3.1 Basis for Design Requirements*

Design requirements should be based on criteria specified in applicable sections of the latest edition of ASCE/SEI 7, *Minimum Design Loads for Buildings and Other Structures*, and other applicable material reference standards, such as ACI 318, *Building Code Requirements for Structural Concrete*, AISC, *Seismic Provisions for Structural Steel Buildings*, ACI 530/ASCE 5/TMS 402, *Building Code Requirements for Masonry Structures*, and ANSI/AF&PA, *National Design Specification for Wood Construction*. The following statements, taken mostly from the *NEHRP Recommended Provisions for Seismic Regulations for New Buildings and Other Structures* (FEMA, 2004a), should be used as a basis for developing design requirements:

- The structure shall include complete lateral- and vertical-force-resisting systems capable of providing adequate strength, stiffness, and energy dissipation capacity to withstand the design ground motions within the prescribed limits of deformation and strength demand.
- Design ground motions shall be assumed to occur along any direction of the structure.
- Adequacy of the systems shall be demonstrated through construction of a mathematical model, and evaluation of this model for the effects of design ground motions. This evaluation shall be based on analysis in which design seismic forces are distributed and applied throughout the height of the structure in accordance with the ASCE/SEI 7.
- Deformations and internal forces in all members of the structure shall be determined and evaluated against acceptance criteria contained or referred to in ASCE/SEI 7, and as developed for the system under consideration.
- A continuous load path, or paths, shall be provided with adequate strength and stiffness to transfer all forces from the point of application to the final point of resistance.

- The foundation shall be designed to accommodate forces developed or movements imparted to the structure by design ground motions. In determining foundation design criteria, special recognition shall be given to the dynamic nature of the forces, the expected ground motions, and the design basis for strength and energy dissipation capacity of the structure.
- Design of a structure shall consider potentially adverse effects on the stability of the structure due to failure of a member, connection, or component of the seismic-force-resisting system.

### *3.3.2 Application Limits and Strength Limit States*

The boundaries of the intended application of the proposed seismic-force-resisting system must be clearly stated, including, for example, any proposed height limitations or restrictions to certain Seismic Design Categories.

Design requirements must integrate from material properties to element, member, connection, assembly, and seismic-force-resisting system overall behavior. With generally accepted modeling criteria and good engineering judgment, design requirements should be of sufficient detail that analytical models of component behavior can be developed. They must address the details of stiffness models for members, connections, assemblies, and the overall system, recognizing that seismic performance factors will be used in the context of linear analyses and response to equivalent static forces. Where size effects are important, they must be included.

Design requirements must provide information necessary to quantify all pertinent strength limit states, including:

- tension, compression, bending, shear;
- yield, rupture, brittle fracture;
- local, member, and global instability.

Proposed systems that rely on standard structural materials, or minor modifications to existing, proven systems, can reference much of the requirements to existing standards. New systems that behave outside the bounds of existing system behavior must include consideration of behavioral effects on other elements of building construction, including the gravity load system and nonstructural components.

### *3.3.3 Overstrength Design Criteria*

It is expected that most seismic-force-resisting systems will rely on inelastic behavior somewhere within the system. Overstrength criteria should be applied to the design of components in a system that are judged to have small

inelastic deformation capacity followed by rapid deterioration in strength. This is especially important if the component is also an essential part of the gravity load system. Design requirements should be written in a manner that clearly identifies all such components so that it is not left up to the judgment of the designer to make this identification.

Design procedures utilizing linear, equivalent static analyses should follow the current standard method of requiring that such components be designed for gravity loads plus $\Omega_0$ times the seismic loads, or for the maximum forces that can be delivered to the component by other elements in the system. It is understood that the overstrength factor used for this purpose is based on judgment, and can vary by a large amount depending on system configuration. To provide adequate protection, this factor should be a high estimate of the expected ratio of maximum force to design force, particularly for systems or materials that are non-ductile, or have significant variability or uncertainty in response.

### *3.3.4 Configuration Issues*

Design requirements should comprehensively address all common system configurations. Emphasis should be placed on criteria that protect against the occurrence of non-ductile failure modes and unintended concentration of inelastic action in limited portions of the system.

When determining the design strength of components that are affected by combined loading, such as axial load/shear friction interaction, consideration should be given to system configurations that might have an effect on the magnitude of combined loads. Beneficial effects of gravity loading must not be permitted in configurations that result in little or no gravity load on the seismic-force-resisting components. Similarly, possible detrimental effects of induced vertical loads should be considered in configurations that generate high axial loads on seismic force resisting components.

Design requirements should address issues of two- and three-directional loading, and simultaneous in-plane and out-of-plane loading, unless the combined load effects are demonstrated to be unimportant.

### *3.3.5 Material Properties*

Design requirements should document all material properties that will serve as reference values for design of components, as well as criteria for determining and measuring these properties. Documentation is not needed for material properties that are prescribed in existing codes and material reference standards. To the extent possible, the experimental determination

of material properties should be based on testing procedures specified in ASTM standards. Material properties of interest include:

- tensile, compressive, and shear stress and strain properties;
- friction properties between parts that possibly will slide;
- bond properties at the interface of two materials;
- other properties on which component behavior depends strongly.

In the determination of material properties, consideration should be given to the simulation of common field conditions during testing, including confinement conditions (e.g., bi-axial or tri-axial states of stress or strain), environmental effects (e.g., temperature, moisture, solar radiation), and cyclic loading. Effects of aging should be quantified, if deemed important to seismic behavior.

Design requirements should include criteria for field testing of material properties for systems in which the reference properties depend strongly on case-specific mix proportions, placement, curing or other similar aspects of construction.

### *3.3.6 Strength and Stiffness Requirements*

Design requirements should contain comprehensive guidance for the determination of design strength and effective elastic stiffness of structural components, and assemblies of components.

- **Stiffness requirements.** Guidance on determination of the effective elastic stiffness of structural components should be provided. The effective elastic stiffness is defined as the stiffness that, if utilized in an analytical model, will provide a good estimate of the interstory drift demand at the design level.
- **Component strength requirements.** The nominal strength of a component should be expressed in terms of material properties, and quantified for the range of loads, and combinations of loads, that might be experienced as the system is subjected to collapse-level ground motions.

  Uncertainty inherent in a strength design equation, as well as the severity of the consequence of failure, should be reflected in the resistance factor ($\phi$-factor) associated with the strength design equation. Resistance factors calibrated for use with common gravity load combinations are recommended for use. Although these factors may not be anchored in reliability analyses for seismic load combinations, design requirements

will be utilized in conjunction with linear analyses and equivalent static forces, and the use of resistance factors will have an important effect on the overall capacity of the system.

If the strength or deformation capacity of one component is affected significantly by interaction with other components, then this interaction should be accounted for in design equations.

If a component is subjected to a load effect, or combination of load effects, that will cause rapid deterioration in strength in the inelastic range, then this load effect, or this combination of load effects, must be clearly identified as a non-ductile mode, and should trigger overstrength design criteria.

Design requirements should be specific about component detailing needed to ensure adequate strength during inelastic deformation.

- **Connection strength requirements.** Design requirements should be specific about design of connections. In general, connections are considered to be non-ductile. If a proposed system is based on a ductile connection, then design requirements must clearly result in connections that will have sufficient deformation capacity to avoid deterioration before any connected components.
- **Sensitivity to gravity loads.** Where the strength of a member or connection is sensitive to compression from gravity loads, design requirements must account for the effect of vertical ground motions. Standard factors in existing standards for additive effects ($1.2 + 0.2S_{DS}$) and counteracting effects ($0.9 – 0.2S_{DS}$) may be used only if justified through studies on structural system archetypes.

### *3.3.7 Quality Rating for Design Requirements*

Quality of information is related to uncertainty, which factors into the performance evaluation for a proposed seismic-force-resisting system. The quality of the proposed design requirements is rated in accordance with the requirements of this section, and approved by the peer review panel.

Design requirements are rated between (A) superior and (D) poor, as shown in Table 3-1. The selection of a quality rating for design requirements considers the completeness and robustness of the requirements, and confidence in the basis for the design equations.

**Table 3-1 Quality Rating of Design Requirements**

| Completeness and Robustness | Confidence in Basis of Design Requirements | | |
|---|---|---|---|
| | High | Medium | Low |
| **High.** Extensive safeguards against poor behavior. All important design and quality assurance issues are addressed. | (A) Superior | (B) Good | (C) Fair |
| **Medium**. Reasonable safeguards against poor behavior. Most of the important design and quality assurance issues are addressed. | (B) Good | (C) Fair | (D) Poor |
| **Low.** Questionable safeguards against poor behavior. Many important design and quality assurance issues are not addressed. | (C) Fair | (D) Poor | -- |

The highest rating of (A) Superior applies to systems that include a complete set of design requirements that provide safeguards against poor, non-ductile behavior and for which there is a high level of confidence that the design equations produce the anticipated results. Existing code requirements for special concrete moment frames, for example, have been vetted with detailed experimental results and real-world earthquake performance. Design and detailing provisions promote a high level of ductility, and include capacity design requirements to safeguard against undesirable behaviors. Such a set of requirements would be rated (A) Superior.

The lowest rating of (D) Poor applies to design requirements that have minimal safeguards against non-ductile failure modes, do not ensure a hierarchy of yielding, and would generally be associated with systems that exhibit non-ductile behavior.

**Completeness and Robustness Characteristics**

Completeness and robustness characteristics are related to how well the design requirements address issues that could potentially lead to smaller strength or ductility than assumed in the design process, as well as proper implementation of designs through fabrication, erection and final construction. Completeness and robustness characteristics are rated from high to low, as follows:

- **High.** Design requirements are extensive, well-vetted and provide extensive safeguards against unanticipated or poor behavior. They establish a definite hierarchy of component yielding. All important issues regarding system behavior have been addressed, resulting in a high reliability in the behavior of the system. Through mature

construction practices, and tightly specified quality assurance requirements, there is a high likelihood that the design provisions will be well executed through fabrication, erection and final construction.

- **Medium.** Design requirements are reasonably extensive and provide reasonable safeguards against poor behavior for a system that consists of moderately-ductile to ductile behavior. Design requirements establish a suggested hierarchy of component yielding, and there is some limited potential for smaller strengths or ductility than expected. While most important behavioral issues have been addressed, some have not, which somewhat reduces the reliability of the system. Quality assurance requirements are specified but do not fully address all the important aspects of fabrication, erection and final construction.
- **Low.** Design requirements provide questionable safeguards against poor behavior for a system that generally consists of non-ductile to moderately-ductile components. Hierarchy of component yielding has been only marginally addressed (if at all), and there is a likelihood of smaller strengths or ductility than expected. While based on experimental results, design requirements do not address important behaviors, resulting in marginally reliable behavior of the system. Quality assurance is lacking, written guidance is not provided, and construction practices are not well-developed for the type of system and materials.

**Confidence in Design Requirements**

Confidence in the basis of the design requirements refers to the degree to which the prescribed material properties, strength criteria, stiffness parameters, and design equations are representative of actual behavior and will achieve the intended result. Confidence is rated from high to low, as follows:

- **High.** There is substantiating evidence (experimental data, history of use, similarity with other systems) that results in a high level of confidence that the properties, criteria, and equations provided in the design requirements will result in component designs that perform as intended.
- **Medium.** There is some substantiating evidence that results in a moderate level of confidence that the properties, criteria, and equations provided in the design requirements will result in component designs that perform as intended.

- **Low.** There is little substantiating evidence (little experimental data, no history of use, no similarity with other systems) that results in a low level of confidence that the properties, criteria, and equations provided in the design requirements will result in component designs that perform as intended.

## 3.4 Data from Experimental Investigation

Analytical modeling alone is not adequate for predicting nonlinear seismic response with confidence, particularly for structural systems that have not been subjected to past earthquakes. A comprehensive experimental investigation program is necessary to establish material properties, confirm behavior, and calibrate analyses for a proposed seismic-force-resisting system. Experimental results from other testing programs can be used to supplement an experimental investigation program, but these results must come from reliable sources, and their applicability to the system under consideration must be demonstrated.

It is understood that there are practical limitations on how comprehensive an experimental testing program can be. It must be understood, however, that limitations on available experimental data will affect the uncertainty and reliability of the collapse assessment of a proposed system, and will factor directly into the performance evaluation process. The scope of an experimental investigation program should be developed in consultation with the peer review panel.

### *3.4.1 Objectives of Testing Program*

Testing is used develop basic information so that the combination of experimental and analytical data is sufficient to achieve the following two objectives:

- Predict the seismic response of structures in the regime of interest to the establishment of seismic performance factors, which occurs when the structure, or any portion of the structure, is subjected to large seismic demands and approaches a state of dynamic instability (collapse). This implies the ability to model strength and stiffness properties of important components, and reliably capture dynamic response until the state of dynamic instability, over the range of possible structural configurations covered by the structural system archetypes,.
- Develop and validate standardized engineering design criteria that can be used to design structures that perform as expected, given the seismic performance factors that are specified.

Achievement of these objectives requires a coordinated material, component, connection, assembly, and system testing program that will provide the following information:

- **Material test data.** Data that serve as reliable reference values for the prediction of strength, stiffness, and deformation properties of structural components and connections under earthquake loading.
- **Component and connection test data.** Information needed to develop and calibrate analytical models of cyclic load-deformation characteristics for components and connections that form an essential part of the seismic-force-resisting system.
- **Assembly and system test data.** Information needed to quantify interactions between structural components and connections that cannot be predicted by analysis with confidence.

### *3.4.2 General Testing Issues*

In developing a comprehensive testing program, the following issues should be considered:

- **Cumulative damage effects.** Structural materials and components experience history-dependent cumulative damage during repeated cyclic loading. The loading history used in testing should be representative of the cyclic response that a material, component, connection, or assembly would experience as part of a typical structural system subjected to a severe earthquake.
- **Size effects.** Tests should be performed on full-size specimens unless it can be shown by theory and experiment that testing of reduced-scale specimens will not significantly affect behavior.
- **Strain rate effects.** If the load-deformation characteristics of the specimen are sensitive to strain rate effects, then testing should be done at strain rates commensurate with those experienced in a typical structural system subjected to a severe earthquake.
- **Boundary conditions.** The boundary conditions of component and assembly tests should be: (1) representative of constraints that a component or assembly conditions would experience in a typical structural system; and (2) sufficiently general so that the results can be applied to boundary conditions that might be experienced in other system configurations. Boundary conditions should not impose beneficial effects on seismic behavior that would not exist in common system configurations.

- **Configuration and number of component/assembly test specimens.** The configuration and number of component and assembly test specimens should be such that common failure modes that could occur in typical system configurations are represented and evaluated. Emphasis should be on the detection and evaluation of failure modes that lead to a rapid deterioration in strength (e.g., brittle failure modes).
- **Interaction between structural components.** Test configurations should consider important interactions between structural components, unless these interactions can be predicted with confidence by analysis.
- **Direction(s) of loading.** Structural components that resist seismic forces in more than one direction (e.g., concrete core walls) should be tested such that the combined load effects are adequately considered, unless these effects can be predicted with confidence by analysis.
- **In-plane and out-of-plane load effects.** Planar structural components (e.g., walls, diaphragms) should be subjected to simultaneous in-plane and out-of-plane loading, unless these effects can be superimposed with confidence by analysis.
- **Gravity load effects.** Effects of gravity loads should be considered in the experimental program, unless these effects can be superimposed on lateral load effects with confidence by analysis.
- **Statistical variability.** A sufficiently large number of tests should be performed so that statistical variations can be evaluated from the data directly, or can be deduced in combination with data from other sources.
- **Environmental conditions.** If environmental conditions during construction or service (e.g., temperature, humidity) will significantly affect behavior, then the range of conditions that could exist in practice should be simulated during testing.
- **Quality of test specimen construction.** Component, connection, assembly, and system specimens should be of a construction quality that is equal to what will be commonly implemented in the field. Special construction techniques or quality control measures should not be employed, unless they are part of the design requirements.
- **Dynamic system validation tests.** If experimental material, component, connection, assembly, or system data, together with analytical modeling, are not sufficient to predict seismic response to collapse, then dynamic system validation tests should be performed (on a shake table, or through other means of dynamic excitation).

- **Past experience.** Laboratory testing cannot fully replace the experience gained from observation of system behavior in actual use. A benefit should be given to structural systems whose performance has been documented in past earthquakes or other use.
- **Documentation of tests and test results.** The documentation of experiments should be comprehensive, and should include: (1) geometric data and important details of the test specimen, including fabrication details, boundary conditions, constraints, and applied loads; (2) locations of instruments for the measurement of primary response parameters; (3) material test data needed for performance evaluation; and (4) experimental data needed for performance evaluation.

The above list should be used as a guide. There may be other issues that are equally important to a given system, but cannot be placed in a general context. Assistance in the identification of important testing issues can be obtained from references available in the literature (e.g., ACI 2001, AISC 2005, ASTM 2003, ATC 1992, Clark et al. 1997, FEMA 2007, and ICBO-ES 2002).

Testing laboratories used to conduct an experimental investigation program should comply with national or international accreditation criteria, such as ICBO ES Acceptance Criteria for Laboratory Accreditation (AC89) (ICBO 2000).

### *3.4.3 Material Testing Program*

A material testing program is required to provide reliable stress-strain relationships for the prediction of strength, stiffness, and deformation properties of structural components and connections under the type of loading experienced during an earthquake. In addition to general testing issues, materials testing should consider the following:

- low-cycle fatigue and fracture properties
- bi-axial and tri-axial stress conditions
- utilization of applicable ASTM Standards
- evaluation of variability in material properties
- effects of aging
- effects of environmental conditions

Material testing programs should be performed in accordance with all applicable ASTM Standards and other testing criteria specified in nationally

accepted industry standards and specifications. Material test data available from past tests that conform to all applicable standards can be used.

### 3.4.4 Component, Connection, and Assembly Testing Program

A component, connection, and assembly testing program is required to provide information for the development and calibration of analytical models of cyclic load-deformation characteristics of components and connections that form an essential part of the seismic-force-resisting system. Components, connections, and assemblies that have low inelastic deformation capacities must be identified, and should undergo sufficient testing so that the results can serve as validation of analytical models that are used to assign strength properties in the design and collapse assessment process.

**Testing of Structural Components**

Component testing serves to identify and quantify component modeling parameters that significantly affect seismic response. Behavior is characterized by a basic hysteresis loop, which deteriorates with the number and amplitude of cycles. It is critical that a test is continued until severe deterioration is evident, and all important characteristics that enter design equations and analytical models have been verified experimentally. No credit should be given in the modeling to any residual strength or deformation capacity beyond the point at which the test is terminated. Two hysteretic responses of a structural component (in this case a steel beam and a plywood panel) are shown in Figure 3-2. In this figure, it appears that the loops stabilize at very large amplitudes, and that more and larger deformation cycles can be sustained; however, the possibility of fracture at large deformations is high. Once this fracture occurs, the resistance will deteriorate rapidly and will approach zero.

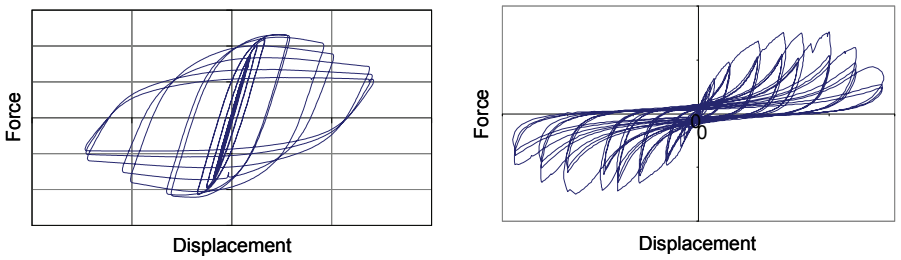


Figure 3-2 Characteristics of force-deformation response (a) steel beam (Uang et al. 2000), (b) plywood shear wall panel (Gatto and Uang 2002)

A sufficiently large number of tests should be performed so that important statistical variations can be evaluated from the data directly, or can be deduced in combination with data from other sources. A minimum of two tests is required for each set of primary variables in a test configuration. If rapid deterioration occurs, such as that caused by fracture behavior, a minimum of three tests should be performed.

Component tests are conducted for the purpose of evaluating all force and deformation characteristics that have a significant effect on the seismic response up to the state of incipient collapse. Gravity loads should be represented, unless it can be shown that their effect is not detrimental to the seismic behavior or can be predicted with confidence from analytical models. The load application and loading history should be representative of what components will experience as part of a typical structural system subjected to a severe earthquake. Instrumentation should permit the measurement of all relevant stiffness and strength properties.

In contrast to "qualification testing", which is intended to gain approval of the use of certain components for specific applications, the main objective of these component tests are to calibrate and validate nonlinear models that are used in the collapse assessment. Types and configurations of component tests, together with the loading protocol, should be planned in conjunction with development of the nonlinear analysis models in Chapter 5.

**Testing of Connections**

A connection is the medium that transfers forces and deformations between adjacent components. Connections should be tested in configurations that simulate gravity load effects as well as seismic load effects, unless gravity loading results in more favorable connection behavior. Connection tests should provide all information necessary to develop connection design criteria in conformance with the latest edition of ASCE/SEI-7, and to permit simulation of connections in analytical models.

**Testing of Assemblies**

An assembly is an arrangement of structural components whose seismic behavior can be described in terms of a single response quantity, such as interstory drift. An assembly testing program is required if important interactions between adjacent components (or between components and connections) cannot be deduced with confidence from a combination of material, component, and connection tests in combination with analytical modeling. Unless strain-rate effects are important, assembly tests can be

performed by imposing load(s) to control point(s) in a quasi-static manner, following a predetermined loading history.

### *3.4.5 Loading History*

Structural elements have limited strength and deformation capacities, and collapse safety depends on the ability to assess these capacities with some confidence. Strength and deformation capacities depend on cumulative damage, which implies that every component has a "memory" of past damaging events, and that all past excursions (or cycles) that have contributed to its current state of health will affect future behavior. Thus, performance depends on the history of previously applied damaging cycles, and assessing the consequences of history requires replication of the load and deformation histories a component will undergo in an earthquake (or several earthquakes, if appropriate). The objective of a loading history is to achieve this in an approximate, but consistent manner.

There is no unique or best loading history, because no two earthquakes are alike, and a specimen may be part of many different structural configurations. The overriding issue is to account for cumulative damage effects through cyclic loading. If there is no cumulative damage, there is no need for cyclic loading. The number and amplitude of cycles applied to the specimen may be derived from analytical studies in which models of representative structural systems are subjected to representative earthquake ground motions, and the response is evaluated statistically. In analytical modeling it should be assumed that specimen resistance deteriorates to zero following the maximum amplitude executed in the test. No credit should be given to deformation capability beyond the largest deformation that a specimen experiences in a test.

Many loading protocols have been proposed in the literature, and several have been used in multi-institutional testing programs (e.g., ATC 1992, Clark et al. 1997, Krawinkler et al. 2000), or are contained in standards or are proposed for standards (e.g., FEMA 2007, AISC 2005, ASTM 2003, ICBO-ES 2002). These protocols recommend somewhat different loading histories, but they differ more in detail than in concept. Comprehensive discussions of loading histories and their origin and objectives are presented in Filiatrault et al. 2008, Krawinkler et al. 2000, and Krawinkler 1996.

Loading history should be deformation-controlled, with the following two exceptions.

- For small excursions in which a component will remain essentially elastic, force-control may be applied. Force-control would be

encouraged for stiff specimens tested in a relatively flexible test set-up, in order to facilitate measurements and test control in the early stages of testing.

- Force-control may be necessary to test components that are an essential part of the load path, but are fully force-controlled in the in-situ condition, and have no reliable inelastic deformation capacity. One such example would be an anchor controlled by the maximum force exerted by a connected component. In such a case, the loading history should be structured based on the strength and deformation capacities of the connected component. Criteria for a force-controlled loading history are presented in FEMA 461 (FEMA 2007).

### *3.4.6 System Testing Program*

Testing of an essentially complete structural system should be performed if important response characteristics or important interactions between components and connections cannot be evaluated with good confidence by analytical models that have been calibrated through material, component, connection, or assembly tests.

System tests should be used as a validation tool for a proposed analytical model rather than as an exploratory test from which analytical models will be developed. System tests should not be used to replace any testing at the material, component, connection, or assembly level.

**Dynamic System Tests**

A dynamic system test should be performed if the response close to collapse depends strongly on dynamic characteristics that cannot be predicted with good confidence by analytical models or from component or assembly tests. Such a test should be performed on an earthquake simulator (shake table) utilizing realistic MCE-level (or collapse level) ground motions, unless it can be demonstrated that equivalent response evaluation can be achieved through alternative means.

**Quasi-Static System Tests**

A quasi-static system test should be performed if important behaviors or interactions between components and connections cannot be evaluated with good confidence by means of calibrated analytical models. Examples include interactions between horizontal and vertical components (floor diaphragms and vertical seismic-force-resisting units) and between vertical components that resist seismic forces in orthogonal directions.

Quasi-static cyclic testing consists of loads that are applied to one or more control points by means of hydraulic actuators whose displacement or load values are varied in a cyclic manner in accordance with a predetermined loading history. The loading history used in testing should be representative of the cyclic response that a material, component, connection, or assembly would experience as part of a typical structural system subjected to a severe earthquake.

### *3.4.7 Quality Rating of Test Data*

Quality of test data is related to uncertainty, which factors into the performance evaluation for a proposed seismic-force-resisting system. The quality of test data obtained from an experimental investigation program is rated in accordance with the requirements of this section, and approved by the peer review panel.

Test data are rated between (A) superior and (D) poor, as shown in Table 3-2. This rating depends not only on the quality of the testing program, but on how well the tests address key parameters and behavioral issues. The selection of a quality rating for test data considers the completeness and robustness of the overall testing program, and confidence in the test results.

**Table 3-2 Quality Rating of Test Data from an Experimental Investigation Program**

| Completeness and Robustness | Confidence in Test Results | | |
|---|---|---|---|
| | High | Medium | Low |
| **High.** Material, component, connection, assembly, and system behavior well understood and accounted for. All, or nearly all, important testing issues addressed. | (A) Superior | (B) Good | (C) Fair |
| **Medium**. Material, component, connection, assembly, and system behavior generally understood and accounted for. Most important testing issues addressed. | (B) Good | (C) Fair | (D) Poor |
| **Low.** Material, component, connection, assembly, and system behavior fairly understood and accounted for. Several important testing issues not addressed. | (C) Fair | (D) Poor | -- |

**Completeness and Robustness Characteristics**

Completeness and robustness characteristics are related to: (1) the degree to which relevant testing issues have been considered in the development of the

testing program, and (2) the extent to which the testing program and other documented experimental evidence quantify the necessary material, component, connection, assembly, and system properties and behaviors. Completeness and robustness characteristics are rated from high to low, as follows:

- **High.** All, or nearly all, important general testing issues of Section 3.4.2 are addressed comprehensively in the testing program and other supporting evidence. All, or nearly all, important behavior aspects at all levels (from material to system) are well understood, and the results can be used to quantify all important parameters that affect design requirements and analytical modeling.
- **Medium.** Most of the important general testing issues of Section 3.4.2 are addressed adequately in the the testing program and other supporting evidence. All, or nearly all, important behavior aspects at all levels (from material to system) are generally understood, and the results can be used to quantify or deduce most of the important parameters that significantly affect design requirements and analytical modeling.
- **Low.** Several important general testing issues of Section 3.4.2 are not addressed adequately in the testing program and other supporting evidence. The most important behavior aspects at all levels (from material to system) are fairly well understood, but the results are not adequate to quantify or deduce many of the important parameters that significantly affect design requirements and analytical modeling.

**Confidence in Test Results**

Confidence in test results is related to the reliability and repeatability of the results obtained from the testing program, and corroboration with available results from other relevant testing programs. It includes consideration as to whether or not experimental results consistently record performance to failure for all modes of behavior (limited ductility to large ductility), and if sufficient information is provided to assess uncertainties within in the design requirements (e.g., $\phi$ factors). Confidence in test results is rated from high to low, as follows:

- **High.** Reliable experimental information is produced on all important parameters that affect design requirements and analytical modeling. Comparable tests from other testing programs have produced results that are fully compatible with those from the system-specific testing program. A sufficient number of tests are performed so that statistical variations in important parameters can be assessed. Test results are fully supported by basic principles of mechanics.

- **Medium.** Moderately reliable experimental information is produced on all important parameters that affect design requirements and analytical modeling. Comparable tests from other testing programs do not contradict, but do not fully corroborate, results from the system-specific testing program. A measure of uncertainty in important parameters can be estimated from the test results. Test results are supported by basic principles of mechanics.
- **Low.** Experimental information produced on many of the important parameters that affect design requirements and analytical modeling is of limited reliability. Comparable tests from other testing programs do not support the results from the system-specific testing program. Insufficient data exists to assess uncertainty in many important parameters. Basic principles of mechanics do not support some of the results of the testing program.

# Chapter 4
# Archetype Development

This chapter describes the development of structural system *archetypes*, which provide a systematic means for characterizing key features and behaviors related to collapse performance of a proposed seismic-force-resisting system. It defines how archetype descriptions and performance characteristics are used to develop a set of building configurations (*index archetype configurations*) that together describe the overall range of permissible configurations (*archetype design space*) of a system, which is then separated into groups sharing common features or behavioral characteristics (*performance groups*) for assessing collapse performance. Structural system archetypes are used to create nonlinear analysis models (*index archetype models*) in Chapter 5.

## 4.1 Development of Structural System Archetypes

Behavior of a proposed seismic-force-resisting system is investigated through the use of archetypes. An *archetype* is a prototypical representation of a seismic-force-resisting system. Archetypes reflect the range of design parameters and system attributes that are judged to have a measurable impact on system response. They are used to bridge the gap between collapse performance of a single specific building and the generalized predictions of behavior needed to quantify performance for an entire class of buildings.

An *index archetype configuration* is a prototypical representation of a seismic-force-resisting system configuration that embodies key features and behaviors related to collapse performance when the system is subjected to earthquake ground motions. Given that building codes permit significant latitude with respect to system configurations within a building class, index archetype configurations are not intended to represent every conceivable configuration of the system of interest. Rather, the intent is to investigate the typical range of parameters that would be representative of typical conditions encountered in design practice.

Collectively, the set of index archetype configurations describe the *archetype design space*, which defines the overall range of permissible configurations, structural design parameters, and other properties that define the application limits for a seismic-force-resisting system. For performance evaluation, the archetype design space is divided into *performance groups*, which are groups

of index archetype configurations that share a common set of features or behavioral characteristics.

Development of structural system archetypes follows the process outlined in Figure 4-1. Using the design requirements and test data developed under Chapter 3 as inputs, development of structural system archetypes considers both structural configuration issues and seismic behavioral effects.

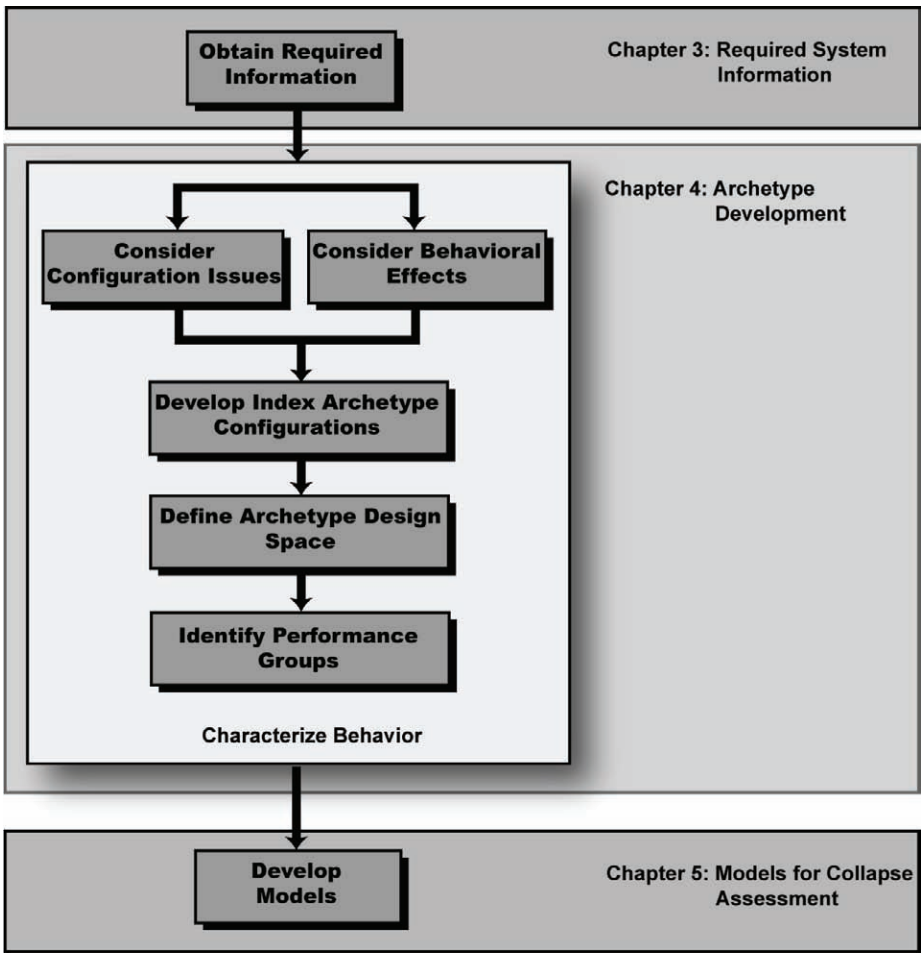


Figure 4-1 Process for developing archetype index configurations and models

## 4.2 Index Archetype Configurations

Index archetype configurations must be sufficiently broad in scope to capture the range of situations that will typically be encountered in practice, but sufficiently limited to be practical to evaluate. The intent is to assess situations that will be generally representative of practice that meets minimum specified requirements for seismic design and construction of a proposed seismic-force-resisting system. In a statistical sense, index archetype configurations are not intended to represent "outliers." They are

also not intended to represent "standard" practices that routinely exceed minimum code requirements. For example, use of one member size at multiple locations in a building is a design and construction practice that can result in member strengths exceeding minimum design requirements at many locations. Benefits from this type of overstrength, however, should not be built into index archetype configurations.

It is expected that the set of index archetype configurations will generally include about twenty to thirty specific structural configurations, though the number will vary depending on the characteristics of the seismic-force-resisting system and the limits of the archetype design space. The final selection of index archetype configurations, and their corresponding design parameters, should be decided in cooperation with the peer review panel.

Development of index archetype configurations involves the following steps:

- Identify key design variables and related physical properties based on structural configuration issues summarized in Table 4-1. Investigate physical properties that affect collapse performance to identify critical design variables that should be reflected in index archetype configurations.
- Establish bounds for key design variables.
- Identify behavioral issues and related design considerations based on behavioral effects summarized in Table 4-2. Investigate possible deterioration modes that could result in local and global collapse scenarios, and assess the likelihood of those scenarios.
- Develop a set of index archetype configurations based on key design variables and behavioral effects that are likely to result in local or global collapse scenarios.

### *4.2.1 Structural Configuration Issues*

Structural configuration issues include occupancy and program influences, framing type and geometric variations, and gravity and lateral load intensities. Typical configuration design variables that can affect the behavior of a seismic-force-resisting system are summarized in Table 4-1. These should be used as a guide in establishing index archetype configurations, as follows:

- **Occupancy and Use:** Building occupancy and use can influence the structural layout, framing system, configuration, and loading intensity. Framing spans, story heights, and live loads for seismic systems intended for residential occupancies are usually quite different from office

occupancies. Similarly, steel moment frames and associated gravity framing used for industrial occupancies can be different from those used for office or institutional buildings. Occupancies with large live load demands may have larger inherent overstrength in comparison to systems for other occupancies. Major changes in structural configuration resulting from different occupancies and use should be reflected in the index archetype configurations.

**Table 4-1 Configuration Design Variables and Related Physical Properties**

| Design Variable | Related Physical Properties |
|---|---|
| Occupancy and Use | • Typical framing layout<br>• Distribution of seismic-force-resisting system components<br>• Gravity load intensity<br>• Component overstrength |
| Elevation and Plan Configuration | • Distribution of seismic-force-resisting components<br>• Typical framing layout<br>• Permitted vertical (strength and stiffness) irregularities<br>• Beam spans, number of framing bays, system regularity<br>• Wall length, aspect ratio, plan geometry, wall coupling<br>• Braced bay size, number of braced bays, bracing configuration<br>• Ratio of seismic mass to seismic-force-resisting components<br>• Ratio of tributary gravity load to seismic load |
| Building Height | • Story heights<br>• Number of stories |
| Structural Component Type | • Moment frame connection types<br>• Bracing component types<br>• Shear wall sheathing and fastener types<br>• Isolator properties and types |
| Seismic Design Category | • Design ground motion intensity<br>• Special design/detailing requirements<br>• Application limits |
| Gravity Load | • Gravity load intensity<br>• Typical framing layout<br>• Ratio of tributary gravity load to seismic load<br>• Component overstrength |

- **Elevation and Plan Configuration:** The range of elevation and plan configurations permitted by the system design requirements should be reflected in the index archetype configurations. This could include, for example, the range of framing span lengths of the seismic-force-resisting

system, alternative configurations of steel bracing (e.g., chevron versus x-bracing), and the extent of gravity framing tributary to the system. These effects may be more significant in some systems than others. Variations in shear wall proportions that result in flexure- versus shear-dominated behavior in a shear wall system are likely to be more significant than variations in framing bay sizes in a moment frame system.

- **Building Height:** The range of story heights and number of stories permitted by the system design requirements should be reflected in the index archetype configurations. To capture the variation in performance over a range of one to 20 stories in height, it is anticipated that as many as six index archetype configurations could be required. Due to significant differences in the response characteristics of very tall buildings, and limited frequency content in the ground motions specified for collapse assessment, use of this Methodology is limited to building heights of about 20 to 30 stories for moment frame systems and 30 to 40 stories for braced frame and shear wall systems.
- **Structural Component Type:** The extent that structural component types can vary within a given seismic-force-resisting system should be reflected in index archetype configurations. Examples include different types of moment connection details, steel bracing members (e.g., HSS, pipe, or W-shape), wood-framed shear wall sheathing and fasteners, and isolators (e.g., sliding versus lead-rubber).
- **Seismic Design Category***:* Systems should be evaluated for the highest (most severe) Seismic Design Category for which they are proposed, and verified in lower Seismic Design Categories. Index archetype configurations within a Seismic Design Category should consider spectral intensities corresponding to the maximum and minimum values for that category, associated design and detailing requirements, and any restrictions on use keyed to Seismic Design Category.
- **Gravity Load:** Large gravity load demands can result in overstrength with respect to seismic demands. For some components (e.g., columns in moment frames) axial load ratio can significantly impact inelastic deformation capacity. The nature, magnitude and variation of gravity loads, including structure self weight, occupancy-related superimposed dead loads, and occupancy-related live loads should be considered, and design parameters that affect tributary gravity load, such as bay sizes and building height, should be reflected in the index archetype configurations. It is anticipated that, for most systems, two levels of gravity load (high and low) would be sufficient.

An example of how configuration issues are considered in the development of index archetype configurations for a special reinforced concrete moment frame system conforming to design requirements contained in ASCE 7-05, is provided in Appendix C.

### *4.2.2 Seismic Behavioral Effects*

Consideration of seismic behavioral effects includes identifying dominant deterioration and collapse mechanisms that are possible, and assessing the likelihood that they will occur. How a component or system behaves under seismic loading is often influenced by configuration decisions, so behavioral effects and configuration issues should be considered concurrently in the development of index archetype configurations.

Seismic collapse resistance depends on the strength, stiffness, and deformation capacity of individual structural components and the overall seismic-force-resisting system. Each of these properties can be addressed directly through system design requirements, but each are also influenced by aspects of the configuration that could change the way a system behaves across the range of an archetype design space. For example, requirements for ductile confinement of reinforced concrete columns will directly affect inelastic deformation capacity, but the magnitude of column axial load, which is influenced by elevation and plan configurations, also has a large impact.

Consideration of behavioral effects is used to help identify major changes in system behavior as the configuration varies. Once potential deterioration and collapse mechanisms are identified, they are addressed through one of the following methods: (1) by ruling out failure modes that are unlikely to occur based on system design and detailing requirements; (2) explicit simulation of failure modes through nonlinear analyses; or (3) evaluation of non-simulated failure modes using alternative limit state checks on demand quantities from nonlinear analyses. Index archetype configurations must address failure modes that will be explicitly simulated in nonlinear analysis models in Chapter 5.

Typical behavioral issues and related design considerations that can have an effect on the behavior of a seismic force-resisting system are summarized in Table 4-2.

**Table 4-2 Seismic Behavioral Effects and Related Design Considerations**

| Behavioral Issue | Related Design Considerations |
|---|---|
| Strength | • Design member forces<br>• Calculated member forces<br>• Capacity design requirements<br>• Component overstrength |
| Stiffness | • Design member forces<br>• Drift limits<br>• Plan and elevation configuration<br>• Calculated inter-story drifts |
| Inelastic deformation capacity | • Component detailing requirements<br>• Member geometric proportions<br>• Capacity design requirements<br>• Calculated member forces<br>• Plan and elevation configuration |
| Seismic Design Category | • Design ground motion intensity<br>• Special design/detailing requirements |
| Inelastic system mobilization | • building height and period<br>• permitted strength and stiffness irregularities<br>• capacity design requirements |

These should be used as a guide in establishing index archetype configurations, as follows:

- **Strength:** Differences between the design strength of components and calculated seismic demands should be reflected in the index archetype configurations. Design strength is a function of the design earthquake intensity, component detailing requirements, capacity design requirements, and overstrength resulting from gravity load effects. Calculated demands are a function of the structural configuration and gravity load (dead and live load) intensity. In cases where gravity load or stiffness considerations control, there can be significant overstrength relative to minimum seismic design forces. Capacity design provisions control yielding by requiring strengths of selected components to be greater than would otherwise be required by minimum seismic design forces.
- **Stiffness:** The elastic lateral stiffness of the seismic-force-resisting system affects the dynamic behavior, sensitivity to sidesway stability (P-Delta) effects, and induced deformation demands on critical components. Stiffness is a function of the design earthquake intensity and imposed drift limits, as well as the system configuration. Index archetype configurations should take into account system types that are more sensitive to drift limits than others, and should identify configurations

that probe limits on minimum stiffness in the system design requirements.

- **Inelastic Deformation Capacity:** Inelastic deformation capacity of components is a function of design requirements (e.g., detailing rules, capacity design provisions), member geometric proportions, and calculated member forces that can vary with structural configuration. Configurations that induce large calculated member forces that affect the deformation capacity should be reflected in index archetype configurations.
- **Seismic Design Category:** Applicable Seismic Design Categories establish the design ground motion intensities, which influence seismic-force-resisting system strength and stiffness. Seismic Design Category designations can also trigger special design and detailing requirements that will influence component inelastic deformation capacity. Index archetype configurations should reflect behavioral effects that are influenced by the Seismic Design Categories for which a system is being proposed.
- **Inelastic System Mobilization:** Inelastic system mobilization is the extent to which inelastic action is distributed throughout the seismic-force-resisting system. Inelastic system mobilization is influenced by limits on stiffness and strength irregularities imposed by system design requirements. Design and configuration decisions can affect whether yielding is distributed across many stories or focused into story mechanisms. Index archetype configurations should identify and test configurations that are permitted by system design requirements, and will result in a lower bound of inelastic system mobilization.

An example of how behavioral effects are considered in the development of index archetype configurations for a special reinforced concrete moment frame system conforming to design requirements contained in ASCE 7-05, is provided in Appendix D.

### *4.2.3 Components Not Designated as Part of the Seismic-Force-Resisting System*

Components not designated as part of the seismic-force-resisting system are not included in the development of index archetype configurations. While it is recognized that other portions of the building (e.g., components of the gravity system) can significantly affect collapse behavior, components that are not controlled by seismic-force-resisting system design requirements may not be present in all cases, and cannot be relied upon for reducing collapse risk.

### 4.2.4 Other Controlling Load Cases

Overstrength due to wind or other controlling load cases that are not specifically attributed to earthquake and gravity load effects is not considered in the development of index archetype configurations. While system overstrength can significantly affect seismic behavior, overstrength that is not controlled by seismic-force-resisting system or gravity load design requirements may not be present in all cases, and cannot be relied upon for reducing collapse risk.

## 4.3 Performance Groups

Index archetype configurations are assembled into performance groups (or bins) that reflect major divisions, or changes in behavior, within the archetype design space. Performance groups should contain multiple index archetype configurations that reflect the expected range of permissible variation in size and other key parameters defined by the archetype design space. For example, each performance group should contain index archetype configurations that cover the range of building heights permitted by the system design requirements.

The binning of index archetype configurations into performance groups provides the basis for statistical assessment of minimum and average collapse margin ratios for performance evaluation in Chapter 7. Performance group populations should not be made larger than necessary, or biased towards certain configurations, in order to manipulate the average collapse statistics for the bin. Binning of index archetype configurations into performance groups should be done in cooperation with the peer review panel.

### 4.3.1 Identification of Performance Groups

Identification of performance groups should consider the following parameters: (1) Seismic Design Category; (2) gravity load intensity; and (3) other key design features that result in major changes in collapse behavior, including component types, span lengths, aspect ratios, or detailing requirements.

As a minimum, two performance groups are required, each with a representative suite of index archetype configurations designed for the maximum and minimum seismic criteria associated with the governing Seismic Design Category (SDC). Typically, only the maximum and minimum earthquake intensities for the highest Seismic Design Category will need to be investigated (for example $D_{max}$ and $D_{min}$ for SDC D). If, however, the trend between the maximum and minimum intensity suggests that lower

intensities may be more critical (e.g., calculated collapse margins are smaller for $D_{min}$ than $D_{max}$) then additional performance groups are necessary to evaluate the possibility that lower Seismic Design Categories (SDC C or SDC B) might control.

When gravity loads significantly influence collapse behavior, binning of index archetype configurations should consider high and low gravity load intensities. In combination with maximum and minimum seismic design criteria for Seismic Design Category D and lower, consideration of gravity loads would result in a minimum of four performance groups:

- Maximum Seismic (SDC $D_{max}$), High Gravity
- Minimum Seismic (SDC $D_{min}$), High Gravity
- Maximum Seismic (SDC $D_{max}$), Low Gravity
- Minimum Seismic (SDC $D_{min}$), Low Gravity

If other design features result in significant changes in collapse behavior, or if trends indicate that lower Seismic Design Categories sometimes control, then additional performance groups would be needed, as shown in the performance group matrix of Table 4-3.

**Table 4-3 Performance Group Matrix**

| Seismic Design Category | Dominant System Characteristic (e.g., Gravity Load Intensity) | |
|---|---|---|
| | High Gravity | Low Gravity |
| $SDC_{max}$ | "N" characteristic sets of index archetype configurations of "Y" heights | "N" characteristic sets of index archetype configurations of "Y" heights |
| $SDC_{min}$ | "N" characteristic sets of index archetype configurations of "Y" heights | "N" characteristic sets of index archetype configurations of "Y" heights |
| SDC-lower | Additional index archetype configuration sets as needed to verify trend for lower SDCs | Additional index archetype configuration sets as needed to verify trend for lower SDCs |

As an example, assume that in addition to Seismic Design Category and gravity load, there are two predominant configuration or component characteristics affecting collapse performance ("N" equals 2), and that 6 index archetype configurations captures the variability over the range of permissible heights ("Y" equals 6). In this case, 48 index archetype

configurations (2 seismic design intensities x 2 gravity load intensities x 2 configuration characteristics x 6 building heights) would be evaluated across 8 performance groups (2 seismic design intensities x 2 gravity load intensities, x 2 configuration characteristics). The number of index archetype configurations and performance groups can be reduced in cooperation with the peer review panel, if there is evidence to indicate that performance evaluation will not change if certain combinations of parameters are omitted.

# Chapter 5
# Nonlinear Model Development

This chapter describes the development of analytical models for collapse assessment of a proposed seismic-force-resisting system. It defines how *index archetype designs* are prepared from index archetype configurations using the proposed design requirements for the system of interest, and how nonlinear member properties are developed and calibrated for use in *index archetype models* for nonlinear simulation of collapse. Index archetype models are based on structural system archetypes defined in Chapter 4, and are used to perform nonlinear analyses in Chapter 6.

## 5.1 Development of Nonlinear Models for Collapse Simulation

Since index archetype configurations are developed with explicit consideration of features that should be investigated through nonlinear collapse simulation, development of nonlinear models is closely related to the development of structural system archetypes. Nonlinear model development includes preparation of: (1) *index archetype designs*, which are index archetype configurations that have been proportioned and detailed using the design requirements for a proposed seismic-force-resisting system; and (2) *index archetype models*, which are idealized mathematical representations of index archetype designs used to simulate collapse in nonlinear static and dynamic analyses.

Development of nonlinear models for collapse simulation follows the process outlined in Figure 5-1. Using structural system archetypes as inputs, design requirements and material test data are applied to each index archetype configuration to develop index archetype designs using trial values of $R$, $C_d$, and $\Omega_o$. Each design is then idealized into an index archetype model. Using data from component, connection, assembly and system tests, models are calibrated for use as inputs to nonlinear analysis in Chapter 6.

## 5.2 Index Archetype Designs

Index archetype designs are prepared by applying design requirements and material test data for a proposed seismic-force-resisting system to a set of index archetype configurations. Index archetype designs should include all significant design features of the proposed system. Member proportions, connection details, and system/material specific detailing requirements

necessary for quantifying the nonlinear response of each index archetype configuration should be designed in accordance with proposed seismic design provisions. Designs should also meet applicable provisions of ASCE/SEI 7-05, material reference standards, or other model building codes.

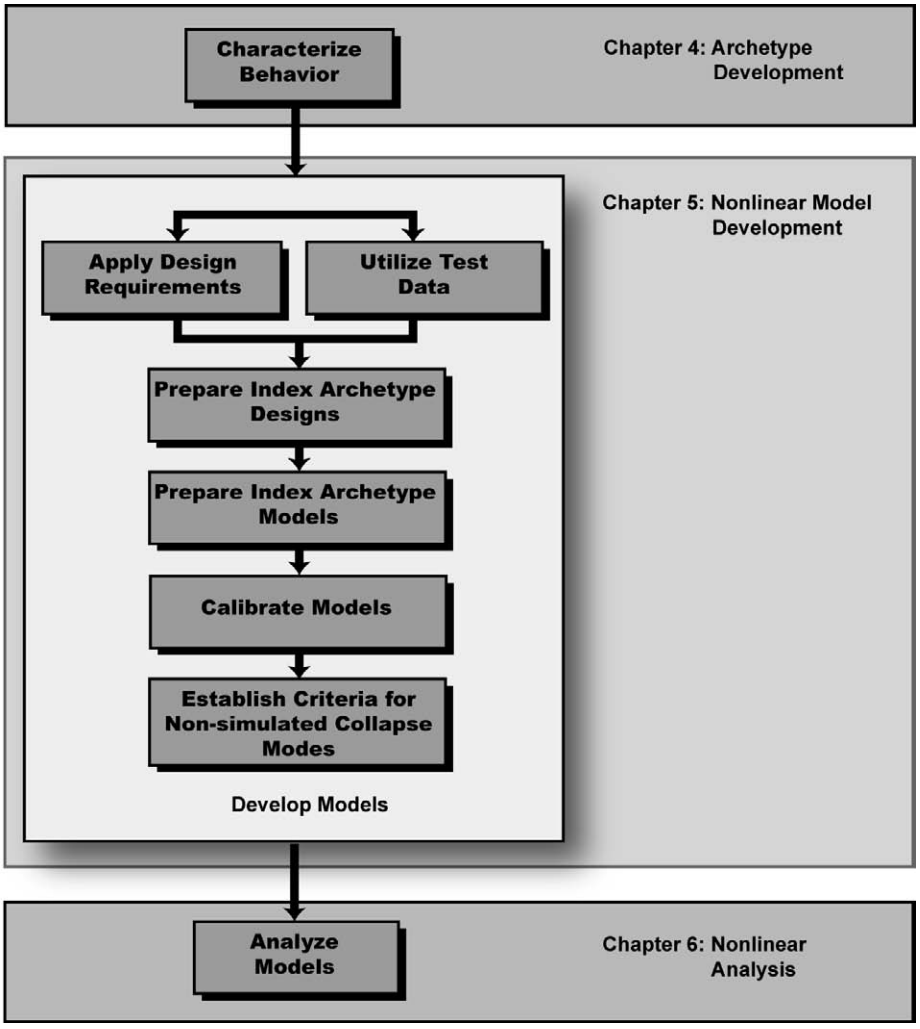


Figure 5-1 Assessment process for Index Archetype Analysis Models by nonlinear analysis

Explicit evaluation of redundancy effects has not been addressed in the development of the Methodology. Evaluation of other generic system effects, such as accidental torsion and configuration irregularities, has also not been specifically addressed. It is assumed that such effects are generic to all systems, and adequately addressed by applicable general analysis and design provisions of ASCE/SEI 7-05. For this reason, it is important that systems comply with these provisions, or that index archetype designs explicitly address any deviations from these provisions.

Index archetype designs should be prepared considering gravity and seismic loading, in accordance with the following load combinations:

$$1.2D + 1.0E + 0.5L \quad (5\text{-}1a)$$

$$0.9D - 1.0E \quad (5\text{-}1b)$$

where $D$ includes the structural self weight and superimposed dead loads, $L$ is the live load (including appropriate live load reduction factors), and $E$ is the earthquake loading effect. For typical cases, roof live loads should be included as a nominal live load of 20 psf. It should be noted that roof snow load is not included in Equation 5-1a, which is different from an analogous equation given in ASCE/SEI 7-05. Since snow load is an environmental load that varies independently of seismic intensity, and is not considered to be a primary factor affecting seismic performance, it has been excluded. For systems in which snow is deemed to be a controlling factor, then provision for snow should be made in the index archetype design.

Earthquake load effects are determined by the following equation, taken directly from ASCE/SEI 7-05:

$$E = \rho Q_E \pm 0.2 S_{DS} D \quad (5\text{-}2)$$

where $Q_E$ is the effect of horizontal seismic forces, $\rho$ is the redundancy factor, and $S_{DS}$ is the design spectral response at short periods. $Q_E$ should be determined in accordance with ASCE/SEI 7-05 as a function of the design ground motion intensity and an initial trial value of the response modification coefficient, $R$. Designs should meet the drift limitations of ASCE/SEI 7-05, based on an initial trial value of the displacement amplification coefficient $C_d$. The redundancy factor, $\rho$, is set to unity for index archetype designs, since the intent is to evaluate seismic performance factors for minimum typical conditions.

Structural components that are subject to rapid deterioration and sensitive to overload conditions should be designed with an initial trial value of the overstrength factor, $\Omega_o$, as follows,

$$E = \Omega_o Q_E \pm 0.2 S_{DS} D \quad (5\text{-}3)$$

Initial trial values of $R$, $C_d$, $\Omega_o$ may need to be revised based on the outcome of the performance evaluation process in Chapter 7.

### *5.2.1 Performance Group Design Variations*

As described Chapter 4, performance groups should consider, as a minimum, design variations related to Seismic Design Category and gravity load

intensity. Index archetype designs should be prepared for the maximum and minimum seismic criteria associated with the governing Seismic Design Category (SDC), assuming a stiff soil site. Resulting design spectral values, $S_{DS}$ and $S_{D1}$, for the upper and lower bounds of each Seismic Design Category are summarized in Table 5-1. The corresponding MCE hazard spectral values are equal to 1.5 times the design spectral values in Table 5-1.

**Table 5-1 Design Spectral Values for Seismic Design Category Boundaries**

| Spectral Accelerations for Design | Seismic Design Category Boundary | | | |
|---|---|---|---|---|
| | $B_{min}$ | $B_{max}/C_{min}$ | $C_{max}/D_{min}$ | $D_{max}$ |
| $S_{DS}$ | 0.167g | 0.33g | 0.50g | 1.00g |
| $S_{D1}$ | 0.067g | 0.133g | 0.20g | 0.60g |

When gravity loads significantly influence collapse behavior, index archetype designs should be prepared for both high and low gravity load intensities reflecting differences in the self weight of alternative gravity systems (e.g., light-weight metal deck versus concrete slabs) and framing configurations (e.g., space frame versus perimeter frame configurations, and bearing versus non-bearing wall components). Design dead load and live load intensities should be established based on the range of permissible values in the archetype design space.

## 5.3 Index Archetype Models

General considerations for developing index archetype models are summarized in Table 5-2. These considerations should be used as a guide in establishing index archetype models, as follows:

- **Model Idealization:** Definition of index archetype models includes selection of the type of idealization used to represent structural behavior. At the one extreme are nonlinear continuum finite element models, which, in theory, are capable of representing the underlying structural mechanics most directly. At the other extreme are phenomenological models, which represent the overall force-deformation response through concentrated springs. A nonlinear beam-column hinge model is an example of such a phenomenological model, in which moment-rotation behavior is related to beam-column design parameters through semi-empirical models that are calibrated to beam-column tests.

  In between these two extremes are models that utilize both continuum phenomenological representations. A "fiber-type" model of a reinforced concrete shear wall is an example of such a combined model, where flexural effects are modeled with uniaxial stress-strain behavior for reinforcing steel and concrete, and where shear (or combined shear-

flexural) behavior is represented through a stress-resultant (force-based) phenomenological model. Regardless of type, models must be validated to assess how accurately they capture nonlinear response and critical limit state behavior.

**Table 5-2 General Considerations for Developing Index Archetype Models**

| Model Attributes | Considerations |
|---|---|
| Mathematical Idealization | • continuum (physics-based) versus phenomenological elements |
| Plan and Elevation Configurations | • number of moment frame bays, regularity.<br>• planar versus 3-D wall representations, openings, coupling beams, regularity.<br>• number of bracing bays, bracing configuration, regularity. |
| 2-D versus 3-D Component Behavior | • prevalence of 2-D versus 3-D systems in design practice<br>• impact on structural response, including provisions for out-of-plane failures in 2-D models |
| 2-D versus 3-D System Behavior | • characteristics of index archetype configurations<br>• impact on structural response that is specific to certain structural systems |

- **Elevation and Plan Configurations:** Representation of elevation and plan configurations in index archetype models will depend on both the index archetype configurations and the structural system behavior. While vertical and horizontal irregularities can contribute to collapse, for the purpose of evaluating general design provisions, currently permissible elevation and plan irregularities in ASCE/SEI 7-05 are not addressed in index archetype models. For moment frame systems, two-dimensional, three-bay frames of regular proportions are judged sufficient to represent typical moment frame behavior. For walls, the issue of planar versus three-dimensional response is a key consideration, as are the presence of wall openings and coupling beams. For braced frame systems, a single bay is likely to be sufficient unless the system relies on the behavior of two bents acting together. Representation of alternative brace configurations is likely to be a dominant variable in the collapse assessment of braced-frame systems.
- **Two-Dimensional versus Three-Dimensional Component Behavior:** Prevalence of applications in design practice, and expected impact on structural response, are major considerations for two-dimensional versus three-dimensional modeling. For most structural framing types, two-dimensional models are likely to be sufficient. However, there may be

cases where three-dimensional behavior (e.g., out-of-plane torsional-flexural instability of laterally unbraced beam-columns) or three-dimensional geometry (e.g., reinforced-concrete C-shaped core walls) is important to simulate. For wall systems, two-dimensional wall models may be appropriate for some system configurations (e.g., wooden shear walls, planar reinforced concrete walls) but inappropriate for others (e.g., reinforced concrete C-shaped and I-shaped core walls).

- **Two-Dimensional versus Three-Dimensional System Behavior:** System behavior involves the interaction of multiple seismic-force-resisting elements distributed spatially within a structure. Introduction of different spatial combinations, however, could lead to an intractable number of index archetype configurations and corresponding index archetype models. Building code provisions regarding plan configuration and three-dimensional effects (e.g., redundancy, accidental torsion) are usually not system specific, so in most cases, a two-dimensional system representation should be adequate.

### *5.3.1 Index Archetype Model Idealization*

Index archetype models should provide the most basic (generic) representation of an index archetype configuration that is still capable of distinguishing between significant behavioral modes and key design features of the proposed seismic-force-resisting system. Index archetype models should be developed in cooperation with the peer review panel.

The mathematical idealization of index archetype models should capture all significant nonlinear effects related to the collapse behavior of the system. This can be done through: (1) explicit simulation of failure modes through nonlinear analyses; or (2) evaluation of non-simulated failure modes using alternative limit state checks on demand quantities from nonlinear analyses.

Analysis models are generally distinguished by overall topology and element type. Topology refers to two-dimensional or three-dimensional modeling configurations. The choice of topology (2-D or 3-D) is largely a function of the index archetype configurations. The choice of element type depends on structural component behavior and the nature of component degradation. Two-dimensional topologies (e.g., planar frames or walls) do not preclude the modeling of three-dimensional effects (e.g., out-of-plane instabilities). Three-dimensional topologies (e.g., space frames or C-shaped walls) do not necessarily employ element types that capture all three-dimensional effects. For simulating collapse, component models must capture strength and stiffness degradation under large deformations.

Structural components are usually idealized as a combination of one-dimensional line-type elements (beam-columns or axial struts) and two-dimensional continuum elements (plane-stress or plate/shell finite elements). Three-dimensional continuum elements (brick finite elements) may be used in some cases. Within each element type, element formulations can be further distinguished by the extent to which the underlying structural behavior is modeled explicitly or through phenomenological representations. For example, nonlinear beam-column elements can range in sophistication from fiber-type continuum elements, in which the geometry and materials in the cross section are modeled explicitly, to concentrated spring models, in which the inelastic response is idealized through a uni-axial or multi-axial spring.

Concentrated spring models will usually be sufficient for simulating nonlinear response of columns, beams, and beam-column connections in frame systems. These models have the practical advantage of providing a straight-forward approach to characterizing strength and inelastic deformation characteristics. Wall systems will typically require two-dimensional continuum models that can capture significant nonlinear stress and strain variations within the walls. Continuum models may include traditional two-dimensional plane stress/strain finite elements, or alternative formulations that utilize combinations of formal finite element approaches and engineering assumptions to represent the nonlinear behavior.

In the case of moment frame systems, for example, an index archetype model might consist of the two-dimensional, three-bay frame shown in Figure 5-2. This model incorporates one-dimensional line-type elements and concentrated spring models to simulate the nonlinear degrading response of beams, columns, beam-column connections, and panel zones. Significant frame behaviors are captured in a two-dimensional representation, and the three-bay configuration captures differences between interior and exterior columns. Additional elements capture P-Delta effects of the seismic mass that is not tributary to the frame.

For shear wall systems, an index archetype model might be as simple as a cantilever element that accounts for inelastic flexure and shear behavior at the base of the wall. However, where punched shear wall geometries are included in the index archetype configurations, then the corresponding index archetype models will need to be more complicated.

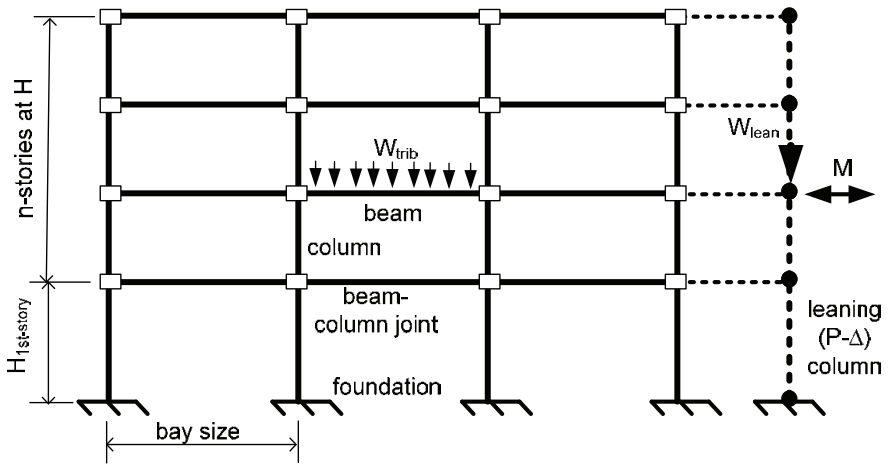


Figure 5-2 Example of Index Archetype Analysis Model for moment resisting frame systems

## 5.4 Simulated Collapse Modes

To the extent possible, index archetype models should directly simulate all significant deterioration modes that contribute to collapse behavior. Typically, this is accomplished through structural component models that simulate the stiffness, strength, and inelastic deformation under reverse cyclic loading. Research has demonstrated that the most significant factors influencing collapse response are the plastic deformation capacity, $\delta_p$, the post-capping tangent stiffness, $K_{pc}$, and the residual strength, $F_r$ (Ibarra et al. 2005). These parameters are used to define a component backbone curve, as shown in Figure 5-3. Degradation of both the backbone curve and the hysteretic response parameters also influences collapse response in nonlinear dynamic analyses. An example of degrading hysteretic response is shown in Figure 5-4. Characterization of component backbone curves and hysteretic responses should represent the mean (average) response properties of structural components.

While of lesser importance than the capping point and post-capping behavior, modeling of the initial stiffness can have a significant effect on the ductility capacity. Element-level initial stiffness should reflect all important contributors to deformation (e.g. flexure, bond-slip, and shear), and should be validated against component and assembly test data. An effective initial stiffness defined as the secant stiffness from the origin through the point of 40% of the yield strength of the element should be considered in phenomenological concentrated spring models. In continuum models, initial stiffness is usually modeled directly, though where results are sensitive to initial stiffness, attention should be given to effects related to initiation of cracking or yielding that may not be considered in the model, such as

shrinkage cracking due to concrete curing and residual stresses due to fabrication.

Figure 5-3 and Figure 5-4 are intentionally portrayed in a generic sense, since critical response parameters will vary for each specific component and configuration. For example, in ductile reinforced concrete components (i.e. special moment frames), nonlinear response is typically associated with moment-rotation in the hinge regions where the capping point and post-capping degradation occurs at large deformations through a combination of concrete crushing, confinement tie yielding/rupture, and longitudinal bar buckling. However, in less ductile reinforced concrete components (i.e., ordinary moment frames), nonlinear response may include shear failures and axial failure following shear failure. Where the seismic-force-resisting system carries significant gravity load, characteristic force and deformation quantities may need to represent vertical deformation effects as well as horizontal response effects.

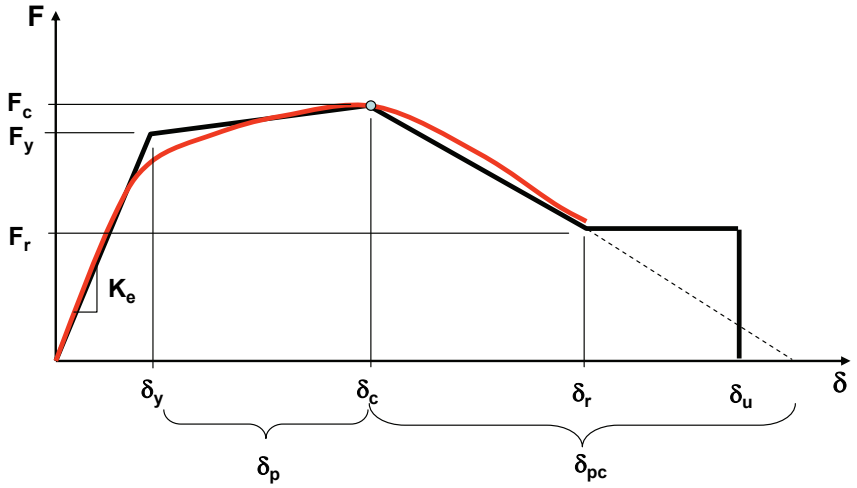


Effective yield strength and deformation ($F_y$ and $\delta_y$)
Effective elastic stiffness, $K_e = F_y/\delta_y$
Capping strength and deformation for monotonic loading ($F_c$ and $\delta_c$)
Plastic deformation capacity for monotonic loading, $\delta_p$
Effective post-yield tangent stiffness, $K_p = (F_c\text{-}F_y)/\ \delta_p$
Post-capping deformation capacity, $\delta_{pc}$
Effective post-capping tangent stiffness, $K_{pc} = F_c/\ \delta_{pc}$
Residual strength, $F_r$
Ultimate deformation capacity, $\delta_u$

Figure 5-3 Parameters of an idealized component backbone curve

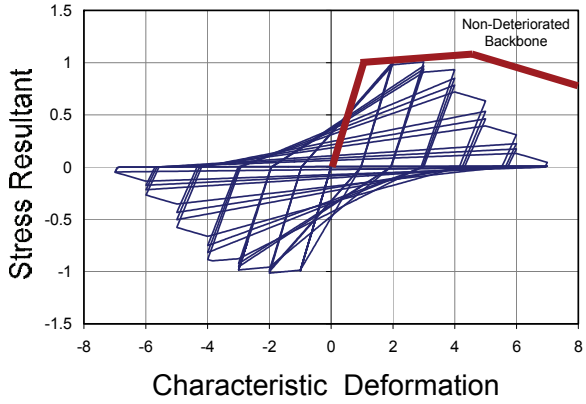


Figure 5-4 Idealized inelastic hysteretic response of structural components with cyclic strength and stiffness degradation.

The development of analytical models is case specific, and no single model is universally applicable. For many realistic steel, reinforced concrete, and wood components, the deterioration model proposed by Ibarra et al. (2005) satisfactorily matches experimental results and analytical predictions. However, this model should be utilized for a proposed system only if it can be justified based on experimental evidence.

Referring to Figure 5-3, the backbone curve provides boundaries within which hysteresis loops are confined. If these boundaries are fixed in the analytical model (i.e., cyclic deterioration is not incorporated explicitly), then estimates of the backbone curve parameters should account for average cyclic deterioration. If the initial stiffness is very different from the effective elastic stiffness, then it may affect the response close to collapse, and should become part of the modeling effort.

Figure 5-5 illustrates the effect of cyclic loading relative to a backbone curve obtained from monotonic loading. In almost all cases, the plastic deformation capacity, $\delta_p$, is reduced by cyclic loading, and in many cases it is reduced by a considerable amount from the monotonic loading case. A backbone curve is difficult to construct from a cyclic test (unless experience exists from other similar specimens) and often necessitates the execution of an additional monotonic test. If this is not done, the skeleton curve enveloping the cyclic test may be used as an estimate of the backbone curve. The implication is that in the analytical model, the load-deformation response is not permitted to move outside this curve.

If the backbone curve is obtained from a monotonic loading test (or is deduced based on a cyclic deterioration model), then cyclic deterioration must be built into the analytical model representing component behavior. Most cyclic deterioration models are energy based (e.g., Ibarra et al. 2005,

Sivaselvan and Reinhorn 2000). Validity of the component model must be demonstrated through satisfactory matching of component, connection, or assembly test date from the experimental program.

Figure 5-5 also illustrates a simplified measure of performance, which is the deformation associated with a force value of 80% of the maximum strength measured in the test, $F_c^c$ (note that $F_c^c$ is not equal to $F_c$ in Figure 5-3; the latter is a reference value without cyclic deterioration). The deformation value, $\delta_c^c$, which is obtained from the intersection of a horizontal line at $0.8F_c^c$ with the skeleton curve, can be viewed as a conservative estimate of the deformation capacity of a component. In simplified analytical models it can be assumed that no deterioration occurs up to this value of deformation, provided that the strength of the component is assumed to drop to zero at deformations larger than this value. Both, $F_c^c$ and $\delta_c^c$, may be different in the positive and negative directions.

While in concept component models are expected to be rigorously calibrated to test data, available data may not be comprehensive enough to fully calibrate the models. Data is often particularly scarce for evaluating the capping point and post-capping behavior that occurs at large deformations in ductile components. In such cases, test data should be augmented by engineering analysis and judgment to establish the modeling parameters.

An example of the development of nonlinear component models for reinforced concrete moment frame systems is provided in Appendix E.

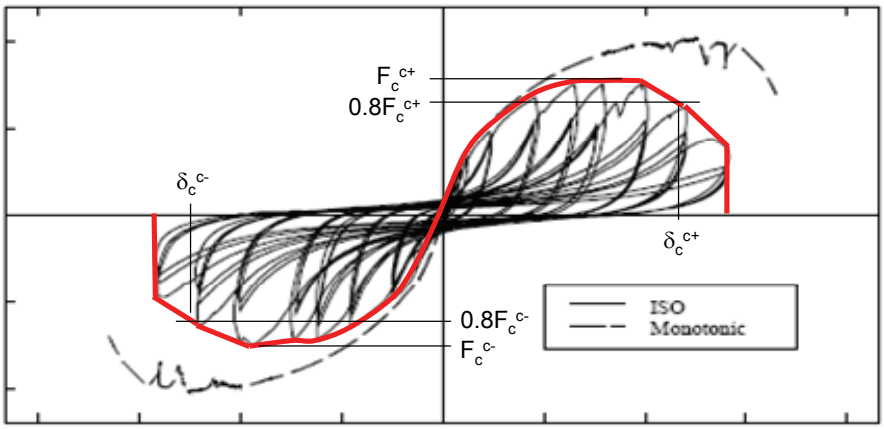


Figure 5-5 Comparison of monotonic and cyclic responses (Gatto and Uang 2002), along with skeleton curve fit to cyclic response

## 5.5 Nonlinear Model Calibration

Nonlinear models should be calibrated to represent the average (mean) properties of structural components. A beam element modeled with

concentrated hinges is shown in Figure 5-6, where inelastic moment-rotation response is described by a montonic backbone curve (Figure 5-6a) that is characterized by five parameters (initial stiffness, plastic moment, plastic rotation capacities in the pre- and post-peak regime, and residual strength). As illustrated in Figure 5-6c, the component analysis model should be capable of simulating strength and stiffness degradation under reverse cyclic loading by employing appropriate history parameters to modify the backbone curve properties and cyclic response parameters (Ibarra et al. 2002, 2005).

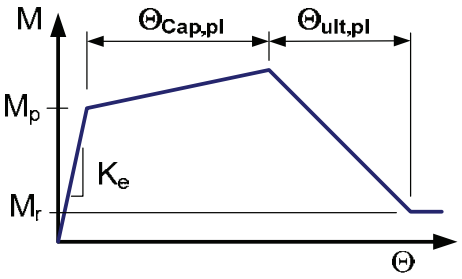


(a)

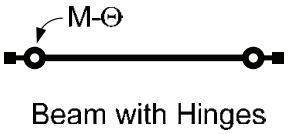


(b)

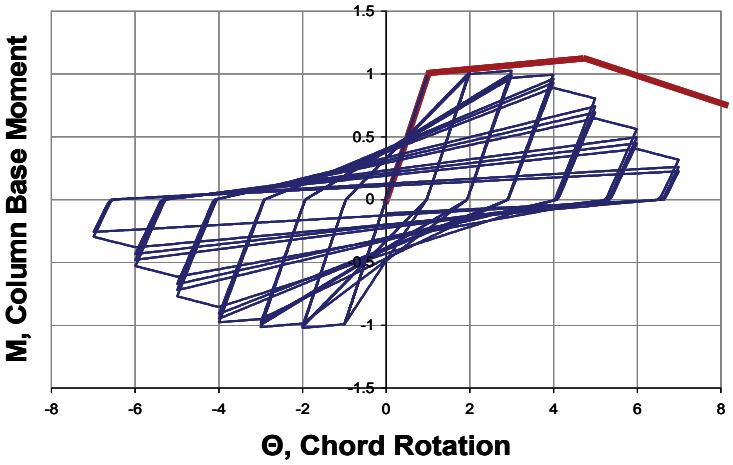


(c)

Figure 5-6 Nonlinear beam element (a) monotonic backbone hinge response curve, (b) idealized element, and (c) montonic backbone curve superimposed on cyclic hinge response

The backbone curve of Figure 5-6 is similar but distinct from the generalized load-displacement curves specified in FEMA 356 (FEMA 2000) and ASCE/SEI 41-06 (ASCE 2006b). In this Methodology, backbone curves are intended to represent mean properties of monotonic loading response where cyclic strength and stiffness degradation are directly modeled in the analysis and statistical variations of the component response are accounted for in the assessment process. This is in contrast to the approach of FEMA 356 and ASCE/SEI 41-06, which apply cyclic skeleton curves that incorporate some degree of cyclic degradation and, in many cases, are conservative estimates of mean values.

An example of the calibration of nonlinear component models for reinforced concrete moment frame systems is provided in Appendix E.

## 5.6 Non-Simulated Collapse Modes

In cases where it is not possible, or not practical to directly simulate all significant deterioration modes contributing to collapse behavior, non-simulated modes should be evaluated using alternative limit state checks on demand quantities from nonlinear analyses. Figure 5-7 shows a non-simulated collapse (NSC) limit state that occurs at a smaller deformation than the peak strength and subsequent deterioration that is directly simulated in the model. Examples of possible non-simulated collapse modes might include shear failure and subsequent axial failure in reinforced concrete column elements, and fracture in the hinge region of steel moment frame elements, both of which are difficult to simulate directly.

In many respects, non-simulated limit state checks are similar to the assessment approach of FEMA 356 and ASCE/SEI 41-06, in which component acceptance criteria are used to evaluate specific performance targets based on demand quantities extracted from analyses. This approach is more of an approximation to the actual behavior of the system, increases the uncertainty in analytical results, and tends to provide conservative estimates of collapse limit states. While not ideal, it is a practical approach that provides a consistent method for evaluating the effects of deterioration and collapse mechanisms that are otherwise difficult, or impossible, to simulate.

It should be understood that non-simulated limit state checks will generally result in a low estimate of the median collapse point, because non-simulated collapse modes are usually associated with a component failure mode. The inherent assumption is that the first occurrence of this failure mode will lead to collapse of the structure, which may not always be the case. For this reason, local failure modes should be directly simulated, if at all possible, in

order to permit redistribution of forces to other elements after a limit state is reached.

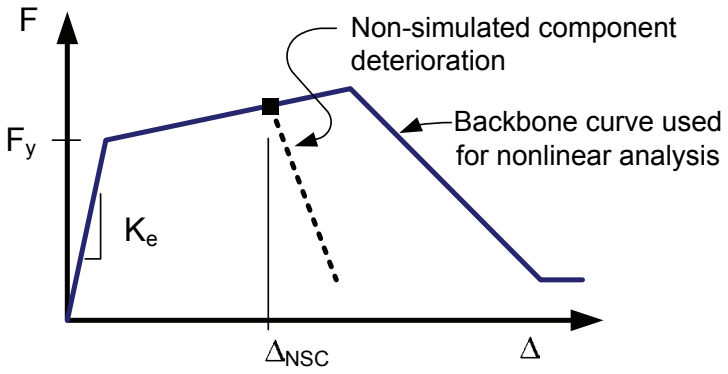


Figure 5-7 Component backbone curve showing a deterioration mode that might not be simulated in the analysis model.

When considered in the context of incremental dynamic analyses, non-simulated component limit state checks are essentially enforcing a collapse limit prior to the point where an analysis would otherwise simulate collapse. Figure 5-8 shows a plot of the results of an incremental dynamic analysis of an index archetype model, which is subjected to a single ground motion that is scaled to increasing intensities. The point denoted SC corresponds to the collapse limit as simulated in the model. The point denoted NSC represents the collapse limit as determined by applying a component limit state check on a potential collapse mode that is not directly simulated in the model. In this figure, the NSC point is represented by interstory drift, but non-simulated collapse checks could be based on any other structural response parameter, such as peak force demand in an element, or peak plastic hinge rotation demand.

Limit state checks for non-simulated collapse modes should be established based on test data and other supporting evidence, and should be calibrated to represent the mean (average) value of the governing response parameter that is associated with the collapse response. When establishing limit state checks, judgment should be exercised in relating the critical condition of a component to the collapse response of the building system, since there are many cases where critical limit states for isolated components will not immediately trigger overall system collapse. It should be understood that once a non-simulated collapse limit state has been reached, the accuracy of nonlinear analysis results is reduced, and the uncertainty is increased. Non-simulated collapse limit states should be developed in cooperation with the peer review panel.

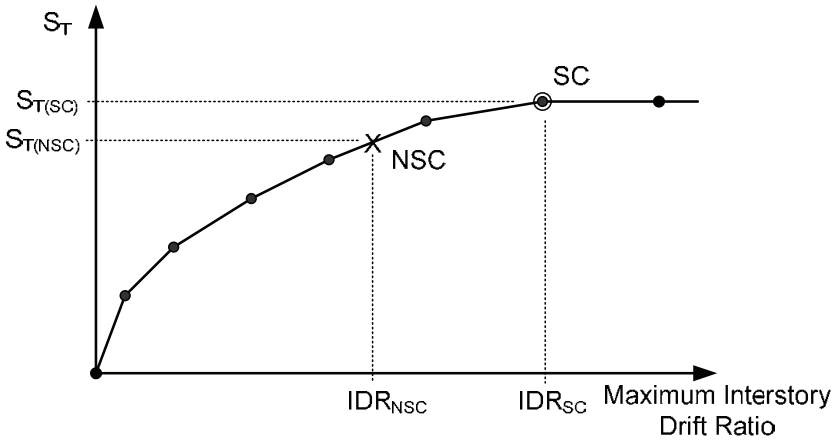


Figure 5-8 Assessment of collapse with simulated and non-simulated modes using incremental dynamic analysis.

## 5.7 Characterization of Modeling Uncertainties

Index archetype models should represent the mean (average) response of the structural components comprising a proposed system. In this Methodology, nonlinear analysis is used to determine the mean value of the median collapse intensity of the index archetype model. Variability in collapse response, due to ground motion variability, modeling, and other uncertainties, is factored into the performance evaluation process in Chapter 7. Therefore, when multiple ground motion records are considered, the median collapse point of all records provides the median collapse estimate of the median model to the entire suite of ground motions.

## 5.8 Quality Rating of Index Archetype Models

Quality of index archetype models is related to uncertainty, which factors into the performance evaluation for a proposed seismic-force-resisting system. The quality of index archetype models is rated in accordance with the requirements of this section, and approved by the peer review panel.

Analytical models are rated between (A) Superior and (D) Poor, as shown in Table 5-3. This rating depends on how well structural behavioral effects are understood, whether or not these effects can be simulated, and the degree to which these effects have been directly incorporated into index archetype models (model fidelity). The selection of a quality rating for index archetype models considers confidence in structural behavioral characteristics, and the accuracy and robustness of the models.

**Table 5-3 Quality Rating of Index Archetype Models**

| Structural Behavioral Characteristics | Accuracy and Robustness of Models | | |
|---|---|---|---|
| | High | Medium | Low |
| **High Confidence.** Response characteristics are well understood, and models for simulating nonlinear behavior are well established. | (A) Superior | (B) Good | (C) Fair |
| **Moderate Confidence.** Response characteristics and models for simulating nonlinear behavior are moderately well understood and established. | (B) Good | (C) Fair | (D) Poor |
| **Limited Confidence.** Response characteristics are sensitive to failure modes that are not well understood or quantifiable, and models for simulating nonlinear behavior are not established. | (C) Fair | (D) Poor | -- |

The highest rating of (A) Superior applies to instances in which structural behavior is well understood, there is a high confidence in the ability of established models to simulate behavior, and a high-fidelity nonlinear model is used. The lowest possible combination, limited confidence in structural behavior characteristics coupled with low-fidelity nonlinear models, is not permitted.

### *5.8.1 Structural Behavioral Characteristics*

Structural behavioral characteristics are related to the extent to which nonlinear strength and stiffness deterioration modes are understood and quantifiable. Confidence in structural behavioral characteristics is not meant to distinguish between structural components with high versus low ductility; rather, it describes how well high and low ductility behavior modes can be simulated. Confidence in structural behavior characteristics is classified as follows:

- **High Confidence.** Mechanisms of strength and stiffness degradation that affect collapse behavior are well understood and can be quantified accurately using analytical models. This implies that key parameters defining a component backbone curve (Figure 5-3) and cyclic degradation (Figure 5-4) are known. Behavioral effects that are predicted well by structural mechanics (e.g., flexural hinging) do not necessarily require extensive test data to provide high confidence in behavioral characteristics. Less predictable effects, however, such as fracture and low-cycle fatigue, will require more extensive test data. For

a high confidence rating, knowledge of structural behavior and accuracy of the models is envisioned to be on par with well-established seismic systems, where behavioral models have been vetted through extensive testing and research.

- **Moderate Confidence.** Mechanisms of strength and stiffness degradation that affect collapse behavior are not fully understood, and models for predicting behavior are approximate. It is envisioned that moderate confidence will be the level typically achieved for most systems, where behavior is fairly well understood, but test data and analytical models have not been validated over the full range of conditions that could be encountered in practical applications.
- **Limited Confidence.** Mechanisms of strength and stiffness degradation that affect collapse behavior are not well understood, and models to predict this behavior are not well developed. Degrading behavior is likely to be highly variable between different design realizations, depending on system configuration and detailing of components. It is envisioned that limited confidence is at the lower end of what would be acceptable for structural design applications.

### *5.8.2 Accuracy and Robustness of Models*

Accuracy and robustness is related to the degree to which nonlinear behaviors are directly simulated in the model. Use of non-simulated collapse limit state checks will lower the accuracy and robustness of a nonlinear model. Accuracy and robustness are characterized as follows:

- **High.** Nonlinear models directly simulate all predominate inelastic effects, from the onset of yielding through strength and stiffness degradation causing collapse. Models employ either concentrated hinges or distributed finite elements to provide spatial resolution appropriate for the proposed system. Computational solution algorithms are sufficiently robust to accurately track inelastic force redistribution, including cyclic loading and unloading, without convergence problems, up to the point of collapse.
- **Medium.** Nonlinear models capture most, but not all, nonlinear deterioration and response mechanisms leading to collapse. Models may not be sufficiently robust to track the full extent of deterioration, so that some component-based limit state checks are necessary to assess collapse.
- **Low.** Nonlinear models capture the onset of yielding and subsequent strain hardening, but do not simulate degrading response. Onset of

degradation is primarily evaluated using non-simulated component limit state checks. Overall uncertainty in response quantities is increased due to inability to capture the effects of deterioration and redistribution.

# Chapter 6
# Nonlinear Analysis

This chapter describes nonlinear analysis procedures for collapse assessment of a proposed seismic-force-resisting system. It defines the set of input ground motions, and specifies how nonlinear static analyses and nonlinear dynamic analyses are conducted on index archetype models developed in Chapter 5. It identifies median response data from nonlinear analysis results that are needed for performance evaluation in Chapter 7.

## 6.1 Nonlinear Analysis Procedures

Nonlinear analysis for collapse assessment follows the process outlined in Figure 6-1.

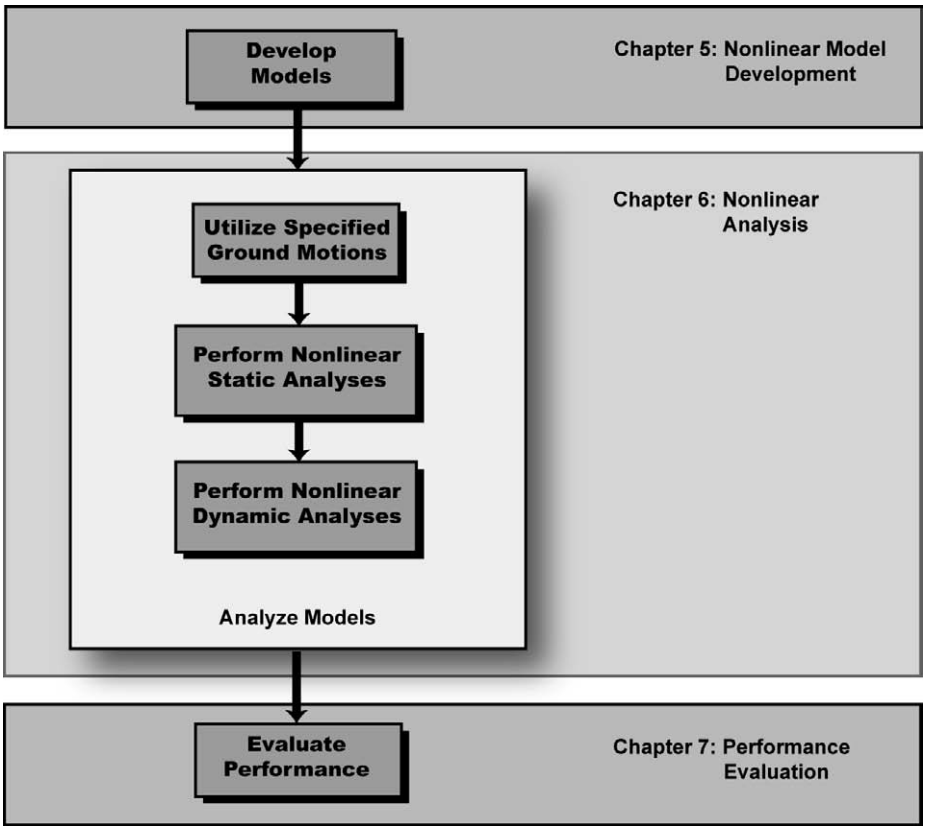


Figure 6-1 Process for developing the nonlinear analysis procedures for collapse assessment

Nonlinear static (pushover) and dynamic (response history) analyses of all index archetype models are performed to obtain statistics for system overstrength, ductility, and collapse capacity. Nonlinear static analyses are

performed first, to help validate the model and to provide statistical data on system overstrength, $\Omega$, and ductility capacity, $\mu_c$. Nonlinear dynamic analyses are then performed using the Far-Field ground motion set to assess median collapse capacities, $\hat{S}_{CT}$, and collapse margin ratios, *CMR*. The median collapse capacity is defined as the ground motion intensity, where half of the ground motions in the Far-Field record set cause collapse of an index archetype model.

In all cases, modeling parameters, including the seismic mass and imposed gravity loads, should represent the mean (average or expected) values of the structure and its components. Expected gravity loads for analysis are different from design gravity loads, and are given by the following load combination:

$$1.05D + 0.25L \tag{6-1}$$

where $D$ is the nominal dead load of the structure and the superimposed dead load, and $L$ is the nominal live load. Load factors in Equation 6-1 are based on expected (mean) values reported in a study on the development of a predecessor document to ASCE 7 (Ellingwood et al. 1980). The live load can be reduced by reduction factors based on influence area, but should not be reduced by additional reduction factors.

Simulations should account for all seismic mass and P-Delta effects associated with gravity loads that are stabilized by the seismic-force-resisting system. This includes gravity loads that are tributary to the index archetype model, as well as gravity loads that rely on the index archetype model for lateral stability.

### *6.1.1 Nonlinear Analysis Software*

Software for nonlinear analysis can be of any type that is: (a) capable of static and dynamic (response history) analyses; and (b) capable of capturing strength and stiffness degradation in structural components at large deformations. A significant computational challenge is to accurately capture the negative post-peak response, sometimes referred to as strain-softening response, in component backbone curves. Strain-softening response leads to the need for robust iterative solution strategies to minimize errors and achieve convergence at large inelastic deformations. Problems with strain-softening response have the potential for non-unique solutions and damage localization that is sensitive to numerical issues. While most modern analysis software can overcome these issues, care must be taken to investigate the sensitivity of the solution to modeling parameters and numerical aspects of the computational solution algorithms.

## 6.2 Input Ground Motions

Nonlinear response is evaluated for a set of pre-defined ground motions that are systematically scaled to increasing intensities until median collapse is established.

### *6.2.1 Ground Motion Hazard*

Collapse safety is evaluated relative to ground motion intensity associated with Maximum Considered Earthquake (MCE), as defined in ASCE/SEI 7-05 (ASCE 2006a), and used as a basis for design. The MCE ground motion intensity is typically defined as rare ground motions (recurrence periods on the order of 1000 to 2500 years) that incorporate adjustment factors to account for local site conditions ($F_a$ and $F_v$) and near field effects. As in ASCE/SEI 7-05, ground motion intensity is defined in terms of spectral acceleration.

For collapse assessment, ground motion levels correspond to maximum and minimum seismic criteria of the Seismic Design Category (SDC) for which a system is qualified. Figure 6-2 shows maximum and minimum MCE ground motion spectral intensities for Seismic Design Categories B, C and D. In all cases, site conditions are based on Site Class D (stiff soil). Table 6-1A and Table 6-1B provide specific values of short-period and 1-second spectral accelerations, respectively, for these categories.

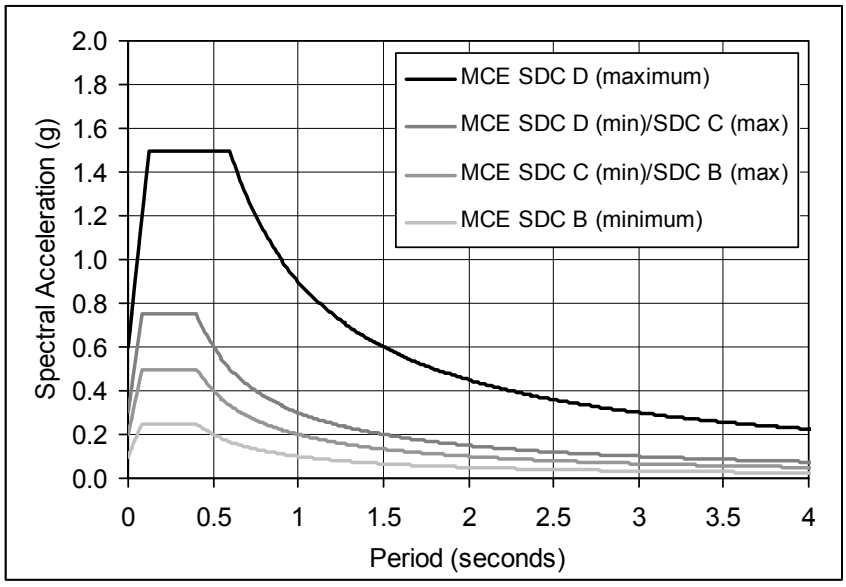


Figure 6-2 MCE response spectra for collapse evaluation of structure archetypes for Seismic Design Categories B through D.

**Table 6-1A Summary of Short-Period Spectral Acceleration, Site Coefficients and Design Parameters Used for Collapse Evaluation of Seismic Design Category D, C and B Structure Archetypes, Respectively**

| Seismic Design Category | | Maximum Considered Earthquake | | | Design |
|---|---|---|---|---|---|
| Maximum | Minimum | $S_S$ (g) | $F_a$ | $S_{MS}$ (g) | $S_{DS}$ (g) |
| D | | 1.5 | 1.0 | 1.5 | 1.0 |
| C | D | 0.55 | 1.36 | 0.75 | 0.50 |
| B | C | 0.33 | 1.53 | 0.50 | 0.33 |
| | B | 0.156 | 1.6 | 0.25 | 0.167 |

**Table 6-1B Summary of 1-Second Spectral Acceleration, Site Coefficients and Design Parameters Used for Collapse Evaluation of Seismic Design Category D, C and B Structure Archetypes, Respectively**

| Seismic Design Category | | Maximum Considered Earthquake | | | Design |
|---|---|---|---|---|---|
| Maximum | Minimum | $S_1$ (g) | $F_v$ | $S_{M1}$ (g) | $S_{D1}$ (g) |
| D | | 0.60 | 1.50 | 0.90 | 0.60 |
| C | D | 0.132 | 2.28 | 0.30 | 0.20 |
| B | C | 0.083 | 2.4 | 0.20 | 0.133 |
| | B | 0.042 | 2.4 | 0.10 | 0.067 |

### *6.2.2 Ground Motion Record Sets*

Two sets of ground motion records are provided for collapse assessment using nonlinear dynamic analysis. One set includes twenty-two ground motion record pairs from sites located greater than or equal to 10 km from fault rupture, referred to as the "Far-Field" record set. The other set includes twenty-eight pairs of ground motions recorded at sites less than 10 km from fault rupture, referred to as the "Near-Field" record set. While both Far-Field and Near-Field record sets are provided, only the Far-Field record set is required for collapse assessment. This is done for reasons of practicality, and in recognition of the fact that there are many unresolved issues concerning the characterization of near-fault hazard and ground motion effects. The Near-Field record set is provided as supplemental information to examine issues that arise due to near-fault directivity effects, if needed.

The ground motion record sets include records from all large-magnitude events in the PEER NGA database (PEER, 2006). Records were selected to meet a number of sometimes conflicting objectives. To avoid event bias, no more than two of the strongest records are taken from each earthquake, yet the record sets have a sufficient number of motions to permit statistical

evaluation of record-to-record (RTR) variability and collapse fragility. Strong ground motions were not distinguished based on either site condition or source mechanism.

Due to inherent limitations in available data, no single set of records can fully meet all desired objectives. Large magnitude events are rare, and few existing earthquake ground motion records are strong enough to collapse large fractions of modern, code-compliant buildings. In the United States, strong-motion records date back to the 1933 Long Beach Earthquake, with only a few records obtained from each event until the 1971 San Fernando Earthquake.

Even with many instruments, existing strong motion instrumentation networks (e.g., Taiwan and California) provide coverage for only a small fraction of all regions of high seismicity. Considering the size of the earth and period of geologic time, the available sample of strong motion records from large-magnitude earthquakes is still quite limited, and potentially biased by records from more recent, relatively well-recorded events. Due to the limited number of very large earthquakes, and the frequency ranges of ground motion recording devices, the ground record sets are primarily intended for buildings with natural (first-mode) periods less than or equal to 4 seconds. Thus, the record set is not necessarily appropriate for tall buildings with long periods.

The record sets, and background information on their selection, are included in Appendix A.

### *6.2.3 Ground Motion Record Scaling*

Ground motions are scaled to represent a range of earthquake intensities up to collapse level ground motions. Record scaling involves two steps. First, individual records in each set are "normalized" by their respective peak ground velocities, as described in Appendix A. This step is intended to remove unwarranted variability between records due to inherent differences in event magnitude, distance to source, source type and site conditions, without eliminating record-to-record variability. Second, normalized ground motions are collectively scaled (or "anchored") to a specific ground motion intensity such that the median spectral acceleration of the record set matches spectral acceleration at the fundamental period of the structure being analyzed.

The first step was performed as part of the ground motion selection process, so the record sets contained in Appendix A already reflect this normalization. The second step is performed as part of the analysis procedure. This two-

step scaling process parallels the ground motion scaling requirements of Section 16.1.3.2 of ASCE/SEI 7-05. Plots of response spectra for the Far-Field record set, and an illustration of intensity anchoring to maximum and minimum MCE design spectra, are shown in Figure 6-3.

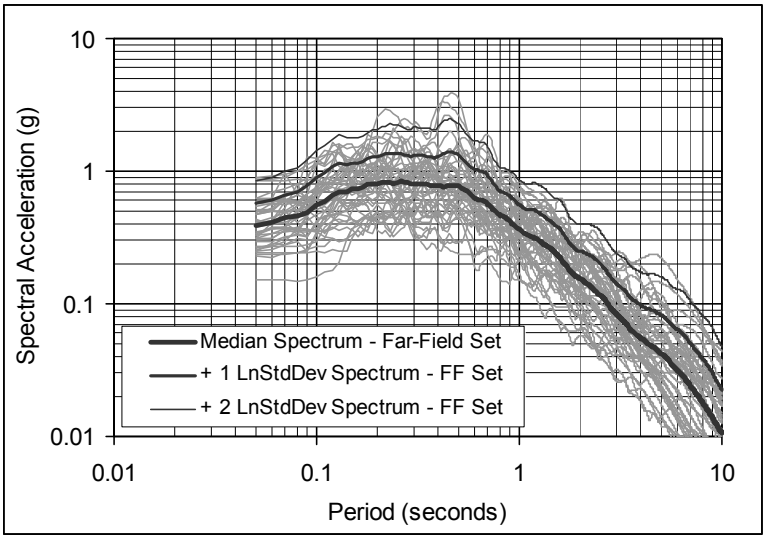


(a)

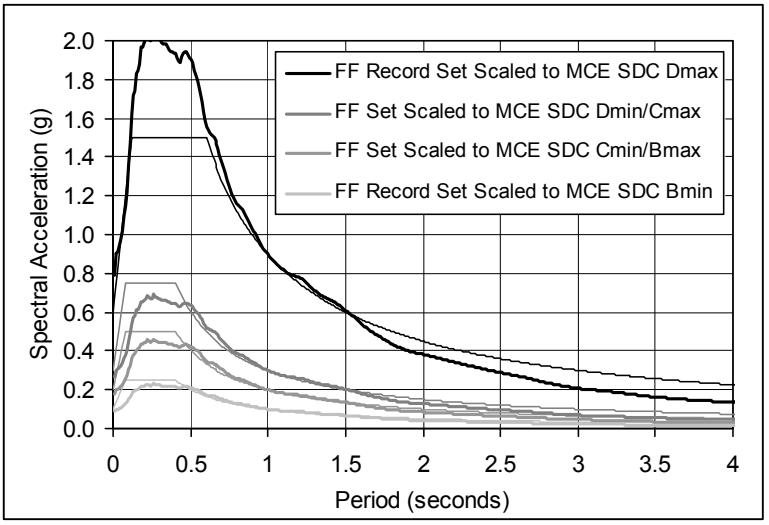


(b)

Figure 6-3 Far-Field record set (a) response spectra plots, (b) illustration of spectral intensity anchoring to maximum and minimum MCE design spectra of Seismic Design Categories B, C and D.

## 6.3 Nonlinear Static (Pushover) Analyses

Nonlinear static (pushover) analyses are conducted under the factored gravity load combination of Equation 6-1 and static lateral earthquake forces. The

distribution of the earthquake forces should be as specified for the equivalent lateral force procedure of ASCE/SEI 7-05:

$$F_x = C_{vx} V \tag{6-2a}$$

and

$$C_{vx} = \frac{w_x h_x^k}{\sum_{i=1}^{n} w_i h_i^k} \tag{6-2b}$$

where $F_x$ is the lateral force applied at each story, $C_{vx}$ is the distribution factor, $V$ is the total applied shear force, $w_i$ and $w_x$ are the portion of the gravity (seismic mass) applied to level $i$ or $x$, $h_i$ and $h_x$ is the height from the base to level $i$ or $x$, and $k$ is an exponent ($k$=1 for structures whose fundamental period is 0.5 seconds or less, $k$=2.5 for structures having a period of 2.5 seconds or more, and $k$ is linearly interpolated for structures with periods between 0.5 to 2.5 seconds).

Figure 6-4 shows a nonlinear static pushover curve and definitions of the maximum base shear capacity ($V_{max}$), effective yield displacement ($\Delta_y$), and the ultimate displacement ($\Delta_{ult}$). $V_{max}$ is taken as the maximum base shear strength at any point on the pushover curve. Similar to the procedure in ASCE/SEI 41-06 (ASCE 2006b), $\Delta_y$ is the displacement where a line through the origin and a point at 60% base shear strength ($0.6V_{max}$) reaches $V_{max}$. $\Delta_{ult}$ is taken as the roof displacement at the point of 20% strength loss ($0.8V_{max}$).

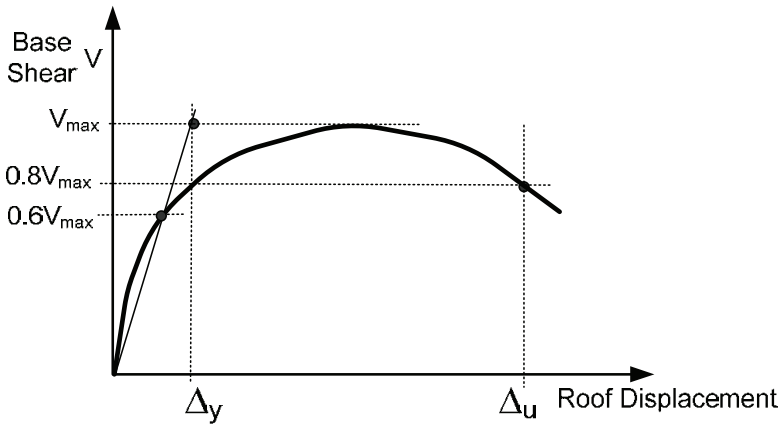


Figure 6-4 Idealized nonlinear static pushover curve

The purpose of static pushover analyses is to quantify $V_{max}$, $\Delta_y$, and $\Delta_{ult}$, and then use them to compute the system overstrength factor and the system ductility capacity. In order to quantify these values, the lateral loads are

monotonically increased until a loss of 20% of the base shear capacity ($0.8V_{max}$) occurs.

The structural system collapse ductility, $\mu_C$, is defined as the ratio of $\Delta_u$ and $\Delta_y$:

$$\mu_C = \frac{\Delta_{ult}}{\Delta_y} \tag{6-3}$$

The system overstrength factor, $\Omega$, is defined as the ratio of the maximum base shear resistance, $V_{max}$, to the design base shear, $V$:

$$\Omega = \frac{V_{\max}}{V} \tag{6-4}$$

Since pushover analyses are intended to verify the models and provide a conservative bound on the system overstrength factor, checks for non-simulated collapse modes are not incorporated directly. Non-simulated collapse modes should be considered when evaluating the ductility displacement capacity, $\Delta_u$.

Ductility capacity is sensitive to evaluation of yield and ultimate displacements, each of which is sensitive to nonlinear modeling assumptions. The yield displacement, $\Delta_y$, can vary significantly depending on the initial stiffness of the model. The ultimate displacement, $\Delta_{ult}$, is sensitive to the degradation and post-peak negative stiffness. To some extent, the sensitivity is minimized by basing these measures on roof drift, rather than peak interstory drift, but the reasonableness of these properties should be checked.

Where three-dimensional analyses are used, separate nonlinear static analyses should be performed to evaluate overstrength and ductility capacity independently along the two principle axes of the index archetype model. The resulting values for overstrength and ductility capacity are calculated by averaging the values from each of the principle loading directions.

## 6.4 Nonlinear Dynamic (Response History) Analyses

Nonlinear dynamic (response history) analyses are conducted under the factored gravity load combination of Equation 6-1 and input ground motions from the Far-Field record set in Appendix A. The objective of the analyses is to establish the median collapse capacity, $\hat{S}_{CT}$, and collapse margin ratio (*CMR*) for each of the index archetype models. Determination of the collapse margin ratio for each index archetype model is expected to require approximately 200 nonlinear response history analyses (approximately 5

analyses of varying intensity for each component of the 22 pairs of earthquake ground motion records).

Ground motion intensity, $S_T$, is defined based on the median spectral intensity of the Far-Field record set, measured at the fundamental period of the structure. The procedure for conducting nonlinear response history analyses is based on the concept of incremental dynamic analysis (IDA) (Vamvatsikos and Cornell 2002), in which each ground motion is scaled to increasing intensities until the structure reaches a collapse point. This concept is illustrated in Figure 6-5. Each point in this figure corresponds to the results of a single response history analysis of one index archetype model subjected to one ground motion record scaled to one intensity level. The lines correspond to plots for different ground motion records, each scaled to the full range of intensity values.

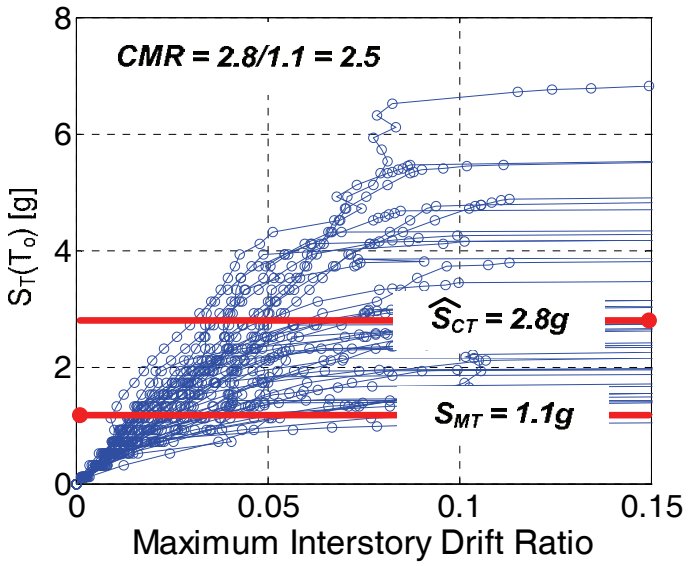


Figure 6-5 Incremental dynamic analysis response plot of spectral acceleration versus maximum interstory drift

Collapse is judged to occur either directly from dynamic analysis results (as evidenced by dynamic instability or excessive lateral displacements) or indirectly through non-simulated component limit state criteria. Using collapse data obtained from nonlinear dynamic analyses, a collapse fragility can be defined through a cumulative distribution function (CDF), which relates the ground motion intensity to the probability of collapse (Ibarra et al. 2002). Figure 6-6 shows an example of a cumulative distribution plot obtained by fitting a lognormal distribution to the collapse data from Figure 6-5.

The lognormal distribution is defined by two parameters, which are the median collapse intensity, $\hat{S}_{CT}$, and the standard deviation of the natural logarithm, $\beta$. The median collapse capacity ( $\hat{S}_{CT}$ = 2.8g in the figure) corresponds to a 50% probability of collapse. The slope of the lognormal distribution is measured by $\beta$, and reflects the variability (uncertainty) in results.

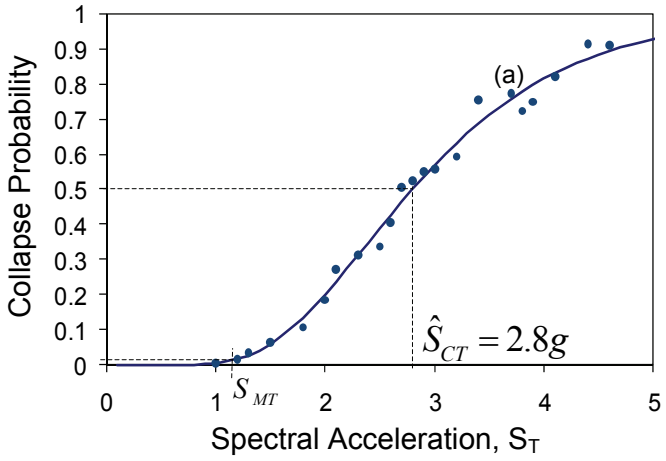


Figure 6-6 Collapse fragility curve, or cumulative distribution function.

While the IDA concept is useful to illustrate the collapse assessment procedure, the Methodology only requires identification of the median collapse point, $\hat{S}_{CT}$, which can be calculated with fewer nonlinear analyses than would otherwise be required to calculate the full IDA curve. Referring to Figure 6-5, $\hat{S}_{CT}$ can be obtained by scaling all the records in the Far-Field record set to the MCE intensity, $S_{MT}$, and then by increasing intensity until one-half of the scaled ground motion records cause collapse. The lowest intensity at which one-half of the records cause collapse is the median collapse intensity, $\hat{S}_{CT}$. Judicious selection of earthquake intensities close to and approaching the median collapse point leads to a significant reduction in the number of required analyses. As a result, nonlinear response history analyses are computationally much less involved than the IDA approach. While the full IDA curve is not required, a sufficient number of response points should be plotted at increasing intensity to help ensure accuracy in calculating the median collapse intensity.

The MCE intensity is obtained from the response spectrum of MCE ground motions at the fundamental period, $T$. In Figure 6-5, the MCE intensity, $S_{MT}$, is 1.1g, taken directly from the response spectrum for SDC D (maximum) in Figure 6-3(b). The ratio between the median collapse intensity and the MCE intensity is the collapse margin ratio (*CMR*), which is the primary parameter used to characterize the collapse safety of the structure.

$$CMR = \frac{\hat{S}_{CT}}{S_{MT}} \tag{6-5}$$

### 6.4.1 Record Scaling

The process of scaling ground motion records is similar, but distinct, from the IDA approach, as developed by Vamvatsikos and Cornell. Both methods involve scaling of records by spectral intensity, but in this Methodology motions are scaled based on the median intensity of the record set, rather than the intensity of each individual record. Conceptually, this envisions Far-Field record set as representative of a suite of records from a major earthquake, in which individual records will have some dispersion about an expected value. Scaling all of the records using a single factor based on the intensity of the median of the record set, means that the actual spectral acceleration for each record will have some dispersion around the median value of the entire set.

The spectral scaling intensity for the ground motion records is determined based on the median spectral acceleration of the Far-Field record set at the fundamental period of the building. For purposes of scaling the spectra and calculating the corresponding MCE hazard spectra, the fundamental period shall be taken as the upper bound value calculated using the simplified formulas and limits in Section 12.8.1 of ASCE/SEI 7-05. The spectral acceleration of the record set at the specified period is $S_T$, and the intensity at the collapse point for each record is $S_{CT}$ (i.e., $S_T$ of the average spectra corresponding to the point when the specified record triggers collapse). The median collapse point for the entire record set (the median of 44 records) is $\hat{S}_{CT}$. The spectral acceleration of the MCE hazard, $S_{MT}$, is calculated as defined in Section 11.4.3 of ASCE/SEI 7-05 for Site Class D.

### 6.4.2 Specified Damping for Nonlinear Dynamic Analyses

In nonlinear dynamic analyses, most structural damping is modeled directly through hysteretic response of the structural components. Added viscous damping is less than would typically be used for linear dynamic analyses. Depending on the type and characteristics of the nonlinear model, additional viscous damping may be used to simulate the portion of energy dissipation that is not otherwise incorporated in the model. When used, viscous damping should be consistent with the inherent damping in the structure that is not already captured by the nonlinear hysteretic response that is directly simulated in the model. For nonlinear dynamic analyses, equivalent viscous damping is typically assumed to be in the range of 2% to 5% of critical damping for the first few vibration modes that tend to dominate the response.

### 6.4.3 Two-Dimensional versus Three-Dimensional Nonlinear Dynamic Analyses

For two-dimensional analyses, all forty-four ground motion records (twenty-two pairs) are applied as independent events to calculate the median collapse intensity, $\hat{S}_{CT}$, for each index archetype model. For three-dimensional analyses, the twenty-two record pairs are applied twice to each model, once with the ground motion records oriented along one principal direction, and then again with the records rotated 90 degrees.

### 6.4.4 Adjustment of Collapse Margin Ratio for Three-Dimensional Nonlinear Dynamic Analyses

Because ground motions records are applied in pairs in three-dimensional nonlinear dynamic analyses, collapse behavior of each index archetype model resulting from each ground motion component is coupled. Notwithstanding other variations between the two-dimensional and three-dimensional analyses, the median collapse point resulting from three-dimensional analyses is on average about 20% less than the median resulting from two-dimensional analyses. The application of pairs of ground motion records in three-dimensional analyses introduces a conservative bias that is not present in two-dimensional analyses.

To achieve parity between two-dimensional and three-dimensional analyses, an adjustment should be made when calculating the collapse margin ratio. The *CMR* calculated using median collapse intensity, $\hat{S}_{CT}$, from three-dimensional analyses should be multiplied by a factor of 1.2. This multiplier is applied in addition to the spectral shape factor (*SSF*) that is used to calculate the adjusted collapse margin ratio, *ACMR*, as part of the performance evaluation process in Chapter 7.

### 6.4.5 Summary of Procedure for Nonlinear Dynamic Analysis

Nonlinear dynamic analysis of each index archetype model includes the following steps:

1. Using the normalized Far-Field earthquake record set in Appendix A, scale all records to an initial scale factor. A suggested initial scale factor is $S_T = 1.3S_{MT,}$, which can be adjusted up or down based on the results of initial analyses.
2. Perform nonlinear response history analyses on each index archetype model using all twenty-two pairs of records in the Far-Field record set. For two-dimensional analyses, models should be analyzed separately for each ground motion component in each pair, for a total of forty-four analyses. For three-dimensional analyses, the twenty-two record pairs

should be applied twice to each model, once with the ground motion records oriented along one principal direction, and then again with the records rotated 90 degrees. Process results to check for simulated collapse (dynamic instability or excessive lateral deformations signaling a sidesway collapse mechanism) or non-simulated collapse (demands that exceed certain component limit state criteria applied external to the analysis).

3. Based on results from the first set of analyses, adjust the ground motion scale factor, and perform additional analyses until collapse is detected for one-half of the response history analyses. Rank the results for the set of forty-four ground motion records in order from least to greatest. The median collapse intensity, $\hat{S}_{CT}$, corresponds to the average of the collapse intensities observed for the 22nd and 23rd records in the ranked set of results.

Other strategies can be used for systematically scaling the records to determine the median collapse capacity. The most straightforward approach, though not necessarily the most efficient, is to systematically scale up the entire record set, in specified increments, until collapse is detected for twenty-three of the records (or record pairs).

## 6.5 Documentation of Analysis Results

Nonlinear analysis results serve as the basis for performance evaluation in Chapter 7, and are subject to review by the peer review panel. As a minimum, information on model development, and data from nonlinear static and dynamic analyses, should be documented in accordance with this section.

### *6.5.1 Documentation of Nonlinear Models*

The following information should be reported on the development of the nonlinear index archetype models:

- Description of analysis model.
- Figure of idealized model showing support and loading conditions and member types.
- Summary of modeling parameters including: material strengths and stress-strain properties, component and connection strengths and deformation capacities, gravity loads and masses, and damping parameters.
- General documentation of analysis software.

### 6.5.2 Data from Nonlinear Static Analyses

The following information should be reported from nonlinear static (pushover) analyses of each index archetype model:

- Fundamental period of vibration, $T$, and design base shear, $V$.
- Distribution of lateral (pushover) loads.
- Plot of base shear versus roof drift.
- Fully yielded strength, $V_{max}$, and static overstrength factor $\Omega = V_{max}/V$.
- The yield and ultimate roof displacements, $\Delta_y$ and $\Delta_{ult}$, and the ductility capacity $\mu_c = \Delta_{ult} / \Delta_{y.}$
- Interstory drift ratios at the design base shear, the maximum load $V_{max}$, and $0.8V_{max}$ (used to gage system behavior).

### 6.5.3 Data from Nonlinear Dynamic Analyses

The following information should be reported from nonlinear dynamic (response history) analyses of each index archetype model:

- MCE ground motion intensity (MCE spectral acceleration), $S_{MT}$, and the period used to calculate this value.
- Median collapse intensity, $\hat{S}_{CT}$, and collapse margin ratio, $CMR$.
- Table of collapse intensity values $S_{CT}$ for each record (or record pair) used to compute the median collapse capacity, along with the response parameter used to identify the collapse condition (e.g., maximum interstory drift ratio for simulated collapse, and limit-state criteria for non-simulated collapse). Accompanying notes, plots, or narratives describing the governing mode(s) of failure.
- Representative plots of hysteresis curves for selected structural components up to the collapse point.

# Chapter 7
# Performance Evaluation

This chapter describes the process of evaluating the performance of a proposed seismic-force-resisting system, assessing the acceptability of a trial value of the response modification coefficient, $R$, determining an appropriate value of the system overstrength factor, $\Omega_O$, and determining an appropriate value of the deflection amplification factor, $C_d$.

Performance evaluation is based on the results of nonlinear analyses conducted in accordance with Chapter 6. It requires judgment in interpreting analytical results, assessing uncertainty, and rounding of values for design. Performance evaluation and selection of appropriate seismic performance factors requires the concurrence of the peer review panel.

## 7.1 Overview of the Performance Evaluation Process

The performance evaluation process utilizes results from nonlinear static (pushover) analyses to determine an appropriate value of the system overstrength factor, $\Omega_O$, and results from nonlinear dynamic (response history) analyses to evaluate the acceptability of a trial value of the response modification coefficient, $R$. The deflection amplification factor, $C_d$, is derived from an acceptable value of $R$, with consideration of the effective damping of the system of interest.

The trial value of the response modification coefficient, $R$, used to design index archetypes, is evaluated in terms of the acceptability of the collapse margin ratio. Acceptability is measured by comparing the collapse margin ratio, after adjustment for the effects of spectral shape, to acceptable values that depend on the quality of information used to define the system, total system uncertainty, and established limits on collapse probability.

Performance evaluation follows the process outlined in Figure 7-1, and includes the following steps:

- Calculate the system overstrength, $\Omega$, and ductility capacity, $\mu_c$, collapse margin ratio, *CMR*, for each index archetype, in accordance with Chapter 6.
- Calculate the adjusted collapse margin ratio, *ACMR*, using the spectral shape factor, *SSF*, which depends on fundamental period, $T$, and ductility capacity, $\mu_c$ (Section 7.2).

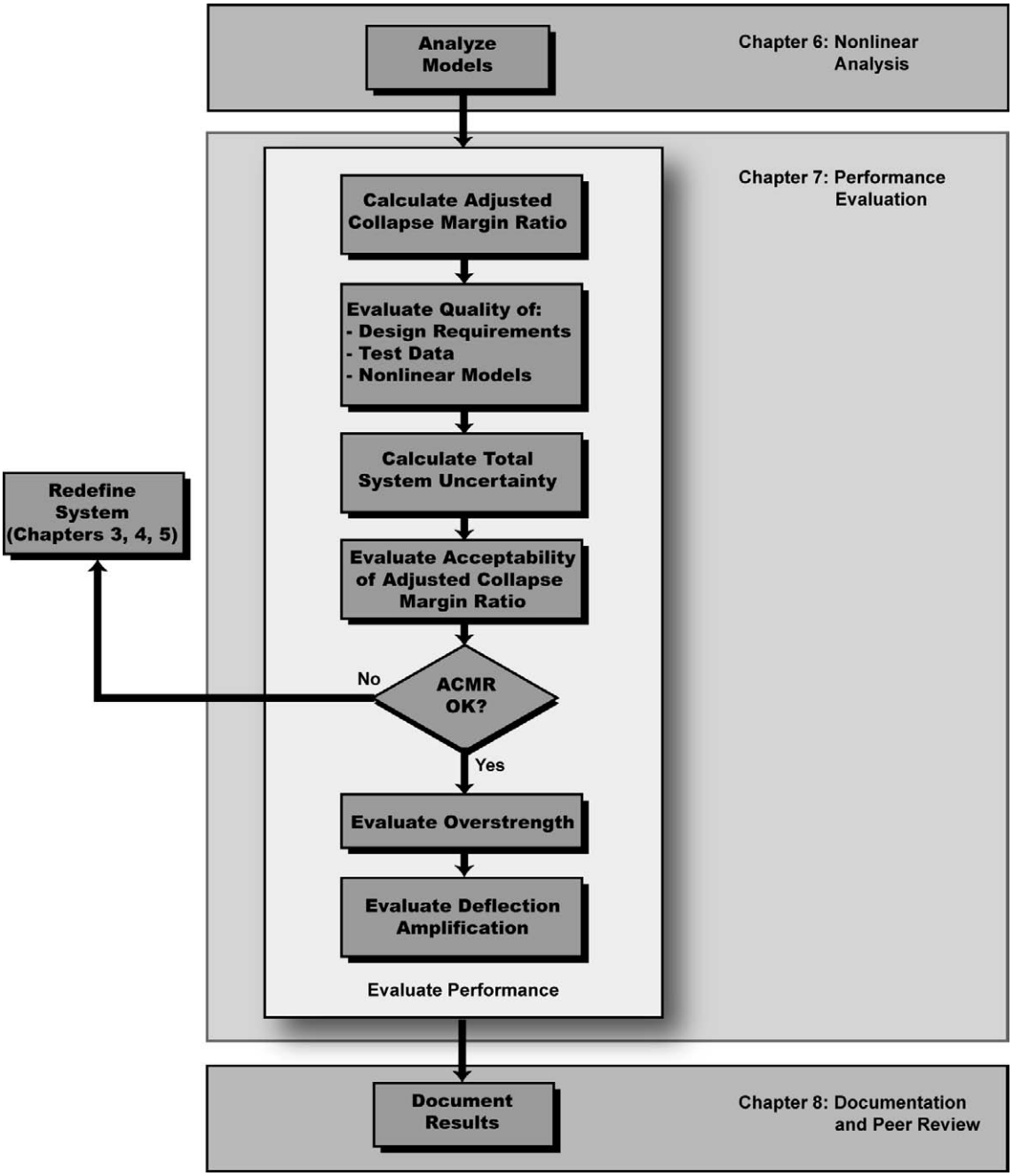


Figure 7-1 Process for Performance Evaluation

- Evaluate the quality of design requirements, test data, and nonlinear models, in accordance with Chapter 3 and Chapter 6, and calculate the total system collapse uncertainty, $\beta_{TOT}$ (Section 7.3).
- Evaluate adjusted collapse margin ratios, *ACMR*, relative to acceptable values of collapse margin ratio, which depend on total system collapse uncertainty, $\beta_{TOT}$, and acceptable probabilities of collapse (Section 7.4, Section 7.5).

- Repeat for each index archetype in each performance group.
- Evaluate the overstrength factor, $\Omega_O$, (Section 7.6).
- Evaluate the displacement amplification factor, $C_d$, (Section 7.7).
- If trial values of $R$, $\Omega_O$, $C_d$ are not acceptable, redefine the system by adjusting the design requirements (Chapter 3), re-characterizing behavior (Chapter 4), or redesigning with new trial values (Chapter 5).

In general, it is expected that more than one iteration will be required to determine the optimal values of the seismic performance factors for the system of interest.

### *7.1.1 Performance Groups*

In general, trial values of seismic performance factors are evaluated for each performance group. Results within each performance group are averaged to determine the value for the group, which is the primary basis for judging acceptability of each trial value. The trial value of the response modification factor, $R$, must be found acceptable for all performance groups. The system overstrength factor, $\Omega_O$, is based on the most critical calculated value of overstrength, $\Omega$, for all performance groups. The deflection amplification factor, $C_d$, is derived from an acceptable value of $R$.

The governing performance group for the response modification factor, $R$, is the one with the smallest value of $R$. The governing performance group for the overstrength factor, $\Omega_O$, is the one with the largest value of $\Omega$. It is possible that the response modification factor, $R$, and the system overstrength factor, $\Omega_O$, will be governed by different performance groups.

Results are also evaluated to identify potential outliers within each performance group (i.e., individual index archetypes that perform significantly worse than the average performance of the group). Outliers can be accommodated by adopting more conservative values of seismic performance factors, or they can be eliminated from the archetype design space by revising the design requirements (e.g., implementation of height limits or other restrictions on use). Revision of seismic performance factors or design requirements will necessitate re-design and re-analysis of index archetypes, and re-evaluation of system performance.

It is not required that all index archetype configurations be used for evaluation, if it can be shown by selective analysis that certain design combinations (configurations) are not critical. Caution should be used in removing non-critical index archetype configurations from a governing

performance group since their removal could adversely affect the average value of the group used for evaluation.

### 7.1.2 Acceptable Probability of Collapse

The fundamental premise of the performance evaluation process is that an acceptably low, yet reasonable probability of collapse can be established as a criterion for assessing the collapse performance of a proposed system.

In this Methodology, the probability of collapse due to MCE ground motions is limited to 10%. Each performance group is required to meet this collapse probability limit, on average, recognizing that some individual archetypes could have collapse probabilities that exceed this value. A limit of twice that value, or 20%, is used as a criterion for evaluating the acceptability of potential "outliers" within a performance group.

It should be noted that these limits were selected based on judgment. Within the performance evaluation process, these values can be adjusted to reflect different values of acceptable probabilities of collapse that are deemed appropriate by governing jurisdictions, or other authorities employing this Methodology to establish seismic design requirements for a proposed system.

## 7.2 Adjusted Collapse Margin Ratio

Collapse capacity, and the calculation of collapse margin ratio can be significantly influenced by the frequency content (spectral shape) of the ground motion record set. To account for the effects of spectral shape, the collapse margin ratio calculated in Chapter 6 is modified to obtain an adjusted collapse margin ratio, *ACMR*, for each index archetype, *i*:

$$ACMR_i = SSF \times CMR_i \tag{7-1}$$

This adjustment is in addition the adjustment made to account for three-dimensional nonlinear dynamic analysis effects in Chapter 6.

### 7.2.1 Effect of Spectral Shape on Collapse Margin

Baker and Cornell (2006) have shown that rare ground motions in the Western United States, such as those corresponding to the MCE, have a distinctive spectral shape that differs from the shape of the design spectrum used for structural design in ASCE/SEI 7-05 (ASCE 2005). In essence, the shape of the spectrum of rare ground motions is peaked at the period of interest, and drops off more rapidly (and has less energy) at periods that are longer or shorter than the period of interest. Where ground motion intensities are defined based on the spectral acceleration at the first-mode

period of a structure, and where structures have sufficient ductility to inelastically soften into longer periods of vibration, this peaked spectral shape, and more rapid drop at other periods, causes these rare records to be less damaging than would be expected based on the shape of the standard design spectrum.

The most direct approach to account for spectral shape would be to select a unique set of ground motions that have the appropriate shape for each site, hazard level, and structural period of interest. This is not feasible, however, in a generalized procedure for assessing the collapse performance of a class of structures, with a range of possible configurations, located on a number of different sites. To remove this conservative bias, simplified spectral shape factors, *SSF*, which depend on fundamental period, *T*, and ductility capacity, $\mu_C$, are used to adjust collapse margin ratios. Background and development of spectral shape factors are described in Appendix B.

### *7.2.2 Spectral Shape Factors*

Spectral shape factors, *SSF*, are a function of the fundamental period, *T*, ductility capacity, $\mu_C$, and the seismic criteria used for design of the index archetypes, as defined by Seismic Design Category. Table 7-1a and Table 7-1b provide values of *SSF* for use in adjusting the collapse margin ratio, *CMR*.

**Table 7-1a Spectral shape factors for archetypes designed using SDC B, SDC C, or SDC $D_{min}$**

| T (sec) | Building Ductility Capacity, $\mu_C$ | | | | | | | |
|---|---|---|---|---|---|---|---|---|
| | 1.0 | 1.1 | 1.5 | 2 | 3 | 4 | 6 | >=8 |
| **<= 0.5** | 1.00 | 1.05 | 1.05 | 1.05 | 1.10 | 1.10 | 1.10 | 1.15 |
| **0.6** | 1.00 | 1.05 | 1.05 | 1.10 | 1.10 | 1.10 | 1.15 | 1.15 |
| **0.7** | 1.00 | 1.05 | 1.05 | 1.10 | 1.10 | 1.15 | 1.15 | 1.20 |
| **0.8** | 1.00 | 1.05 | 1.10 | 1.10 | 1.15 | 1.15 | 1.20 | 1.20 |
| **0.9** | 1.00 | 1.05 | 1.10 | 1.10 | 1.15 | 1.15 | 1.20 | 1.25 |
| **1.0** | 1.00 | 1.05 | 1.10 | 1.15 | 1.15 | 1.20 | 1.20 | 1.25 |
| **1.1** | 1.00 | 1.05 | 1.10 | 1.15 | 1.20 | 1.20 | 1.25 | 1.30 |
| **1.2** | 1.00 | 1.05 | 1.10 | 1.15 | 1.20 | 1.20 | 1.25 | 1.30 |
| **1.3** | 1.00 | 1.05 | 1.15 | 1.15 | 1.20 | 1.25 | 1.30 | 1.35 |
| **1.4** | 1.00 | 1.10 | 1.15 | 1.15 | 1.20 | 1.25 | 1.30 | 1.35 |
| **>= 1.5** | 1.00 | 1.10 | 1.15 | 1.20 | 1.25 | 1.30 | 1.35 | 1.40 |

Since spectral shape factors are considerably different between SDC $D_{max}$ and other Seismic Design Categories, the governing performance group for the adjusted collapse margin ratio, *ACMR*, may not be the same as the one for the collapse margin ratio, *CMR*, before adjustment.

**Table 7-1b Spectral shape factors for archetypes designed using SDC $D_{max}$**

| T (sec) | Building Ductility Capacity, $\mu_C$ | | | | | | | |
|---|---|---|---|---|---|---|---|---|
| | 1.0 | 1.1 | 1.5 | 2 | 3 | 4 | 6 | >=8 |
| <= 0.5 | 1.00 | 1.05 | 1.15 | 1.15 | 1.20 | 1.25 | 1.30 | 1.35 |
| 0.6 | 1.00 | 1.10 | 1.15 | 1.20 | 1.25 | 1.25 | 1.30 | 1.35 |
| 0.7 | 1.00 | 1.10 | 1.15 | 1.20 | 1.25 | 1.30 | 1.35 | 1.40 |
| 0.8 | 1.00 | 1.10 | 1.15 | 1.20 | 1.25 | 1.30 | 1.35 | 1.40 |
| 0.9 | 1.00 | 1.10 | 1.15 | 1.20 | 1.30 | 1.30 | 1.40 | 1.45 |
| 1.0 | 1.00 | 1.10 | 1.20 | 1.25 | 1.30 | 1.35 | 1.40 | 1.45 |
| 1.1 | 1.00 | 1.10 | 1.20 | 1.25 | 1.30 | 1.35 | 1.45 | 1.50 |
| 1.2 | 1.00 | 1.10 | 1.20 | 1.25 | 1.35 | 1.40 | 1.45 | 1.55 |
| 1.3 | 1.00 | 1.10 | 1.20 | 1.25 | 1.35 | 1.40 | 1.50 | 1.55 |
| 1.4 | 1.00 | 1.10 | 1.20 | 1.30 | 1.35 | 1.40 | 1.50 | 1.60 |
| >= 1.5 | 1.00 | 1.15 | 1.20 | 1.30 | 1.40 | 1.45 | 1.55 | 1.65 |

## 7.3 Total System Collapse Uncertainty

Many sources of uncertainty contribute to variability in collapse capacity. Larger variability in the overall collapse prediction will necessitate larger collapse margins in order to limit the collapse probability to an acceptable level at the MCE intensity. It is important to evaluate all significant sources of uncertainty in collapse response, and to incorporate their effects in the collapse assessment process.

### *7.3.1 Sources of Uncertainty*

The following sources of uncertainty are considered in the collapse assessment process:

- **Record-to-Record (RTR) Uncertainty.** Uncertainty due to variability in the response of index archetypes to different ground motion records. Record-to-record variability is evident in the incremental dynamic response plots in Figures 6-5. Variability in response is due to the combined effects of: (a) variations in frequency content and dynamic characteristics of the various records; and (b) variability in the hazard characterization as reflected in the Far-Field ground motion record set. Values of record-to-record variability, $\beta_{RTR}$, ranging from 0.35 to 0.45 are fairly consistent among various building types (Haselton 2006, Ibarra and Krawinkler 2005a, 2005b, Zareian et al. 2006, Zareian 2006). Based on this, and other related research, a fixed value of $\beta_{RTR}$ = 0.40 is assumed in the performance evaluation.
- **Design Requirements-Related (DR) Uncertainty.** Uncertainty associated with the design requirements for the system of interest, based on qualitative evaluation of the completeness and robustness of the

design requirements, and the extent to which index archetype configurations represent structural designs that are likely to result in actual design and construction practice. To some extent design uncertainty is reflected in variations between index archetype configurations, but this finite set of examples may not be representative of the full range of possible variations in practice. Design requirements-related uncertainty is quantified in terms of the quality of design requirements, which is rated in accordance with the requirements in Chapter 3.

- **Test Data-Related (TD) Uncertainty.** Collapse uncertainty associated with the test data for the system of interest, based on qualitative evaluation of the completeness and robustness of the test data used to define the system. Test data-related uncertainty is closely associated with, but distinct from, modeling uncertainty. Test data-related uncertainty is quantified in terms of the quality of test data, which is rated in accordance with the requirements in Chapter 3.
- **Modeling (MDL) Uncertainty.** Uncertainty associated with nonlinear modeling, based on qualitative evaluation of the accuracy and robustness of nonlinear models, and ability to simulate component nonlinear behavior. Modeling-related uncertainty is quantified in terms of the quality of nonlinear models, which is rated in accordance with the requirements in Chapter 5.

### *7.3.2 Combining Uncertainties in Collapse Evaluation*

The total uncertainty is obtained by combining *RTR, DR, TD,* and *MDL* uncertainties. Formally, the collapse fragility of each index archetype is defined by the random variable, $S_{CT}$, assumed to be equal to the product of the median value of the collapse ground motion intensity, $\hat{S}_{CT}$ , as calculated by NDA, and the random lognormal variable, $\lambda_{TOT}$:

$$S_{CT} = \hat{S}_{CT}\lambda_{TOT} \tag{7-2}$$

where $\lambda_{TOT}$ is a lognormal random variable with a median value of unity and a lognormal standard deviation of $\beta_{TOT.}$ The lognormal random variable is assumed to be comprised of four component random variables according to the following equation:

$$\lambda_{TOT} = \lambda_{RTR}\lambda_{DR}\lambda_{TD}\lambda_{MDL} \tag{7-3}$$

where $\lambda_{RTR}$, $\lambda_{MDL,}$ $\lambda_{DR,}$ and $\lambda_{TD}$ are lognormal random variables with median values of unity, and lognormal standard deviation parameters, $\beta_{RTR}$, $\beta_{DR,}$ $\beta_{TD}$, and $\beta_{MDL,}$ respectively. Since these parameters are assumed to be statistically

independent, the lognormal standard deviation parameter, $\beta_{TOT}$, describing total collapse uncertainty, is given by:

$$\beta_{TOT} = \sqrt{\beta_{RTR}^2 + \beta_{DR}^2 + \beta_{TD}^2 + \beta_{MDL}^2} \quad (7\text{-}4)$$

where: $\beta_{TOT}$ = total system collapse uncertainty
$\beta_{RTR}$ = record-to-record collapse uncertainty (0.40)
$\beta_{DR}$ = design requirements-related collapse uncertainty (0.20 – 0.65)
$\beta_{TD}$ = test data-related collapse uncertainty (0.20 – 0.65)
$\beta_{MDL}$ = modeling-related collapse uncertainty (0.20 – 0.65).

The performance evaluation process does not require explicit calculation of the lognormal distribution given by Equation 7-2 and Equation 7-3. Acceptance criteria, however, are based on the composite uncertainty, $\beta_{TOT}$, developed on the basis of Equation 7-4.

### *7.3.3 Effect of Uncertainty on Collapse Margin*

Uncertainty influences the shape of a collapse fragility curve plotted from the results of incremental dynamic analyses. Figure 7-2 shows two collapse fragility curves reflecting two different levels of uncertainty. The dashed curve "a" reflects a $\beta_{RTR} = 0.4$, and the solid curve "b" reflects a $\beta_{TOTAL} = 0.65$. As indicated in the figure, additional uncertainty has the effect of "flattening" the curve. While the median collapse intensity, $\hat{S}_{CT}$, is unchanged, additional uncertainty causes a large increase in the probability of collapse at the MCE intensity, $S_{MT}$.

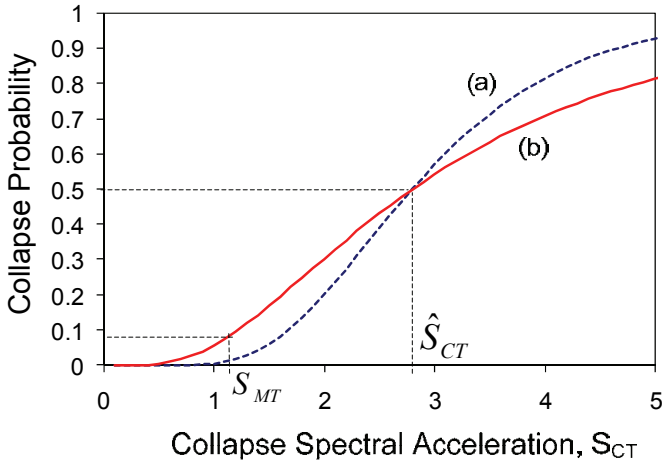


Figure 7-2 Collapse fragility curves considering (a) ground motion record-to-record uncertainty, (b) modifications for total uncertainty

Changes in the probability of collapse at the MCE intensity will affect the collapse margin ratio, *CMR*. Figure 7-3 shows collapse fragility curves for two hypothetical seismic-force-resisting systems that have different levels of collapse uncertainty. In this example, both systems have been designed for the same seismic response coefficient, $C_S$, and happen to have the same median collapse intensity, $\hat{S}_{CT}$. System No. 1, however, has a larger uncertainty and a "flatter" collapse fragility curve. To achieve the same 10 percent probability of collapse for MCE ground motions, a larger collapse margin ratio is required for System No. 1 than is required for System No. 2 (i.e., $CMR_1 > CMR_2$). Thus, System No. 1 would have to be designed using a smaller response modification coefficient, *R*, than System No. 2.

Figure 7-4 shows collapse fragility curves for another set of hypothetical seismic-force-resisting systems with different levels of collapse uncertainty. As in Figure 7-3, both systems are designed for the same seismic response coefficient, $C_S$, but in this case, the two systems are also designed for the same response modification coefficient, *R*. The difference in uncertainty, however, requires different collapse margin ratios to achieve the same median probability of collapse. In order to utilize the same response modification coefficient, *R*, System No. 1, with larger uncertainty and flatter collapse fragility, is required to have a larger collapse margin ratio than System No. 3 (i.e., $CMR_1 > CMR_3$).

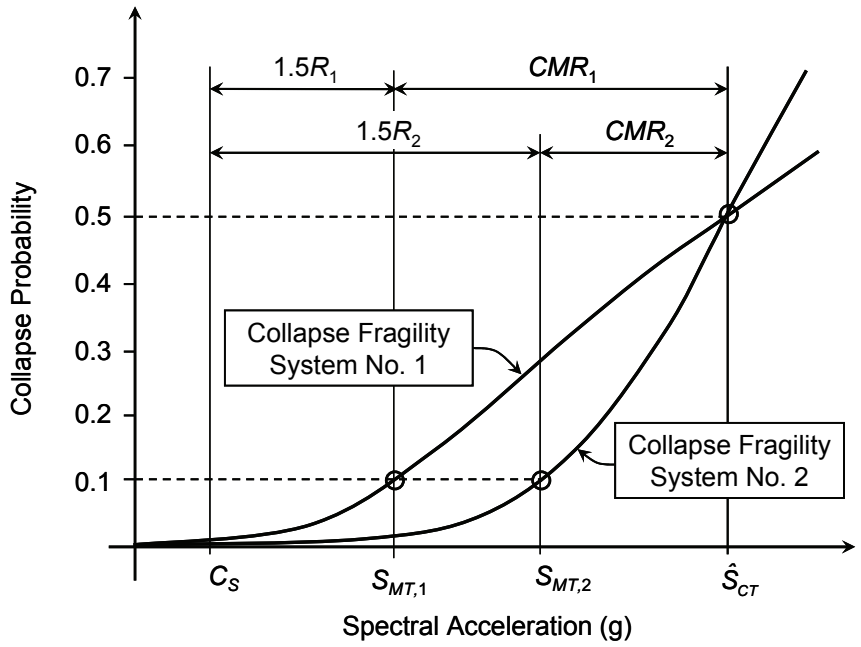


Figure 7-3 Illustration of fragility curves and collapse margin ratios for two hypothetical seismic-force-resisting systems – same median collapse level.

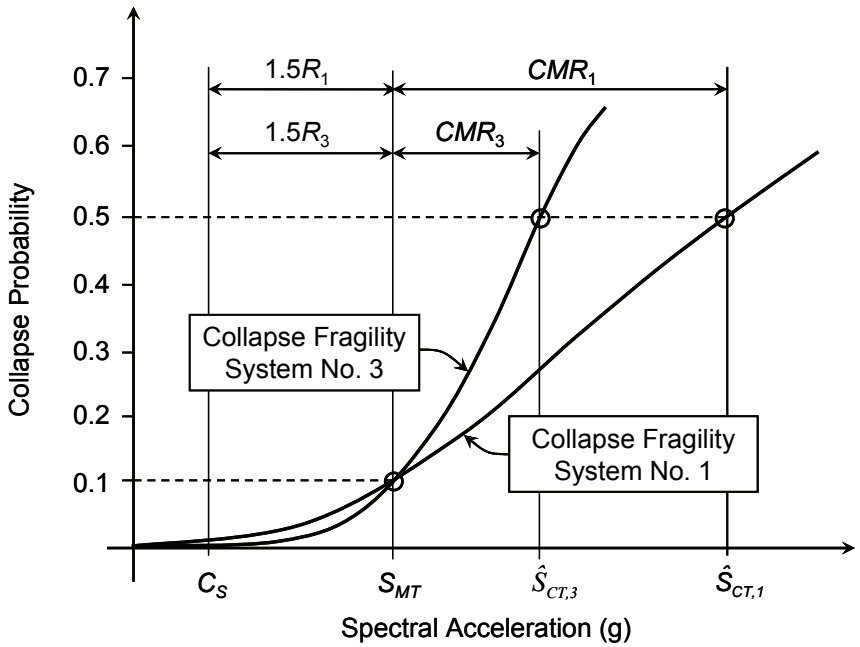


Figure 7-4 Illustration of fragility curves and collapse margin ratios for two hypothetical seismic-force-resisting systems – same *R* factor.

### *7.3.4 Total System Collapse Uncertainty*

Total system collapse uncertainty is calculated based on Equation 7-4, and is a function of record-to-record (RTR) uncertainty, design requirements-related (DR) uncertainty, test data-related (TD) uncertainty, and modeling (MDL) uncertainty.

Uncertainty due to record-to-record variability is taken as $\beta_{RTR} = 0.40$ in all cases. Quality ratings for design requirements, test data, and nonlinear modeling are translated into quantitative values of uncertainty based on the following scale: (A) Superior, $\beta = 0.20$; (B) Good, $\beta = 0.30$; (C) Fair, $\beta = 0.45$; and (D) Poor, $\beta = 0.65$.

Values of total system collapse uncertainty, $\beta_{TOT}$, are provided in Table 7-2a through Table 7-2d. Each table is specific to model quality ratings of (A) Superior, (B) Good, (C) Fair, or (D) Poor. Values in each table are based on Equation 7-4 and the applicable combination of quality ratings for test data and design requirements.

**Table 7-2a Total System Collapse Uncertainty ($\beta_{TOT}$) for Model Quality (A) Superior**

| Quality of Test Data | Quality of Design Requirements | | | |
|---|---|---|---|---|
| | A – Superior | B – Good | C – Fair | D - Poor |
| (A) Superior | 0.55 | 0.55 | 0.65 | 0.80 |
| (B) Good | 0.55 | 0.60 | 0.70 | 0.85 |
| (C) Fair | 0.65 | 0.70 | 0.80 | 0.90 |
| (D) Poor | 0.80 | 0.85 | 0.90 | 1.00 |

**Table 7-2b Total System Collapse Uncertainty ($\beta_{TOT}$) for Model Quality (B) Good**

| Quality of Test Data | Quality of Design Requirements | | | |
|---|---|---|---|---|
| | A – Superior | B – Good | C – Fair | D - Poor |
| (A) Superior | 0.55 | 0.60 | 0.70 | 0.85 |
| (B) Good | 0.60 | 0.65 | 0.75 | 0.85 |
| (C) Fair | 0.70 | 0.75 | 0.80 | 0.95 |
| (D) Poor | 0.85 | 0.85 | 0.95 | 1.05 |

**Table 7-2c Total System Collapse Uncertainty ($\beta_{TOT}$) for Model Quality (C) Fair**

| Quality of Test Data | Quality of Design Requirements | | | |
|---|---|---|---|---|
| | A – Superior | B – Good | C – Fair | D - Poor |
| (A) Superior | 0.65 | 0.70 | 0.80 | 0.90 |
| (B) Good | 0.70 | 0.75 | 0.80 | 0.95 |
| (C) Fair | 0.80 | 0.80 | 0.90 | 1.00 |
| (D) Poor | 0.90 | 0.95 | 1.00 | 1.10 |

**Table 7-2d Total System Collapse Uncertainty ($\beta_{TOT}$) for Model Quality (D) Poor**

| Quality of Test Data | Quality of Design Requirements | | | |
|---|---|---|---|---|
| | A – Superior | B – Good | C – Fair | D - Poor |
| (A) Superior | 0.80 | 0.85 | 0.90 | 1.00 |
| (B) Good | 0.85 | 0.85 | 0.95 | 1.05 |
| (C) Fair | 0.90 | 0.95 | 1.00 | 1.10 |
| (D) Poor | 1.00 | 1.05 | 1.10 | 1.20 |

## 7.4 Acceptable Values of Adjusted Collapse Margin Ratio

Acceptable values of adjusted collapse margin ratio are based on total system collapse uncertainty, $\beta_{TOT}$, and established values of acceptable probabilities of collapse. They are based on the assumption that the distribution of collapse level spectral intensities is lognormal, with a median value, $\hat{S}_{CT}$, and a lognormal standard deviation equal to the total system collapse uncertainty, $\beta_{TOT}$.

Table 7-3 provides acceptable values of adjusted collapse margin ratio, *ACMR10%* and *ACMR20%*, based on total system collapse uncertainty and values of acceptable collapse probability, taken as 10% and 20%, respectively. Other values of collapse probability ranging from 5% - 25% are shown for comparison and reference. Lower values of acceptable collapse probability and higher levels of collapse uncertainty result in higher required values of adjusted collapse margin ratio.

**Table 7-3 Acceptable Values of Adjusted Collapse Margin Ratio (*ACMR10%* and *ACMR20%*)**

| Total System Collapse Uncertainty | Collapse Probability | | | | |
|---|---|---|---|---|---|
| | 5% | 10% | 15% | 20% | 25% |
| | | *(ACMR10%)* | | *(ACMR20%)* | |
| 0.55 | 2.47 | 2.02 | 1.77 | 1.59 | 1.45 |
| 0.60 | 2.68 | 2.16 | 1.86 | 1.66 | 1.50 |
| 0.65 | 2.91 | 2.30 | 1.96 | 1.73 | 1.55 |
| 0.70 | 3.16 | 2.45 | 2.07 | 1.80 | 1.60 |
| 0.75 | 3.43 | 2.61 | 2.18 | 1.88 | 1.66 |
| 0.80 | 3.73 | 2.78 | 2.29 | 1.96 | 1.72 |
| 0.85 | 4.05 | 2.97 | 2.41 | 2.05 | 1.77 |
| 0.90 | 4.40 | 3.16 | 2.54 | 2.13 | 1.84 |
| 0.95 | 4.77 | 3.37 | 2.68 | 2.23 | 1.90 |
| 1.00 | 5.18 | 3.60 | 2.82 | 2.32 | 1.96 |
| 1.05 | 5.63 | 3.83 | 2.97 | 2.42 | 2.03 |
| 1.10 | 6.11 | 4.09 | 3.13 | 2.52 | 2.10 |
| 1.15 | 6.63 | 4.36 | 3.30 | 2.63 | 2.17 |
| 1.20 | 7.20 | 4.65 | 3.47 | 2.75 | 2.25 |

## 7.5 Evaluation of the Response Modification Coefficient, *R*

Acceptable performance is defined by the following two basic collapse prevention objectives:

- The probability of collapse for MCE ground motions is approximately ten percent, or less, on average across a performance group.
- The probability of collapse for MCE ground motions is approximately twenty percent, or less, for each index archetype within a performance group.

Acceptable performance is achieved when, for each performance group, adjusted collapse margin ratios, *ACMR*, for each index archetype meet the following two criteria:

- the average value of adjusted collapse margin ratio for each performance group exceeds *ACMR10%*:

$$\overline{ACMR_i} \geq ACMR10\% \tag{7-5}$$

- individual values of adjusted collapse margin ratio for each index archetype within a performance group exceeds *ACMR20%*:

$$ACMR_i \geq ACMR20\% \tag{7-6}$$

## 7.6 Evaluation of the Overstrength Factor, $\Omega_O$

The average value of archetype overstrength, $\Omega$, is calculated for each performance group. The value of the system overstrength factor, $\Omega_O$, for use in design should not be taken as less than the largest average value of calculated archetype overstrength, $\Omega$, from any performance group. The system overstrength factor, $\Omega_O$, should be conservatively increased to account for variation in overstrength results of individual index archetypes, and judgmentally rounded to half unit intervals (e.g., 1.5, 2.0, 2.5, and 3.0).

The system overstrength factor, $\Omega_O$, need not exceed 1.5 times the response modification coefficient, *R*. A practical limit on the value of $\Omega_O$ is about 3.0, consistent with the largest value of this factor specified in Table 12.2-1 of ASCE 7-05 for all current approved seismic-force-resisting systems.

## 7.7 Evaluation of the Deflection Amplification Factor, $C_d$

The deflection amplification factor, $C_d$, is based on the acceptable value of the response modification factor, *R*, reduced by the damping factor, $B_{1E}$,

corresponding to the inherent and added viscous damping of the system of interest:

$$C_d = \frac{R}{B_{1E}} \tag{7-7}$$

Where: $C_d$ = deflection amplification factor

$R$ = system response modification factor (Section 7.4)

$B_{1E}$ = numerical coefficient as set forth in Table 18.6-1 of ASCE 7-05 for effective damping equal to $\beta_I + \beta_{V1}$ and period, $T$

$\beta_I$ = component of effective damping of the structure due to the inherent dissipation of energy by elements of the structure, at or just below the effective yield displacement of the seismic-force-resisting system, Section 18.6.2.1 of ASCE 7-05

$\beta_{V1}$ = component of effective damping of the 1st mode of vibration of the structure in the direction of interest due to viscous dissipation of energy by damping devices (for systems with such devices), at or just below the effective yield displacement of the seismic force-resisting system, Section 18.6.2.3 of ASCE 7-05.

Most systems do not include damping devices (i.e., $\beta_{VI} = 0$) and have only inherent damping, $\beta_I$. In general, inherent damping may be assumed to be 5 percent of critical, and a corresponding value of the damping coefficient, $B_{1E} = 1.0$ (Table 18.6-1, ASCE 7-05). Thus, for most systems the value of $C_d$ will be equal to the value of $R$.

# Chapter 8
# Documentation and Peer Review

This chapter describes documentation and peer review requirements for a proposed seismic-force-resisting system. It identifies recommended qualifications, expertise, and responsibilities for personnel involved with the development and review of a proposed system. It lists information that should be included in a report documenting the development of a system, and discusses requirements for review at each step of the developmental process.

## 8.1 Recommended Qualifications, Expertise and Responsibilities for a System Development Team

In order to collect the necessary data and apply the procedures of this Methodology, a system development team will need to have certain qualifications, experience, and expertise. These include the ability to: (1) adequately test materials, components and assemblies; (2) develop comprehensive design and construction requirements; (3) develop archetype designs; and (4) analyze archetype models.

A development team is responsible for following the procedures of this Methodology in determining seismic performance factors for a proposed system, defining the limits under which a system will be applicable, obtaining approval of the peer review panel, and documenting results.

### *8.1.1 System Sponsor*

The system sponsor is a person or organization that has conceived a new seismic-force-resisting system and will benefit from its use. The system sponsor is responsible for assembling a development team, selecting a peer review panel, and submitting a proposed system for approval and use.

### *8.1.2 Testing Qualifications, Expertise and Responsibilities*

The testing facilities engaged in the development of a proposed system must have the capability to perform material, component, connection, assembly, and system tests necessary for quantifying the material and behavioral properties of the system. The testing laboratory used to conduct experimental tests should comply with national or international accreditation

criteria, such as ICBO ES Acceptance Criteria for Laboratory Accreditation (AC89) (ICBO 2000).

Testing facility staff should have the necessary expertise to establish and execute an experimental program, conduct the tests, and mine existing research for other relevant available test data.

### *8.1.3 Engineering and Construction Qualifications, Expertise and Responsibilities*

Member(s) of a development team must have sufficient experience and expertise to develop comprehensive design and construction requirements, and to perform trial system designs. This should include familiarity with seismic design requirements specified in ASCE/SEI 7, and material design and detailing requirements for other similar systems. To be viable for use, a proposed system must be feasible to construct. Familiarity with proposed construction techniques, or established construction techniques for other similar systems is needed.

### *8.1.4 Analytical Qualifications, Expertise and Responsibilities*

Member(s) of a development team must have sufficient experience and expertise to interpret test data and develop sophisticated nonlinear models capable of simulating potential collapse failure modes of a proposed system. This should include knowledge and experience in the analytical approaches specified in the Methodology, knowledge of material, component, connection, and overall system performance, and experience with analysis software capable of simulating system response.

## 8.2 Documentation of System Development and Results

The results of system development efforts must be thoroughly documented at each step of the process for: (1) review and approval by the peer review panel; (2) review and approval by an authority having jurisdiction over its eventual use; and (3) use in design and construction.

Documentation of the development of seismic performance factors for a proposed system should include, but is not necessarily limited to the following:

- description of intended system applications and expected performance
- limitations on system use
- typical horizontal and vertical geometric configurations

- clear and complete design requirements and specifications for the system providing information to quantify strength limit states, proportion and detail components, analyze predicted response, and confirm satisfactory behavior
- summary of test data and other supporting evidence from an experimental investigation program validating material properties and component behavior, calibrating nonlinear analysis models, and establishing performance acceptance criteria
- description of index archetype configurations and extent of archetype design space
- identification of performance groups, applicable Seismic Design Categories, and gravity load intensities
- idealized model configurations, nonlinear modeling parameters, documentation of analysis software, and information used in model calibration
- criteria for non-simulated collapse modes
- summary of nonlinear model results, demand parameters, and response quantities
- quality ratings for design requirements, test data, and nonlinear models
- summary of performance evaluation results, derived quantities, and acceptance criteria
- proposed seismic performance factors ($R$, $\Omega_O$, and $C_d$)

## 8.3 Peer Review Panel

Implementation of this Methodology involves much uncertainty, judgment and potential for variation. Deciding on an appropriate level of detail to adequately characterize performance of a proposed system should be performed at each step in the process in collaboration with a peer review panel.

It is recommended that a peer review panel consisting of knowledgeable experts be retained for this purpose. The peer review panel should be familiar with the procedures of this Methodology, should have sufficient knowledge to render an informed opinion on the developmental process, and should include expertise in each of the following areas:

- Material, component, and assembly testing
- Engineering design and construction

- Nonlinear collapse simulation

Members of the peer review panel must be qualified to critically evaluate the development of the proposed system including testing, design, and analysis. If a unique computer code is developed by the development team, the peer review panel should be capable of performing independent analyses of the proposed system using other analysis platforms.

### *8.3.1 Peer Review Panel Selection*

It is envisioned that the cost of the peer review panel will be borne by the system sponsor. As such, it is expected that members of the peer review panel will be selected by the system sponsor. It is intended, however, that the peer review panel be an independent set of reviewers who will advise and guide the development team at each step in the process. It is recommended that other stakeholders, including authorities with jurisdiction over the eventual use of the system in design and construction, be consulted in the selection of peer review panel members.

### *8.3.2 Peer Review Roles and Responsibilities*

The peer review panel is responsible for reviewing and commenting on the approach taken by the development team including the extent of the experimental program, testing procedures, design requirements, development of structural system archetypes, analytical approaches, extent of the nonlinear analysis investigation, and the final selection of the proposed seismic performance factors.

The peer review panel is responsible for reporting their opinion on the work performed by the developmental team, their findings, recommendations, and conclusions.

If there are any areas where concurrence between the peer review panel and the development team was not reached, or where the peer review panel was not satisfied with the approach or extent of the work performed, this should be reflected in the total uncertainty used in calculating the system acceptance criteria, and in determining the final values of proposed seismic performance factors.

## 8.4 Submittal

It is expected that a system sponsor will wish to submit a proposed system to an authority for approval and use. For national building codes and standards, one such authority is the Building Seismic Safety Council (BSSC) Provisions Update Committee (PUC), which has jurisdiction over the National

Earthquake Hazards Reduction Program *(NEHRP) Recommended Provisions for Seismic Regulations for New Buildings and Other Structures* (*NEHRP Recommended Provisions*). BSSC's PUC, along with its technical subcommittees, is a nationally recognized leader in reviewing and endorsing new seismic force-resisting systems for ultimate inclusion in national building codes and standards. Systems can also be submitted directly to model building codes through the code change process.

Another approach is to promote a new system through a relevant material standard organization, such as the American Concrete Institute (ACI), American Institute of Steel Construction (AISC), American Iron and Steel Institute (AISI), or the American Forest & Paper Association (AF&PA). Approval through one of these organizations, however, will still require adoption by national building codes or standards before use.

If a proposed system is intended for a single project application, then documentation should be submitted, along with drawings and calculations for the single application, to the authority having jurisdiction over the site where it is being proposed.

# Chapter 9
# Example Applications

This chapter presents examples illustrating the application of the Methodology to reinforced concrete (RC) special moment frame (SMF), reinforced concrete (RC) ordinary moment frame (OMF), and wood light-frame shear wall seismic force-resisting systems.

## 9.1 General

Three seismic-force-resisting systems are evaluated using the methods of Chapters 3 through 7. The examples span different system types, design requirements, test data, archetype models, and analysis software. Models include both simulated and non-simulated collapse modes. Each system is currently contained in Table 12.2-1 of ASCE/SEI 7-05 (ASCE 2006a), and the examples utilize design requirements and test data currently available for these approved systems. For new (proposed) systems, design requirements will generally not exist, and would need to be developed.

These examples illustrate the application of the Methodology, and show how system design requirements might need to be modified so that the proposed structural system will meet the prescribed collapse performance objectives. These examples also demonstrate general alignment between the acceptance criteria of the Methodology and the inherent safety against collapse intended by current seismic codes.

These examples are intended for illustration only, and are not intended to propose any specific changes to current building code requirements for any currently approved system.

## 9.2 Example Application - Reinforced Concrete Special Moment Frame System

### *9.2.1 Introduction*

In this example, a reinforced concrete (RC) special moment frame (SMF) system (as defined by ACI 318-05) is considered as if it were a new system proposed for inclusion in ASCE/SEI 7-05.

### 9.2.2 Overview and Approach

In the case of this RC SMF example, the detailing requirements of ACI 318-05 (ACI 2005) are assumed to be given. The system design requirements of ASCE/SEI 7-05 are used as the framework, and seismic performance factors (SPFs) are determined by iteration until the acceptance criteria of the Methodology are met. Seismic performance factors under consideration in this example include the $R$ factor, $C_d$ factor, and $\Omega_0$ factor.

All pertinent design requirements of ASCE/SEI 7-05, including drift limits and minimum base shear requirements are assumed to apply initially. In the Methodology, the user has full flexibility to define and modify any aspect of the proposed system design requirements, as long as modifications are tested within the index archetype configurations. This includes the $R$ factor, stiffness requirements, detailing requirements, capacity design requirements, minimum base shear requirements, and any other requirements that control the design of the structural system.

The iterative assessment process begins with initial assumptions of $R = 8$, $C_d = 5.5$[1], inter-story drift limits of 2%, and minimum design base shear requirements consistent with ASCE/SEI 7-05. Overstrength, $\Omega_0$, is not assumed initially, but is determined from the overstrengths of the archetype designs. A set of structural system archetypes are developed for RC SMF buildings, nonlinear models are developed to simulate structural collapse, models are analyzed to predict the collapse capacities of each design, and the collapse margin ratio (*CMR*) is evaluated and compared to acceptance criteria.

After completing an assessment using the initial set of SPFs, selected archetypes (e.g., taller building configurations) did not meet the acceptance criteria, and were found to have inadequate collapse safety. Aspects of the structural design requirements were modified, and the system was reassessed.

This example has been adapted from collaborative research on the development of structural archetypes for RC SMFs, calibration of nonlinear element models for collapse simulation, simulation of structural response to collapse, spectral shape considerations, and treatment of uncertainties (Haselton and Deierlein 2007).

[1] $C_d = 5.5$ is used in this example, based on the value specified for reinforced concrete special moment frames in ASCE/SEI 7-05. In future applications of the Methodology, $C_d = R$ should be used unless $C_d < R$ can be substantiated.

### *9.2.3 Structural System Information*

**Design Requirements**

This example utilizes ACI 318-05 design requirements in place of the requirements that would be developed for a newly proposed system. For the purpose of assessing uncertainty, ACI 318-05 design requirements are categorized as A-Superior since they represent many years of development and include lessons learned from a number of major earthquakes.

In the process of completing the assessment of the class of RC SMF buildings, it was found that often seemingly subtle design requirements have important effects on the design and resulting structural performance; the various design requirements often interact and affect the design and performance differently than one might expect. Therefore, for newly proposed systems, it is important that the set of design requirements be well developed and clearly specified, and that the requirements are applied in their totality when designing the archetype structures.

**Test Data**

This example assessment relies on existing published test data in place of test data that would be developed for a newly proposed system. Specifically, this relies on the Pacific Earthquake Engineering Research Center's Structural Performance Database that was developed by Berry, Parrish, and Eberhard (PEER 2006a, Berry et al. 2004). To develop element models, the data are utilized from cyclic and monotonic tests of 255 rectangular columns failing in flexure and flexure-shear.

The quality of the test data is an important consideration when quantifying the uncertainty in the overall collapse assessment process. The test data used in this example cover a wide range of column design configurations and contain both monotonic and cyclic loading protocols. Even so, many of the loading protocols are not continued to deformations large enough for the capping point to be observed, and it is difficult to use such data to calibrate models for structural collapse assessment. These test data also do not include beam elements with attached slabs. Additionally, these data include no systematic test series that both (a) subject similar specimens to different loading protocols (e.g. monotonic and cyclic) and (b) continue the loading to deformations large enough for the capping behavior to be observed. Lastly, only column element tests were utilized when used to calibrate the element model, while sub-assemblage tests and/or full-scale tests were not used. Based on these observations, for the purpose of assessing uncertainty, this test data set is categorized as "B-Good."

### *9.2.4 Identification of RC SMF Archetypes Configurations*

Figure 9-1 shows the two-dimensional three-bay multi-story frame that is considered an appropriate archetype configuration for reinforced concrete frame buildings. This archetype model includes joint panels, beam and column elements, elastic foundation springs, and a leaning column to account for the P-Delta effect from loads on the gravity system. This two-dimensional model, not accounting for torsional effects, is considered acceptable because most RC SMF buildings will not be highly sensitive to torsional effects, and the goal is to verify the performance of a full class of buildings, rather than one specific building with a unique torsional issue. Appendix C provides more background of the development of this archetype configuration and model.

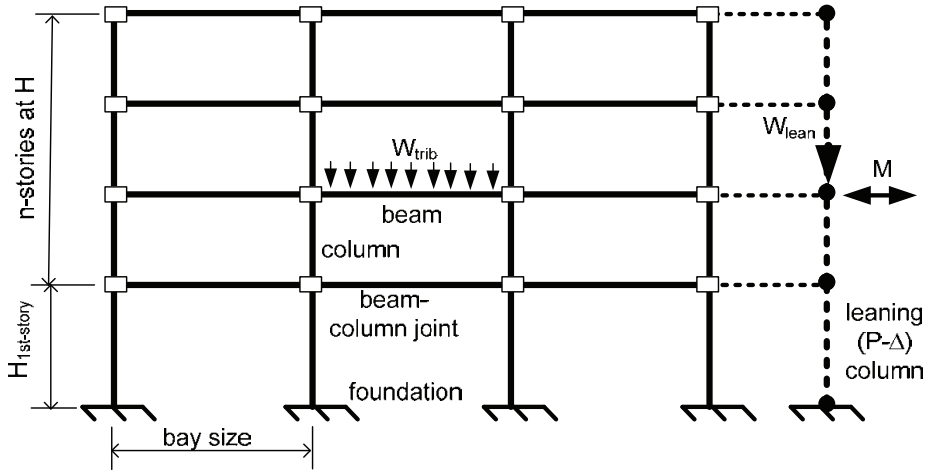


Figure 9-1 Archetype analysis model for moment frame buildings (after Haselton and Deierlein 2007, chapter 6)

Using the above archetype model configuration, a set of structural archetype designs was developed to represent the archetype design space. This set of designs was organized into four performance groups that represent the range of design ground motion intensities and the range of gravity loading conditions:

- Maximum of highest SDC (SDC $D_{max}$), high gravity loading
- Maximum of highest SDC (SDC $D_{max}$), low gravity loading
- Minimum of highest SDC (SDC $D_{min}$), high gravity loading
- Minimum of highest SDC (SDC $D_{min}$), low gravity loading

Appendix C provides a detailed discussion on the development of structural system archetypes for this system. High and low gravity load intensities are represented by space-frame (S) and perimeter-frame (P) systems,

respectively. For the buildings used in this study, the ratio of gravity load to lateral load effects is typically six times larger for space frame buildings.

Within each performance group, buildings are designed within a range of expected bay spacing (20' span and 30' span), and a range building heights (six heights between 1-story and 20-stories, as expected for RC frames buildings with no walls). To represent these four performance groups and ranges of design parameters, 48 archetypes could have been used to evaluate the RC SMF system (four seismic/gravity combinations, two bay spacings, and six heights). Instead of designing and assessing all 48 buildings, initial pilot studies were used to find the more critical design cases, which were high-seismic designs with 20' bay spacing. By utilizing these pilot studies and then focusing on the critical design cases, use of 18 archetypes were found to be sufficient.

Note that this approach of focusing on the critical design cases is not required in the Methodology, and this approach adds conservatism into the assessment process. The benefit of this approach is that it can significantly reduce the number of required archetype buildings and allow a wider range of design conditions to be considered in the assessment. When this approach is utilized, the peer review panel should closely review how the analysts chose the critical design cases.

Table 9-1 shows the properties for each of these designs. The high- and low-seismic demands are represented by the minimum and maximum demands possible in Seismic Design Category (SDC) D. The archetypes are designed for a soil site (Site Class D) conditions and design lateral loads of $S_s$ = 1.5g and $S_1$ = 0.6g for SDC $D_{max}$ and $S_s$ = 0.55g and $S_1$ = 0.13g for SDC $D_{min}$[2]. The space-frame buildings are denoted by "S" and the perimeter-frame buildings are denoted by "P". The computed value of T, in Table 9-1, is based on Section 12.8.2 of ASCE/SEI 7-05.

Each archetype configuration was fully designed in accordance with the governing design requirements. Additional information on archetype designs in provided in Appendix C.

[2] This class of buildings was designed for $Ss$ = 0.38g and $S_1$ = 0.1g, which differs slightly from the $Ss$ = 0.55g and $S_1$ = 0.13g required by these guidelines for SDC $D_{min}$.

**Table 9-1 Archetype Structural Design Properties**

| Archetype Design ID Number | No. of Stories | Key Archetype Design Parameters | | | | | |
|---|---|---|---|---|---|---|---|
| | | Framing / Gravity Loads | Seismic Design Criteria | | | | $S_{MT}$ [*T*] (g) |
| | | | *SDC* | *R* | *T* (sec.) | *V*/*W* (g) | |
| Maximum Seismic ($D_{max}$) and Low Gravity (Perimeter Frame) Designs, 20' Bay Width | | | | | | | |
| 2069 | 1 | P | $D_{max}$ | 8 | 0.26 | 0.125 | 1.50 |
| 2064 | 2 | P | $D_{max}$ | 8 | 0.45 | 0.125 | 1.50 |
| 1003 | 4 | P | $D_{max}$ | 8 | 0.81 | 0.092 | 1.11 |
| 1011 | 8 | P | $D_{max}$ | 8 | 1.49 | 0.050 | 0.60 |
| 5013 | 12 | P | $D_{max}$ | 8 | 2.13 | 0.035 | 0.42 |
| 5020 | 20 | P | $D_{max}$ | 8 | 3.36 | 0.022 | 0.27 |
| Maximum Seismic ($D_{max}$) and High Gravity (Space Frame) Designs, 20' Bay Width | | | | | | | |
| 2061 | 1 | S | $D_{max}$ | 8 | 0.26 | 0.125 | 1.50 |
| 1001 | 2 | S | $D_{max}$ | 8 | 0.45 | 0.125 | 1.50 |
| 1008 | 4 | S | $D_{max}$ | 8 | 0.81 | 0.092 | 1.11 |
| 1012 | 8 | S | $D_{max}$ | 8 | 1.49 | 0.050 | 0.60 |
| 5014 | 12 | S | $D_{max}$ | 8 | 2.13 | 0.035 | 0.42 |
| 5021 | 20 | S | $D_{max}$ | 8 | 3.36 | 0.022 | 0.27 |
| Minimum Seismic (SDC $D_{min}$) Designs, 20' Bay Width | | | | | | | |
| 6011 | 8 | P | $D_{min}$ | 8 | 1.60 | 0.013 | 0.15 |
| 6013 | 12 | P | $D_{min}$ | 8 | 2.28 | 0.010 | 0.10 |
| 6020 | 20 | P | $D_{min}$ | 8 | 3.60 | 0.010 | 0.065 |
| 6021 | 20 | S | $D_{min}$ | 8 | 3.60 | 0.010 | 0.065 |
| 30-Foot Bay Width Designs (SDC $D_{max}$) | | | | | | | |
| 1009 | 4 | P | $D_{max}$ | 8 | 1.03 | 0.092 | 1.03 |
| 1010 | 4 | S | $D_{max}$ | 8 | 1.03 | 0.092 | 1.03 |

Figure 9-2 shows example design documentation for the four-story high-seismic design with 30’ bay width (ID 1010); the notation used in this figure is defined in the notation list. This example building will be used throughout this illustrative assessment, to more clearly show how the methods described in this document should be applied in assessing each archetype design.

### *9.2.5 Development of Nonlinear Structural Archetype Models*

Implementation of the Methodology includes explicit modeling of structural collapse. Additional discussion on nonlinear modeling of RC SMF systems is provided in Appendix E.

**Archetype Analysis Models**

The system-level modeling follows the three-bay multi-story frame configuration shown in Figure 9-1. This model consists of elastic joint elements, plastic hinge RC beam and column elements, a leaning column to account for P-Delta effects, and elastic foundation springs.

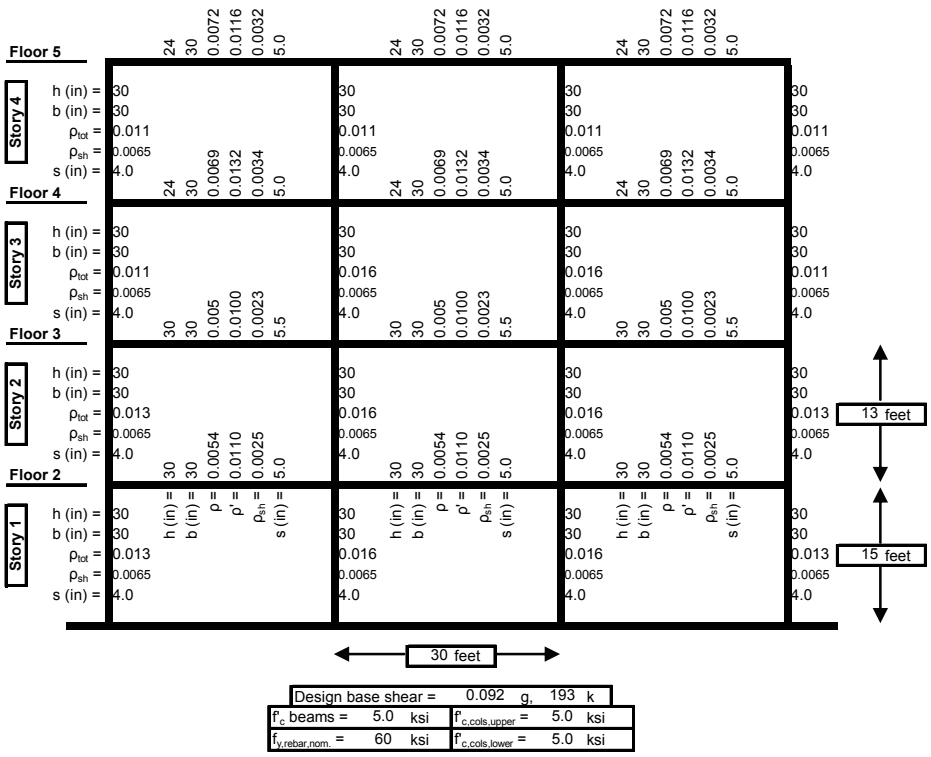


(a)

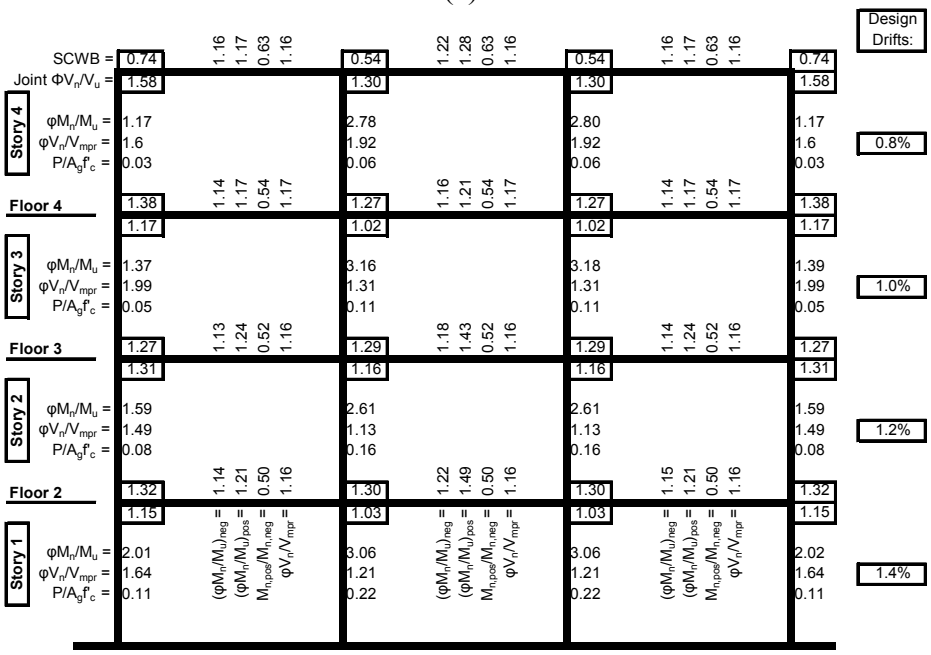


(b)

Figure 9-2 Design documentation for a four-story space frame archetype with 30′ bay spacing (building ID 1010) (after Haselton and Deierlein 2007, chapter 6).

**Nonlinear Beam-Column Element Models**

Many RC element models exist, but most cannot be used to simulate structural collapse. Recent research by Ibarra, Medina, and Krawinkler (2005) has resulted in an element model that is capable of capturing the severe deterioration that precipitates sideway collapse (Appendix E). Figure 9-3 shows the tri-linear monotonic backbone curve and associated hysteretic behavior of this model. An important aspect of this model is the "capping point," where monotonic strength loss begins, and the post-capping negative stiffness; these enables modeling of the strain softening behavior associated with concrete crushing, rebar buckling and fracture, or bond failure. Direct simulation of sidesway structural collapse is not possible without modeling this post-capping behavior.

Figure 9-4 shows an example of the experimental and calibrated response of an RC column specimen. Appendix E presents a detailed discussion of how this element model was calibrated using cyclic and monotonic tests of 255 rectangular RC elements. This Appendix shows how carefully the calibration needs to be completed, in order to avoid substantial errors in the collapse capacity prediction. Often various deterioration modes are improperly mixed together in the calibration process (e.g. cyclic strength deterioration versus in-cycle strength loss) and can lead to errors in collapse predictions.

The calibration results for the 255 tests were subsequently used to create empirical equations to predict the element model parameters (as shown in Figure 9-3), when knowing element design information such as axial load ratio and confinement ratio. These equations were used to predict the modeling parameters for the archetype designs used in this example. For illustration, Figure 9-5 shows the predicted modeling parameters for each element of design ID1010 (see Table 9-1); the notation is defined in the notation list.

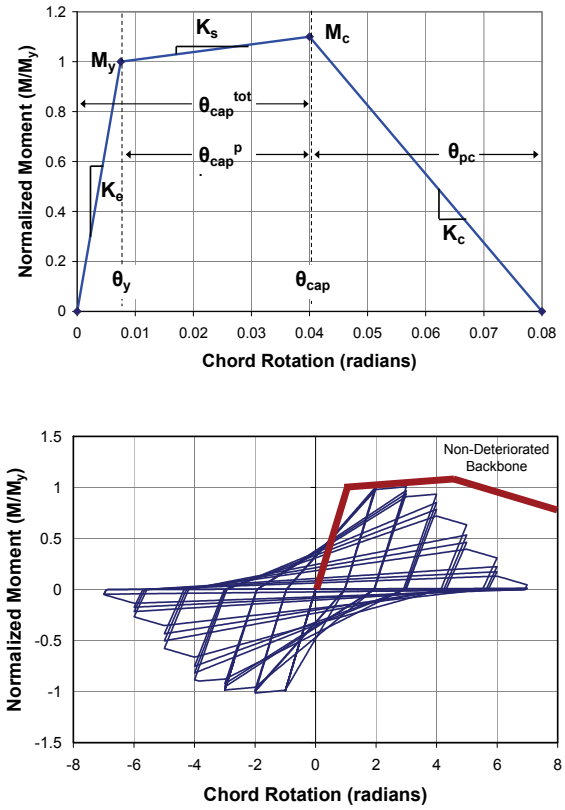


Figure 9-3 Monotonic and cyclic behavior of component model used in this study (after Haselton and Deierlein 2007, chapter 4).

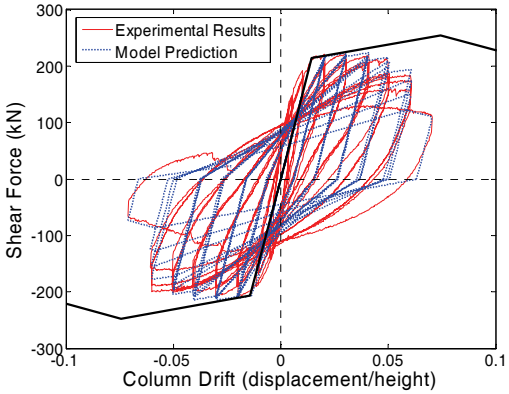


Figure 9-4 Illustration of experimental and calibrated element response (Saatciolgu and Grira, specimen BG-6) (after Haselton and Deierlein 2007, chapter 4). The solid black line shows the calibrated monotonic backbone.

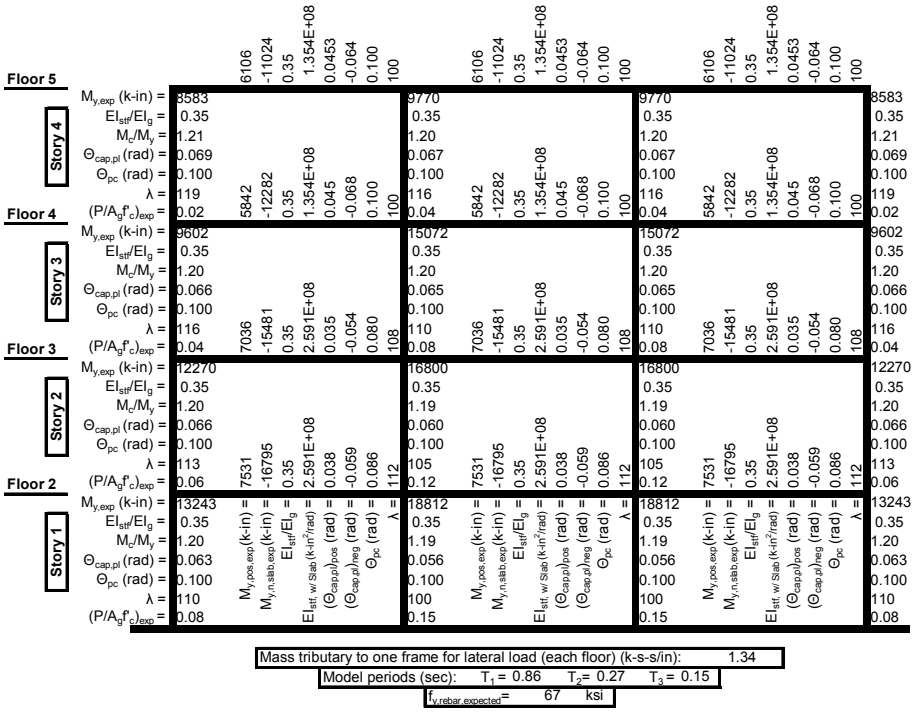


Figure 9-5 Structural modeling documentation for a four-story space frame archetype with 30′ bay spacing (building ID 1010) (after Haselton and Deierlein 2007, chapter 6).

**Uncertainty due to Model Quality**

For the purpose of assessing uncertainty, this modeling is rated as "A-Superior." RC SMF buildings are controlled by many detailing and capacity design requirements, which limit possible failure modes. The primary expected failure mode is flexural hinging leading to sidesway collapse, which the modeling approach can simulate reasonably well by capturing post-peak degrading response (under both monotonic and cyclic loading). A rating of "A-Superior" by no means indicates that this modeling approach is perfect, but the rating does recognize that the modeling approach is able to directly simulate structural response up to collapse (simulating all expected modes of damage that could lead to collapse), and is well calibrated to large amounts of data.

### *9.2.6 Nonlinear Structural Analyses*

The structural analysis software selected for completing this example is the Open Systems for Earthquake Engineering Simulation (OpenSees 2006), which was developed by the Pacific Earthquake Engineering Research (PEER) Center. This software includes the modeling aspects required for collapse simulation of RC SMF buildings: the Ibarra element model, joint models, a large deformation geometric transformation, several numerical

algorithms for solving the systems of equations associated with nonlinear dynamic and static analyses, etc.

To compute the system overstrength factor ($\Omega_0$) and to help verify the structural model, monotonic static pushover analysis is used. This pushover is based on the lateral load pattern prescribed in ASCE/SEI 7-05. Figure 9-6 shows an example of the pushover curve and inter-story drift distributions for archetype ID1010.

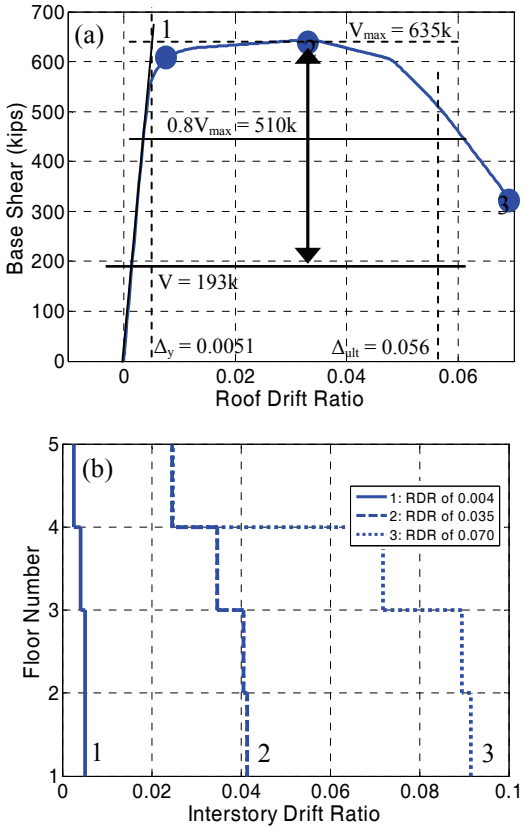


Figure 9-6 (a) Monotonic static pushover, and (b) peak interstory drift ratios at three deformation levels during pushover. The pushover is based on the building code specified lateral load distribution (ASCE 2005) (after Haselton and Deierlein 2007, chapter 6).

For this example RC SMF building, yielding occurs at about a 0.005 interstory and roof drift ratio ($\Delta_y$ = 0.0051), a maximum strength of 635 kips is reached, and then capping (the onset of negative stiffness) occurs at about a 0.040 interstory and 0.035 roof drift ratio. This is followed with 20% strength loss at $\Delta_{ult}$ = 0.056. Using these values, the overstrength factor can be computed as $\Omega$ = 635k/193k = 3.3, and the building ductility capacity can be computed as $\mu_c$ = 0.056/0.0051 = 11.0.

To compute the collapse capacity for each archetype design, the incremental dynamic analysis (IDA) approach is used (Chapter 6), with the Far-Field ground motion set and ground motion scaling method presented in Appendix A. Note that Chapter 6 does not require a full IDA (as is shown in Figure 9-7) only a simplified version of this analysis is required, which has the goal of quantifying the median collapse capacity of each archetype model.

Figure 9-7 illustrates how the IDA method is used to compute the collapse capacity of archetype ID1010. The spectral acceleration at collapse ($S_{CT}$) is computed for each of the 44 ground motions of the Far-Field Set, then the median collapse level ( $\hat{S}_{CT}$ ) is computed, which is 2.58 g for this example. The collapse margin ratio (*CMR*), defined as the ratio of $\hat{S}_{CT}$ to the Maximum Considered Earthquake ground motion demand ($S_{MT}$), is 2.50 for archetype ID1010.

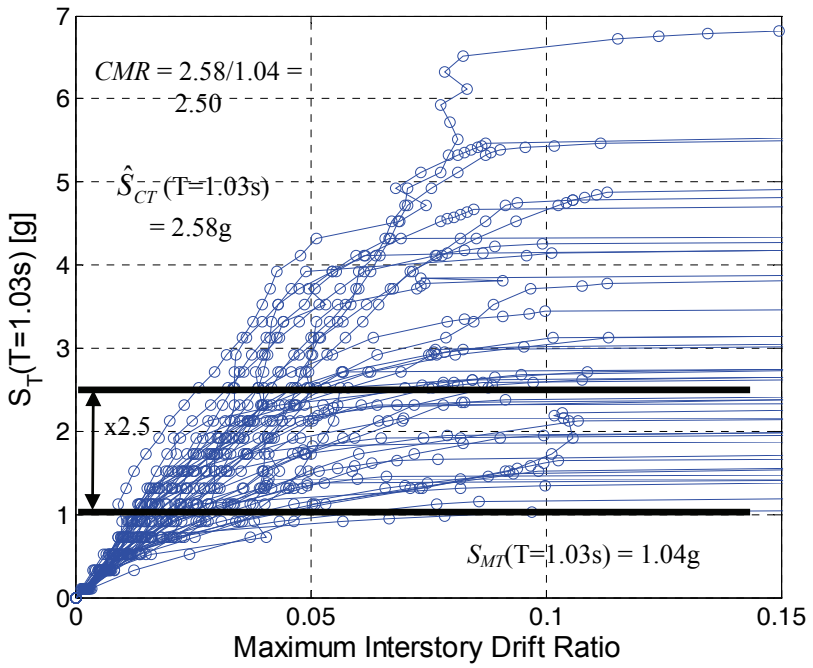


Figure 9-7 Incremental Dynamic Analysis to collapse, showing the Maximum Considered Earthquake ground motion ($S_{MT}$), median collapse capacity ( $\hat{S}_{CT}$ ), and collapse margin ratio (*CMR*) for ID1010.

In this example, it is assumed that RC SMF buildings collapse in a sideway mechanism, which can be directly simulated using the structural analysis model. This assertion is made due to the many detailing, continuity, and capacity design provisions preventing other collapse modes (Appendix D). For structural systems where some collapse modes are not simulated by the

structural model, these additional modes must be accounted for using component limit state checks for non-simulated collapse modes (Chapter 5).

Static pushover analyses were completed and the IDA method was applied to each of the 18 archetype designs, and Table 9-2 summarizes the results of these analyses. These IDA results shows that the average *CMR* is 1.26 for perimeter frames and 1.71 for space frames, however, note that these values have not yet been adjusted for the beneficial effects of spectral shape (Appendix B). Allowable *CMR* values and acceptance criteria are discussed later.

**Table 9-2 Summary of Collapse Results for Archetype Designs**

| Archetype Design ID Number | Design Configuration | | | Pushover and IDA Results | | | |
|---|---|---|---|---|---|---|---|
| | No. of Stories | Framing / Gravity Loads | Seismic SDC | Static $\Omega$ | $S_{MT}$ [$T$] (g) | $S_{CT}$ [$T$] (g) | *CMR* |
| Maximum Seismic ($D_{max}$) and Low Gravity (Perimeter Frame) Designs, 20' Bay Width | | | | | | | |
| 2069 | 1 | P | $D_{max}$ | 1.6 | 1.50 | 1.77 | 1.18 |
| 2064 | 2 | P | $D_{max}$ | 1.8 | 1.50 | 2.25 | 1.50 |
| 1003 | 4 | P | $D_{max}$ | 1.6 | 1.11 | 1.79 | 1.61 |
| 1011 | 8 | P | $D_{max}$ | 1.6 | 0.60 | 0.76 | 1.25 |
| 5013 | 12 | P | $D_{max}$ | 1.7 | 0.42 | 0.51 | 1.22 |
| 5020 | 20 | P | $D_{max}$ | 2.6 | 0.27 | 0.22 | 0.82 |
| Mean: | -- | -- | -- | 1.8 | -- | -- | 1.26 |
| Maximum Seismic ($D_{max}$) and High Gravity (Space Frame) Designs, 20' Bay Width | | | | | | | |
| 2061 | 1 | S | $D_{max}$ | 4.0 | 1.50 | 2.94 | 1.96 |
| 1001 | 2 | S | $D_{max}$ | 3.5 | 1.50 | 3.09 | 2.06 |
| 1008 | 4 | S | $D_{max}$ | 2.7 | 1.11 | 1.97 | 1.78 |
| 1012 | 8 | S | $D_{max}$ | 2.3 | 0.60 | 0.98 | 1.63 |
| 5014 | 12 | S | $D_{max}$ | 2.8 | 0.42 | 0.67 | 1.59 |
| 5021 | 20 | S | $D_{max}$ | 3.5 | 0.27 | 0.34 | 1.25 |
| Mean: | -- | -- | -- | 3.1 | -- | -- | 1.71 |
| Comparison of Results – SDC $D_{max}$ & $D_{min}$ Seismic Design Conditions, 20' Bay Width | | | | | | | |
| 1011 | 8 | P | $D_{max}$ | 1.6 | 0.56 | 0.71 | 1.25 |
| 6011 | 8 | P | $D_{min}$ | 1.8 | 0.15 | 0.32 | 2.12 |
| 5013 | 12 | P | $D_{max}$ | 1.7 | 0.35 | 0.43 | 1.22 |
| 6013 | 12 | P | $D_{min}$ | 1.8 | 0.10 | 0.21 | 2.00 |
| 5020 | 20 | P | $D_{max}$ | 2.6 | 0.22 | 0.19 | 0.82 |
| 6020 | 20 | P | $D_{min}$ | 1.8 | 0.07 | 0.24 | 3.70 |
| 5021 | 20 | S | $D_{max}$ | 3.5 | 0.24 | 0.31 | 1.25 |
| 6021 | 20 | S | $D_{min}$ | 3.4 | 0.07 | 0.11 | 1.73 |
| Comparison of Results - 20-Foot and 30-Foot Bay Width Designs (SDC $D_{max}$) | | | | | | | |
| 1003 | 4 | P-20 | $D_{max}$ | 1.6 | 1.04 | 1.67 | 1.61 |
| 1009 | 4 | P-30 | $D_{max}$ | 1.6 | 1.04 | 2.05 | 1.98 |
| 1008 | 4 | S-20 | $D_{max}$ | 2.7 | 1.04 | 1.84 | 1.78 |
| 1010 | 4 | S-30 | $D_{max}$ | 3.3 | 1.04 | 2.58 | 2.50 |

In addition, these results verify that the buildings designed in low-seismic regions have higher *CMR* (lower collapse risk) than those designed in high-

seismic regions. Additionally, buildings with 30' bay width tend to have higher *CMR*, as compared to building with 20' bay width (due to gravity load effects in the design). Therefore, the remaining assessment focuses on the 12 more critical archetype buildings, which were designed for high-seismic sites (SDC Dmax) and with 20' bay width. This approach substantially reduced the number of required structural designs and analyses, but did introduce some conservatism in this assessment example.

### 9.2.7 Evaluation of Collapse Margin and Acceptance Criteria

The previous section discussed how to simulate structural collapse, compute median collapse level ( $\hat{S}_{CT}$ ), and compute the collapse margin ratio (*CMR*). However, *CMR* does not account for unique spectral shape of rare ground motions. Appendix B discusses spectral shape and how it affects the predicted collapse capacity. Appendix B also develops simplified spectral shape factors (*SSFs*) that can be used to adjust the median collapse level ( $\hat{S}_{CT}$ ) to account for spectral shape effects. Table 9-3 (taken from Table 7.1a) and Table 9-4 (taken from Table 7.1b) show these factors for SDC B/C/$D_{min}$ and SDC $D_{max}$, respectively. The values in these tables depend on the building period (*T*), building ductility capacity ($\mu_c$), and the properties of nearby faults (approximately quantified by the seismic design category). The tables show that the *SSF* values range from 1.0 to 1.38 for SDC B/C/$D_{min}$ and from 1.0 to 1.65 for SDC $D_{max}$.

**Table 9-3 Spectral Shape Factors for SDC B/C/$D_{min}$**

| Spectral Shape Factor (SSF) - Seismic Design Category B/C/$D_{min}$ | | | | | | | | |
|---|---|---|---|---|---|---|---|---|
| *T* (sec) | Building Ductility Capacity, $\mu_C$ | | | | | | | |
| | 1.0 | 1.1 | 1.5 | 2 | 3 | 4 | 6 | >=8 |
| **<= 0.5** | 1.00 | 1.03 | 1.06 | 1.07 | 1.09 | 1.10 | 1.12 | 1.14 |
| **0.6** | 1.00 | 1.04 | 1.06 | 1.08 | 1.10 | 1.12 | 1.14 | 1.16 |
| **0.7** | 1.00 | 1.04 | 1.07 | 1.09 | 1.12 | 1.14 | 1.16 | 1.18 |
| **0.8** | 1.00 | 1.05 | 1.08 | 1.10 | 1.13 | 1.15 | 1.18 | 1.21 |
| **0.9** | 1.00 | 1.05 | 1.09 | 1.11 | 1.15 | 1.17 | 1.20 | 1.23 |
| **1.0** | 1.00 | 1.06 | 1.10 | 1.13 | 1.16 | 1.19 | 1.22 | 1.25 |
| **1.1** | 1.00 | 1.06 | 1.11 | 1.14 | 1.18 | 1.20 | 1.25 | 1.28 |
| **1.2** | 1.00 | 1.07 | 1.12 | 1.15 | 1.19 | 1.22 | 1.27 | 1.30 |
| **1.3** | 1.00 | 1.07 | 1.13 | 1.16 | 1.21 | 1.24 | 1.29 | 1.33 |
| **1.4** | 1.00 | 1.08 | 1.14 | 1.17 | 1.22 | 1.26 | 1.31 | 1.35 |
| **>= 1.5** | 1.00 | 1.08 | 1.14 | 1.19 | 1.24 | 1.28 | 1.34 | 1.38 |

The adjusted collapse margin ratio (*ACMR*) is computed by multiplying *SSF* (from Table 9-3 or Table 9-4) and *CMR* (from Table 9-2). Later, Table 9-7 will show this margin adjustment for the RC archetypes.

**Table 9-4 Spectral Shape Factors for SDC $D_{max}$**

| Spectral Shape Factor (SSF) - Seismic Design Category $D_{max}$ | | | | | | | | |
|---|---|---|---|---|---|---|---|---|
| *T* (sec) | Building Ductility Capacity, $\mu_C$ | | | | | | | |
| | 1.0 | 1.1 | 1.5 | 2 | 3 | 4 | 6 | >=8 |
| **<= 0.5** | 1.00 | 1.07 | 1.13 | 1.17 | 1.21 | 1.25 | 1.30 | 1.34 |
| **0.6** | 1.00 | 1.08 | 1.14 | 1.18 | 1.23 | 1.26 | 1.32 | 1.36 |
| **0.7** | 1.00 | 1.08 | 1.15 | 1.19 | 1.24 | 1.28 | 1.34 | 1.39 |
| **0.8** | 1.00 | 1.09 | 1.16 | 1.20 | 1.26 | 1.30 | 1.37 | 1.42 |
| **0.9** | 1.00 | 1.09 | 1.17 | 1.21 | 1.28 | 1.32 | 1.39 | 1.45 |
| **1.0** | 1.00 | 1.10 | 1.18 | 1.23 | 1.29 | 1.34 | 1.41 | 1.47 |
| **1.1** | 1.00 | 1.11 | 1.19 | 1.24 | 1.31 | 1.36 | 1.44 | 1.50 |
| **1.2** | 1.00 | 1.11 | 1.20 | 1.25 | 1.33 | 1.38 | 1.46 | 1.53 |
| **1.3** | 1.00 | 1.12 | 1.21 | 1.26 | 1.34 | 1.40 | 1.49 | 1.56 |
| **1.4** | 1.00 | 1.12 | 1.22 | 1.28 | 1.36 | 1.42 | 1.52 | 1.59 |
| **>= 1.5** | 1.00 | 1.13 | 1.22 | 1.29 | 1.38 | 1.44 | 1.54 | 1.62 |

In addition to quantifying the *ACMR*, the composite uncertainty ($\beta_{TOT}$) in collapse capacity is also needed.

Table 9-5 is replicated from Chapter 7, and shows composite uncertainties, which account for the variability between ground motion records of a given intensity (defined as a constant $\beta_{RTR} = 0.40$), the uncertainty in the nonlinear structural modeling (A – superior), the quality of the test data used to calibrate the element models (B – good), and the quality of the structural system design requirements (A – superior). For this example assessment, the composite uncertainty is $\beta_{TOT} = 0.55$ and is shown in bold.

Knowing the composite uncertainty and an acceptable conditional collapse probability ($P[C|S_{MT}]$), the acceptable collapse margin can be computed. Table 9-6 shows these acceptable *ACMR* computed assuming a lognormal distribution of collapse capacity. The performance criteria in Chapter 7 include a conditional collapse probability of $\leq$ 20% for all archetype buildings, and $\leq$ 10% for the average of the buildings in each performance group. This corresponds to a required *ACMR* of 1.59 (using $\beta_{TOT} = 0.60$) for every archetype building and a required average *ACMR* of 2.02 for each Performance Group.

**Table 9-5 Total Uncertainties ($\beta_{TOT}$) Accounting for the Quality of Test Data, Quality of Structural Design Requirements, and Uncertainty in Nonlinear Model**

| Uncertainty - Nonlinear Model | **A - Superior** | | | |
|---|---|---|---|---|
| Uncertainty - Quality of Test Data | Uncertainty - Quality of Design Requirements | | | |
| | **A - Super.** | B - Good | C - Fair | D - Poor |
| A - Superior | 0.55 | 0.55 | 0.65 | 0.80 |
| **B - Good** | **0.55** | 0.60 | 0.70 | 0.85 |
| C - Fair | 0.65 | 0.70 | 0.80 | 0.90 |
| D - Poor | 0.80 | 0.85 | 0.90 | 1.00 |

**Table 9-6 Acceptable Adjusted Collapse Margin Ratios (*ACMR*), as Based on the Composite Uncertainty and the Acceptable Conditional Collapse Probability**

| Composite Uncertainty | Target Conditional Collapse Probability | | | | |
|---|---|---|---|---|---|
| | 5% | 10% | 15% | 20% | 25% |
| 0.55 | 2.47 | **2.02** | 1.77 | **1.59** | 1.45 |
| 0.60 | 2.68 | 2.16 | 1.86 | 1.66 | 1.50 |
| 0.65 | 2.91 | 2.30 | 1.96 | 1.73 | 1.55 |
| 0.70 | 3.16 | 2.45 | 2.07 | 1.80 | 1.60 |
| 0.75 | 3.43 | 2.61 | 2.18 | 1.88 | 1.66 |
| 0.80 | 3.73 | 2.78 | 2.29 | 1.96 | 1.72 |
| 0.85 | 4.05 | 2.97 | 2.41 | 2.05 | 1.77 |
| 0.90 | 4.40 | 3.16 | 2.54 | 2.13 | 1.84 |
| 0.95 | 4.77 | 3.37 | 2.68 | 2.23 | 1.90 |
| 1.00 | 5.18 | 3.60 | 2.82 | 2.32 | 1.96 |
| 1.15 | 6.63 | 4.36 | 3.30 | 2.63 | 2.17 |
| 1.20 | 7.20 | 4.65 | 3.47 | 2.75 | 2.25 |

Table 9-7 presents the final results and acceptance criteria for each of the 18 archetype designs. This shows the collapse margin ratio computed directly from IDA (*CMR*), the *SSF*, and the final adjusted collapse margin ratio (*ACMR*). The acceptable margins are then shown, and each archetype is shown to either pass of fail the acceptance criteria. Average margin results are also shown for the two groups of six high-seismic designs with 20' bay spacing; these sets of buildings represent the critical design conditions of the two high-seismic performance groups.

The comparisons in the second half of the table show that the high-seismic designs control and have lower *ACMR*. Therefore, the low-seismic performance groups were not focused on in this assessment. Also, the 20-foot bay widths control with lower *ACMR*, so the 30-foot bay width buildings were not focused on in this assessment.

In reviewing the critical subsets of the two controlling performance groups, namely perimeter- and space-frame buildings designed for a high-seismic location and having 20' bay spacing, results show that the majority of the archetype buildings have acceptable *ACMR*, but a disturbing trend is evident. For space- and perimeter-frame buildings taller than four-stories, the *ACMR* decreases substantially with increased building height. This causes the 20-story perimeter frame building to have an unacceptable *ACMR* and causes the average *ACMR* of the perimeter frame buildings to also be unacceptable. In addition, the one-story perimeter frame building has an *ACMR* that is slightly below the acceptable value.

**Table 9-7 Summary of Final Collapse Margins and Comparison to Acceptance Criteria**

| Archetype Design ID Number | Design Configuration | | | Computed Collapse Margin | | | | Acceptance Check | |
|---|---|---|---|---|---|---|---|---|---|
| | No. Stories | Framing / Gravity Loads | Seismic SDC | *CMR* | $\mu_c$ | *SSF* | *ACMR* | Accept. *ACMR* | Pass/Fail |
| Maximum Seismic ($D_{max}$) and Low Gravity (Perimeter Frame) Designs, 20' Bay Width | | | | | | | | | |
| 2069 | 1 | P | $D_{max}$ | 1.18 | 16.1 | 1.34 | 1.58 | 1.59 | Near Pass |
| 2064 | 2 | P | $D_{max}$ | 1.50 | 19.5 | 1.34 | 2.01 | 1.59 | Pass |
| 1003 | 4 | P | $D_{max}$ | 1.61 | 9.2 | 1.42 | 2.29 | 1.59 | Pass |
| 1011 | 8 | P | $D_{max}$ | 1.25 | 7.9 | 1.62 | 2.02 | 1.59 | Pass |
| 5013 | 12 | P | $D_{max}$ | 1.22 | 5.9 | 1.54 | 1.88 | 1.59 | Pass |
| 5020 | 20 | P | $D_{max}$ | 0.82 | 3.3 | 1.40 | 1.14 | 1.59 | **FAIL** |
| Mean/Acceptable: | | -- | -- | -- | | -- | 1.82 | 2.02 | **FAIL** |
| Maximum Seismic ($D_{max}$) and High Gravity (Space Frame) Designs, 20' Bay Width | | | | | | | | | |
| 2061 | 1 | S | $D_{max}$ | 1.96 | 16.1 | 1.34 | 2.62 | 1.59 | Pass |
| 1001 | 2 | S | $D_{max}$ | 2.06 | 14.3 | 1.34 | 2.76 | 1.59 | Pass |
| 1008 | 4 | S | $D_{max}$ | 1.78 | 9.6 | 1.42 | 2.53 | 1.59 | Pass |
| 1012 | 8 | S | $D_{max}$ | 1.63 | 6.2 | 1.55 | 2.52 | 1.59 | Pass |
| 5014 | 12 | S | $D_{max}$ | 1.59 | 6.9 | 1.58 | 2.51 | 1.59 | Pass |
| 5021 | 20 | S | $D_{max}$ | 1.25 | 3.5 | 1.41 | 1.76 | 1.59 | Pass |
| Mean/Acceptable: | | -- | -- | -- | | -- | 2.45 | 2.02 | Pass |
| Comparison of Results - SDC $D_{max}$ & $D_{min}$ Seismic Design Conditions, 20' Bay Width | | | | | | | | | |
| 1011 | 8 | P | $D_{max}$ | 1.25 | 7.9 | 1.62 | 2.02 | 1.59 | Pass |
| 6011 | 8 | P | $D_{min}$ | 2.12 | 2.3 | 1.20 | 2.55 | 1.59 | Pass |
| 5013 | 12 | P | $D_{max}$ | 1.22 | 5.9 | 1.54 | 1.88 | 1.59 | Pass |
| 6013 | 12 | P | $D_{min}$ | 2.00 | 2.5 | 1.22 | 2.43 | 1.59 | Pass |
| 5020 | 20 | P | $D_{max}$ | 0.82 | 3.3 | 1.40 | 1.14 | 1.59 | **FAIL** |
| 6020 | 20 | P | $D_{min}$ | 3.70 | 1.8 | 1.17 | 4.32 | 1.59 | Pass |
| 5021 | 20 | S | $D_{max}$ | 1.25 | 3.5 | 1.41 | 1.76 | 1.59 | Pass |
| 6021 | 20 | S | $D_{min}$ | 1.73 | 2.4 | 1.21 | 2.09 | 1.59 | Pass |
| Comparison of Results - 20-Foot and 30-Foot Bay Width Designs (SDC $D_{max}$) | | | | | | | | | |
| 1003 | 4 | P-20 | $D_{max}$ | 1.61 | 9.2 | 1.42 | 2.29 | 1.59 | Pass |
| 1009 | 4 | P-30 | $D_{max}$ | 1.98 | 11.4 | 1.42 | 2.81 | 1.59 | Pass |
| 1008 | 4 | S-20 | $D_{max}$ | 1.78 | 9.6 | 1.42 | 2.53 | 1.59 | Pass |
| 1010 | 4 | S-30 | $D_{max}$ | 2.5 | 11.0 | 1.42 | 3.55 | 1.59 | Pass |

At this point, the "newly proposed" RC SMF system, as currently defined, does not meet the collapse performance objectives of this Methodology, and would need an adjustment in the design requirements to meet the performance intent. To address the problem of decreasing *ACMR* for taller buildings, adjustments to the design requirements are considered. One alternative would be to limit the proposed system to a maximum height of 12-stories (or 160'), or to require a space frame system for buildings taller than 160'. Even with such a height limit, however, the average *ACMR* for the first performance group would still not meet the required value of 2.02, so additional adjustments would be needed to improve the overall performance of the perimeter frame buildings.

### 9.2.8 Iteration: Adjustment of Design Requirements to Meet Performance Goals

The RC SMF system did not meet the performance criteria with the initially used set of design requirements and SPFs. For the initially assessed designs, the *ACI 318-05* design requirements were used along with $R = 8$, $C_d = 5.5$, an inter-story drift limit of 2%, and the minimum design base shear requirement from ASCE/SEI 7-05. These requirements must now be modified in some way that will improve the RC SMF collapse performance and cause the system to meet the performance criteria.

When deciding how to change the design requirements and SPFs, the specific performance problems should be addressed to the extent possible. For the initial RC SMF assessment, Table 9-7 showed that the one-story perimeter frame building does not meet the *ACMR* requirement of 1.59; this deficiency would need to be addressed for this RC SMF system to attain the collapse performance required by this document. For brevity, this example does not address this short period issue. If this were to be addressed, it could be addressed in many ways, such as an added strength requirement for short-period structures. This could be accomplished through a period-dependent R-factor that is lower for shorter period buildings (Miranda et al. 1994), but this approach is inconsistent with the current structure of ASCE/SEI 7-05, which only includes a single value for R, independent of period. Another approach would be to include an added strength requirement that only affects perimeter frame buildings, since they tend to have low $\Omega$ and lower collapse capacity.

Table 9-7 also showed a more important and disturbing trend, that the adjusted collapse margin ratio (*ACMR*) decreased (higher collapse risk) with increasing height. Haselton (2006) showed that this poor performance is caused by the damage localizing more for taller moment resisting frames (MRFs); this is driven primarily by higher P-Delta effects as the building height increases. This issue could be addressed in various ways. More conservative beam-column strength ratios could be developed for taller buildings, in order to cause the damage to spread more uniformly over the height of the building. To reduce P-Delta effects, more restrictive drift limits could be imposed. Strength requirements could also be increased for taller buildings, by using a period dependent R factor; in a recent paper, Krawinkler and Zareian (2007) illustrated how the R factor would need to change, as a function of period, in order to create uniform collapse probabilities for moment frame buildings of varying height.

In this example, the minimum design base shear is increased in the effort to solve this problem. This solution is not the most direct way to solve the specifically identified problems of damage localization and P-Delta for taller MRF buildings, but it is a simple solution that works. Specifically, the ASCE/SEI 7-05 minimum base shear requirement (ASCE 2006a, equation 12.8-5) is replaced by the ASCE 7-02 requirement (ASCE 2002, equation 9.5.5.2.1-3). The ASCE 7-02 minimum based shear requirement equation is shown as Equation 9-1.

$$C_s \geq 0.044 S_{DS} I \tag{9-1}$$

This change to the design requirements impacted only the design of the 12- and 20-story buildings in SDC $D_{max}$ and the 8-, 12-, and 20-story buildings in SDC $D_{min}$. Table 9-8 shows the design information for the redesigned buildings. To get a sense of how this impacts the design base shear strengths, comparison to Table 9-1 shows that the design base shear coefficient ($V/W$) increased from 0.022 to 0.044 for the 20-story building in SDC $D_{max}$, and increased from 0.010 to 0.017 for the 20-story building in SDC $D_{min}$. The base shear coefficient also increased, to a lesser extent, for the other buildings shown in Table 9-8.

The building designs were revised and the collapse assessments were completed for the revised designs. Table 9-9 shows the updated collapse performance results, with the bold italic lines highlighting the designs that were affected by the change to the minimum base shear requirement. This shows that each archetype building meets the performance requirement of $ACMR \geq 1.59$ (i.e. 20% conditional collapse probability) and the average $ACMR \geq 2.02$ for each Performance Group (i.e. 10% conditional collapse probability)[3]. This shows that after modifying the minimum design base shear requirement, the "newly proposed" RC SMF system attains the required collapse performance and could be added as a "new system" in the building code provisions[4].

Table 9-9 shows that building archetypes were only assessed up to a height of 20 stories. Taller buildings were not assessed because of the limitations of the ground motion record set, which is applicable only to buildings with elastic fundamental periods below 4.0 seconds (Appendix A, Chapter 11).

[3] The performance of the one-story building causes the *ACMR* values to be slightly below the required values for the perimeter frame SDC $D_{max}$ Performance Group. For simplicity, this is not addressed in this example, and it is assumed that the SDC $D_{max}$ perimeter frame Performance Group meets the performance requirements. In the context of a complete performance assessment, this deficiency would need to be addressed.

Even so, Table 9-9 shows a trend that the collapse safety increases with building height. As long as this trend is observed for buildings with fundamental periods below 4.0 seconds, and the peer review committee believes that the trend is stable and defensible, then a height limit would not need to be imposed for this RC SMF structural system.

**Table 9-8 Archetype Structural Design Properties, for Buildings Redesigned Considering a Minimum Base Shear Requirement**

| Archetype Design ID Number | No. of Stories | Key Archetype Design Parameters | | | | | |
|---|---|---|---|---|---|---|---|
| | | Framing / Gravity Loads | Seismic Design Criteria | | | | $S_{MT}$ [$T$] (g) |
| | | | SDC | $R_{eff}$ [1] | $T$ (sec.) | $V/W$ (g) | |
| Re-Design Maximum Seismic ($D_{max}$) Perimeter Frame Designs, 20' Bay Width | | | | | | | |
| 1013 | 12 | P | $D_{max}$ | 6.4 | 2.13 | 0.044 | 0.42 |
| 1020 | 20 | P | $D_{max}$ | 4.1 | 3.36 | 0.044 | 0.27 |
| Re-Design - Maximum Seismic ($D_{max}$) Space Frame Designs, 20' Bay Width | | | | | | | |
| 1014 | 12 | S | $D_{max}$ | 6.4 | 2.13 | 0.044 | 0.42 |
| 1021 | 20 | S | $D_{max}$ | 4.1 | 3.36 | 0.044 | 0.27 |
| Re-Design - Low Seismic Designs, 20' Bay Width (SDC $D_{min}$) | | | | | | | |
| 4011 | 8 | P | $D_{min}$ | 5.8 | 1.60 | 0.017 | 0.15 |
| 4013 | 12 | P | $D_{min}$ | 6.6 | 2.28 | 0.017 | 0.10 |
| 4020 | 20 | P | $D_{min}$ | 4.2 | 3.60 | 0.017 | 0.065 |
| 4021 | 20 | S | $D_{min}$ | 8.0 | 3.60 | 0.017 | 0.065 |

1. Effective value of R due to limits on the seismic coefficient, Cs.

### Calculation of $\Omega_0$ using Final Set of Archetype Designs

At this point, the $\Omega_0$ value can be established for use in the proposed design provisions. Chapter 7 specifies that the $\Omega_o$ value should be conservatively based on individual $\Omega$ values, and the average values for each performance group. The final $\Omega_o$ value should be rounded to the nearest 0.5, and limited to a maximum value of 3.0.

This portion of this example is not entirely complete, because the full set of six archetypes was only completed for the two collapse-critical high-seismic performance groups. Only a subset of buildings from the low-seismic performance groups was evaluated, since we reasoned that this subset possessed the critical collapse performance of that performance group.

The average $\Omega$ values for the high-seismic performance groups are 1.7 and 2.8, for low- and high-gravity loading, respectively. The average $\Omega$ value for the subset of low-seismic designs considered is 2.1, but this includes mostly perimeter frame buildings (which tend to have lower $\Omega$ values) and does not include low-rise buildings (which tend to have higher $\Omega$ values). This average would be larger if the full set of buildings were utilized.

**Table 9-9 Summary of Final Collapse Margins and Comparison to Acceptance Criteria, for Buildings Redesigned with an Updated Minimum Base Shear Requirement**

| Arch. Design ID Number | Design Configuration | | | | Computed Collapse Margin | | | | Acceptance Check | |
|---|---|---|---|---|---|---|---|---|---|---|
| | No. of Stories | Framing / Gravity Loads | Seismic SDC | Static $\Omega$ | *CMR* | $\mu_c$ | *SSF* | *ACMR* | Accept. *ACMR* | Pass/Fail |
| Maximum Seismic ($D_{max}$) and Low Gravity (Perimeter Frame) Designs, 20' Bay Width | | | | | | | | | | |
| 2069 | 1 | P | $D_{max}$ | 1.6 | 1.18 | 16.1 | 1.34 | 1.58 | 1.59 | Near Pass |
| 2064 | 2 | P | $D_{max}$ | 1.8 | 1.50 | 19.5 | 1.34 | 2.01 | 1.59 | Pass |
| 1003 | 4 | P | $D_{max}$ | 1.6 | 1.61 | 9.2 | 1.42 | 2.29 | 1.59 | Pass |
| 1011 | 8 | P | $D_{max}$ | 1.6 | 1.25 | 7.9 | 1.62 | 2.02 | 1.59 | Pass |
| ***1013*** | ***12*** | ***P*** | ***$D_{max}$*** | ***1.7*** | ***1.45*** | ***10.0*** | ***1.62*** | ***2.35*** | ***1.59*** | ***Pass*** |
| ***1020*** | ***20*** | ***P*** | ***$D_{max}$*** | ***1.6*** | ***1.66*** | ***7.2*** | ***1.59*** | ***2.64*** | ***1.59*** | ***Pass*** |
| Mean/Acceptable: | | -- | -- | ***1.7*** | -- | | -- | ***2.15*** | ***2.02*** | **Pass** |
| Maximum Seismic ($D_{max}$) and High Gravity (Space Frame) Designs, 20' Bay Width | | | | | | | | | | |
| 2061 | 1 | S | $D_{max}$ | 4.0 | 1.96 | 16.1 | 1.34 | 2.62 | 1.59 | Pass |
| 1001 | 2 | S | $D_{max}$ | 3.5 | 2.06 | 14.3 | 1.34 | 2.76 | 1.59 | Pass |
| 1008 | 4 | S | $D_{max}$ | 2.7 | 1.78 | 9.6 | 1.42 | 2.53 | 1.59 | Pass |
| 1012 | 8 | S | $D_{max}$ | 2.3 | 1.63 | 6.2 | 1.55 | 2.52 | 1.59 | Pass |
| ***1014*** | ***12*** | ***S*** | ***$D_{max}$*** | ***2.1*** | ***1.59*** | ***5.8*** | **1.53** | ***2.44*** | ***1.59*** | ***Pass*** |
| ***1021*** | ***20*** | ***S*** | ***$D_{max}$*** | ***2.0*** | ***1.98*** | ***9.1*** | **1.62** | ***3.21*** | ***1.59*** | ***Pass*** |
| Mean/Acceptable: | | -- | -- | ***2.8*** | -- | | -- | ***2.68*** | ***2.02*** | ***Pass*** |
| Comparison of Results - SDC $D_{max}$ & $D_{min}$ Seismic Design Conditions, 20' Bay Width | | | | | | | | | | |
| 1011 | 8 | P | $D_{max}$ | 1.6 | 1.25 | 7.9 | 1.62 | 2.02 | 1.59 | Pass |
| ***4011*** | ***8*** | ***P*** | ***$D_{min}$*** | ***1.8*** | ***1.93*** | ***2.8*** | 1.23 | ***2.37*** | ***1.59*** | ***Pass*** |
| ***1013*** | ***12*** | ***P*** | ***$D_{max}$*** | ***1.7*** | ***1.45*** | ***10.0*** | 1.62 | ***2.35*** | ***1.59*** | ***Pass*** |
| ***4013*** | ***12*** | ***P*** | ***$D_{min}$*** | ***1.8*** | ***2.29*** | ***3.4*** | 1.25 | ***2.87*** | ***1.59*** | ***Pass*** |
| ***1020*** | ***20*** | ***P*** | ***$D_{max}$*** | ***1.6*** | ***1.66*** | ***7.2*** | 1.59 | ***2.64*** | ***1.59*** | ***Pass*** |
| ***4020*** | ***20*** | ***P*** | ***$D_{min}$*** | ***1.8*** | ***2.36*** | ***3.0*** | 1.24 | ***2.92*** | ***1.59*** | ***Pass*** |
| ***1021*** | ***20*** | ***S*** | ***$D_{max}$*** | ***2.0*** | ***1.98*** | ***9.1*** | 1.62 | ***3.21*** | ***1.59*** | ***Pass*** |
| ***4021*** | ***20*** | ***S*** | ***$D_{min}$*** | ***2.8*** | ***3.87*** | ***3.0*** | 1.24 | ***4.80*** | ***1.59*** | ***Pass*** |
| Comparison of Results - 20-Foot and 30-Foot Bay Width Designs (SDC $D_{max}$) | | | | | | | | | | |
| 1003 | 4 | P-20 | $D_{max}$ | 1.6 | 1.61 | 9.2 | 1.42 | 2.29 | 1.59 | Pass |
| 1009 | 4 | P-30 | $D_{max}$ | 1.6 | 1.98 | 11.4 | 1.42 | 2.81 | 1.59 | Pass |
| 1008 | 4 | S-20 | $D_{max}$ | 2.7 | 1.78 | 9.6 | 1.42 | 2.53 | 1.59 | Pass |
| 1010 | 4 | S-30 | $D_{max}$ | 3.3 | 2.50 | 11.0 | 1.42 | 3.55 | 1.59 | Pass |

The proposed $\Omega_o$ value can now be based on the above values, subject to the Peer Review process. For this example, the upper-bound value of $\Omega_o$ = 3.0 is warranted, due to the average $\Omega$ value of 2.8 observed for one of the performance groups and the large values of 3.5 and 4.0 observed for some individual archetype buildings.

### *9.2.9 Summary Observations - Reinforced Concrete Special Moment Frame System*

This example shows that current seismic provisions for RC SMF systems in ACI 318-05 and ASCE/SEI 7-05 provide an acceptable level of collapse safety in SDC D, with an important modification of imposing an additional

minimum base shear requirement from the ASCE 7-02 provisions. In addition, it demonstrates that the Methodology is reasonably calibrated in that recent building code design provisions lead to acceptable collapse safety, as defined by the Methodology. This example also illustrates how the Methodology could be used as a tool for testing possible changes to building code requirements, and informing code change proposals.

## 9.3 Example Application - Reinforced Concrete Ordinary Moment Frame System

### *9.3.1 Introduction*

In this example, a reinforced concrete (RC) ordinary moment frame (OMF) system (as defined by ACI 318-05 and ASCE/SEI 7-05) is considered as if it were a new system proposed for inclusion in ASCE/SEI 7-05.

This example illustrates the Methodology for limited ductility systems, which are only permitted in lower seismic design categories, are typical of construction in the Central and Eastern United States, and are designed for a much lower ratio of lateral load to gravity load. Since these systems lack the capacity design and ductile detailing provisions of special moment frames, OMF systems are susceptible to additional damage modes, such as column shear failure leading to rapid strength and stiffness deterioration. This also creates the need to incorporate component limit state checks for collapse modes that are not simulated directly in the nonlinear analysis.

### *9.3.2 Overview and Approach*

The structural system is defined by the design and detailing provisions of ASCE/SEI 7-05 and ACI 318-05, and is evaluated using the methods of Chapters 3 through 7. Once design requirements are specified, a set of structural system archetypes are developed for RC OMF buildings, nonlinear models are developed to simulate structural collapse, models are analyzed to predict the collapse capacities of each design, and collapse margin ratios (*CMR*) are evaluated and compared to acceptance criteria.

This example has been adapted from collaborative research on the development of structural archetypes for RC OMFs, calibration of nonlinear element models for collapse simulation, simulation of structural response to collapse, spectral shape considerations, and treatment of uncertainties (Liel and Deierlein 2008).

### 9.3.3 *Structural System Information*

**Design Requirements**

This example utilizes ACI 318-05 design requirements, which are extremely detailed and represent years of accumulated research and building code development. As such, for the purpose of assessing composite uncertainty, the design requirements are categorized as "A-Superior" to reflect the high degree of confidence in the design equations for reinforced concrete.

**Test Data**

The element models used in this study are the same as those in the RC SMF study, and based on existing published test data from the Pacific Earthquake Engineering Research Center's Structural Performance Database (PEER 2006, Berry et al. 2004). Although extensive data is available for reinforced concrete elements, due to limitations and variations of experimental procedures and intentions, the test data can not provide the exact requirements of model parameters and behavior. Accordingly, for the purpose of assessing the total uncertainty, the test data is categorized as "B-Good" (again, in agreement with the SMF example).

### 9.3.4 *Seismic Design Criteria*

RC OMFs are permitted only in SDCs B and below. The highest SDC category will typically govern the evaluation of structural performance factors. Accordingly, the lateral load levels used in the RC OMF system example are shown in Figure 9-8, labeled $B_{min}$ and $B_{max}$. A subset of archetype models is also evaluated at the limits of SDC C, where OMFs are not permitted, to assess whether the Methodology will confirm the validity of the current code limits.

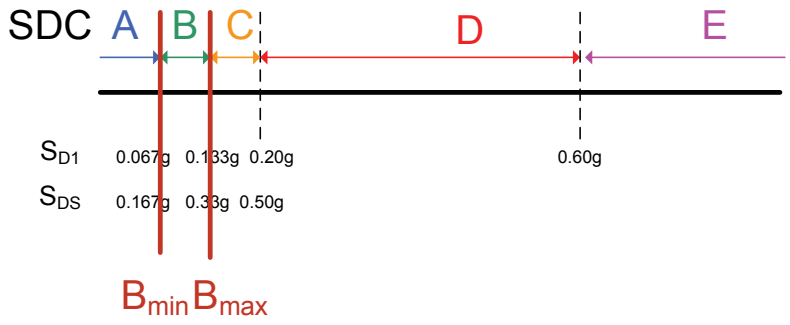


Figure 9-8 Definition of SDCs according to ASCE/SEI 7-05, as well as the seismic design criteria used in RC OMF example for evaluating SDC B.

### 9.3.5 Identification of RC OMF Archetype Configurations

Figure 9-9 shows the two-dimensional three-bay multi-story frame that is used to model reinforced concrete frame buildings in this example. This model is the same to the one used to evaluate the RC SMF system, and includes joint panel elements, beam and column elements, elastic foundation springs, and a leaning column to account for P-Delta effects due to the load on the gravity system.

A set of index archetype designs was developed to explore the range of possible configurations represented by an RC OMF system definition. The intent of this example is to demonstrate the applicability of the Methodology to RC OMF systems in general. Since it is not intended to be a comprehensive assessment of the system, the total number of archetype structures and performance groups are smaller than those used in the RC SMF study, and do not include all possible design variations that would be permitted by the code.

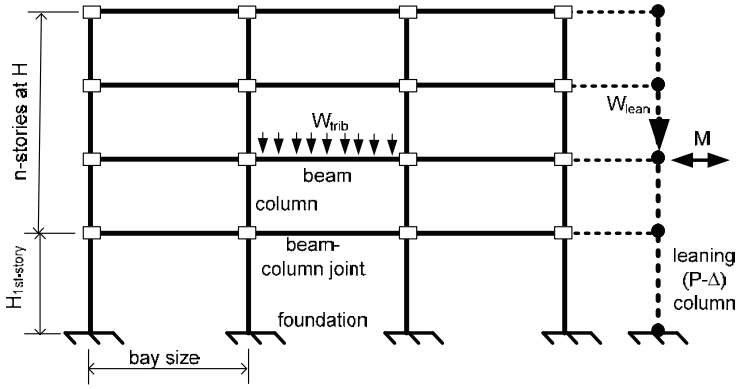


Figure 9-9 Archetype analysis model for RC OMFs

Archetype designs are organized into four performance groups that represent the range of allowable design ground motion intensities (lateral loading) and gravity load intensities. These performance groups are similar to those used in the evaluation of the RC SMF systems.

- Maximum seismic design criteria (SDC $B_{max}$), high gravity loading
- Maximum seismic design criteria (SDC $B_{max}$), low gravity loading
- Minimum seismic design criteria (SDC $B_{min}$), high gravity loading
- Minimum seismic design criteria (SDC $B_{min}$), low gravity loading

The "high gravity" systems are space frames, which are typical for OMF designs. "Low gravity" systems could represent either perimeter frames of a flat plate system or the perimeter framing of a one-way joist system (frames running parallel to the joist system). Figure 9-10 and Figure 9-11 show the

layout of the archetype space and perimeter frame systems. Buildings have a bay spacing of 30’ and cover a range of building heights (2, 4, 8, or 12 stories). The span length is different from the default of 20’ used in the SMF study, but is chosen here to better reflect the typical configurations of gravity-dominated OMF designs. For space frames, a transverse span (*W*) of 35’ was used to maximize the gravity load contribution, whereas a smaller transverse span (*W*) of 30’ was used for the lightly loaded perimeter frames.

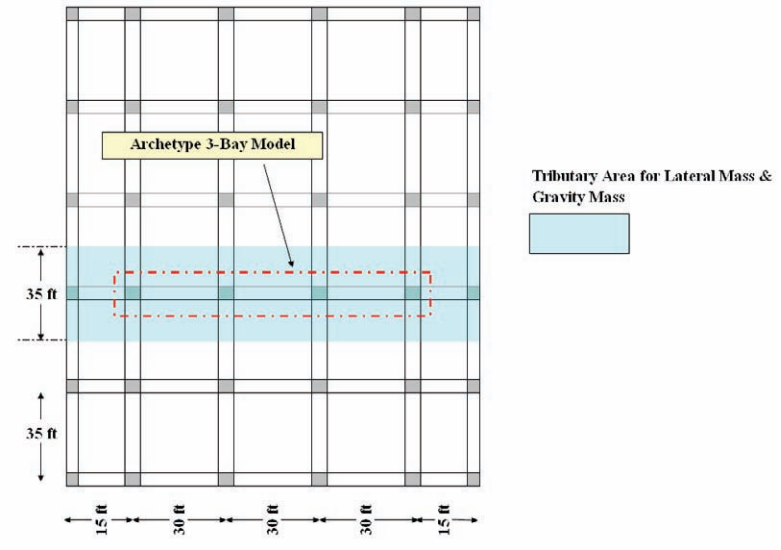


Figure 9-10 High gravity (space frame) layout.

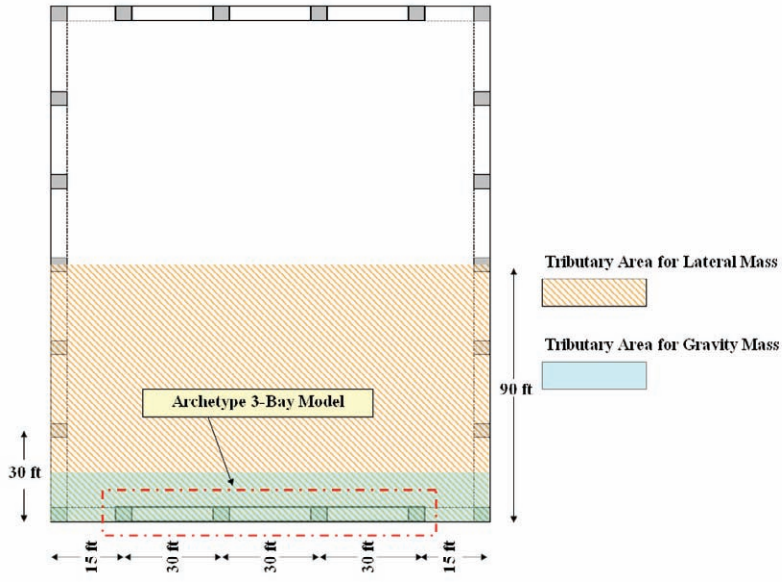


Figure 9-11 Low gravity (perimeter frame) layout.

Each of the index archetype configurations was fully designed in accordance with the governing design requirements (ASCE/SEI 7-05, ACI 318-05). Additional information on archetype designs in provided in Appendix C.

Table 9-10 summarizes the properties of the OMF archetype designs needed to evaluate SDC B, including the design base shear and code-calculated structural period. The design documentation provided is consistent with that provided for the SMF models. The documentation for Design ID 9203 is shown in Figure 9-12. Similar documentation has been maintained for all other archetype designs.

**Table 9-10 Archetype Design Properties, SDC B**

| Archetype Design ID Number | No. of Stories | Key Archetype Design Parameters | | | | | |
|---|---|---|---|---|---|---|---|
| | | Framing / Gravity Loads | Seismic Design Criteria | | | | $S_{MT}$ [$T$] (g) |
| | | | SDC | $R$ | $T$ (sec.) | $V/W$ (g) | |
| Minimum Seismic, SDC $B_{min}$, Low Gravity (Perimeter Frame) Designs | | | | | | | |
| 9101 | 2 | P | $B_{min}$ | 3 | 0.55 | 0.041 | 0.18 |
| 9103 | 4 | P | $B_{min}$ | 3 | 0.99 | 0.023 | 0.10 |
| 9105 | 8 | P | $B_{min}$ | 3 | 1.81 | 0.012 | 0.06 |
| 9107 | 12 | P | $B_{min}$ | 3 | 2.59 | 0.010 | 0.04 |
| Minimum Seismic, SDC $B_{min}$, High Gravity (Space Frame) Designs | | | | | | | |
| 9102 | 2 | S | $B_{min}$ | 3 | 0.55 | 0.041 | 0.18 |
| 9104 | 4 | S | $B_{min}$ | 3 | 0.99 | 0.023 | 0.1 |
| 9106 | 8 | S | $B_{min}$ | 3 | 1.81 | 0.012 | 0.06 |
| 9108 | 12 | S | $B_{min}$ | 3 | 2.59 | 0.010 | 0.04 |
| Maximum Seismic, SDC $B_{max}$, Low Gravity (Perimeter Frame) Designs | | | | | | | |
| 9201 | 2 | P | $B_{max}$ | 3 | 0.51 | 0.087 | 0.39 |
| 9203 | 4 | P | $B_{max}$ | 3 | 0.93 | 0.048 | 0.22 |
| 9205 | 8 | P | $B_{max}$ | 3 | 1.70 | 0.026 | 0.12 |
| 9207 | 12 | P | $B_{max}$ | 3 | 2.44 | 0.018 | 0.08 |
| Maximum Seismic, SDC $B_{max}$, High Gravity (Space Frame) Designs | | | | | | | |
| 9202 | 2 | S | $B_{max}$ | 3 | 0.51 | 0.087 | 0.39 |
| 9204 | 4 | S | $B_{max}$ | 3 | 0.93 | 0.048 | 0.22 |
| 9206 | 8 | S | $B_{max}$ | 3 | 1.70 | 0.026 | 0.12 |
| 9208 | 12 | S | $B_{max}$ | 3 | 2.44 | 0.018 | 0.08 |

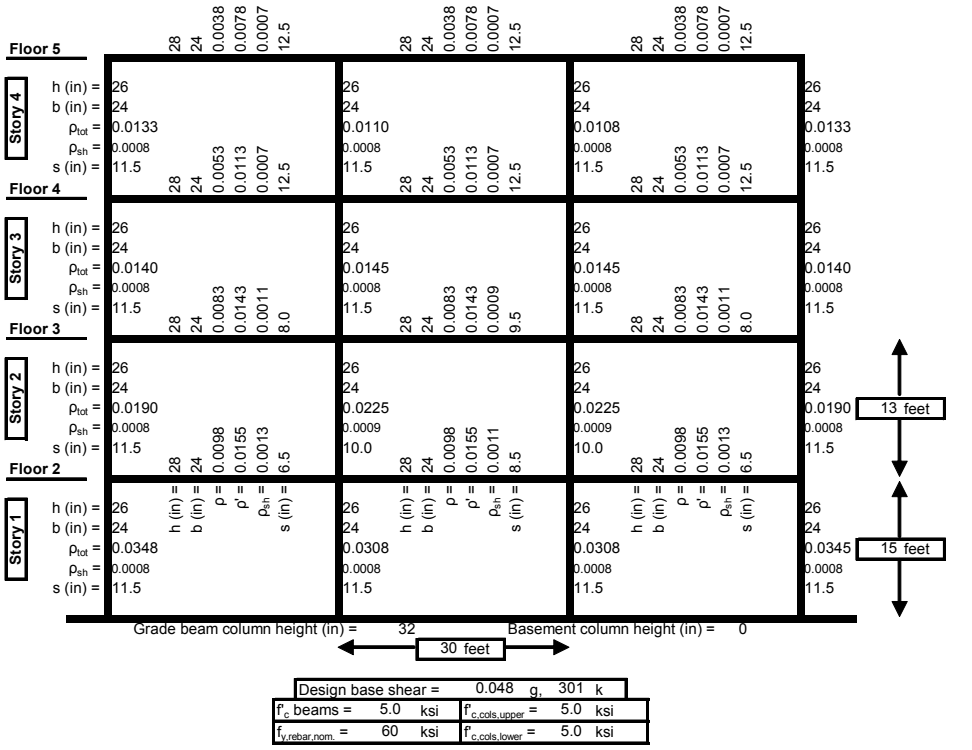


(a)

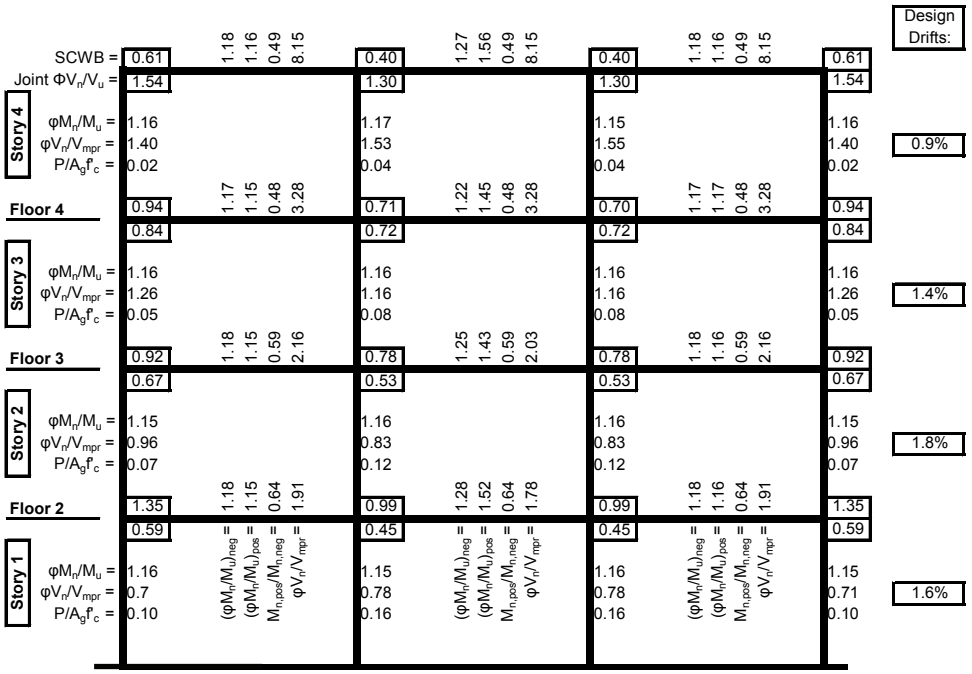


(b)

Figure 9-12 Design documentation for a 4-story RC OMF perimeter frame

### 9.3.6 Nonlinear Analysis Models and Results

The parameters used in the nonlinear models were developed in the same manner as those used in the RC SMF system study. For illustration, Figure 9-13 shows the predicted modeling parameters for each element of design ID 9203. As expected, these structures are modeled to have substantially less ductility than their SMF counterparts. These differences are reflected in the deformation capacity ($\theta_{cap,pl}$ and $\theta_{pc}$) and cyclic deterioration parameters ($\lambda$). As with the SMF example, these models were implemented in the OpenSees software platform, developed by the Pacific Earthquake Engineering Research Center (OpenSees 2006).

Shear failure in columns is not explicitly included in the analysis models, and is incorporated through post-processing as a non-simulated failure mode. Shear failure is difficult to simulate using available technologies and test data, and is accounted for in post-processing for this reason; however, if possible, it would be better to incorporate this failure mode directly into the simulation.

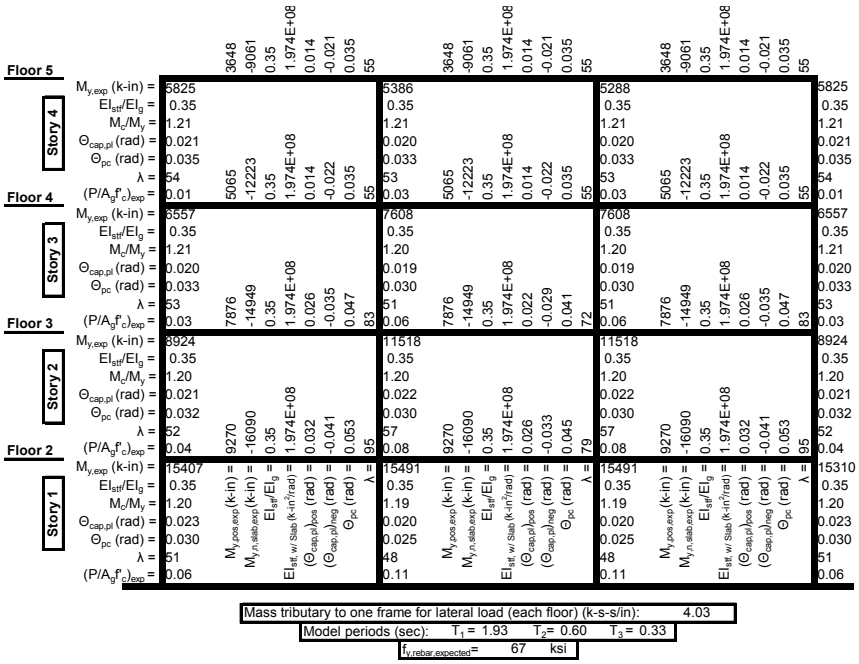


Figure 9-13 Structural modeling documentation for a 4-story RC OMF archetype (9203).

For the purpose of assessing uncertainty, the modeling is rated "B-Good". The same modeling techniques were implemented for the OMFs as in the SMF study, capturing post-peak degrading response, as well the modes of strength and stiffness deterioration associated with flexure and flexure-shear degradation. However, because of only moderate confidence in the ability to

predict collapse modes that occur after shear failure, which is not explicitly modeled but is only accounted for using non-simulated collapse criteria, the modeling in rated as "B-Good" rather than "A-Superior."

**Static Pushover Analysis**

To compute the system overstrength ($\Omega$) of each archetype design, the lateral load pattern prescribed in ASCE/SEI 7-05 is applied in monotonic static pushover analysis. Static pushover analysis results for design ID 9203 are illustrated in Figure 9-14. For this example RC OMF, yielding occurs at about 0.004 roof drift ratio (*RDR*), and capping (the onset of negative stiffness) occurs at about 0.014 roof drift ratio. These structures have substantially less ductility than their SMF counterparts (compare to Figure 9-6).

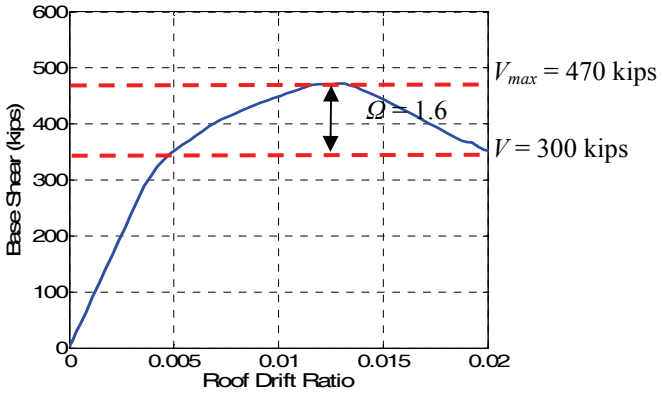


Figure 9-14 Monotonic static pushover.

The results of static pushover analysis are tabulated in Table 9-11 for all performance groups in SDC B. Pertinent results include computed static overstrength ($\Omega$) and the building ductility capacity ($\mu_c$). The building ductility capacity is used in computing the spectral shape factor (*SSF*). When non-simulated collapse modes are considered in the collapse assessment, the building ductility capacity must be adjusted to account for these modes when a non-simulated collapse is detected.

**Nonlinear Dynamic Analysis and Simulation**

The collapse capacity for each archetype design is computed using dynamic analysis and the Far-Field record set and scaling procedures described in Appendix A. Figure 9-15 illustrates how the incremental dynamic analysis method (IDA) is used to compute the sidesway collapse margin ratio of design ID 9203 (4-story perimeter frame, designed for $B_{max}$).

**Table 9-11 Pushover Analysis Results, SDC B**

| Archetype Design ID Number | Design Configuration | | | | Pushover and IDA Results | |
|---|---|---|---|---|---|---|
| | No. of Stories | Framing / Gravity Loads | Seismic SDC | *V*/*W* | $\Omega$ | $\mu_c$* |
| Minimum Seismic, SDC $B_{min}$, Low Gravity (Perimeter Frame) Designs | | | | | | |
| 9101 | 2 | Perimeter | $B_{min}$ | 0.041 | 2.0 | 3.4 |
| 9103 | 4 | Perimeter | $B_{min}$ | 0.023 | 1.8 | 2.7 |
| 9105 | 8 | Perimeter | $B_{min}$ | 0.012 | 2.6 | 2.4 |
| 9107 | 12 | Perimeter | $B_{min}$ | 0.010 | 2.3 | 2.7 |
| Minimum Seismic, SDC $B_{min}$, High Gravity (Space Frame) Designs | | | | | | |
| 9102 | 2 | Space | $B_{min}$ | 0.041 | 6.6 | 2.1 |
| 9104 | 4 | Space | $B_{min}$ | 0.023 | 5.3 | 1.8 |
| 9106 | 8 | Space | $B_{min}$ | 0.012 | 6.0 | 2.4 |
| 9108 | 12 | Space | $B_{min}$ | 0.010 | 6.0 | 3.5 |
| Maximum Seismic, SDC $B_{max}$, Low Gravity (Perimeter Frame) Designs | | | | | | |
| 9201 | 2 | Perimeter | $B_{max}$ | 0.087 | 1.6 | 3.2 |
| 9203 | 4 | Perimeter | $B_{max}$ | 0.048 | 1.6 | 2.9 |
| 9205 | 8 | Perimeter | $B_{max}$ | 0.026 | 1.5 | 2.2 |
| 9207 | 12 | Perimeter | $B_{max}$ | 0.018 | 1.7 | 2.1 |
| Maximum Seismic, SDC $B_{max}$, High Gravity (Space Frame) Designs | | | | | | |
| 9202 | 2 | Space | $B_{max}$ | 0.087 | 2.9 | 3.2 |
| 9204 | 4 | Space | $B_{max}$ | 0.048 | 3.0 | 2.0 |
| 9206 | 8 | Space | $B_{max}$ | 0.026 | 3.1 | 2.4 |
| 9208 | 12 | Space | $B_{max}$ | 0.018 | 3.8 | 5.0 |

* Due to time constraints, these values do not account for non-simulated collapse modes. Even so, these must be included when computing $\mu_c$ for use in this Methodology.

The IDA results for the 16 archetype designs are summarized in Table 9-12. These results reflect only the sidesway collapse mechanisms, which are directly simulated in the structural analysis model. The subscript "SS" denotes consideration of side-sway collapse only. As such, $CMR_{SS}$ is *not used for system evaluation*, but is presented here for illustrative purposes only.

**Non-Simulated Collapse Modes**

In this example, only sidesway collapse mechanisms based on strength and stiffness degradation due to flexural and flexural-shear effects are simulated directly in the analysis. Nonlinear models do not capture column shear failure, which may occur because OMF columns lack the capacity design requirements of SMF design and, as a result, have light transverse reinforcement. Although shear failure in itself is not a collapse mechanism, it may precipitate axial failure as a column loses ability to carry lateral loads. A detailed discussion of possible failure modes in RC moment frames is included in Appendix D.

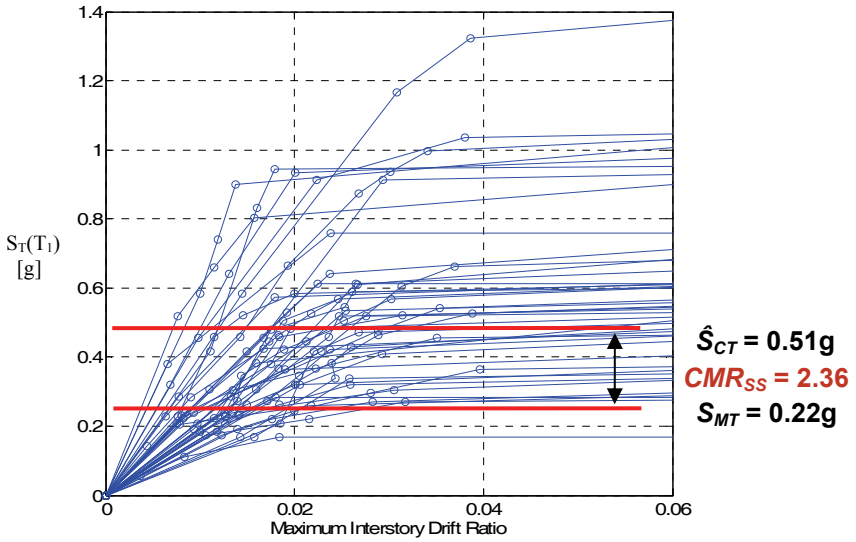


Figure 9-15 Incremental dynamic analysis to collapse showing the Maximum Considered Earthquake ground motion (*SMT*), Median Collapse Capacity ($\hat{S}_{CT}$), and Sidesway Collapse Margin Ratio ($CMR_{SS}$) for design ID 9203.

**Table 9-12 Summary of IDA Sidesway Collapse Results for Archetype Designs, SDC B**

| Archetype Design ID Number | Design Configuration | | | Pushover and IDA Results | | |
|---|---|---|---|---|---|---|
| | No. of Stories | Framing / Gravity Loads | Seismic SDC | $S_{MT}$ [*T*] (g) | $S_{CT}$ [*T*] (g) | *CMR* |
| Minimum Seismic, SDC $B_{min}$, Low Gravity (Perimeter Frame) Designs | | | | | | |
| 9101 | 2 | Perimeter | $B_{min}$ | 0.18 | 0.91 | 4.99 |
| 9103 | 4 | Perimeter | $B_{min}$ | 0.10 | 0.33 | 3.30 |
| 9105 | 8 | Perimeter | $B_{min}$ | 0.06 | 0.18 | 3.31 |
| 9107 | 12 | Perimeter | $B_{min}$ | 0.04 | 0.14 | 3.68 |
| Mean: | -- | -- | -- | -- | -- | 3.82 |
| Minimum Seismic, SDC $B_{min}$, High Gravity (Space Frame) Designs | | | | | | |
| 9102 | 2 | Space | $B_{min}$ | 0.18 | 1.40 | 7.69 |
| 9104 | 4 | Space | $B_{min}$ | 0.10 | 0.68 | 6.70 |
| 9106 | 8 | Space | $B_{min}$ | 0.06 | 0.39 | 7.05 |
| 9108 | 12 | Space | $B_{min}$ | 0.04 | 0.35 | 9.07 |
| Mean: | -- | -- | -- | -- | -- | 7.63 |
| Maximum Seismic, SDC $B_{max}$, Low Gravity (Perimeter Frame) Designs | | | | | | |
| 9201 | 2 | Perimeter | $B_{max}$ | 0.39 | 1.07 | 2.72 |
| 9203 | 4 | Perimeter | $B_{max}$ | 0.22 | 0.51 | 2.36 |
| 9205 | 8 | Perimeter | $B_{max}$ | 0.12 | 0.25 | 2.11 |
| 9207 | 12 | Perimeter | $B_{max}$ | 0.08 | 0.18 | 2.22 |
| Mean: | -- | -- | -- | -- | -- | 2.36 |
| Maximum Seismic, SDC $B_{max}$, High Gravity (Space Frame) Designs | | | | | | |
| 9202 | 2 | Space | $B_{max}$ | 0.39 | 1.36 | 3.47 |
| 9204 | 4 | Space | $B_{max}$ | 0.22 | 0.83 | 3.87 |
| 9206 | 8 | Space | $B_{max}$ | 0.12 | 0.41 | 3.49 |
| 9208 | 12 | Space | $B_{max}$ | 0.08 | 0.38 | 4.65 |
| Mean: | -- | -- | -- | -- | -- | 3.87 |

To capture these failure modes, further post-processing of the nonlinear dynamic results is required. This post-processing is also required as a part of the static pushover analysis so that the computed ductility capacity accounts for such modes. This is important because the ductility capacity affects the SSF, which is used to determine the adjusted collapse margin ratio. Fragility functions (adopted from Aslani, 2005) are introduced to determine the drift at which a column experiences shear failure and, subsequently, the drift at which a column loses its ability to carry gravity loads following shear failure. To determine if the shear-induced axial failure mode has occurred, the column drift level is extracted from the analysis data and compared to the median drift level associated with column axial failure from the fragility functions. If the median drift level has been exceeded in any column, the non-simulated collapse mode is assumed to have occurred. This approach can be highly conservative because is assumes that when a limit is exceeded in one element, it is exceeded for the entire building. In many cases, gravity loads can be redistributed to nearby elements, and the axial failure of a single column will not cause complete collapse of an entire structure.

Using the post-processing approach, the collapse fragility is adjusted to reflect the probability of both the simulated and non-simulated failure modes, reducing the collapse margin ratio. This reduction is more significant in space frame structures that have higher axial loads in the columns. The effect of non-simulated failure modes on the computed collapse margin ratios for the 16 archetype structures is shown in Table 9-13. The final collapse results are summarized in Table 9-14.

Table 9-15 shows the SSF values as a function of the building ductility capacity ($\mu_c$) and structural period ($T$). When using this table, the ductility capacity values should include non-simulated collapse modes, assuming that when a non-simulated collapse mode occurs then the building looses at least 20% lateral strength. Since the OMF archetypes are designed for SDC B, where the benefit of spectral shape is more limited, and they have limited ductility, the *SSF* values are smaller than in the SMF example.

To assess the OMF system, the composite uncertainty ($\beta_{TOT}$) in collapse capacity is needed. The same assumptions as the SMF example are considered, including uncertainty in the nonlinear structural modeling ("B-Good"), uncertainty in the test data ("B-Good") and the quality of the structural system design requirements ("A-Superior"). For the OMF example, the composite uncertainty determined to be $\beta_{TOT} = 0.60$ from Table 7-2.

**Table 9-13 Effect of Non-Simulated Collapse Modes on Computed Collapse Margin Ratios, SDC B**

| Archetype Design ID Number | Design Configuration | | $S_{MT}$ [$T$] (g) | $CMR_{ss}$ | $CMR_{non\text{-}simulated}$ | Percent Decrease |
|---|---|---|---|---|---|---|
| | No. of Stories | Seismic SDC | | | | |
| Minimum Seismic, SDC $B_{min}$, Low Gravity (Perimeter Frame) Designs | | | | | | |
| 9101 | 2 | $B_{min}$ | 0.18 | 4.99 | 4.96 | 0.6% |
| 9103 | 4 | $B_{min}$ | 0.10 | 3.30 | 3.08 | 6.7% |
| 9105 | 8 | $B_{min}$ | 0.06 | 3.31 | 2.57 | 22.3% |
| 9107 | 12 | $B_{min}$ | 0.04 | 3.68 | 2.96 | 19.5% |
| Mean | -- | -- | -- | 3.82 | 3.39 | 11.2% |
| Minimum Seismic, SDC $B_{min}$, High Gravity (Space Frame) Designs | | | | | | |
| 9102 | 2 | $B_{min}$ | 0.18 | 7.69 | 3.98 | 48.2% |
| 9104 | 4 | $B_{min}$ | 0.10 | 6.70 | 2.79 | 58.4% |
| 9106 | 8 | $B_{min}$ | 0.06 | 7.05 | 4.36 | 38.2% |
| 9108 | 12 | $B_{min}$ | 0.04 | 9.07 | 4.19 | 53.8% |
| Mean | -- | -- | -- | 7.63 | 3.83 | 49.8% |
| Maximum Seismic, SDC $B_{max}$, Low Gravity (Perimeter Frame) Designs | | | | | | |
| 9201 | 2 | $B_{max}$ | 0.39 | 2.72 | 2.04 | 25.0% |
| 9203 | 4 | $B_{max}$ | 0.22 | 2.36 | 1.99 | 15.6% |
| 9205 | 8 | $B_{max}$ | 0.12 | 2.11 | 1.68 | 20.5% |
| 9207 | 12 | $B_{max}$ | 0.08 | 2.22 | 1.93 | 13.4% |
| Mean | -- | -- | -- | 2.36 | 1.91 | 18.9% |
| Maximum Seismic, SDC $B_{max}$, High Gravity (Space Frame) Designs | | | | | | |
| 9202 | 2 | $B_{max}$ | 0.39 | 3.47 | 1.79 | 48.5% |
| 9204 | 4 | $B_{max}$ | 0.22 | 3.87 | 2.08 | 46.3% |
| 9206 | 8 | $B_{max}$ | 0.12 | 3.49 | 2.48 | 28.9% |
| 9208 | 12 | $B_{max}$ | 0.08 | 4.65 | 1.95 | 58.0% |
| Mean | -- | -- | -- | 3.87 | 2.08 | 46.4% |

The acceptable collapse margin is determined from the composite uncertainty and the acceptable conditional probability of collapse under the maximum considered earthquake ground motion. The required performance criteria in Chapter 7 are: (1) a conditional collapse probability of ≤ 20% for all archetype buildings, and (2) a conditional collapse probability of ≤ 10% for the average of the buildings in each performance group. For the OMF structures with a composite uncertainty of 0.60, this corresponds to a required *ACMR* of 1.66 for each archetype building, with a required average *ACMR* of 2.16 for each performance group. These values are taken from Table 7-3.

**Table 9-14 Summary of Collapse Results for Archetype Designs, SDC B**

| Archetype Design ID Number | Design Configuration | | | Pushover and IDA Results | | |
|---|---|---|---|---|---|---|
| | No. of Stories | Framing / Gravity Loads | Seismic SDC | $S_{MT}$ [$T$] (g) | $S_{CT}$ [$T$] (g) | *CMR* |
| Minimum Seismic, SDC $B_{min}$, Low Gravity (Perimeter Frame) Designs | | | | | | |
| 9101 | 2 | Perimeter | $B_{min}$ | 0.18 | 0.90 | 4.96 |
| 9103 | 4 | Perimeter | $B_{min}$ | 0.10 | 0.31 | 3.08 |
| 9105 | 8 | Perimeter | $B_{min}$ | 0.06 | 0.14 | 2.57 |
| 9107 | 12 | Perimeter | $B_{min}$ | 0.04 | 0.11 | 2.96 |
| Mean | -- | -- | -- | -- | -- | 3.39 |
| Minimum Seismic, SDC $B_{min}$, High Gravity (Space Frame) Designs | | | | | | |
| 9102 | 2 | Space | $B_{min}$ | 0.18 | 0.72 | 3.98 |
| 9104 | 4 | Space | $B_{min}$ | 0.10 | 0.28 | 2.79 |
| 9106 | 8 | Space | $B_{min}$ | 0.06 | 0.24 | 4.36 |
| 9108 | 12 | Space | $B_{min}$ | 0.04 | 0.16 | 4.19 |
| Mean | -- | -- | -- | -- | -- | 3.83 |
| Maximum Seismic, SDC $B_{max}$, Low Gravity (Perimeter Frame) Designs | | | | | | |
| 9201 | 2 | Perimeter | $B_{max}$ | 0.39 | 0.80 | 2.04 |
| 9203 | 4 | Perimeter | $B_{max}$ | 0.22 | 0.43 | 1.99 |
| 9205 | 8 | Perimeter | $B_{max}$ | 0.12 | 0.20 | 1.68 |
| 9207 | 12 | Perimeter | $B_{max}$ | 0.08 | 0.16 | 1.93 |
| Mean | -- | -- | -- | -- | -- | 1.91 |
| Maximum Seismic, SDC $B_{max}$, High Gravity (Space Frame) Designs | | | | | | |
| 9202 | 2 | Space | $B_{max}$ | 0.39 | 0.70 | 1.79 |
| 9204 | 4 | Space | $B_{max}$ | 0.22 | 0.45 | 2.08 |
| 9206 | 8 | Space | $B_{max}$ | 0.12 | 0.29 | 2.48 |
| 9208 | 12 | Space | $B_{max}$ | 0.08 | 0.16 | 1.95 |
| Mean | -- | -- | -- | -- | -- | 2.08 |

**Table 9-15 Spectral shape factors for SDC B/C/$D_{min}$ archetypes**

| $T$ (sec) | Spectrum Shape Factor (SSF) - Seismic Design Category B/C/$D_{min}$ | | | | | | | |
|---|---|---|---|---|---|---|---|---|
| | Building Ductility Capacity, $\mu_C$ | | | | | | | |
| | 1.0 | 1.1 | 1.5 | 2 | 3 | 4 | 6 | >=8 |
| **<= 0.5** | 1.00 | 1.03 | 1.06 | 1.07 | 1.09 | 1.10 | 1.12 | 1.14 |
| **0.6** | 1.00 | 1.04 | 1.06 | 1.08 | 1.10 | 1.12 | 1.14 | 1.16 |
| **0.7** | 1.00 | 1.04 | 1.07 | 1.09 | 1.12 | 1.14 | 1.16 | 1.18 |
| **0.8** | 1.00 | 1.05 | 1.08 | 1.10 | 1.13 | 1.15 | 1.18 | 1.21 |
| **0.9** | 1.00 | 1.05 | 1.09 | 1.11 | 1.15 | 1.17 | 1.20 | 1.23 |
| **1.0** | 1.00 | 1.06 | 1.10 | 1.13 | 1.16 | 1.19 | 1.22 | 1.25 |
| **1.1** | 1.00 | 1.06 | 1.11 | 1.14 | 1.18 | 1.20 | 1.25 | 1.28 |
| **1.2** | 1.00 | 1.07 | 1.12 | 1.15 | 1.19 | 1.22 | 1.27 | 1.30 |
| **1.3** | 1.00 | 1.07 | 1.13 | 1.16 | 1.21 | 1.24 | 1.29 | 1.33 |
| **1.4** | 1.00 | 1.08 | 1.14 | 1.17 | 1.22 | 1.26 | 1.31 | 1.35 |
| **>= 1.5** | 1.00 | 1.08 | 1.14 | 1.19 | 1.24 | 1.28 | 1.34 | 1.38 |

Table 9-16 presents the final results and acceptance criteria for the 16 RC OMF archetypes in SDC B. As shown in Table 9-16, the RC OMF structural system passes for each of the two performance groups in both $B_{max}$ and $B_{min}$, in some cases with *ACMRs* considerably above the required level. The large ACMRs tend to occur for structures with substantial overstrength, which resulted from the dominance of gravity loading in the design.

**Table 9-16 Summary of Final Collapse Margins and Comparison to Acceptance Criteria for SDC B**

| Arch. Design ID Number | Design Configuration | | | Computed Collapse Margin | | | Acceptance Check | |
|---|---|---|---|---|---|---|---|---|
| | No. of Stories | Framing / Gravity Loads | Seismic SDC | *CMR* | *SSF* | *ACMR* | Accept. *ACMR* | Pass/Fail |
| Minimum Seismic, SDC $B_{min}$, Low Gravity (Perimeter Frame) Designs | | | | | | | | |
| 9101 | 2 | Perimeter | $B_{min}$ | 4.96 | 1.10 | 5.46 | 1.66 | Pass |
| 9103 | 4 | Perimeter | $B_{min}$ | 3.08 | 1.15 | 3.54 | 1.66 | Pass |
| 9105 | 8 | Perimeter | $B_{min}$ | 2.57 | 1.22 | 3.13 | 1.66 | Pass |
| 9107 | 12 | Perimeter | $B_{min}$ | 2.96 | 1.24 | 3.67 | 1.66 | Pass |
| Mean | -- | -- | -- | -- | -- | 3.95 | 2.16 | **Pass** |
| Minimum Seismic, SDC $B_{min}$, High Gravity (Space Frame) Designs | | | | | | | | |
| 9102 | 2 | Space | $B_{min}$ | 3.98 | 1.08 | 4.30 | 1.66 | Pass |
| 9104 | 4 | Space | $B_{min}$ | 2.79 | 1.13 | 3.15 | 1.66 | Pass |
| 9106 | 8 | Space | $B_{min}$ | 4.36 | 1.22 | 5.31 | 1.66 | Pass |
| 9108 | 12 | Space | $B_{min}$ | 4.19 | 1.28 | 5.36 | 1.66 | Pass |
| Mean | -- | -- | -- | -- | -- | 4.53 | 2.16 | **Pass** |
| Maximum Seismic, SDC $B_{max}$, Low Gravity (Perimeter Frame) Designs | | | | | | | | |
| 9201 | 2 | Perimeter | $B_{max}$ | 2.04 | 1.10 | 2.25 | 1.66 | Pass |
| 9203 | 4 | Perimeter | $B_{max}$ | 1.99 | 1.15 | 2.29 | 1.66 | Pass |
| 9205 | 8 | Perimeter | $B_{max}$ | 1.68 | 1.21 | 2.03 | 1.66 | Pass |
| 9207 | 12 | Perimeter | $B_{max}$ | 1.93 | 1.21 | 2.33 | 1.66 | Pass |
| Mean | -- | -- | -- | -- | -- | 2.23 | 2.16 | **Pass** |
| Maximum Seismic, SDC $B_{max}$, High Gravity (Space Frame) Designs | | | | | | | | |
| 9202 | 2 | Space | $B_{max}$ | 1.79 | 1.10 | 1.97 | 1.66 | Pass |
| 9204 | 4 | Space | $B_{max}$ | 2.08 | 1.10 | 2.29 | 1.66 | Pass |
| 9206 | 8 | Space | $B_{max}$ | 2.48 | 1.22 | 3.03 | 1.66 | Pass |
| 9208 | 12 | Space | $B_{max}$ | 1.95 | 1.33 | 2.60 | 1.66 | Pass |
| Mean | -- | -- | -- | -- | -- | 2.47 | 2.16 | **Pass** |

### *9.3.7 Evaluation of RC OMF System in SDC C*

A smaller subset of archetypes was considered to assess whether RC OMF systems pass the collapse safety criteria in SDC C. The archetype designs and results for $B_{max}$ are used in this assessment, since $B_{max}$ is identical to $C_{min}$. In addition, we consider four additional archetype RC OMFs, designed for $C_{max}$, as shown in Table 9-17. The archetypes are binned into the same four performance groups used in the evaluation for SDC B.

Seismic performance factors are assessed using the same procedure as described for the evaluation of RC OMFs in SDC B. Table 9-18 shows the

computed overstrength factors from static pushover analysis. The computed collapse margin ratios, including both simulated and non-simulated failure modes, are reported in Table 9-19. This table also compares the adjusted collapse margin ratios to the acceptance criteria.

**Table 9-17 Archetype Design Properties, SDC C**

| Archetype Design ID Number | No. of Stories | Key Archetype Design Parameters | | | | | |
|---|---|---|---|---|---|---|---|
| | | Framing / Gravity Loads | Seismic Design Criteria | | | | $S_{MT}$ [$T$] (g) |
| | | | SDC | $R$ | $T$ (sec.) | $V/W$ (g) | |
| Minimum Seismic, SDC $C_{min}$, Low Gravity (Perimeter Frame) Designs | | | | | | | |
| 9201 | 2 | P | $C_{min}$ | 3 | 0.51 | 0.087 | 0.39 |
| 9203 | 4 | P | $C_{min}$ | 3 | 0.93 | 0.048 | 0.22 |
| 9205 | 8 | P | $C_{min}$ | 3 | 1.70 | 0.026 | 0.12 |
| 9207 | 12 | P | $C_{min}$ | 3 | 2.44 | 0.018 | 0.08 |
| Minimum Seismic, SDC $C_{min}$, High Gravity (Space Frame) Designs | | | | | | | |
| 9202 | 2 | S | $C_{min}$ | 3 | 0.51 | 0.087 | 0.39 |
| 9204 | 4 | S | $C_{min}$ | 3 | 0.93 | 0.048 | 0.22 |
| 9206 | 8 | S | $C_{min}$ | 3 | 1.70 | 0.026 | 0.12 |
| 9208 | 12 | S | $C_{min}$ | 3 | 2.44 | 0.018 | 0.08 |
| Maximum Seismic, SDC $C_{max}$, Low Gravity (Perimeter Frame) Designs | | | | | | | |
| 9303 | 4 | P | $C_{max}$ | 3 | 0.87 | 0.077 | 0.34 |
| 9307 | 12 | P | $C_{max}$ | 3 | 2.29 | 0.029 | 0.13 |
| Maximum Seismic, SDC $B_{max}$, High Gravity (Space Frame) Designs | | | | | | | |
| 9304 | 4 | S | $C_{max}$ | 3 | 0.87 | 0.077 | 0.34 |
| 9308 | 12 | S | $C_{max}$ | 3 | 2.29 | 0.029 | 0.13 |

**Table 9-18 Pushover Analysis Results, SDC C**

| Archetype Design ID Number | Design Configuration | | | | Pushover and IDA Results | |
|---|---|---|---|---|---|---|
| | No. of Stories | Framing / Gravity Loads | Seismic SDC | $V/W$ | $\Omega$ | $\mu_c$* |
| Minimum Seismic, SDC $C_{min}$, Low Gravity (Perimeter Frame) Designs | | | | | | |
| 9201 | 2 | Perimeter | $C_{min}$ | 0.087 | 1.6 | 3.2 |
| 9203 | 4 | Perimeter | $C_{min}$ | 0.048 | 1.6 | 2.9 |
| 9205 | 8 | Perimeter | $C_{min}$ | 0.026 | 1.5 | 2.2 |
| 9207 | 12 | Perimeter | $C_{min}$ | 0.018 | 1.7 | 2.1 |
| Minimum Seismic, SDC $C_{min}$, High Gravity (Space Frame) Designs | | | | | | |
| 9202 | 2 | Space | $C_{min}$ | 0.087 | 2.9 | 3.2 |
| 9204 | 4 | Space | $C_{min}$ | 0.048 | 3.0 | 2.0 |
| 9206 | 8 | Space | $C_{min}$ | 0.026 | 3.1 | 2.4 |
| 9208 | 12 | Space | $C_{min}$ | 0.018 | 3.8 | 5.0 |
| Maximum Seismic, SDC $C_{max}$, Low Gravity (Perimeter Frame) Designs | | | | | | |
| 9303 | 4 | Perimeter | $C_{max}$ | 0.077 | 1.5 | 3.3 |
| 9307 | 12 | Perimeter | $C_{max}$ | 0.029 | 1.4 | 2.0 |
| Maximum Seismic, SDC $C_{max}$, High Gravity (Space Frame) Designs | | | | | | |
| 9304 | 4 | Space | $C_{max}$ | 0.077 | 2.1 | 2.7 |
| 9308 | 12 | Space | $C_{max}$ | 0.029 | 2.7 | 3.7 |

* Due to time constraints, these values do not account for non-simulated collapse modes. Even so, these must be included when computing $\mu_c$ for use in this Methodology.

**Table 9-19 Summary of Final Collapse Margins and Comparison to Acceptance Criteria, SDC C**

| Arch. Design ID Number | Design Configuration | | | Computed Collapse Margin | | | Acceptance Check | |
|---|---|---|---|---|---|---|---|---|
| | No. of Stories | Framing / Gravity Loads | Seismic SDC | *CMR* | *SSF* | *ACMR* | Accept. *ACMR* | Pass/Fail |
| Minimum Seismic, SDC $C_{min}$, Low Gravity (Perimeter Frame) Designs | | | | | | | | |
| 9201 | 2 | Perimeter | $C_{min}$ | 2.04 | 1.10 | 2.25 | 1.66 | Pass |
| 9203 | 4 | Perimeter | $C_{min}$ | 1.99 | 1.15 | 2.29 | 1.66 | Pass |
| 9205 | 8 | Perimeter | $C_{min}$ | 1.68 | 1.21 | 2.03 | 1.66 | Pass |
| 9207 | 12 | Perimeter | $C_{min}$ | 1.93 | 1.21 | 2.33 | 1.66 | Pass |
| Mean | | | | | | 2.23 | 2.16 | **Pass** |
| Minimum Seismic, SDC $C_{min}$, High Gravity (Space Frame) Designs | | | | | | | | |
| 9202 | 2 | Space | $C_{min}$ | 1.79 | 1.1 | 1.97 | 1.66 | Pass |
| 9204 | 4 | Space | $C_{min}$ | 2.08 | 1.1 | 2.29 | 1.66 | Pass |
| 9206 | 8 | Space | $C_{min}$ | 2.48 | 1.22 | 3.03 | 1.66 | Pass |
| 9208 | 12 | Space | $C_{min}$ | 1.95 | 1.33 | 2.60 | 1.66 | Pass |
| Mean | | | | | | 2.47 | 2.16 | **Pass** |
| Maximum Seismic, SDC $C_{max}$, Low Gravity (Perimeter Frame) Designs | | | | | | | | |
| 9303 | 4 | Perimeter | $C_{max}$ | 1.55 | 1.15 | 1.78 | 1.66 | Pass |
| 9307 | 12 | Perimeter | $C_{max}$ | 1.03 | 1.2 | 1.24 | 1.66 | Fail |
| Mean | | | | | | 1.51 | 2.16 | **Fail** |
| Maximum Seismic, SDC $C_{max}$, High Gravity (Space Frame) Designs | | | | | | | | |
| 9304 | 4 | Space | $C_{max}$ | 1.97 | 1.14 | 2.25 | 1.66 | Pass |
| 9308 | 12 | Space | $C_{max}$ | 1.58 | 1.29 | 2.04 | 1.66 | Pass |
| Mean | | | | | | 2.15 | 2.16 | **Near Pass** |

As shown in Table 9-19, archetype structures fail the acceptance criteria for $C_{max}$ at both the individual and the performance group level. At $C_{min}$, as at $B_{max}$, the archetype structures pass the acceptance criteria, but barely. These results indicate that the exclusion of OMFs in SDC C is appropriate. In order to be permitted in SDC C, a lower *R*-factor, or other change in design requirements, is needed.

### *9.3.8 Evaluation of $\Omega_o$ using Archetype Designs*

Development of the overstrength factor ($\Omega_o$) is based on SDC B archetype designs, since this is the highest SDC that is currently allowed for this system. If the system were being approved for use in SDC C, then the SDC C archetypes would be used for establishing $\Omega_o$.

The first step is to compute the overstrength values ($\Omega$) for each individual archetype building. There is a relatively wide range of overstrength observed for the set of archetype designs ($\Omega$ ranges from 1.5 to 6.6, as reported in Table 9-11). The performance group that governs the R-factor, maximum seismic/low gravity, has computed $\Omega$ values ranging from 1.5 to 1.7, with an average of 1.6. Maximum seismic/high gravity structures have higher computed overstrengths, between 2.9 and 3.8, with an average of 3.2. The minimum seismic/high gravity archetypes have the largest overstrength

values, ranging up to 6.6, with an average of 6.0. The $\Omega_o$ value should be conservatively based on these individual values, rounded to the nearest 0.5, and limited to a maximum value of 3.0. This process is subject to judgment, and should be done in cooperation with the peer review panel. For this example, the upper-bound value of $\Omega_o = 3.0$ is warranted, due to large average $\Omega$ values observed for several of the archetype buildings, and average values higher than 3.0 for two performance groups.

### 9.3.9 Summary Observations - Reinforced Concrete Ordinary Moment Frame System

This example shows that current seismic provisions for RC OMF systems provide an acceptable level of collapse safety in SDC B, but not in SDC C. These results are consistent with the provisions for use of RC OMFs in ASCE/SEI 7-05.

To account for non-simulated failure mode, component limit state checks are incorporated through post-processing of dynamic analysis results. In some cases incorporation of the non-simulated failure modes significantly affects the collapse margin ratio, demonstrating the importance of carefully considering and including all critical failure modes either explicitly in the simulation models or in non-simulated limit state checks.

The RC OMF system example also illustrates more generally the interrelated nature of structural design requirements and building code provisions. Assessment of seismic performance factors represents an evaluation of the complete set of design provisions. Many different design and detailing rules can have unexpected influences collapse behavior. These include conservatism in the code-calculated period, the stability coefficient, and gravity load versus lateral load ratios.

## 9.4 Example Application - Wood Light-Frame System

### 9.4.1 Introduction

In this example, a wood light-frame system with structural panel sheathing is considered as if it were a new system proposed for inclusion in ASCE/SEI 7-05. This example is intended for illustration only, and is not intended to propose any specific changes to current building code provisions for this system.

### 9.4.2 Overview and Approach

Wood light-frame system design requirements of ASCE/SEI 7-05 are used as the framework. A set of structural archetypes are developed for wood light-

frame buildings, nonlinear models are developed to simulate structural collapse, models are analyzed to predict the collapse capacities of each design, and the collapse margin ratio, *CMR*, is evaluated and compared to acceptance criteria.

Seismic performance factors (SPFs) are determined by iteration until the acceptance criteria of the Methodology are met. The iterative process begins with an initial value of $R = 6$. This value is different from the current value of $R = 6.5$ for wood light-frame shear wall systems with wood structural panel sheathing in ASCE/SEI 7-05. It has been rounded to the nearest whole number for simplicity, and because developmental studies have shown that there is no discernable difference in collapse performance of structures design for fractional *R* factors (e.g., R = 6 versus R = 6.5). Initially, minimum design base shear requirements consistent with ASCE/SEI7-05 are utilized, without consideration of wall finish materials. The $\Omega_0$ factor is not assumed initially, but is determined from the actual overstrengths factors, $\Omega$, calculated for the archetype designs.

After completing an assessment using the initial set of SPFs, selected archetypes (e.g., $R = 6$, wood-only designs) did not meet the acceptance criteria, and were found to have inadequate collapse safety. Aspects of the structural design requirements were modified, and the system was reassessed. Modifications included consideration of lateral strength and stiffness contributions from gypsum wallboard applied to the interior surfaces of the wood structural walls, and reduced *R* factors (increased initial design base shear strength).

### *9.4.3 Design Requirements*

This example utilizes design requirements for engineered wood light-frame buildings included in ASCE/SEI 7-05 in place of the requirements that would need to be developed for a newly proposed system. For the purpose of assessing uncertainty, the ASCE/SEI 7-05 design requirements are categorized as "A-Superior" since they represent many years of development, include lessons learned from a number of major earthquakes, and consider recent results obtained from large research programs on wood light-frame systems, such as the FEMA-funded CUREE-Caltech Woodframe Project and the NSF/NEES-funded NEESWood Project.

### *9.4.4 Test Data*

This example relies on existing published sheathing-to-framing connection test data and wood shear wall assembly test data. Specifically, this example relies on information developed during the CUREE-Caltech Woodframe

Project (Fonseca et al. 2002; Folz and Filiatrault, 2001), the NEESWood Project (Ekiert and Hong, 2006), and the CoLA wood shear wall test program (CoLA, 2001). When gypsum wallboard sheathing is considered, the equivalent gypsum-to-wood framing connector model developed recently by Pang and Rosowsky (2007) is used.

The quality of the test data is an important consideration when quantifying the uncertainty in the overall collapse assessment process. The monotonic and cyclic test data used in this example cover a wide range of wood sheathing types and thicknesses (e.g. Oriented Strand Board and Plywood), framing grades and species and connector types (e.g. common vs box nails). All loading protocols were continued to deformations large enough for the capping strength to be observed, which allows a better calibration of models for structural collapse assessment. Nevertheless, some uncertainties still exist with these test data sets including a) premature failures in some of the CUREE data set caused by specimens with smaller connector edge distances than specified, b) the use of the Sequential Phased Displacement, SPD, loading protocol in the CoLA tests that tends to cause premature specimen failure by connectors fatigue, which is seldom observed after real earthquakes and c) the inherent large variability associated with the material properties of wood. Therefore, for the purpose of assessing uncertainty, this test data set is conservatively categorized as "B-Good."

### *9.4.5 Identification of Wood Light-Frame Archetype Configurations*

Figure 9-16 shows the two different building configurations used to define the two-dimensional archetype configurations for wood light-frame shear wall systems with wood structural panel sheathing. The first configuration is representative of residential building dimensions, while the second configuration is associated with office, retail, educational, and warehouse/light manufacturing wood buildings.

Table 9-20 lists the range of design parameters considered for the development of the two-dimensional archetype wall models. Two-dimensional archetype wall models, not accounting for torsional effects, are considered acceptable because the intended use of the Methodology is to verify the performance of a full class of buildings, rather than one specific building with a unique torsional issue. Wall finishes, such as stucco and gypsum wallboard, were not considered for the initial design of the archetype wall models. Depending on their type, wall finishes may greatly influence the seismic response of wood buildings.

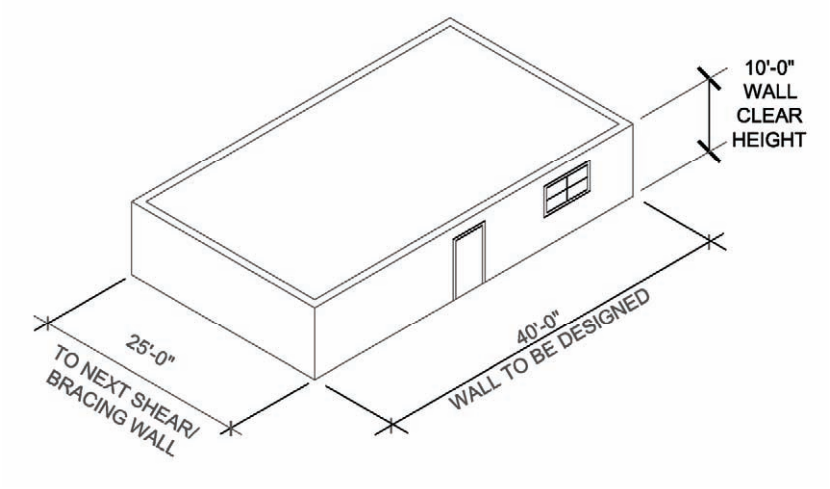


Residential Building Dimensions

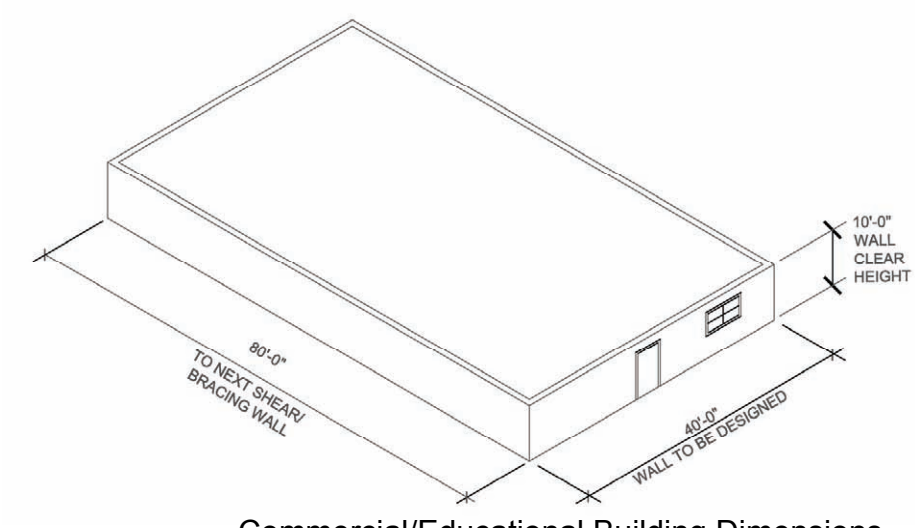


Commercial/Educational Building Dimensions

Figure 9-16 Building Configurations Considered for the Definitions of Wood Light-Frame Archetype Buildings.

**Table 9-20 Range of Variables Considered for the Definition of Wood Light-Frame Archetype Buildings**

| Variable | Range |
|---|---|
| Number of stories | 1 to 5 |
| Seismic Design Categories (SDC) | $D_{max}$ and $D_{min}$ |
| Story height | 10 ft |
| Interior Nonstructural wall finishes | Not considered in design<br>Considered in Modeling |
| Exterior Nonstructural wall finishes | Not considered |
| Wood shear wall pier aspect ratios | High/Low |

The influence of interior gypsum wallboard was introduced once it was realized that the wood-only archetypes designed with $R = 6$ did not meet the acceptance criteria of the Methodology. Introducing gypsum wallboard was deemed reasonable since it is likely that it will be incorporated to the interior surfaces of structural wood walls of most wood buildings. The influence of nonstructural gypsum wallboard partitions, however, was not considered since the amount of partitions will vary greatly depending on the architectural layouts of wood buildings. Similarly, the influence of exterior wall finishes, such as stucco, can not be relied upon when considering the performance of an entire class of wood buildings for which various types of wall finishes may be used. Low aspect ratio (1:1 to 1.43:1) and high aspect ratio (2.70:1 to 3.33:1) walls were incorporated in the archetype designs to consider the influence of the aspect ratio strength adjustment factor for wood shear walls contained in ASCE/SEI 7-05.

To represent these ranges of design parameters, 40 archetypes could have been used to evaluate the system (two building configurations, five story heights, two shear wall aspect ratios and two seismic design categories). However, 16 archetypes were found to be sufficient. These 16 wood archetypes were divided in four performance groups: (1) three low aspect ratio wall buildings designed for the maximum ground motions of the Seismic Design Category D, SDC $D_{max}$; (2) five SDC $D_{max}$ - high aspect ratio wall buildings; (3) one low aspect ratio shear wall building designed for the minimum ground motions of SDC $D_{min}$; and (4) seven SDC $D_{min}$ - high aspect ratio shear wall buildings. It is believed that this ensemble of 16 archetypes covers the current design space for wood light-frame buildings. Appendix C provides detailed descriptions of the 16 archetype models developed for wood light-frame buildings.

Table 9-21 shows the properties for each of these 16 archetype designs. The high- and low-seismic demands are represented by the maximum and minimum ground motions of Seismic Design Category (SDC) D, respectively. The archetypes are designed for a soil type D and acceleration parameters $S_{DS} = 1.0$ g and $S_{D1} = 0.6$ g for SDC $D_{max}$ (High Seismic in Table 9-21) and $S_{DS} = 0.50$ g and $S_{D1} = 0.20$ g for SDC $D_{min}$ (Low Seismic in Table 9-21). Note that the low seismic archetype buildings were originally designed for acceleration parameters $S_{DS} = 0.38$ g and $S_{D1} = 0.16$ g, corresponding to SDC B/C, and were not modified for this example because the low seismic performance groups did not govern the determination of the SPFs for the wood light-frame system, as it will be shown below.

**Table 9-21 Wood Light-Frame Archetype Structural Design Properties**

| Model No. | No. of Stories | Building Configuration | Wall Aspect Ratio | Period $T$ (sec) | V/W | $S_{MT}$ (g) |
|---|---|---|---|---|---|---|
| **High Seismic (SDC $D_{max}$) - Low Aspect Ratios - R = 6** | | | | | | |
| 1 | 1 | Commercial | Low | 0.25 | 0.167 | 1.50 |
| 5 | 2 | Commercial | Low | 0.26 | 0.167 | 1.50 |
| 9 | 3 | Commercial | Low | 0.36 | 0.167 | 1.50 |
| **High Seismic (SDC $D_{max}$) - High Aspect Ratios - R = 6** | | | | | | |
| 2 | 1 | 1&2 Family | High | 0.25 | 0.167 | 1.50 |
| 6 | 2 | 1&2 Family | High | 0.26 | 0.167 | 1.50 |
| 10 | 3 | Multi-Family | High | 0.36 | 0.167 | 1.50 |
| 13 | 4 | Multi-Family | High | 0.45 | 0.167 | 1.50 |
| 15 | 5 | Multi-Family | High | 0.53 | 0.167 | 1.50 |
| **Low Seismic (SDC $D_{min}$) - Low Aspect Ratios - R = 6** | | | | | | |
| 11 | 3 | Commercial | Low | 0.41 | 0.063 | 0.75 |
| **Low Seismic (SDC $D_{min}$) - High Aspect Ratios - R = 6** | | | | | | |
| 3 | 1 | Commercial | High | 0.25 | 0.063 | 0.75 |
| 4 | 1 | 1&2 Family | High | 0.25 | 0.063 | 0.75 |
| 7 | 2 | Commercial | High | 0.30 | 0.063 | 0.75 |
| 8 | 2 | 1&2 Family | High | 0.30 | 0.063 | 0.75 |
| 12 | 3 | Multi-Family | High | 0.41 | 0.063 | 0.75 |
| 14 | 4 | Multi-Family | High | 0.51 | 0.063 | 0.75 |
| 16 | 5 | Multi-Family | High | 0.60 | 0.063 | 0.75 |

The Maximum Considered Earthquake, MCE, ground motion spectral response accelerations, $S_{MT}$, shown in Table 9-21 and utilized in the analysis of the archetype buildings are based on the ASCE/SEI 7-05 mapped values given in Table A-1A of Appendix A. The periods reported in Table 9-21 are the fundamental period of the buildings based on the upper limit of Section 12.8.2 of ASCE/SEI 7-05 ($T = C_u T_a$) with a lower bound of 0.25 sec.

### *9.4.6 Development of Nonlinear Structural Archetype Models*

Structural modeling of the wood light-frame archetypes is based on a "pancake" approach (Isoda et al., 2001). This system-level modeling approach simulates the three-dimensional seismic response of a wood light-frame building through a degenerated two-dimensional planar analysis. The computer program SAWS: Seismic Analysis of Woodframe Structures, developed within the CUREE-Caltech Woodframe Project (Folz and Filiatrault, 2004a, b), was used to analyze the wood light-frame archetype models.

In the SAWS model, the building structure is composed of rigid horizontal diaphragms and nonlinear lateral load resisting shear wall elements. The pinched, strength and stiffness degrading hysteretic behavior of each wood shear wall in the building can be characterized using an associated numerical model (Folz and Filiatrault, 2001) that predicts the load-displacement response of whole wall assemblies under general quasi-static cyclic loading

based on sheathing-to-framing connection cyclic test data. Alternatively, cyclic test results on full-scale walls can be used directly to characterize their hysteretic response. In the SAWS model, the hysteretic behavior of each wall panel is represented by an equivalent nonlinear shear spring element. The hysteretic behavior of this shear spring element includes pinching, stiffness and strength degradation and is governed by 10 different physically identifiable parameters (Folz and Filiatrault 2004a, b), as shown in Figure 9-17. The predictive capabilities of the SAWS program have been demonstrated by comparing its predictions with the results of shake table tests performed on full-scale wood light-frame buildings (Folz and Filiatrault, 2004b; White and Ventura, 2007).

Table 9-22 shows the hysteretic parameters used to construct the equivalent nonlinear shear spring element of each wood and gypsum wall contained in the archetype models. For wood structural walls incorporating Oriented Strand Board (OSB) sheathing with 8d common nails and for the gypsum walls attached with #6 1-1/4 in. long screws, the shear elements were constructed from sheathing-to-framing connector test data. The hysteretic model used for those sheathing-to-framing connectors is the same as that for the entire wall panel assemblies shown in Figure 9-17. For wood structural walls incorporating plywood sheathing and 10d common nails, results from cyclic tests on full wall assemblies were used to construct the shear elements of those walls. The hysteretic parameters for plywood walls shown in Table 9-22 are associated with 8 ft long x 10 ft high walls. These parameters were linearly scaled in the models based on the lengths of individual wall piers.

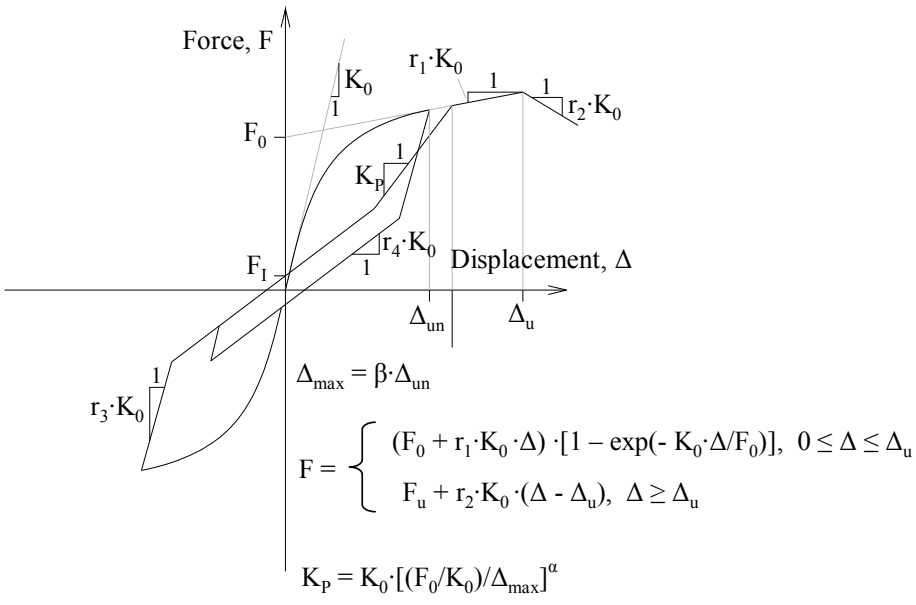


Figure 9-17 Hysteretic Model of Shear Spring Element Included in SAWS Program (after Folz and Filiatrault 2004a, b).

**Table 9-22 Hysteretic Parameters Used to Construct Shear Elements for Wood Light-Frame Archetype Models**

| Element Type | Connection Type | $K_0$ (lbs/in) | $r_1$ | $r_2$ | $r_3$ | $r_4$ | $F_o$ (lbs) | $F_1$ (lbs) | $\Delta_u$ (in) | $\alpha$ | $\beta$ |
|---|---|---|---|---|---|---|---|---|---|---|---|
| Framing to Sheathing Connector | 7/16" OSB - 8d common nails | 3203 | 0.061 | -0.078 | 1.4 | 0.050 | 169 | 32 | 0.51 | 0.8 | 1.1 |
| Framing to Sheathing Connector | 1/2" Gypsum fastened with #6-1/4" long screws | 10000 | 0.015 | -0.030 | 1.1 | 0.007 | 100 | 20 | 0.20 | 0.8 | 1.1 |
| 8′ x10′ Wall | 19/32" Plywood - 10d common nails @ 4" oc | 21250 | 0.037 | -0.04 | 1.3 | 0.012 | 8366 | 1744 | 2.44 | 0.74 | 1.1 |
| 8′ x10′ Wall | 19/32" Plywood - 10d common nails @ 2" oc | 36125 | 0.037 | -0.04 | 1.3 | 0.012 | 14223 | 2966 | 2.44 | 0.74 | 1.1 |

### *9.4.7 Uncertainty due to Model Quality*

For the purpose of assessing uncertainty, the structural modeling approach for the wood light-frame archetypes captures the primary shear deterioration modes of the shear walls that precipitate side-sway collapse. However, not all behavioral aspects are captured by this system-level modeling, such as axial-flexural interaction effects of the wall elements, the uplift of narrow wall ends, and the slippage of sill and top plates. These effects are secondary for walls with low aspect ratios, which deform mainly in a shear mode, but are important for archetypes incorporating walls with high aspect ratios. Therefore, the structural model for the archetypes incorporating low-aspect ratio walls is rated as "B-Good", while the same structural model for the archetypes incorporating high-aspect ratio walls is rated as "C-Fair".

### *9.4.8 Nonlinear Structural Analyses*

To compute the system overstrength, $\Omega$, and help verify the structural model, monotonic static pushover analysis is used with an inverted triangular lateral load pattern. Figure 9-18 shows an example of the pushover curve for the two-story archetype model No. 5 without gypsum wallboard. For this example wood light-frame building, the design LRFD seismic coefficient $V/W = 0.167$ and occurs at a roof drift ratio (lateral roof displacement divided by the building height) of 0.0043. Capping (the onset of negative stiffness) occurs for a seismic coefficient of 0.339 and at a roof drift ratio of 0.0321. Therefore, $\Omega = 2.04$ for this archetype model

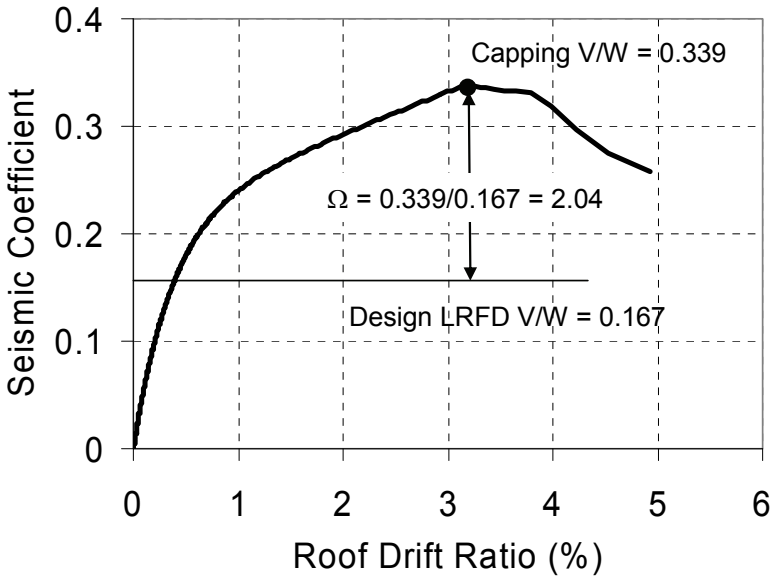


Figure 9-18 Monotonic Static Pushover Curve and Computation of $\Omega$ for Two-Story Wood Light-Frame Archetype No. 5 without Gypsum Wallboard.

To compute the collapse capacity of each wood light-frame archetype design, the Incremental Dynamic Analysis (IDA) approach is used with the Far-Field record set and ground motion scaling method presented in Appendix A. The intensity of the ground motion causing collapse of the wood light-frame archetype models is defined as the point on the intensity-drift IDA plot having a nearly horizontal slope but without exceeding a peak inter-story drift of 7% in any wall of a model. This collapse inter-story drift limit was selected based on recent collapse shake table testing conducted on full-scale two-story wood buildings in Japan (Isoda et al. 2007).

Figure 9-19 and Figure 9-20 illustrate how the IDA method is used to compute the collapse margin ratio, *CMR*, for the two-story archetype model No. 5 without gypsum wallboard. The spectral acceleration at collapse is computed for each of the 44 ground motions of the Far-Field Set, as shown in Figure 9-19. The collapse fragility curve can then be constructed from the IDA plots, as shown in Figure 9-20. The collapse level earthquake spectral acceleration (spectral acceleration causing collapse in 50% of the analyses) is $\hat{S}_{CT}(T = 0.26 \text{ sec}) = 2.15$ g for this example. The collapse margin ratio, *CMR*, of 1.43 is then computed as the ratio of $\hat{S}_{CT}$ to the spectral acceleration value at period $T = 0.26$ sec for the MCE $S_{MT} = 1.50$ g.

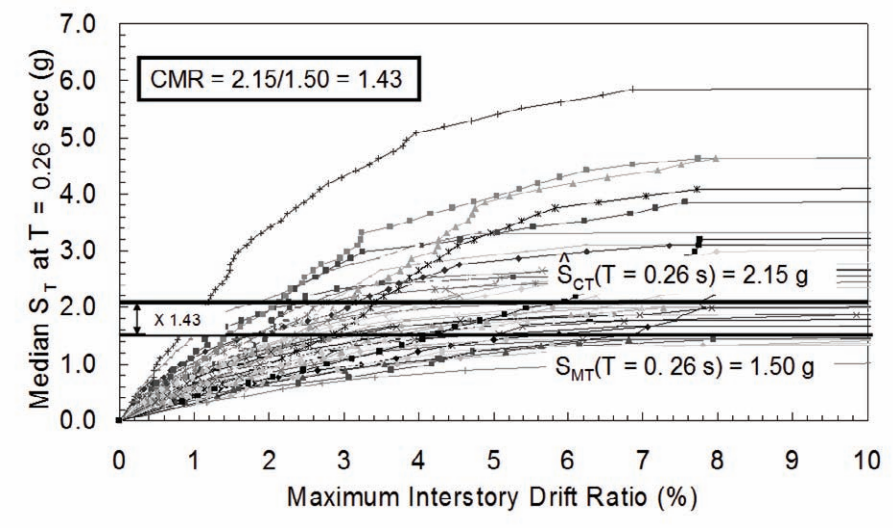


Figure 9-19 Results of Incremental Dynamic Analysis to Collapse for Two-Story Wood Light-Frame Archetype No. 5 without Gypsum Wallboard.

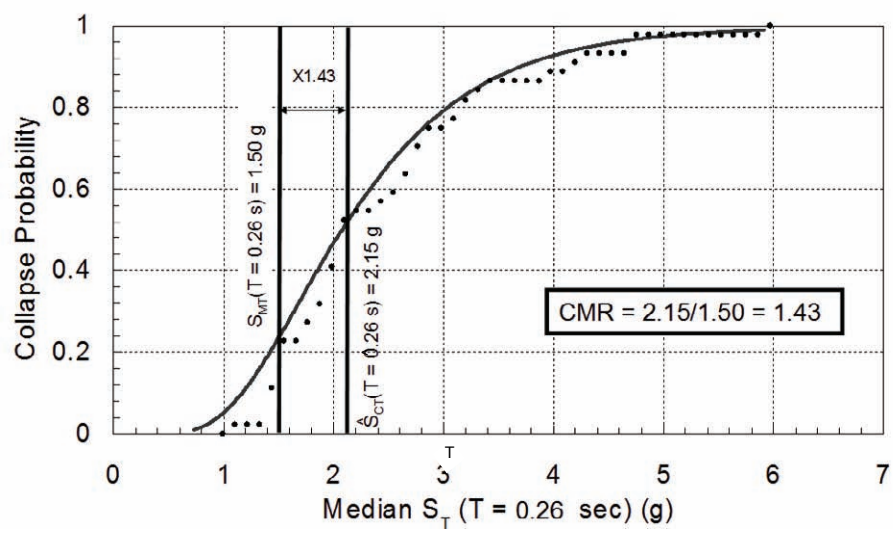


Figure 9-20 Collapse Fragility Curve for Two-Story Wood Light-Frame Archetype No. 5 without Gypsum Wallboard.

Static pushover analyses were conducted and the IDA method was applied to each of the 16 wood light-frame archetype designs without gypsum wallboard. Table 9-23 summarizes the results of these analyses. These IDA results indicate that the average collapse margin ratio is 1.42 for the SDC $D_{max}$ – low aspect ratio buildings, 1.85 for the SDC $D_{max}$ – high aspect ratio buildings, 2.35 for the SDC $D_{min}$ – low aspect ratio buildings and 2.46 for the SDC $D_{min}$ – high aspect ratio buildings. These margin values, however, have not yet been adjusted for the beneficial effects of spectral shape (as described

in Appendix B). Allowable collapse margins and acceptance criteria are discussed later.

The results shown in Table 9-23 show that the wood light-frame buildings without gypsum wallboard designed in low-seismic regions (SDC $D_{min}$) have higher collapse margin ratios (lower collapse risk) compared with the performance group of buildings designed in high-seismic regions (SDC-$D_{max}$). It is believed that this result originates from the longer periods of vibration for the low-seismic buildings compared to those of the high-seismic buildings, since the longer periods reduce seismic demands. Also, buildings incorporating walls with high aspect ratios have higher collapse margin ratios than those for buildings incorporating low aspect ratios. This is the result of the ASCE/SEI 7-05 strength reduction factor applied to walls with high aspect ratios, which cause an increase in required number of nails to reach a given strength. This increased nailing density causes an increase in the shear capacity of the walls with high aspect ratios, but the model does not account for the associated increase in flexural deformations.

**Table 9-23 Summary of Collapse Results for Wood Light-Frame Archetype Designs without Gypsum Wallboard**

| Model No. | No. of Stories | Building Configuration | Wall Aspect Ratio | Period $T$ (sec) | V/W | $S_{MT}$ (g) | Static $\Omega$ | $S_{CT}$ (g) | CMR |
|---|---|---|---|---|---|---|---|---|---|
| **High Seismic (SDC $D_{max}$) - Low Aspect Ratios - R = 6** | | | | | | | | | |
| 1 | 1 | Commercial | Low | 0.25 | 0.167 | 1.50 | 1.55 | 1.94 | 1.29 |
| 5 | 2 | Commercial | Low | 0.26 | 0.167 | 1.50 | 2.04 | 2.15 | 1.43 |
| 9 | 3 | Commercial | Low | 0.36 | 0.167 | 1.50 | 1.56 | 2.28 | 1.52 |
| Mean | | | | | | | 1.72 | | 1.42 |
| **High Seismic (SDC $D_{max}$) - High Aspect Ratios - R = 6** | | | | | | | | | |
| 2 | 1 | 1&2 Family | High | 0.25 | 0.167 | 1.50 | 3.06 | 2.51 | 1.67 |
| 6 | 2 | 1&2 Family | High | 0.26 | 0.167 | 1.50 | 2.80 | 2.93 | 1.95 |
| 10 | 3 | Multi-Family | High | 0.36 | 0.167 | 1.50 | 2.81 | 2.98 | 1.99 |
| 13 | 4 | Multi-Family | High | 0.45 | 0.167 | 1.50 | 2.71 | 2.77 | 1.85 |
| 15 | 5 | Multi-Family | High | 0.53 | 0.167 | 1.50 | 2.37 | 2.71 | 1.81 |
| Mean | | | | | | | 2.75 | | 1.85 |
| **Low Seismic (SDC $D_{min}$) - Low Aspect Ratios - R = 6** | | | | | | | | | |
| 11 | 3 | Commercial | Low | 0.41 | 0.063 | 0.75 | 1.56 | 1.76 | 2.35 |
| Mean | | | | | | | 1.56 | | 2.35 |
| **Low Seismic (SDC $D_{min}$) - High Aspect Ratios - R = 6** | | | | | | | | | |
| 3 | 1 | Commercial | High | 0.25 | 0.063 | 0.75 | 2.72 | 1.67 | 2.23 |
| 4 | 1 | 1&2 Family | High | 0.25 | 0.063 | 0.75 | 4.09 | 1.81 | 2.41 |
| 7 | 2 | Commercial | High | 0.30 | 0.063 | 0.75 | 3.10 | 1.90 | 2.53 |
| 8 | 2 | 1&2 Family | High | 0.30 | 0.063 | 0.75 | 2.51 | 1.76 | 2.35 |
| 12 | 3 | Multi-Family | High | 0.41 | 0.063 | 0.75 | 3.07 | 2.13 | 2.84 |
| 14 | 4 | Multi-Family | High | 0.51 | 0.063 | 0.75 | 2.59 | 1.98 | 2.64 |
| 16 | 5 | Multi-Family | High | 0.60 | 0.063 | 0.75 | 2.44 | 1.68 | 2.24 |
| Mean | | | | | | | 2.93 | | 2.46 |

### *9.4.9 Evaluation of Collapse Margin Ratio and Acceptance Criteria for Light-Frame Wood Archetypes without Gypsum Wallboard*

The collapse margin ratios computed above do not account for the unique spectral shape of rare ground motions. Spectral shape adjustment factors, *SSF*, must be applied to the collapse spectral acceleration, $S_{CT}$, to account for spectral shape effect. Based on the simplified method contained in Appendix

B, the *SSF* can be established for each archetype model based on its global ductility capacity, $\mu_c$, obtained from the pushover curve. Figure 9-21 shows an example of the calculation of $\mu_c$ from the pushover curve for the two-story archetype model No. 5 without gypsum wallboard. An idealized elastic-perfectly plastic pushover curved is defined through a secant stiffness anchored at 60% of the capping strength. This secant stiffness then intercepts a horizontal line passing through the capping strength. The ductility capacity, $\mu_c$, of 4.36 is then computed as the ratio of the ultimate roof drift ratio (defined as the drift ratio at 80% of the capping strength in the descending branch of the pushover curve) $\Delta_{ult}$ = 0.0454 to the equivalent yield roof drift ratio $\Delta_y$ = 0.0104.

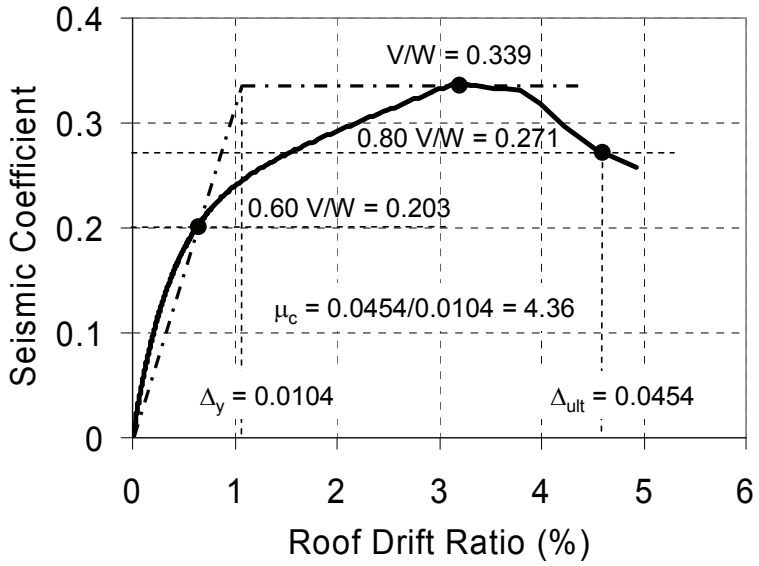


Figure 9-21 Monotonic Static Pushover Curve and Computation of $\mu_c$ for Two-Story Wood Light-Frame Archetype No. 5 without Gypsum Wallboard.

The adjusted collapse margin ratio, *ACMR*, is then computed for each wood light-frame archetype design without gypsum wallboard as the multiple of the *SSF* (from Table 7-1b for SDC D) and *CMR* (from Table 9-23). Table 9-24 shows the resulting adjusted collapse margin ratios for the wood light-frame archetypes.

To calculate acceptable values of the adjusted collapse margin ratio, the total system uncertainty is needed. Chapter 7 provides guidance for this calculation. Table 7-2 shows these composite uncertainties, which account for the variability between ground motion records of a given intensity (defined as a constant $\beta_{RTR}$ = 0.40), the uncertainty in the nonlinear structural modeling, the quality of the test data used to calibrate the element models, and the quality of the structural system design requirements. For this

example assessment, the composite uncertainty was based on a "B-Good" model quality for archetypes with low aspect ratio walls and a "C-Fair" for archetypes with high aspect ratio walls, "A-Superior" quality of design requirements" and "B-Good" quality of test data. Thus, $\beta_{TOT} = 0.60$ for archetype buildings incorporating low aspect ratio walls (Table 7-2b) and $\beta_{TOT} = 0.70$ for archetype buildings incorporating high aspect ratio walls (Table 7-2c).

An acceptable collapse margin ratio must now be selected based on a composite uncertainty, $\beta_{TOT}$, and a target collapse prevention probability. Table 7-3 presents acceptable values of adjusted collapse margin ratio computed assuming a lognormal distribution of collapse capacity. Chapter 7 defines the collapse performance objectives as: (1) a conditional collapse probability of 20% for all wood light-frame archetype models, and (2) a conditional collapse probability of 10% for the average of each of the four performance groups of wood light-frame archetypes (two SDC and two wall aspect ratios). For archetype buildings incorporating low aspect ratio walls, this corresponds to an acceptable collapse margin ratio *CMR20*% of 1.66 for every wood light-frame archetype and a *CMR10*% of 2.16 for each performance group. For archetype buildings incorporating high aspect ratio walls, this corresponds to an acceptable collapse margin ratio *CMR20*% of 1.80 for every wood light-frame archetype and a *CMR10*% of 2.45 for each performance group.

Table 9-24 presents the final results and acceptance criteria for each of the 16 wood light-frame archetype designs without gypsum wallboard. The table presents the collapse margin ratios computed directly from the collapse fragility curves, *CMR*, the ductility capacities, $\mu_c$, the *SSF*, and the adjusted collapse margin ratio, *ACMR*. The acceptable adjusted collapse margin ratios are shown and each archetype is shown to either pass or fail the acceptance criteria. Average collapse margin ratios are also shown for the four different performance groups of archetypes.

The results shown in Table 9-24 indicate that the high-seismic designs control and have lower adjusted collapse margins ratios than the low-seismic designs. Similarly, the archetype buildings incorporating low-aspect ratio walls control with lower collapse margin ratios than the high-aspect ratio designs.

The results shown in Table 9-24 indicate also that all but one (Archetype No. 1) of the 16 wood light-frame archetype designs have acceptable individual adjusted collapse margin ratios. The two high seismic performance groups (SDC $D_{max}$), however, do not have acceptable average collapse margin ratios,

and fail the acceptance criteria of the Methodology. Therefore, if wood light-frame buildings without consideration of gypsum wallboard were a "newly proposed" seismic-force-resisting system with $R = 6$, it would not meet the collapse performance objectives of the Methodology, and would need adjustments in the design requirements to meet the performance intent.

**Table 9-24 Adjusted Collapse Margin Ratios and Acceptable Collapse Margin Ratios for Wood Light-Frame Archetype Designs without Gypsum Wallboard**

| Model No. | Period $T$ (sec) | Static $\Omega$ | CMR | $\mu_c$ | SSF | ACMR | Acceptable ACMR | Pass/Fail |
|---|---|---|---|---|---|---|---|---|
| **High Seismic (SDC $D_{max}$) - Low Aspect Ratios - R = 6** | | | | | | | | |
| 1 | 0.25 | 1.55 | 1.29 | 4.45 | 1.26 | 1.63 | 1.66 | Fail |
| 5 | 0.26 | 2.04 | 1.43 | 4.36 | 1.26 | 1.81 | 1.66 | Pass |
| 9 | 0.36 | 1.56 | 1.52 | 4.05 | 1.25 | 1.90 | 1.66 | Pass |
| Mean | | 1.72 | 1.42 | | | 1.78 | 2.16 | Fail |
| **High Seismic (SDC $D_{max}$) - High Aspect Ratios - R = 6** | | | | | | | | |
| 2 | 0.25 | 3.06 | 1.67 | 3.89 | 1.24 | 2.07 | 1.80 | Pass |
| 6 | 0.26 | 2.80 | 1.95 | 3.91 | 1.24 | 2.42 | 1.80 | Pass |
| 10 | 0.36 | 2.81 | 1.99 | 4.74 | 1.27 | 2.52 | 1.80 | Pass |
| 13 | 0.45 | 2.71 | 1.85 | 2.99 | 1.21 | 2.23 | 1.80 | Pass |
| 15 | 0.53 | 2.37 | 1.81 | 2.98 | 1.22 | 2.20 | 1.80 | Pass |
| Mean | | 2.75 | 1.85 | | | 2.29 | 2.45 | Fail |
| **Low Seismic (SDC $D_{min}$) - Low Aspect Ratios - R = 6** | | | | | | | | |
| 11 | 0.41 | 1.56 | 2.35 | 2.73 | 1.08 | 2.53 | 1.66 | Pass |
| Mean | | 1.56 | 2.35 | | | 2.53 | 2.16 | Pass |
| **Low Seismic (SDC $D_{min}$) - High Aspect Ratios - R = 6** | | | | | | | | |
| 3 | 0.25 | 2.72 | 2.23 | 4.20 | 1.10 | 2.45 | 1.80 | Pass |
| 4 | 0.25 | 4.09 | 2.41 | 4.18 | 1.10 | 2.65 | 1.80 | Pass |
| 7 | 0.30 | 3.10 | 2.53 | 3.06 | 1.09 | 2.76 | 1.80 | Pass |
| 8 | 0.30 | 2.51 | 2.35 | 3.55 | 1.10 | 2.58 | 1.80 | Pass |
| 12 | 0.41 | 3.07 | 2.84 | 3.25 | 1.09 | 3.10 | 1.80 | Pass |
| 14 | 0.51 | 2.59 | 2.64 | 2.60 | 1.08 | 2.85 | 1.80 | Pass |
| 16 | 0.60 | 2.44 | 2.24 | 2.58 | 1.10 | 2.46 | 1.80 | Pass |
| Mean | | 2.93 | 2.46 | | | 2.69 | 2.45 | Pass |

The fact that $R = 6$ does not work for these short period (0.25-0.6 second) systems is not surprising. The need for higher strengths in short period systems has been shown by many researchers (Newmark and Hall 1973; Takeda et al. 1988; Nassar and Krawinkler 1991; Miranda and Bertero 1994; and many others). Using single degree of freedom systems, Newmark showed that, for constant ductility demands, systems that are designed for R = 6 at periods greater than 0.6 seconds, should be designed for reduced values (R = 3.5) for periods between 0.15 and 0.3 seconds, and further reduced values (R = 1) for periods below 0.1 seconds. Such trends look generally consistent with the observations of this example (specifically for periods in the range of 0.25-0.35 seconds), but additional buildings with periods greater than 0.6 seconds would need to be added to confirm Newmark's trends for single degree of freedom systems.

The concept of a period-dependent $R$ factor is not consistent with ASCE/SEI 7-05, so this option is not pursued in this example. Instead, additional

strength and stiffness provided by the gypsum wallboard, applied on the interior faces of the structural wood walls, is considered, with the goal of determining whether or not the addition of gypsum wallboard will increase the collapse capacity enough so that $R = 6$ leads to acceptable collapse performance for wood light-frame buildings.

### *9.4.10 Consideration of Gypsum Wallboard*

Since the $R = 6$ for light-frame wood archetype buildings without consideration of gypsum wallboard did not pass the acceptance criteria, archetype buildings are re-analyzed with ½ in. thick gypsum wallboard applied to the interior surfaces of all wood structural panel shear walls in the archetype designs. Although gypsum wallboard is not specifically considered by ASCE/SEI 7-05 in the design process for light-frame wood buildings braced by structural panel shear walls, it is applied to the interior surfaces of structural wood walls in the vast majority of buildings, making it reasonable to consider gypsum wood panels in the analytical model. The collapse capacity of each wood light-frame archetype building with gypsum wallboard in addition to wood structural panel sheathing is re-evaluated using the Incremental Dynamic Analysis, IDA, approach described above and the Far-Field ground motion set.

First, the gypsum wallboard is assumed to be attached with #6 1-1/4 in. long drywall screws spaced at 16 in. on center along the vertical studs only of all wood structural walls. This spacing of the screws is first considered since it is commonly used in residential construction. Table 9-25 presents the IDA results and acceptance criteria for each of the 16 wood light-frame archetype buildings including this configuration of gypsum wallboard. The results shown in Table 9-25 indicate that the incorporation of the gypsum wallboard with screws spaced at 16 in. on center improved the collapse capacity of the wood light-frame archetype buildings. Note also the significant increase in ductility capacities, $\mu_c$, of the archetypes incorporating gypsum wallboard. This is the result of the increase in initial lateral stiffness caused by the gypsum wallboard, which results in lower yield roof drift ratios $\Delta_y$.

The results shown in Table 9-25 indicate also that all of the 16 wood light-frame archetype designs now have acceptable individual adjusted collapse margin ratios. However, the two high seismic performance groups (SDC $D_{max}$) still do not have an acceptable average collapse margin ratio, and again fail the acceptance criteria of the Methodology. Therefore, a different configuration of gypsum wallboard is considered.

**Table 9-25 Adjusted Collapse Margin Ratios and Acceptable Collapse Margin Ratios for Wood Light-Frame Archetype Designs with ½ in. thick Gypsum Wallboard Attached with #6 1-1/4 Drywall Screws Spaced at 16 in.**

| Model No. | Period $T$ (sec) | Static $\Omega$ | CMR | $\mu_c$ | SSF | ACMR | Acceptable ACMR | Pass/Fail |
|---|---|---|---|---|---|---|---|---|
| **High Seismic (SDC $D_{max}$) - Low Aspect Ratios - R = 6** | | | | | | | | |
| 1 | 0.25 | 1.57 | 1.34 | 7.25 | 1.32 | 1.77 | 1.66 | Pass |
| 5 | 0.26 | 2.02 | 1.45 | 7.27 | 1.32 | 1.92 | 1.66 | Pass |
| 9 | 0.36 | 1.70 | 1.70 | 6.05 | 1.30 | 2.21 | 1.66 | Pass |
| Mean | | 1.76 | 1.50 | | | 1.97 | 2.16 | Fail |
| **High Seismic (SDC $D_{max}$) - High Aspect Ratios - R = 6** | | | | | | | | |
| 2 | 0.25 | 3.05 | 1.87 | 7.61 | 1.33 | 2.49 | 1.80 | Pass |
| 6 | 0.26 | 2.88 | 1.95 | 5.27 | 1.28 | 2.50 | 1.80 | Pass |
| 10 | 0.36 | 2.89 | 2.13 | 5.85 | 1.29 | 2.75 | 1.80 | Pass |
| 13 | 0.45 | 2.78 | 1.81 | 3.89 | 1.24 | 2.24 | 1.80 | Pass |
| 15 | 0.53 | 2.43 | 1.75 | 3.43 | 1.23 | 2.16 | 1.80 | Pass |
| Mean | | 2.81 | 1.90 | | | 2.43 | 2.45 | Fail |
| **Low Seismic (SDC $D_{min}$) - Low Aspect Ratios - R = 6** | | | | | | | | |
| 11 | 0.26 | 1.62 | 2.35 | 3.70 | 1.10 | 2.58 | 1.73 | Pass |
| Mean | | 1.62 | 2.35 | | | 2.58 | 2.30 | Pass |
| **Low Seismic (SDC $D_{min}$) - High Aspect Ratios - R = 6** | | | | | | | | |
| 3 | 0.25 | 2.71 | 2.25 | 7.70 | 1.14 | 2.57 | 1.88 | Pass |
| 4 | 0.25 | 4.06 | 2.71 | 8.23 | 1.14 | 3.09 | 1.88 | Pass |
| 7 | 0.30 | 3.08 | 2.49 | 4.20 | 1.10 | 2.74 | 1.88 | Pass |
| 8 | 0.30 | 2.47 | 2.37 | 5.25 | 1.12 | 2.66 | 1.88 | Pass |
| 12 | 0.41 | 3.01 | 2.84 | 4.38 | 1.11 | 3.15 | 1.88 | Pass |
| 14 | 0.51 | 2.59 | 2.79 | 3.54 | 1.10 | 3.07 | 1.88 | Pass |
| 16 | 0.60 | 2.40 | 2.08 | 3.23 | 1.11 | 2.31 | 1.88 | Pass |
| Mean | | 2.90 | 2.50 | | | 2.80 | 2.61 | Pass |

During an iterative process involving various spacing of drywall screws, it was found that the collapse capacity of the wood light-frame archetypes was mainly governed by the spacing of the screws in the first story of the archetypes. Spacing of screws in the upper stories had very little influence on the collapse capacity. This makes intuitive sense because the collapse mechanism associated with the wood light-frame archetype buildings is mainly governed by a weak first story side-sway collapse mechanism.

Table 9-26 presents the results of the analyses and acceptance criteria for each of the 16 wood light-frame archetype buildings incorporating gypsum wallboard attached with #6 1-1/4 in. long screws spaced at 4 in on center along the vertical studs and top and bottom plates in the first story and at 16 in. on center along the vertical studs only in the upper stories of the archetypes buildings. The results of Table 9-26 show that all of the 16 wood light-frame archetype designs have acceptable individual adjusted collapse margin ratios.

**Table 9-26 Adjusted Collapse Margin ratios and Acceptable Collapse Margin Ratios for Wood Light-Frame Archetype Designs with ½ in. Thick Gypsum Wallboard Attached with #6 1-1/4 Drywall Screws spaced at 4 in. in First Story and 16 in. in all other Upper Stories**

| Model No. | Period $T$ (sec) | Static $\Omega$ | CMR | $\mu_c$ | SSF | ACMR | Acceptable ACMR | Pass/Fail |
|---|---|---|---|---|---|---|---|---|
| **High Seismic (SDC $D_{max}$) - Low Aspect Ratios - R = 6** | | | | | | | | |
| 1 | 0.25 | 2.41 | 1.52 | 8.05 | 1.34 | 2.04 | 1.66 | Pass |
| 5 | 0.26 | 2.05 | 1.63 | 6.13 | 1.30 | 2.12 | 1.66 | Pass |
| 9 | 0.36 | 1.71 | 1.67 | 6.29 | 1.30 | 2.17 | 1.66 | Pass |
| Mean | | 2.06 | 1.61 | | | 2.11 | 2.16 | Near Pass |
| **High Seismic (SDC $D_{max}$) - High Aspect Ratios - R = 6** | | | | | | | | |
| 2 | 0.25 | 4.79 | 1.98 | 7.64 | 1.33 | 2.63 | 1.80 | Pass |
| 6 | 0.26 | 2.88 | 1.99 | 7.49 | 1.33 | 2.64 | 1.80 | Pass |
| 10 | 0.36 | 2.90 | 2.07 | 6.64 | 1.31 | 2.72 | 1.80 | Pass |
| 13 | 0.45 | 3.02 | 2.09 | 5.83 | 1.29 | 2.70 | 1.80 | Pass |
| 15 | 0.53 | 2.47 | 1.89 | 3.07 | 1.22 | 2.30 | 1.80 | Pass |
| Mean | | 3.21 | 2.00 | | | 2.60 | 2.45 | Pass |
| **Low Seismic (SDC $D_{min}$) - Low Aspect Ratios - R = 6** | | | | | | | | |
| 11 | 0.41 | 1.62 | 1.99 | 3.90 | 1.10 | 2.19 | 1.66 | Pass |
| Mean | | 1.62 | 1.99 | | | 2.19 | 2.16 | Pass |
| **Low Seismic (SDC $D_{min}$) - High Aspect Ratios - R = 6** | | | | | | | | |
| 3 | 0.25 | 4.23 | 2.47 | 8.63 | 1.14 | 2.81 | 1.80 | Pass |
| 4 | 0.25 | 6.35 | 2.89 | 7.77 | 1.14 | 3.30 | 1.80 | Pass |
| 7 | 0.30 | 3.20 | 2.61 | 6.05 | 1.12 | 2.93 | 1.80 | Pass |
| 8 | 0.30 | 3.06 | 2.59 | 7.09 | 1.13 | 2.92 | 1.80 | Pass |
| 12 | 0.41 | 3.07 | 2.47 | 3.66 | 1.10 | 2.71 | 1.80 | Pass |
| 14 | 0.51 | 2.59 | 2.59 | 3.75 | 1.10 | 2.85 | 1.80 | Pass |
| 16 | 0.60 | 2.42 | 2.00 | 3.30 | 1.11 | 2.22 | 1.80 | Pass |
| Mean | | 3.56 | 2.52 | | | 2.82 | 2.45 | Pass |

Only the high seismic/low aspect ratios performance group slightly underachieves the acceptable average collapse margin ratio ($ACMR$ = 2.11 vs. Acceptable $ACMR$ = 2.16). Considering that other gypsum partition walls will contribute to the collapse capacities of the archetype buildings, it could be concluded that the current seismic provisions for engineered wood light-frame construction included in the ASCE/SEI 7-05 are adequate to provide an acceptable collapse safety with $R$ = 6, if ½-inch thick gypsum wallboard is attached to the interior surfaces of the structural wood walls with #6 x 1-1/4 inch long screws spaced at least at 4 inches on center along the vertical studs and the top and bottom plates in the first stories, and 16 in. on center along the vertical studs in all the other upper stories of the buildings.

### *9.4.11 Calculation of $\Omega_0$ using Set of Archetype Designs*

The value of the overstrength factor, $\Omega_0$, that would be used in the design provisions for the "newly-proposed" wood light-frame system incorporating the final configuration of gypsum wallboard is computed. Table 9-26 shows the calculated $\Omega$ values for each of the archetypes, with a range of values from 1.6 to 6.4, and an average value of 3.2. The average values for each

Performance Group, are 2.1, 3.2, 1.6, and 3.6, with the largest value of 3.6 being for the high aspect ratio walls designed for low-seismic demands.

Tthe $\Omega_o$ value should be conservatively based on these individual values, rounded to the nearest 0.5, and limited to a maximum value of 3.0; this is subject to judgment and the Peer Review process. For this example, the upper-bound value of $\Omega_o = 3.0$ is warranted, due to the large average $\Omega$ values observed for several of the archetype buildings, and the average values being greater than 3.0 for two of the Performance Groups.

### *9.4.12 Alternative Wood-Only Designs with Reduced R Factors*

As an alternative to relying on the application of gypsum wallboard on the interior surfaces of wood structural walls design with $R = 6$, wood-only structures could also be designed with a lower value of the $R$ factor, and still meet the acceptance criteria of the Methodology. An iterative process is used to identify a reduced value of $R$ that meets these criteria without consideration of the effects of gypsum wallboard. Only the high seismic - low aspect ratios archetype models are considered since, from the results presented above, this performance group controls the selection of $R$.

First, the three archetype buildings of the high seismic/low aspect ratio performance group were re-designed with a value of $R = 4$. Appendix C provides detailed descriptions of these re-designed archetype models. Table 9-27 presents the results of the IDA analyses and acceptance criteria for each of these $R = 4$ archetype buildings. The results shown in Table 9-27 indicate that archetypes designed for $R = 4$ still do not meet the acceptable average values of adjusted collapse margin ratio. Based on this, a lower value of $R$ must be considered.

**Table 9-27 Adjusted Collapse Margin Ratios and Acceptable Collapse Margin Ratios for Wood Light-Frame Archetypes Re-Designed for $R = 4$ and without Gypsum Wallboard**

| Model No. | Period $T$ (sec) | Static $\Omega$ | CMR | $\mu_c$ | SSF | ACMR | Acceptable ACMR | Pass/Fail |
|---|---|---|---|---|---|---|---|---|
| **High Seismic (SDC $D_{max}$) - Low Aspect Ratios - R = 4** | | | | | | | | |
| 1A | 0.25 | 1.65 | 1.52 | 3.90 | 1.25 | 1.90 | 1.66 | Pass |
| 5A | 0.26 | 1.70 | 1.73 | 3.84 | 1.24 | 2.14 | 1.66 | Pass |
| 9A | 0.36 | 1.70 | 1.65 | 3.54 | 1.23 | 2.03 | 1.66 | Pass |
| Mean | | 1.68 | 1.63 | | | 2.02 | 2.16 | Fail |

The three archetypes buildings of the high seismic/low aspect ratio performance group were re-designed again for a value of $R = 3$. Appendix C provides detailed descriptions of these re-designed archetype models. Table 9-28 presents the results of the IDA analyses and acceptance criteria for each of these $R = 3$ archetype buildings. The results shown in Table 9-28 indicate

that the archetypes designed for $R = 3$ now meet the acceptable average collapse margin ratio.

The average $\Omega$ value from Table 9-28 is 1.55, but this is only based on data for the performance group that was critical for determining the appropriate $R$ factor (low aspect ratio, high seismic). This is not enough information to determine an appropriate value of the system overstrength factor, $\Omega_0$, because Table 9-26 previously showed that walls with high aspect ratios tend to have much higher $\Omega$ values. To determine an appropriate value of $\Omega_0$, archetype designs would need to be completed and analyzed for the performance groups that are expected to have higher $\Omega$ values, which are the high aspect ratio walls for this example.

**Table 9-28 Adjusted Collapse Margin Ratios and Acceptable Collapse Margin Ratios for Wood Light-Frame Archetypes Re-designed for R = 3 and without Gypsum Wallboard**

| Model No. | Period $T$ (sec) | Static $\Omega$ | CMR | $\mu_c$ | SSF | ACMR | Acceptable ACMR | Pass/Fail |
|---|---|---|---|---|---|---|---|---|
| High Seismic (SDC $D_{max}$) - Low Aspect Ratios - R = 3 | | | | | | | | |
| 1B | 0.25 | 1.51 | 1.67 | 4.09 | 1.25 | 2.09 | 1.66 | Pass |
| 5B | 0.26 | 1.59 | 2.21 | 4.38 | 1.26 | 2.79 | 1.66 | Pass |
| 9B | 0.36 | 1.55 | 1.99 | 4.71 | 1.27 | 2.53 | 1.66 | Pass |
| Mean | | 1.55 | 1.96 | | | 2.47 | 2.16 | Pass |

### *9.4.13 Summary Observations - Wood Light-Frame System*

This example shows that current seismic provisions for engineered wood light-frame construction included in the ASCE/SEI 7-05 are not necessarily adequate to provide an acceptable level of collapse safety if the effects of nonstructural wall finishes materials are ignored. This result is supported by past research on the behavior of short period systems.

Acceptable collapse safety is obtained with $R = 6$ only when the contribution of ½ in. thick gypsum wallboard attached with #6 1-1/4 in. long screws to the interior surfaces of all wood structural walls is considered. Specifications for gypsum wallboard would need to be included directly in the seismic design requirements of engineered wood light-frame for an $R = 6$ to be valid using this Methodology. Alternatively, a value of $R = 3$ would be adequate if the contribution of gypsum wallboard is ignored.

## 9.5 Example Applications - Summary Observations and Conclusions

### *9.5.1 Short Period Structures*

The wood light-frame system showed that additional strength was needed in in order to meet collapse performance objectives. These wood light-frame

buildings all have periods from 0.25-0.60 seconds. A similar trend can be observed in the one-story RC SMF perimeter frame archetype, with a period of 0.26 seconds.

This points to a general observation that short period systems need additional strength to meet collapse performance objectives. This finding is not new, but rather has been reported in research starting with Newmark and Hall in 1973 (Newmark 1973). Similar findings, based on single degree of freedom systems, have since been reported by a large number of researchers (Lai and Biggs 1980; Elghadamsi and Mohraz 1987; Riddell, Hidalgo, and Cruz 1989; Nassar and Krawinkler 1991; Vidic, Fajfar, and Fischinger 1992; Miranda and Bertero 1994). Similar findings have also been derived using simple MDOF systems (Takeda et al. 1998; Krawinkler and Zareian 2007).

Past research has clearly shown, and the example applications of this chapter have verified, that strength requirements should be higher for short period systems. This suggests the use of a period dependent *R* factor, which is lower for shorter period buildings, as is proposed in many of the referenced papers and reports on this topic. Currently, the ASCE/SEI 7 document utilizes period-independent *R* factors. Future work should look more closely at the question of period-dependent *R* factors and whether or not they should be considered for use in future versions of ASCE/SEI 7.

### *9.5.2 Tall Moment Frame Structures*

The reinforced concrete special moment frame (RC SMF) system example found a disturbing trend in that taller perimeter frame buildings (above 12 stories) designed based on ASCE/SEI 7-05 do not meet the collapse performance objectives of this methodology, with collapse safety getting worse with increased building height. This is caused by localization of the damage for taller buildings, which is driven primarily by higher P-Delta effects as the building height increases.

This issue could be addressed in various ways. More conservative beam-column strength ratios could be developed for taller buildings, more restrictive drift limits could be imposed, a period-dependent R factor could be used, or other approaches could be taken. In the example, the minimum base shear requirement of ASCE 7-02 was reintroduced into the design requirements. This was successful in reversing the trends and created increasing collapse safety with increasing building height.

This information was made available to the ASCE 7 Seismic Committee and a special code change proposal was passed in 2007 (Supplement No. 2),

amending the minimum base shear requirements of ASCE/SEI 7-05 to correct this potential deficiency.

### 9.5.3 Collapse Performances for Different Seismic Design Categories

Example applications generally found lower collapse safety for buildings designed in seismic design categories (SCDs) with higher levels of ground motion. For example, the *CMR* is typically lower for a building designed for SDC $D_{max}$, as compared to a building design for SDC $D_{min}$. This trend is primarily caused by the increasing effects of gravity loads for lower levels of seismic demand, which increases the overstrength of the structural system, and in turn increases the collapse capacity of the system.

This finding suggests that the *R* factor will be governed by the SDC with the strongest ground motion for which the system is proposed. Based on this observation, the Methodology requires that the SDC with the strongest ground motion be used when verifying the *R* factor. It is expected that such *R* factors will be conservative for other SDCs, but this trend should be confirmed in the archetype investigation.

# Chapter 10
# Supporting Studies

This chapter describes additional studies performed in support of the development of the Methodology. These studies supplement the illustrative examples presented in Chapter 9, and serve to illustrate selected aspects of the Methodology as applied to different seismic-force-resisting systems.

## 10.1 General

Two supporting studies are presented. One study assesses non-simulated failure modes in a steel special moment frame system. This study illustrates the use of component limit state checks to evaluate failure modes that are not explicitly simulated in the nonlinear analysis. This study also demonstrates the application of the Methodology to steel moment frame systems.

A second study performs collapse assessments on seismically-isolated systems. This study illustrates application of the Methodology to isolated structural systems, which have fundamentally different dynamic response characteristics, performance properties and collapse failure modes than those of conventional, fixed-base structures. This study also demonstrates the potential use of the Methodology as a tool for assessing the validity and developing improvements to current design requirements, in this case requirements for isolated structures.

## 10.2 Assessment of Non-Simulated Failure Modes in a Steel Special Moment Frame System

### *10.2.1 Overview and Approach*

The purpose of this example is to illustrate the use of separate component limit state checks to evaluate failure modes that are not explicitly simulated in the nonlinear analysis. This example follows the approach for non-simulated collapse modes described in Chapter 5.

The procedure for evaluating non-simulated collapse modes is illustrated through the evaluation of a steel special moment frame (SMF) structure, designed using pre-qualified Reduced Beam Section (RBS) connection details in accordance with current design standards (ASCE/SEI 7-05 and AISC 2005). This example focuses on assessment of a single steel SMF building, which in concept could be one of many index archetype

configurations serving to describe the full archetype design space for all steel SMFs. The procedures applied to this one building would be extended to the full set of index archetype models in order to evaluate the entire class of steel SMFs.

The primary inelastic deterioration of this special moment frame occurs through hinging in the RBS regions of the beams and the columns, which can lead to sidesway collapse under large deformations. While gradual deterioration of the inelastic hinges associated with yielding and local buckling is simulated in the analyses, sudden strength and stiffness degradation associated with ductile fractures are not explicitly modeled. In this example, ductile fracture is not simulated because of software limitations.

The use of separate non-simulated limit state checks is supported by a number of related factors. First, through the use of pre-qualified connections, the initiation of ductile fracture is unlikely to occur until large inelastic rotations have been reached and sidesway collapse has occurred or nearly occurred. Hence, the simplified limit state check for fracture is not expected to dominate the results. Second, available test data suggests that the location where ductile fracture may occur and the deformations at which ductile fracture may occur are highly variable, and simulation models would need to define correlations relating fracture probabilities at multiple connections. In this particular structure, where the large columns tend to enforce equal rotations across a story, the assumed correlations would be a dominant factor in spatial distributions of fractures. Thus, apart from the challenges of modeling sudden strength and stiffness degradation associated with ductile fracture directly in the model, without explicitly modeling uncertainties and correlations directly in the analysis, fractures would tend to form simultaneously across an entire story, similar to how non-simulated limit state checks would affect collapse results.

In order to ensure that the collapse assessment process represents the behavior of the structural system of interest, the choice to incorporate a particular failure mode using a limit state check in lieu of direct simulation should be based on careful consideration of these factors. Where non-simulated failure modes dominate the results, or where their exclusion jeopardizes simulation accuracy before the non-simulated limit state is reached, the appropriateness of the nonlinear model must be re-examined.

### *10.2.2 Structural System Information*

The steel SMF archetype design analyzed in this example (Figure 10-1) is one of four perimeter moment frames that comprise the seismic-force-resisting system of a four-story building. The building is designed assuming a high seismic site located in Seismic Design Category D, based on $T = 0.94$ second and an MCE spectral demand, $S_{MT}$, of 0.96g (corresponding to $D_{max}$). The structure has a design base shear, $V = 0.08W$. As designed according to ASCE/SEI 7-05 and AISC 2005, beams range in size from W24 to W30 (Figure 10-1), and are governed by minimum stiffness (drift limit) requirements. The RBS sections have 45% flange reduction. W24 columns are sized to satisfy the connection panel zone strength requirements without the use of web doubler plates. As such, they automatically satisfy other requirements, including the strong-column weak-beam (SCWB) requirement. The resulting SCWB ratio is about 2.5 times larger than the minimum requirement. This large column overstrength reflects a possible design decision that is representative of current practice in California; however, it implies that this example will not necessarily demonstrate the lower-bound performance of code-conforming steel SMFs. The design requirements for this system are well-established, reflecting a high degree of confidence and completeness. For the purpose of assessing system uncertainty, the design requirements are rated "A-Superior".

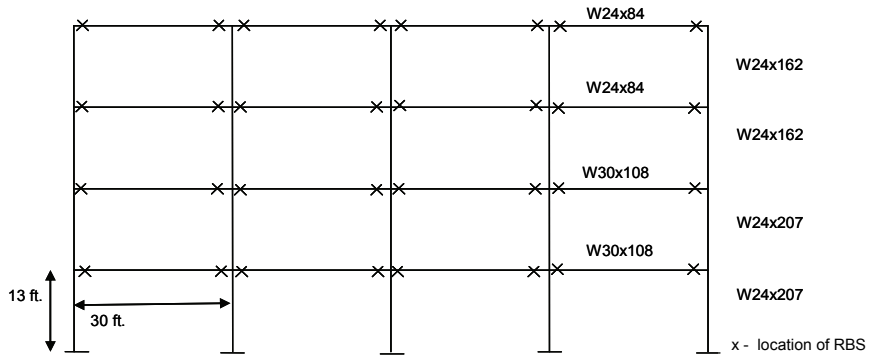


Figure 10-1 Archetype analysis model of steel special moment frame (SMF) seismic-force-resisting system

### *10.2.3 Nonlinear Analysis Model*

This structure is judged to have primarily two collapse modes: (1) sidesway collapse associated with beam and column hinging, and (2) collapse triggered by ductile fracture in one or more reduced beam section. The nonlinear response history analyses were run using the OpenSees (OpenSees 2006) software, employing elements with concentrated inelastic springs to capture

flexural hinging in beams and columns and an inelastic (finite size) joint model for the beam-column panel zone.

The model parameters for the beam and column (plastic rotation capacity, cyclic deterioration parameters, etc.) were calibrated to experimental test data (Lignos and Krawinkler, 2007) and use expected values for the steel yield strength. An example monotonic backbone curve and key modeling parameters for the column and beam hinges are shown in Figure 10-2. The joint panel zone yield point and hardening parameters are based on *AISC 05* Equation 9-1 and Krawinkler (1971, 1978); the panel zone spring is modeled as non-deteriorating with a bilinear kinematic hardening model.

As noted previously, the fracture failure mode is not modeled directly in the frame analysis, but rather is evaluated through a separate limit state check. Other modeling assumptions are consistent with the requirements of Chapter 5. The model is rated "B-Good" in accordance with Table 5-2; the model is judged to have a high degree of accuracy and robustness, but because of the potential for ductile fracture the structural behavior is judged to be "moderately controlled." The available test data is also rated "B-Good."

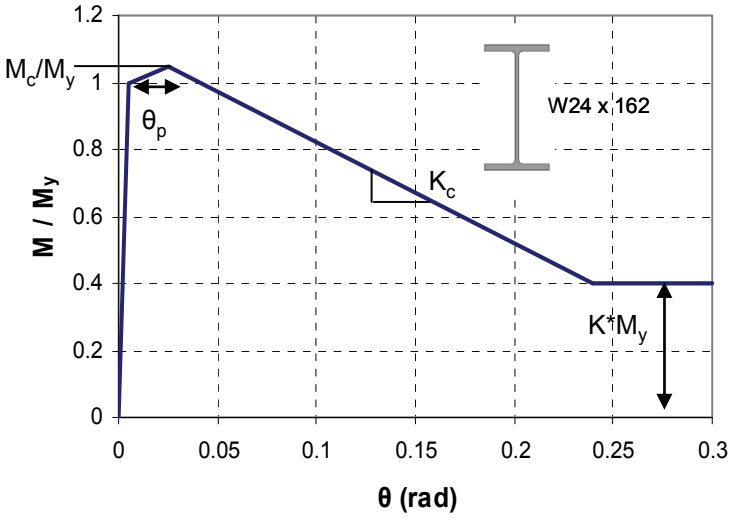


Figure 10-2 Modeling parameters used for beams and columns, based on calibration to experimental data by Lignos and Krawinkler (2007). Interested readers should refer to the notation and discussion in Appendix E.

### *10.2.4 Nonlinear Structural Analysis*

**Static Pushover Analysis**

The overstrength calculated by a static pushover analysis is $\Omega = 3.4$. The building ductility capacity, computed from the pushover,, is $\mu_c = 7.2$. Since all the failure modes are not simulated, $\mu_c$ is computed such that

$\Delta_u = \Delta_{fracture\ failure\ mode\ occurs}$. Occurrence of the fracture failure mode is based on the component limit established in Step (3) below.

The results of static pushover analysis for this structure are illustrated in Figure 10-3.

**Nonlinear Time History Analysis and Simulation**

The 4-story steel SMF was analyzed using the Far-Field record set (Appendix A) and nonlinear dynamic analyses (Chapter 6). From this analysis a median collapse capacity, $\hat{S}_{CT}$, of 2.36g is obtained. In comparison with MCE spectral demand, $S_{MT}$, of 0.96g, this corresponds to a collapse margin ratio, *CMR,* of 2.5. The total system collapse uncertainty (Chapter 7) is $\beta_{TOT} = 0.60$. Note that these values do not yet include the adjustment for the spectral shape factor (*SSF*). Due to very strong columns relative to the beams, the sidesway collapse mode is a full four-story mechanism with hinges in all the beam RBS regions and at the fixed column bases, for all ground motions.

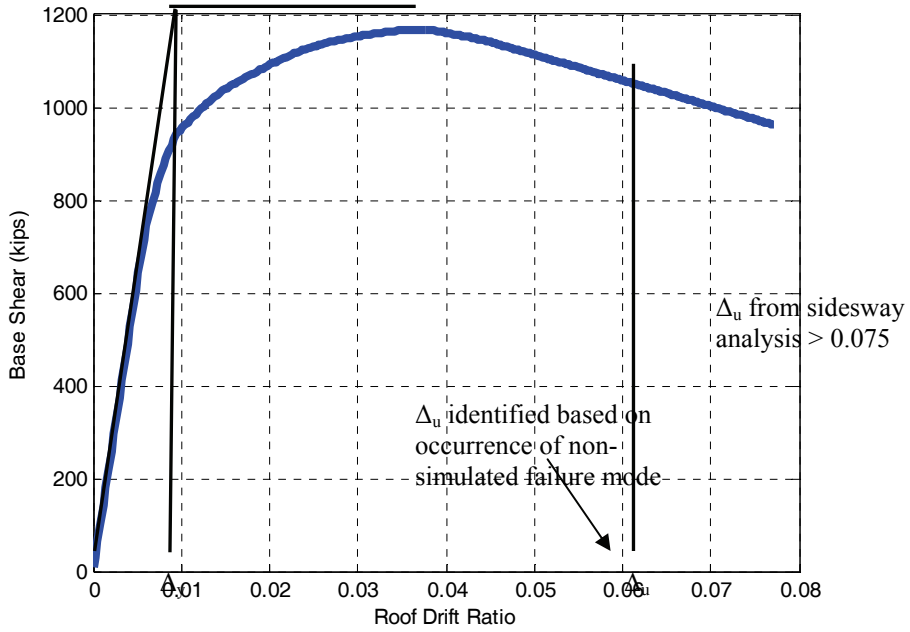


Figure 10-3 Static pushover analysis of steel frame model, illustrating computation of ductility ($\mu_c$).

### *10.2.5 Procedure for Incorporating Non-Simulated Failure Modes*

At this stage, however, results do not yet reflect consideration of non-simulated ductile fracture deterioration modes. Assessment of the collapse margin ratio including the non-simulated fracture models begins with the identification and calibration of appropriate limit-state models, followed by

limit-state checks on demand parameters resulting from the nonlinear dynamic analyses. Based on these limit-state checks, the computed CMR is modified to account for both simulated and non-simulated failure modes. After adjustment for spectral shape effects with *SSF*, the resulting *ACMR* is then compared to the acceptance criteria in Chapter 7.

**(1) Identify Non-Simulated Collapse Modes**

The collapse assessment results reported thus far account only for the sidesway collapse mode due to hinging and gradual deterioration associated with yielding and local buckling that is incorporated in the simulation model. However, experimental data (e.g., Engelhardt et al. 1998; Ricles et al. 2004; Lignos and Krawinkler 2007) suggests that the steel frame may also experience ductile fracture in RBS sections, or possibly at the joint between the beam and column. For example, in testing done as part of the SAC Steel Project, Engelhardt et al. (1998) reported fractures in qualifying connections at inelastic rotations between 0.05 and 0.07 radians, as illustrated in Figure 10-3. It should be emphasized that the fracture being considered here is triggered by ductile crack initiation, and occurs after significant inelastic yielding has occurred, in contrast to the connection fractures observed in steel frame structures during the 1994 Northridge earthquake.

For the purposes of this example, fracture-induced collapse is conservatively assumed to occur when the fracture limit state is first breached at any RBS hinge location. Given the nature of the governing sidesway mechanism in this frame, where the strong columns lead to similar peak rotations in all the RBS hinges, the degree to which fracture occurs at multiple locations would primarily be a function of correlations in fracture occurrence, rather than spatial variations in hinge demands. This reasoning suggests that the assumption of equating the first instance of a fractured connection with fracture-induced collapse may not be too unreasonable (overly conservative) for this particular example. It would, of course, generally be desirable to incorporate fracture deterioration directly in the response history analyses. Since it is not directly incorporated in this analysis, a conservative judgment is made about what constitutes collapse for the fracture limit state.

**(2) Develop Component Fragility**

Calculation of the non-simulated collapse mode requires the definition of a fracture fragility function, which relates the probability of fracture in the RBS hinge to an engineering demand parameter (EDP), in this case, plastic rotations at each hinge; that is, the probability of fracture in each RBS is associated with the maximum rotation that has occurred in the plastic hinge. Figure 10-5 shows the resulting fragility function, P[Fracture|$\theta_p$], which is

based on available data (Lignos and Krawinkler 2007) and engineering judgment. The fragility function for fracture is assumed to follow a lognormal distribution, and has a median capacity of $\hat{\theta}_p$ = 0.063 radians and a logarithmic standard deviation of $\beta_F$ = 0.35. The dispersion ($\beta_F$ ) reflects both test data statistics (from 10 tests) and judgment as to the additional variability that may be encountered in actual buildings. Assuming that the parameters associated with fracture are the same throughout the building, the fragility function is applicable to every RBS in the building. A typical representation of the deformations at fracture are illustrated in Figure 10-4.

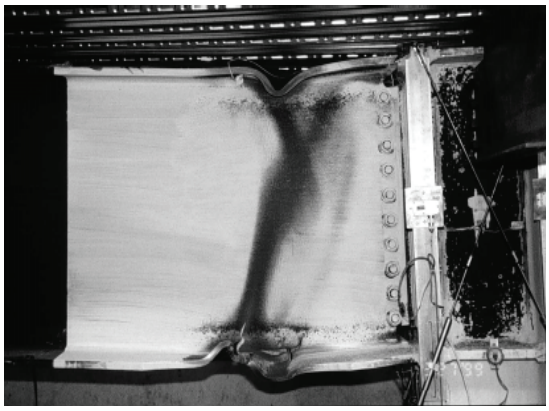

Figure 10-4 Illustration of fracture behavior (Engelhardt et al., 1998).

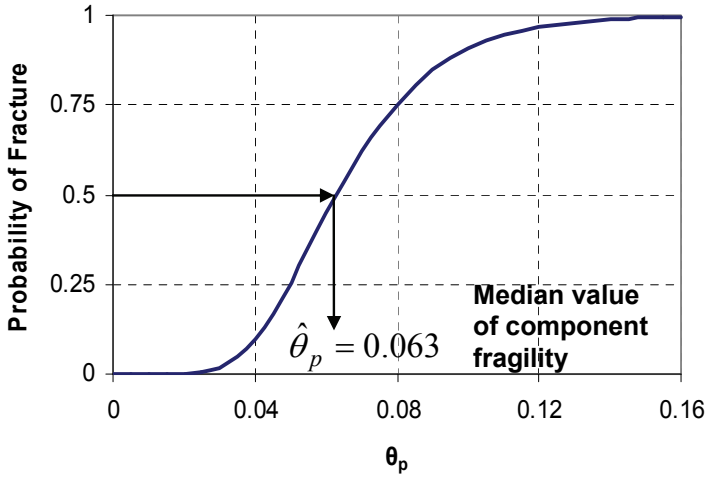


Figure 10-5 Component fragility function: P[Fracture$|\theta_p$]. According to this fragility function, ductile fracture occurs on average when the plastic rotation in an RBS reaches 0.063 radians.

**(3) Identify Collapse Limit based on Component Fragility**

The collapse limit point for the non-simulated collapse mode is defined by the median value of the fragility function defined for the component failure. The median value of the fragility function is for ductile fracture of RBS is

$\hat{\theta}_p$ = 0.063, as illustrated in Figure 10-5. In this formulation, dispersion ($\beta_F$) is ignored and collapse due to ductile fracture (the non-simulated failure mode) is assumed to occur when the plastic rotation in any RBS during dynamic analysis exceeds this median value (0.063). This assumption is reasonable, since component dispersion is relatively small ($\beta_F$ = 0.35) and does not have a significant effect on total collapse uncertainty, $\beta_{TOT}$.

**(4) Compute Collapse Fragility**

The collapse fragility is now computed based on both simulated and non-simulated collapse modes. This procedure is illustrated graphically in Figure 10-6, using representative curves from incremental dynamic analysis for this structure (each curve contains the dynamic analysis results for one ground motion, scaled until collapse). For the purposes of this figure, the component collapse limit of $\hat{\theta}_p$ = 0.063 is shown as approximately equal to the interstory drift ratio; this assumption is made for illustration purposes, and is not actually used in computing the occurrence of non-simulated failure modes. Of the three curves shown in Figure 10-6, the lowest reaches the sidesway collapse limit state and the non-simulated collapse point at approximately the same intensity level. The other ground motions reach the non-simulated collapse point before the structure collapses in sidesway simulation. In computing the collapse fragility, the more critical of these two limit states is taken as the governing collapse point for each ground motion record.

The combined collapse fragility is illustrated in Figure 10-7, where the composite uncertainty is $\beta_{TOT}$ = 0.60, as determined from Table 7-3. In this figure, the horizontal axis fragility parameter, $S_{CT}$, is normalized by MCE demand, $S_{MT}$. to permit direct comparison of the collapse margin ratio (*CMR*) for the structure with and without consideration of non-simulated fracture-induced failure modes. For this structure, the net result of including the fracture-induced collapse is to reduce the collapse margin ratio (*CMR*) by 32%, from 2.5 for the simulated sidesway-only case to 1.9. The conditional probability of collapse at the MCE increases from 8% to 14%. (Note: these margins and the collapse probabilities do not include the spectral shape factor, which is considered in the evaluation of acceptance criteria.)

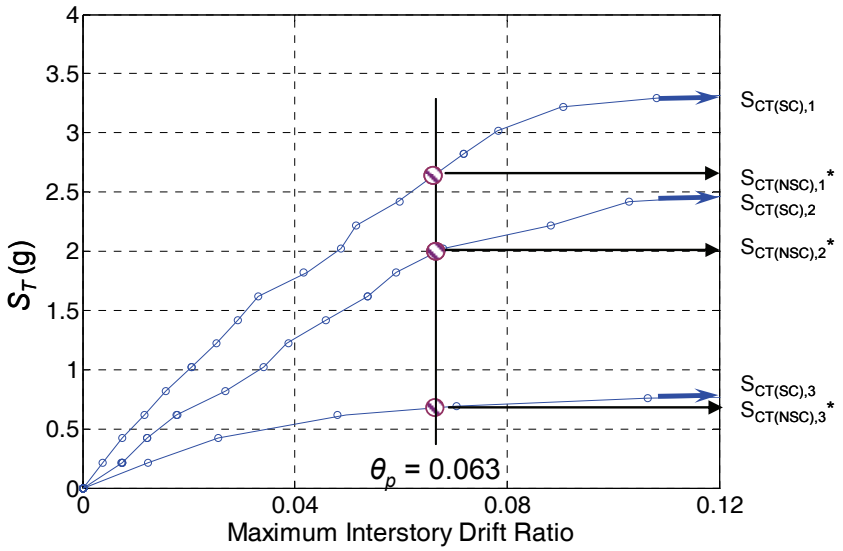


Figure 10-6 Selected simulation results for the steel SMF, for the purpose of illustrating the identification of non-simulated collapse modes. Sidesway collapse points ($S_{CT(SC)}$), based on results from simulation, are shown with short bold pointers. Non-simulated (fracture-induced) collapse points ($S_{CT(NSC)}$) are shown with pointers from hatched circles corresponding to maximum interstory drift at fracture ($\theta_P$ = 0.063 radians). The governing collapse point for each ground motion record is identified with an asterisk (*).

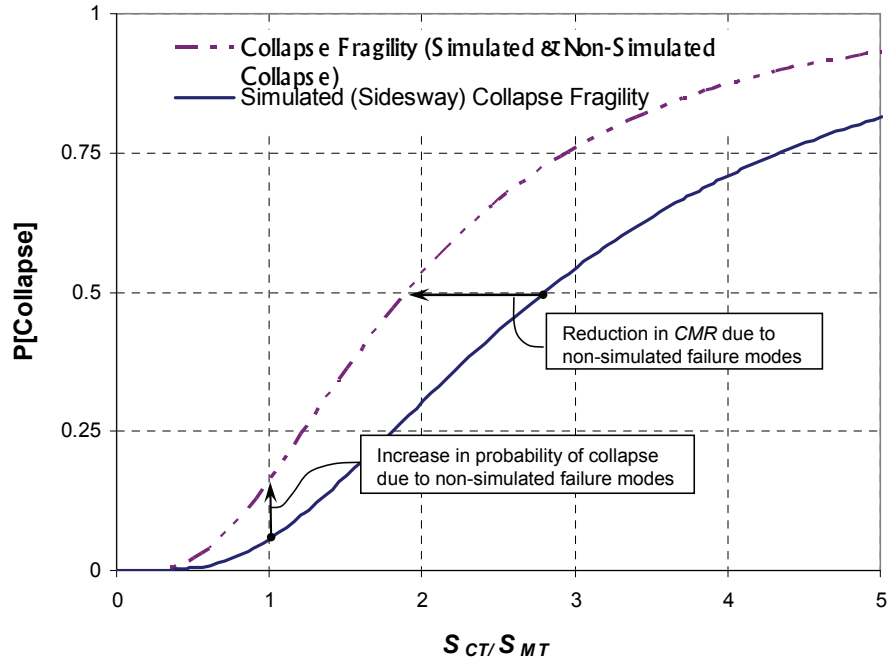


Figure 10-7 Comparison of steel SMF collapse fragilities for sidesway-only and combined simulated and non-simulated (sidesway and fracture-induced) collapse. (These fragilities are not adjusted for spectral shape).

**(5) Compare to Acceptance Criteria**

Finally, the combined fragility data, reflecting the likelihood of both simulated and non-simulated collapse, should be compared to the acceptance criteria, as specified in Chapter 7. For this structure, the spectral shape factor (*SSF*) of 1.43 is determined from Table 7-1b with $T = 0.94$ seconds and $\mu_c = 7.2$, which the increases collapse margin ratio from 1.9 to 2.8, thus easily satisfying the acceptance criteria given in Section 7.6. Here, acceptance is based on a total system collapse uncertainty of $\beta_{TOT} = 0.60$, which provides an acceptable collapse margin ratio of 2.16, as given in Table 7-2.

## 10.3 Collapse Evaluation of Seismically Isolated Structures

### *10.3.1 Introduction*

Seismic isolation (commonly known as base isolation) is a technology that is intended to protect facility function and provide substantially greater damage control than conventional, fixed-base, structures for moderate and strong earthquake ground motions. For extreme (e.g. MCE) ground motions, seismically isolated structures are expected to be at least as safe against collapse as their conventional counterparts. To ensure adequate performance, ASCE/SEI 7-05 requires that every design for an isolated structure be explicitly evaluated under MCE ground motions, and comprehensive testing of prototype isolator units to verify design properties and demonstrate stability for MCE loads.

The provisions of ASCE/SEI 7-05 require the seismic-force-resisting system of the structure above the isolation system (superstructure) to be designed for response modification factors, $R_I$, that are a fraction of the $R$ factors permitted for conventional structures. Reduced values of the response modification factor are intended to keep the superstructure "essentially elastic" for design earthquake ground motions. To protect against potential brittle failure for extreme (MCE) ground motions, ASCE/SEI 7-05 requires the superstructure to have the same ductile capacity as that required for a conventional structure (with the same type of seismic-force-resisting system). The provisions of ASCE/SEI 7-05 are generally considered to be conservative with respect to design of the superstructure, although the degree of conservatism, if any, is not known.

**Objectives**

This study is intended to test the application of the Methodology to isolated structures, which have fundamentally different dynamic response

characteristics, performance properties and collapse failure modes than those of conventional, fixed-base structures. Special issues include the following:

*Period Definition.* The fundamental-mode "effective" period of an isolated structure is based on secant stiffness (at the response amplitude of interest), rather than "elastic" stiffness used to define the period, *T*, of a conventional structures.

*Record-to-Record (RTR) Variability.* Is the record-to-record (RTR) variability of isolated structures essentially the same as that of conventional structures (which is assumed in the Methodology to be about 0.4 in all cases)? If substantially different, can the RTR variability still be assumed to be 0.4 without adversely affecting collapse results?

*Test Data and Modeling Uncertainty*. Should the collapse margin ratio (*CMR*) of isolated structures be evaluated using the same uncertainty (associated with test data and modeling of the superstructure) as that of a conventional structure (with the same type of seismic-force-resisting system)?

*Spectrum Shape Factor (SSF)*. Can the spectrum shape factor (*SSF*) used to adjust the *CMR* of isolated structures be calculated using the same methods as those specified by the Methodology for conventional structures?

This study is also intended to illustrate how the Methodology can be used as a tool for assessing the validity and developing improvements to current design requirements in Chapter 17 of ASCE/SEI 7-05, "Seismic Design Requirements for Seismically Isolated Structures." In order to evaluate the design requirements for isolated structures, this study specifically explores the sensitivity of collapse performance to the following key design properties of isolated structures:

*Superstructure Strength*. How does collapse performance vary for superstructures that have different levels of design strength (e.g., superstructures designed for different effective values of the $R_I$ factor)?

*Superstructure Ductility.* How does superstructure ductility influence collapse performance (e.g., performance of special moment frame superstructures as compared to that of ordinary moment frame superstructures)?

*Moat Wall Clearance.* How does collapse performance vary for isolated structures that have different amounts of clearance between the isolated structure and the moat wall?

**Scope and Approach**

The scope of this study is necessarily limited and relies on archetypical models available from other studies to represent the superstructures of isolated archetypes. Specifically, superstructures are based on the 2-dimensional, archetypical models of 4-story reinforced-concrete (RC) special moment frame (SMF) and ordinary moment frame (OMF) systems, from the example applications included in Sections 9.2 and 9.3, respectively. The benefits of using these models, which explicitly incorporate detailed non-linear, degrading behavior of elements, outweighs any possible shortcomings.

The archetypical models of isolated structures incorporate force-deflection properties of isolation systems typical of actual projects that use either (1) elastomeric, rubber bearings (RB), or (2) sliding, friction-pendulum (FP) bearings. These two isolation system types are designed and archetypical models of the isolated structure evaluated for maximum and minimum SDC D ground motions (SDC $D_{max}$ and SDC $D_{min}$). SDC $D_{max}$ ground motions are typical of those used for most seismic isolation projects (e.g., projects in high seismic regions of coastal California).

This study includes discussion of background information necessary for proper application of the Methodology to isolated structures and related development of isolated archetypes. Archetype configurations, nonlinear analysis techniques, and collapse performance methods are described with reference to specific differences in applying the methodology to isolated structures. Collapse evaluation results are reported for archetypes that comply fully with the design requirements of ASCE/SEI 7-05 (referred to herein as Code-Compliant archetypes) and for archetypes that deviate, in some manner, from current requirements (Non-Code-Compliant archetypes). The latter case demonstrates potential use of the Methodology as a Code development tool by evaluating collapse performance for archetype models that have weaker (or stronger) superstructures, less ductility, or different moat clearances than those now required by ASCE/SEI 7-05.

### *10.3.2 Isolator and Structural System Information – Quality Ratings*

As required by the Methodology (Chapter 3), archetypes of isolated structures must be designed using established design requirements and

modeling of isolated archetypes must be supported by appropriate test data. Further, the quality of the design requirements and test data must be rated for establishing collapse uncertainty (as described in Chapter 7).

**Design Requirements**

Archetypes of isolated structures are designed according to the provisions of ASCE/SEI 7-05 and related superstructure design codes, including ACI 318-05, except as such provisions are modified, or ignored, to evaluate the effects of reduced superstructure strength, or limited ductility, or moat clearance in the non-code-compliant archetypes. Chapter 17 of ASCE/SEI 7-05*,"Seismic Design Requirements for Seismically isolated Structures*" requires thorough and rigorous design of the isolated structure, including explicit evaluation of the isolation system for MCE ground motions, and peer review.

For the purpose of assessing the composite uncertainty in the Methodology, the isolation system and superstructure design requirements are rated as "A-Superior," as they are thorough, detailed and vetted through the building code process.

**Test Data**

The requirements for test data relate both to testing of superstructure components (i.e., RC beams, columns and connections), and testing of prototype isolator units. The test data related to RC elements is discussed, in detail, in Sections 9.2 and 9.3, and rated "B-Good." While there is a large amount of test data of RC components, there are still several areas where test data are not complete (i.e. tests of beams with slabs, tests to very large deformations, etc).

Test data related to isolation systems is both qualitatively and quantitatively different. For the purposes of fixed-base (superstructure) modeling and evaluation, test data is taken from a variety of different researchers regarding components which are similar, but not identical to, the components being modeled in the structure. In contrast, the provisions ASCE/SEI 7-05 require prototype testing of isolator units for the purpose of establishing and validating the design properties of the isolation system and verifying stability for MCE response. These tests are specific to the isolation system installed in a particular building, and follow detailed requirements for force-deflection response outlined in the design requirements. As a result, there is substantially smaller uncertainty related to the test data in an isolated system than the superstructure.

A rating of "B-Good" is conservatively assigned to the uncertainty assessment for test data for these systems. This rating is largely associated

with uncertainty in test data related to superstructure modeling. Also, isolator failure is not considered in this study. If considered, then the quality of data on isolator failure should be also be weighted in.

### *10.3.3 Definition of Properties and Methods Unique to Collapse Evaluation of Isolated Structures*

This section defines certain properties and methods that are, in some manner, unique to collapse evaluation of isolated structures, including the definition of the fundamental period (used to evaluate the *CMR*), nonlinear static (pushover) analysis of the isolated structure (used to assess system ductility), and related evaluation of the spectrum shape factor (*SSF*). Additional discussion of the reasonableness of these parameters and methods, considering results from isolated archetype analyses, is provided in Section 10.3.7.

**Definition of Fundamental Period**

For conventional, fixed-base, systems, the Methodology defines the period of interest as the fundamental (first mode) period of vibration of the structure, *T*, as computed according to code equations (see Chapter 2). This period is used to evaluate the spectral acceleration at which median failure occurs and the corresponding collapse margin ratio (*CMR*).

As shown by the example pushover plot in Figure 10-8, isolated systems tend to be initially stiff, but yield early, and then become very flexible. This flexible region (post-yield stiffness of the isolator) dominates the response. Use of the initial stiffness to compute the period would significantly underestimate the period, except for very small deformation levels. For isolated structures, ASCE/SEI 7-05 defines two amplitude-dependent fundamental-mode periods based on secant stiffness, $T_D$, (period at the design displacement), and $T_M$, (period at the MCE displacement). Values of $T_D$ and $T_M$ are typically close together.

In this study, collapse margin ratios are evaluated for the MCE fundamental-mode period, $T_M$, as defined by ASCE/SEI 7-05:

$$T_M = 2\pi \sqrt{\frac{W}{k_{Mmin}\, g}} \tag{10-1}$$

Where:

$T_M$ = effective period, in seconds, of the seismically isolated structure at the maximum displacement in the direction under consideration, as prescribed by Eq. 17.5-4 of ASCE/SEI 7-05,

$W$ = effective seismic weight of the structure above the isolation interface, as defined in Section 17.5.3.4 of ASCE/SEI 7-05, and

$k_{Mmin}$ = minimum effective stiffness, in kips/in., of the isolation system at the maximum displacement in the horizontal direction under consideration, as prescribed by Eq. 17.8-6 of ASCE/SEI 7-05.

**Nonlinear Static (Pushover) Analysis**

The Methodology requires a nonlinear static (pushover) analysis to determine the overstrength of the archetype and to evaluate system ductility. Evaluation of overstrength is not needed for isolated structures, but provides a useful tool for understanding the strength of the superstructure relative to the level of lateral force in the isolation system.

Figure 10-8 illustrates nonlinear static (pushover) analysis results for an isolated structure and for same structure (i.e., same superstructure) on a fixed-base. While the same value of overstrength is obtained from the two analyses, the isolated structure effectively shares system ductility between displacement of the isolation system and displacement of the superstructure.

In this study, pushover analysis is performed on isolated structures with the isolation system free to displace. Pushover forces are based on a uniform pattern of lateral load (i.e., pushover forces are proportional to floor mass) emulating the approximate pattern of uniform lateral displacement of the isolated structure (at displacements up to significant yielding of the superstructure).

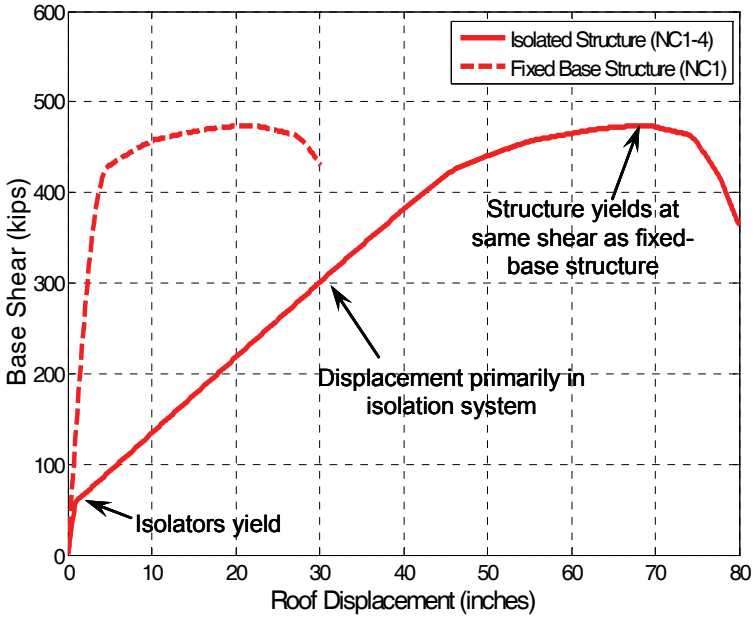


Figure 10-8 Example pushover curves of an isolated structure and the same structure (superstructure) on a fixed base.

**System Ductility and Spectrum Shape Factor**

As required by the Methodology, NSA results are used to evaluate the system ductility for the purpose of evaluating system ductility. The ductility is computed from the pushover of the isolated structure following the procedures described in Chapter 6, as illustrated in Figure 10-9.

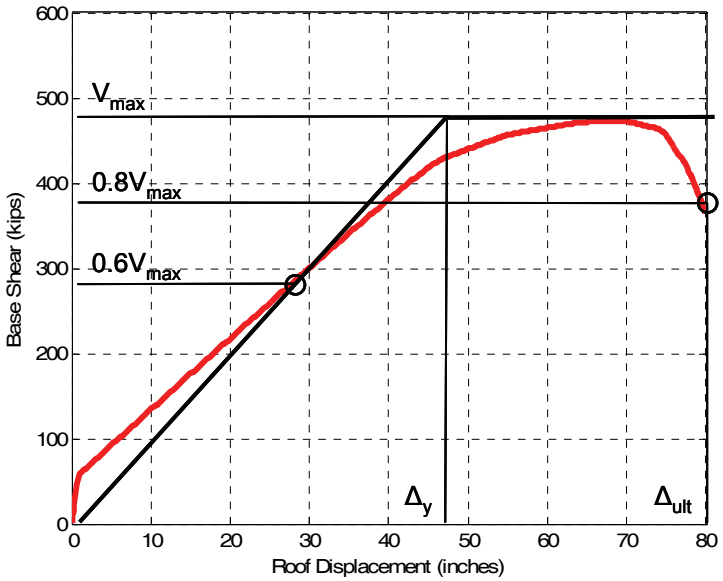


Figure 10-9 Example illustration of system ductility used to evaluate Spectrum Shape Factor (*SSF*) of an isolated structure.

Since the *SSF* is based on the ductility obtained from the isolated structure pushover, the *SSF* is smaller for the isolated system than for its fixed-base counterpart (larger $\Delta_y$, relative to $\Delta_{ult}$). Note that in conducting static pushover analysis, the moat wall springs (discussed later and illustrated in Figure 10-12) were not included in the models. Further discussion of the calculation of system ductility and spectrum shape factor is provided in Chapter 6.

### *10.3.4 Modeling Isolated Structure Archetypes*

This section identifies the basic configuration, systems and elements of the isolated structures of this study and provides a general overview of the index archetype models used to evaluate collapse performance. Section 10.3.5 describes specific design properties for the isolation system, moat wall clearance, and the superstructure of each model.

The seismic-force-resisting system of an isolated structure includes: (1) the isolation system, and (2) the seismic-force-resisting system of the superstructure above the isolation system. The isolation system includes individual isolator units (e.g., elastomeric or sliding bearings), structural

elements that transfer seismic force between elements of the isolation system (e.g., beams just above isolators) and connections to other structural elements. Energy dissipation devices (dampers) are sometimes used to supplement damping of isolator units, but such devices are not considered in this study.

Isolated structures are typically low-rise or mid-rise buildings that have relatively stiff superstructures. This study assumes that the seismic-force-resisting system of the superstructure is a reinforced-concrete (RC) moment frame system to make use of existing models that explicitly capture side-sway collapse. A relatively short height (4 stories) is used to assure adequate stiffness of the superstructure.

Isolated structures typically have a "moat" around all or part of the perimeter of the building at the 1st-floor level. The moat is usually covered by architectural components (e.g., cover plates) that permit access to the building, but do not inhibit lateral earthquake displacement of the isolated structure. In most cases, building occupants are not aware that the building is isolated, or has a moat around the perimeter.

Impact with the moat wall is a potential failure mode that can significantly influence collapse performance of the superstructure. Accordingly, Section 17.2.5.2 of ASCE/SEI 7-05 requires a minimum building separation to "retaining walls and other fixed obstructions" not less than the total maximum (MCE) displacement of the isolation system. The intent of this provision is to limit the likelihood of such impacts, even for strong ground motions.

Section 17.2.4.5 of ASCE/SEI 7-05 recognizes that providing clearance for MCE ground motions may not be practical for some systems and permits isolation system design to incorporate a "displacement restraint" that would limit MCE displacement, provided certain criteria are met. These criteria include the requirement that "the structure above the isolation system is checked for stability and ductility demand of the maximum considered earthquake." This study shows how the Methodology can be used to perform this check.

**Index Archetype Models**

Models of the isolated systems consist of a superstructure model, an isolator model, and a moat wall model. Each of these components must be capable of capturing the inelastic effects in the structure up until the point at which the structure collapses. The analyses are two-dimensional, and neglect possible

torsional effects. The index archetype model for isolated systems is illustrated in Figure 10-10.

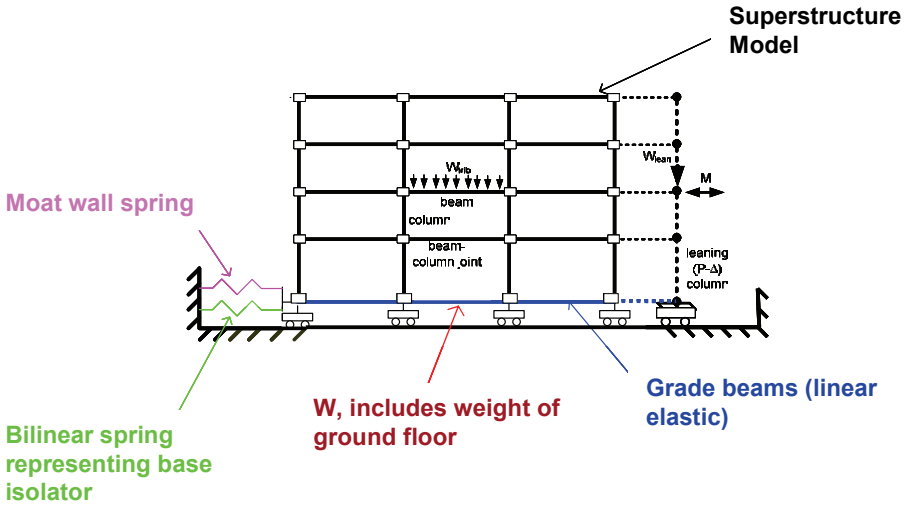


Figure 10-10 Archetype analysis model for isolated systems.

The superstructures are modeled using the same assumptions as described in Section 9.2 (RC SMF) and Section 9.3 (RC OMF). Each model captures material nonlinearities in beams, columns and beam column joints, as well as cyclic deterioration of strength and stiffness. As before, the superstructure model includes a leaning (P-Δ) column to account for the effect of the seismic mass on the gravity system.

**Isolator Modeling**

The isolation system bearings (isolators) are modeled using a bilinear spring between the foundation and the 1st floor of the superstructure, as shown in Figure 10-10. The bilinear spring is assumed to be a non-degrading, fully hysteretic element. Some types of isolators tend to change properties with repeated cycles of loading, but modeling such behavior was beyond the scope of this study. Bilinear springs are commonly used in practice and provide sufficiently accurate estimates of nonlinear response when their stiffness and damping properties are selected to match those of the isolators (Kircher, 2006).

Figure 10-11 illustrates nominal, upper-bound and lower-bound values of bilinear springs used in this study to model isolators (i.e., isolator force is normalized by the weight of the building in Figure 10-11). In general, isolators are modeled with nominal spring properties. In certain cases, isolators are modeled with upper-bound and lower-bound spring properties to evaluate the effects of these properties on collapse. Upper-bound and lower-bound properties are also needed for isolation system design. Section 17.5 of

ASCE/SEI 7-05 requires lower-bound properties for calculation of isolation system displacements, and upper-bound properties for calculation of design forces. The range of upper-bound and lower-bound bilinear spring properties used to model isolators is based on prototype testing acceptance criteria of Section 17.8.4 of ASCE/SEI 7-05.

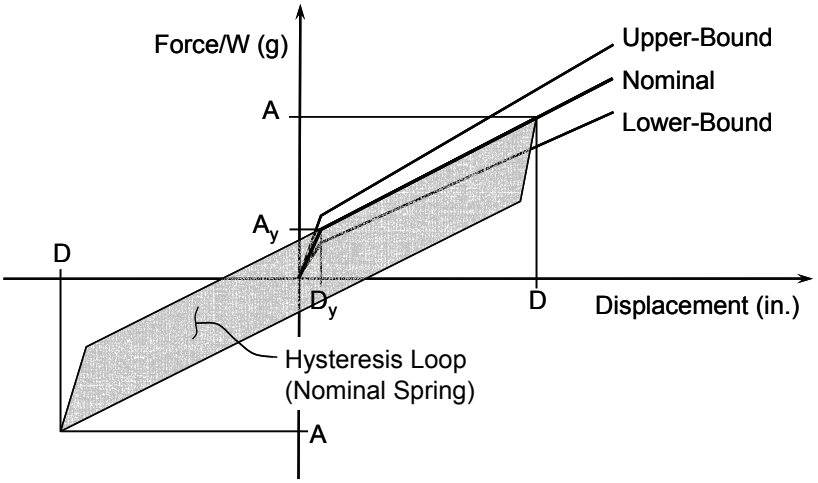


Figure 10-11 Example nominal, upper-bound and lower-bound bilinear springs and hysteretic properties used to model the isolation system.

Bilinear curves in Figure 10-11 are defined by a yield point ($D_y$, $A_y$) and a post-yield point ($D$, $A$) located somewhere on the yielded portion of the curve. The properties are assumed to be symmetric for positive and negative displacements. Amplitude-dependent values of effective stiffness, $k_{eff}$, effective period, $T_{eff}$ (in seconds), and effective damping, $\beta_{eff}$, of the isolation system may be calculated by the following equations:

$$k_{eff} = \frac{AW}{D} \tag{10-2}$$

$$T_{eff} = 2\pi\sqrt{\frac{D}{gA}} \tag{10-3}$$

$$\beta_{eff} = \frac{2}{\pi}\sqrt{\frac{A_y D - D_y A}{D\,A}} \tag{10-4}$$

Equations (10-2), (10-3) and (10-4) are consistent with the definitions of effective stiffness, $k_{eff}$, and effective damping, $\beta_{eff}$, of Section 17.8.5 of ASCE/SEI 7-05 used to determine the force-deflection characteristics of the isolation system from the tests of prototype isolators.

**Moat Wall Modeling**

This study includes nonlinear springs to represent the effects of impact with the moat wall when the seismic demand on the isolated system exceeds the clearance provided. The moat wall is represented by 5 symmetrical gap springs implemented in parallel as illustrated in Figure 10-12.

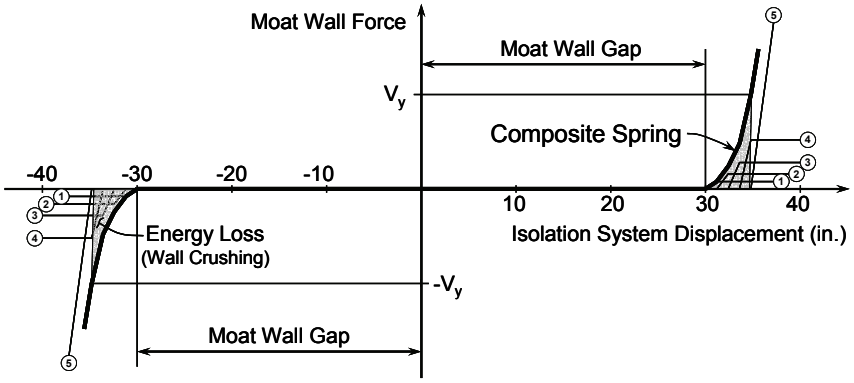


Figure 10-12 Example five Individual springs and effective composite spring used to model moat wall resistance (30-inch moat wall gap).

Gap springs have zero force until the isolated structure reaches the moat wall, and then begin to resist further displacement of the isolated structure. The five springs engage sequentially to effect increasing stiffness and nonlinear resistance as the structure pushes into the moat wall. Gap springs are modeled as inelastic elements to account for energy loss due to localized crushing at the structure-wall interface. Gap spring properties are defined relative to the strength of the superstructure such that moat wall force is equal to the strength of the superstructure, $V_{max}$, at about 4 inches of moat wall displacement.

It should be noted that the models used in this study, and illustrated in Figures 10-11 and 10-12, are relatively simplistic representations of isolated systems and neglect many complex aspects of isolator performance. As noted earlier, bilinear properties of the isolator neglect hardening that can occur at high displacements and reduction in effective stiffness that can occur for repeated cycles of loading in certain elastomeric bearings. It may also be noted that the isolation system model neglects potential uplift at isolators (i.e., when overturning loads exceed gravity loads and isolator tension capacity, if any). Local uplift of isolators is a potential failure mode, but permitted by Section 17.2.4.7 of ASCE/SEI 7-05 provided "resulting deflections do not cause overstress or instability of isolator units or other structure elements." Despite these limitations, the models represented in Figures 10-10, 10-11, and 10-12 are expected to give reasonable predictions

of dynamic response and collapse performance, as well as relative differences in performance associated with variability in design parameters.

**Uncertainty due to Model Quality**

Model quality is rated as “A-Superior” for the purpose of assessing the composite uncertainty in the performance predictions of archetype analysis models with a RC SMF superstructure and rated as "B-Good” for archetype analysis models with a RC OMF superstructure: These ratings reflect the uncertainty in the superstructure models, which are rated "A-Superior" and “B-Good” for fixed-base RC SMF and RC OMF systems, respectively, as reported in Chapter 9. The models of the entire isolated system (including isolator, moat wall, and superstructure) are judged to have the same model quality as the superstructure.

### *10.3.5 Design Properties of Isolated Structure Archetypes*

Specific design properties of index archetype models in this study include isolation system properties, moat wall clearance and superstructure properties. The archetypes probe the effects of the critical design parameters on collapse performance. The goal of considering a wide variety of archetype configurations is to assess the validity of current code provisions. As such, archetypes are developed for both "Code-Compliant" systems that comply fully with ASCE/SEI 7-05 requirements, and "Non-Code-Compliant" systems that deviate from ASCE/SEI 7-05 requirements in terms of superstructure strength, superstructure ductility, and/or moat wall clearance.

**Isolation System Design Properties**

Design properties of the isolation system of isolated are developed using the equations and design requirements of the “Equivalent Lateral Force Procedure,” Section 17.5 of ASCE/SEI 7-05. These equations provide a convenient basis for design and are commonly used for preliminary design and review of isolated structures.

As shown in Figure 10-11, the isolation system is defined by two control points, the “yield” point ($D_y$, $A_y$) and the post-yield point ($D$, $A$). The yield point represents dynamic friction level of sliding bearings (e.g., FP bearings) and approximates the yield level (normalized by weight) of elastomeric bearings (e.g., lead-rubber or high-damping rubber bearings). The post-yield point is used simply to define the slope of yielded system (and the isolation system is assumed capable of displacing without failure beyond this point).

Values of the yield and the post-yield control points are selected such that the corresponding values of maximum (MCE) displacement, $D_M$, effective

period, $T_M$, effective stiffness, and effective damping, $\beta_M$, meet the following criteria:

(1) Values of $D_M$, $T_M$ and $\beta_M$ comply fully with the equations and requirements of Section 17.5 of ASCE/SEI 7-05,

(2) Values of effective stiffness and damping are consistent with actual isolation system properties (i.e. for isolations systems with either elastomeric or sliding bearings), and

(3) Values of effective stiffness and damping reduce response such that forces required for design of the superstructure are approximately the same as the design base shear required for conventional fixed-base system (of the same type and configuration), so that existing models of Code-Compliant systems can be used for the superstructure (without re-design).

This study considers different types of isolation systems representative of systems with either elastomeric, rubber bearings (RB) or sliding, friction pendulum (FP) bearings, respectively. Isolation systems are designed for either SDC $D_{max}$ or SDC $D_{min}$ seismic criteria (Site Class D).

The response characteristics of isolation systems with either RB or FP bearings are sufficiently similar for strong (SDC $D_{max}$) ground motions to permit modeling both systems with the same set of bilinear springs properties (i.e., a single set of "generic" properties is used to represent both systems). Such is not the case for moderate (SDC $D_{min}$) ground motions, and different spring properties are used to model isolation systems with RB and FP bearings.

Nominal isolation system design properties (i.e., yield and post-yield control points that define bilinear springs) are given in Table 10-1 for the generic (GEN) system, the RB system and FP system, respectively. Nominal, upper-bound and lower-bound spring properties are also given for the GEN system. Only nominal properties are shown for the RB and FP systems (although MCE design parameters still utilize upper-bound and lower-bound properties, as required by Section 17.5 of ASCE/SEI 7-05).

Table 10-1 also provides design values of the effective period, $T_M$, effective damping, $\beta_M$, and total maximum displacement, $D_{TM}$, for each system. Calculation of $D_{TM}$ was based on the Equivalent Lateral Procedure of ASCE/SEI 7-05. Total maximum displacement includes an additional 15 percent of torsional displacement, consistent with Equation (17.5-6) of ASCE/SEI 7-05 (assuming a square configuration of the building in plan):

$$D_{TM} = 1.15\, D_M \tag{10-5}$$

**Table 10-1 Isolation System Design Properties**

| Isolator Properties | | Force-Deflection Curve | | | | MCE Design Parameters | | |
|---|---|---|---|---|---|---|---|---|
| | | Yield Point | | Post-Yield | | $T_M$ (sec) | $\beta_M$ (% crit) | $D_{TM}$ (in.) |
| Type | Range | $D_y$ (in) | $A_y$ (g) | $D$ (in) | $A$ (g) | | | |
| *High-Damping Rubber or Friction Pendulum System - $D_{max}$ Design* | | | | | | | | |
| GEN | Nominal | 0.5 | 0.05 | 23.3 | 0.225 | 3.47 | 10.5% | 29.3 |
| GEN-UB | Upper-Bound | 0.5 | 0.06 | 21.1 | 0.23 | | | |
| GEN-LB | Lower-Bound | 0.5 | 0.04 | 25.5 | 0.22 | | | |
| *High-Damping Rubber and Friction Pendulum Systems - $D_{min}$ Designs* | | | | | | | | |
| RB | Nominal | 1.5 | 0.04 | 6.5 | 0.081 | 3.18 | 12.5% | 8.5 |
| FP | Nominal | 0.1 | 0.04 | 4.2 | 0.072 | 2.78 | 28% | 5.7 |

**Isolation System Clearance**

The performance of isolated structures can also be dependent on the clearance of the isolated system. As a result, a moat wall is incorporated into each of archetype analysis models. Table 10-2 summarizes values of moat wall clearance (gap) distances. For the GEN isolation system (SDC $D_{max}$ design), five different moat wall distances are used to investigate the effects of this parameter on collapse performance.

Moat wall clearance is based on a fraction of the total maximum displacement, $D_{TM}$, plus a little extra displacement for fit-up tolerance: Moat wall clearance is nominally modeled as $1.0D_{TM}$. Unless dynamic analysis can justify a smaller value, $1.0D_{TM}$ is the minimum clearance permitted by Section 17.5 of ASCE/SEI 7-05. For the GEN system, moat wall gap displacements of $0.6D_{TM}$ and $0.8D_{TM}$ test the consequences of restricting isolation system displacement, and clearances of $1.2D_{TM}$ and $1.4D_{TM}$ evaluate the benefits of having extra clearance.

Moat wall clearance is influenced by site conditions (e.g., sloping site), building configuration and architectural features, but economic considerations usually dictate design at or near the minimum required displacement, so that moat wall clearances between approximately $0.8D_{TM}$ and $1.0D_{TM}$ are typical (when the configuration has a moat wall). Moat wall clearance of $1.4D_{TM}$ is not practical, as it would likely result in a more costly design. ASCE/SEI 7-05 does not permit moat wall clearance less than $0.8D_{TM}$ unless the superstructure is explicitly evaluated for stability for MCE demand (which is not common).

**Table 10-2 Summary of Moat Wall Clearance (Gap) Distances.**

| Isolation System Properties | | | Moat Wall Gap Distance (inches) | | | | |
|---|---|---|---|---|---|---|---|
| Type | Displacement (in.) | | Approximate Fraction of Code Minimum ($D_{TM}$) | | | | |
| | $D_{TM}$ | Fit-up | 0.6 $D_{TM}$ | 0.8 $D_{TM}$ | 1.0 $D_{TM}$ | 1.2 $D_{TM}$ | 1.4 $D_{TM}$ |
| *Generic Elastomeric or Sliding Systems - $D_{max}$ Design* | | | | | | | |
| GEN | 29.3 | 0.7 | 18 | 24 | 30 | 36 | 42 |
| GEN-UB | 29.3 | 0.7 | | | 30 | | |
| GEN-LB | 29.3 | 0.7 | | | 30 | | |
| *Rubber (RB) or Friction Pendulum (FP) Systems - $D_{min}$ Designs* | | | | | | | |
| RB | 8.5 | 0.5 | | | 9 | | |
| FP | 5.7 | 0.3 | | | 6 | | |

**Superstructure Design Properties**

In this study, isolated structure archetypes are grouped as Code-Compliant and Non-Code-Compliant archetypes. Code-Compliant archetypes include systems with reinforced-concrete special moment frame (RC SMF) superstructures that conform to the design requirements of Chapter 17 of ASCE/SEI 7-05, in terms of both strength and ductility (i.e., detailing requirements). Non-Code-Compliant archetypes include systems that do not conform either in terms of design strength, e.g., RC SMF superstructure designed for less than the minimum required base shear, or in terms of ductility, e.g., reinforced-concrete ordinary moment frame (RC OMF) superstructure not permitted for use as a SDC D system.

Table 10-3 summarizes design properties for the 3 superstructures of Code-Compliant archetypes used in this study:

(C1) a RC SMF (perimeter frame) system, designed for base shear, $V_s = 0.092W$ ($R_I = 2.0$),

(C2) a RC SMF (space frame) system, designed for base shear, $V_s = 0.092W$ ($R_I = 2.0$), and

(C3) a RC SMF (space frame) system, designed for base shear, $V_s = 0.077W$.

The first two systems are superstructures of isolated archetypes designed for SDC $D_{max}$ seismic criteria, and the last system is the superstructure of isolated archetypes designed for SDC $D_{min}$ seismic criteria.

**Table 10-3 Isolated Structure Design Properties for Code-Compliant Archetypes.**

| Arch. No. | Isolated Structure Archetype Design Properties | | | | | | |
|---|---|---|---|---|---|---|---|
| | Superstructure | | | Isolation System | | Isolated Structure | |
| | $V_s/W$ | $\Omega$ | $V_{max}/W$ | Type | Gap (in.) | $\mu_c$ | $T_M$ (sec.) |
| *RC SMF Perimeter Systems Evaluated at $D_{max}$* | | | | | | | |
| C1-1 | 0.092 | 1.6 | 0.15 | GEN | 18 | 4.2 | 3.47 |
| C1-2 | 0.092 | 1.6 | 0.15 | GEN | 24 | 4.2 | 3.47 |
| C1-3 | 0.092 | 1.6 | 0.15 | GEN | 30 | 4.2 | 3.47 |
| C1-4 | 0.092 | 1.6 | 0.15 | GEN | 36 | 4.2 | 3.47 |
| C1-5 | 0.092 | 1.6 | 0.15 | GEN | 42 | 4.2 | 3.47 |
| *RC SMF Space Frame Systems Evaluated at $D_{max}$* | | | | | | | |
| C2-1 | 0.092 | 3.3 | 0.30 | GEN | 18 | 2.0 | 3.47 |
| C2-2 | 0.092 | 3.3 | 0.30 | GEN | 24 | 2.0 | 3.47 |
| C2-3 | 0.092 | 3.3 | 0.30 | GEN | 30 | 2.0 | 3.47 |
| C2-4 | 0.092 | 3.3 | 0.30 | GEN | 36 | 2.0 | 3.47 |
| C2-5 | 0.092 | 3.3 | 0.30 | GEN | 42 | 2.0 | 3.47 |
| C2-3U | 0.092 | 3.3 | 0.30 | GEN-UB | 30 | 2.3 | 3.47 |
| C2-3B | 0.092 | 3.3 | 0.30 | GEN-LB | 30 | 1.7 | 3.47 |
| *RC SMF Space Frame Systems Evaluated at $D_{min}$* | | | | | | | |
| C3-1 | 0.077 | 3.7 | 0.28 | RB | 9 | 1.9 | 3.18 |
| C3-2 | 0.077 | 3.7 | 0.28 | FP | 6 | 2.0 | 2.78 |

Note: The base shear of the last system is governed by the limit of Section 17.5.4.3 of ASCE/SEI 7-05 that requires the base shear, $V_s$, to not be less than 1.5 times either the "yield level" of an elastomeric system or the "breakaway" friction level of a sliding system. In this case, the base shear ($V_s = 0.077W$) is approximately equal to 1.5 times 0.05, the upper-bound yield level of systems designed for SDC $D_{min}$ seismic criteria with either RB or FP bearings.

**Superstructure Overstrength Properties**

A static pushover analysis of each of the archetypes listed in Table 10-3 (C1 - C3) and Table 10-4 (NC1 – NC5), respectively, was performed to determine the actual maximum strength, $V_{max}$, and to compare actual strength with design strength, $V_s$. Overstrength results are illustrated in Figure 10-13. Note that the pushover results for the superstructure alone and the isolated system (isolator and superstructure) provide approximately the same ultimate base shear, as shown in Figure 10-8. As Figure 10-13 shows, the maximum

strength of the superstructure is system dependent and does not decrease in proportion to design base shear.

**Table 10-4 Isolated Structure Design Properties for Non-Code-Compliant Archetypes.**

| Arch. No. | Isolated Structure Archetype Design Properties | | | | | | |
|---|---|---|---|---|---|---|---|
| | Superstructure | | | Isolation System | | Isolated Structure | |
| | $V_s/W$ | $\Omega$ | $V_{max}/W$ | Gap (in.) | Type | $\mu_c$ | $T_M$ (sec.) |
| *RC SMF Space Frame Systems Evaluated at $D_{max}$* | | | | | | | |
| NC1-1 | 0.164 | 2.8 | 0.46 | 18 | GEN | 1.7 | 3.47 |
| NC1-2 | 0.164 | 2.8 | 0.46 | 24 | GEN | 1.7 | 3.47 |
| NC1-3 | 0.164 | 2.8 | 0.46 | 30 | GEN | 1.7 | 3.47 |
| NC1-4 | 0.164 | 2.8 | 0.46 | 42 | GEN | 1.7 | 3.47 |
| NC2-1 | 0.046 | 5.2 | 0.24 | 18 | GEN | 2.3 | 3.47 |
| NC2-2 | 0.046 | 5.2 | 0.24 | 24 | GEN | 2.3 | 3.47 |
| NC2-3 | 0.046 | 5.2 | 0.24 | 30 | GEN | 2.3 | 3.47 |
| NC2-4 | 0.046 | 5.2 | 0.24 | 42 | GEN | 2.3 | 3.47 |
| *RC OMF Space Frame Systems Evaluated at $D_{max}$* | | | | | | | |
| NC3-1 | 0.246 | 1.9 | 0.47 | 30 | GEN | 1.4 | 3.47 |
| NC3-2 | 0.246 | 1.9 | 0.47 | 42 | GEN | 1.4 | 3.47 |
| NC4-1 | 0.164 | 1.8 | 0.30 | 30 | GEN | 1.5 | 3.47 |
| NC4-2 | 0.164 | 1.8 | 0.30 | 42 | GEN | 1.5 | 3.47 |
| NC5-1 | 0.092 | 1.9 | 0.17 | 30 | GEN | 1.7 | 3.47 |
| NC5-2 | 0.092 | 1.9 | 0.17 | 42 | GEN | 1.6 | 3.47 |

When designed with a base shear of $0.092W$, the perimeter RC SMF has an ultimate strength $0.15W$, the space RC SMF has an ultimate strength of $0.30W$ and the space RC OMF has an ultimate strength of $0.17W$. Space frames typically have higher overstrength (relative to the design lateral load) than perimeter frames due to the higher contribution of gravity loads to designs with less base shear. RC OMFs typically have lower overstrength because of the lack of capacity-design provisions. The relative strength of the superstructure and isolation system can have a big impact on the performance of isolated structures under extreme loadings.

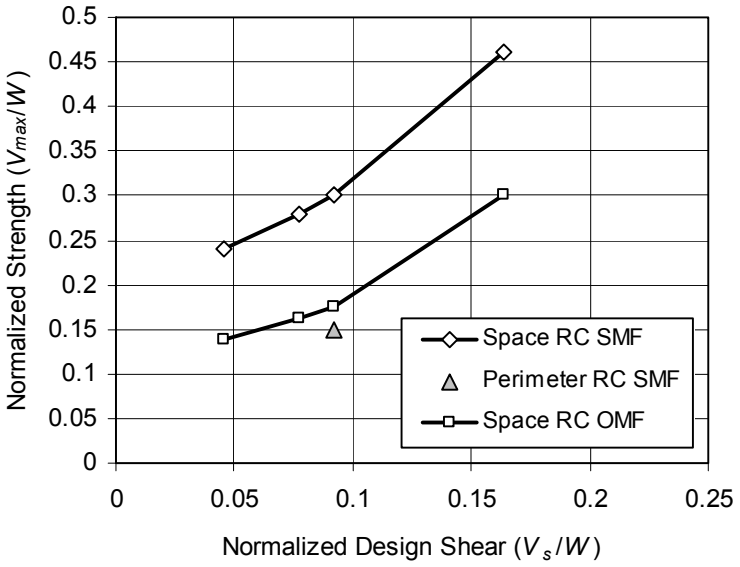


Figure 10-13 Normalized design shear ($Vs/W$) and strength ($V_{max}/W$) of superstructures. Note. Some of the structures shown in Figure 10-13 were designed for this study, but are not discussed in this report.

### *10.3.6 Collapse Evaluation Results*

**Evaluation Process and Acceptance Criteria**

The base isolated systems listed in Tables 10-3 and 10-4 are analyzed and evaluated according to the Methodology (as described in Chapters 5 – 7). Nonlinear dynamic analyses, using the far-field record set (Appendix A), determine the median spectral acceleration at which the structure collapses ($\hat{S}_{CT}$). The collapse margin ratio, *CMR*, is computed as the ratio of the median collapse capacity, $\hat{S}_{CT}$ , and the MCE demand, $S_{MT}$.

As described in the Methodology, and further illustrated in Chapter 9, the acceptance criteria are based on the adjusted collapse margin ratio (*ACMR*) which is the *CMR* modified by the spectrum shape factor (*SSF*) to account for the unique spectral shape of rare ground motions. Note that the effects of spectral shape are somewhat different for base isolated structures than for the fixed-base structures (and these differences are discussed in more detail in Section 10.3.7). The computed values of ductility capacity ($\mu_c$) for base isolated systems are listed in Table 10-3 and Table 10-4. The spectrum shape factor, *SSF*, is determined from Tables 7-1a and 7-1b as a function of ductility capacity and building period (e.g., $T > 1.5$ seconds).

The composite (total) uncertainty associated with collapse must be assessed in order to compare the *ACMR* to the acceptance criteria. This assessment requires rating the "quality" of modeling, test data (e.g., used to develop

nonlinear properties) and design requirements. For isolated archetypes with ductile (SMF) superstructures, with ratings of "A-Superior" for modeling, "B-Good" for test data and "A-Superior" for design requirements, a total uncertainty, $\beta_{TOT}$, of 0.55 is obtained from Table 7-3a. The non-code compliant isolated archetypes, with non-ductile (OMF) superstructures, have a modeling rating of "B-Good" and a total uncertainty (from Table 7-3b) of $\beta_{TOT} = 0.60$. Additional discussion of special issues related to the determination of composite uncertainty in the evaluation of base isolated structures is included in Section 10.3.7.

The acceptance criteria of Chapter 7 require archetypes with a total uncertainty of $\beta_{TOT} = 0.55$ and $\beta_{TOT} = 0.60$ to have average *ACMR* values greater than 2.02 and 2.16, respectively (See Table 7-2). Although *ACMR* results are not averaged (since the study did not develop performance groups of isolated archetypes), values of the *ACMR* > 2.02 (for code-compliant archetypes) and *ACMR* > 2.16 (for non-code compliant archetypes) are used in this study to evaluate isolated structures. In essence, each isolated archetype is evaluated using criteria that require collapse performance equivalent to that of conventional fixed-base systems, on average.

**Collapse Results for Code-Compliant Archetypes**

The collapse results for the code-compliant base isolation system archetypes are tabulated in Tables 10-5a, 10-5b and 10-5c. For these systems, with an SMF superstructure, the collapse margin ratio is acceptable if the *ACMR* is greater than 2.16. A quick examination of the results in the final column of each table reveals that the code-compliant base isolation systems easily meet the acceptance criteria in this Methodology. The perimeter frame system (C1) has consistently smaller *ACMR*s than the space frame system (C2), due to the smaller lateral overstrength inherent in perimeter frame systems (see Section 10.3.5, Superstructure Overstrength Properties).

Table 10-5a and Figure 10-14 illustrate the effect of the moat wall clearance distance or gap size. The smallest gap sizes (18 in. and 24 in.) would not generally be allowed by Chapter 17 of ASCE/SEI 7-05, and are not code-compliant. These results are included here for comparison purposes. It is noted that even those systems with moat clearances less than the code allowed minimum are acceptable according to the criteria laid out in this Methodology. For small gap sizes, values of the *ACMR* are very stable, and are quite close to the *ACMR* values of fixed-base systems that have the same superstructure (i.e., *ACMR* values shown in Figure 10-14 for "0" gap size). This study indicates that base isolated systems have comparable levels of safety to code-conforming, conventional fixed-base structures. Even isolated

systems with smaller gap sizes than permitted in the code (gap sizes < 30 inches) meet the acceptable *ACMR* requirements.

**Table 10-5a Collapse Results for Code-Compliant Archetypes: Various Gap Sizes**

| Arch. No. | Gap Size (in.) | $S_{MT}[T_M]$ (g) | NDA (IDA) Results | | Computed Collapse Margin | | |
|---|---|---|---|---|---|---|---|
| | | | $\beta_{RTR}$ | $\hat{S}_{CT}[T_M]$ (g) | *CMR* | *SSF* | *ACMR* |
| *Perimeter RC SMF Systems Evaluated at $D_{max}$* | | | | | | | |
| C1-1 | 18 | 0.26 | 0.44 | 0.40 | 1.54 | 1.46 | 2.24 |
| C1-2 | 24 | 0.26 | 0.45 | 0.43 | 1.66 | 1.46 | 2.42 |
| C1-3 | 30 | 0.26 | 0.46 | 0.43 | 1.67 | 1.46 | 2.43 |
| C1-4 | 36 | 0.26 | 0.46 | 0.44 | 1.70 | 1.46 | 2.48 |
| C1-5 | 42 | 0.26 | 0.47 | 0.44 | 1.70 | 1.46 | 2.48 |
| *Space RC SMF Systems Evaluated at $D_{max}$* | | | | | | | |
| C2-1 | 18 | 0.26 | 0.46 | 0.50 | 1.92 | 1.30 | 2.50 |
| C2-2 | 24 | 0.26 | 0.47 | 0.56 | 2.16 | 1.30 | 2.81 |
| C2-3 | 30 | 0.26 | 0.45 | 0.57 | 2.19 | 1.30 | 2.85 |
| C2-4 | 36 | 0.26 | 0.47 | 0.62 | 2.40 | 1.30 | 3.12 |
| C2-5 | 42 | 0.26 | 0.48 | 0.66 | 2.52 | 1.30 | 3.28 |

**Table 10-5b Collapse Results for Code-Compliant Isolated Archetypes: Nominal (GEN), Upper-Bound (GEN-UB) and Lower-Bound (GEN-LB) Isolator Properties**

| Arch. No. | Isolator Prop's. | $S_{MT}[T_M]$ (g) | NDA (IDA) Results | | Collapse Margin Evaluation | | |
|---|---|---|---|---|---|---|---|
| | | | $\beta_{RTR}$ | $\hat{S}_{CT}[T_M]$ (g) | *CMR* | *SSF* | *ACMR* |
| *Space RC SMF Space Frame Systems Evaluated at $D_{max}$ - 30-inch Gap* | | | | | | | |
| C2-3 | GEN | 0.26 | 0.45 | 0.57 | 2.19 | 1.30 | 2.85 |
| C2-3U | GEN-UB | 0.26 | 0.47 | 0.54 | 2.08 | 1.33 | 2.77 |
| C2-3L | GEN-LB | 0.26 | 0.47 | 0.57 | 2.20 | 1.24 | 2.73 |

**Table 10-5c Collapse Results for Code-Compliant Isolated Archetypes: Moderate Seismic ($D_{min}$) Criteria**

| Arch. No. | Isolator Type | $S_{MT}[T_M]$ (g) | NDA (IDA) Results | | Collapse Margin Evaluation | | |
|---|---|---|---|---|---|---|---|
| | | | $\beta_{RTR}$ | $\hat{S}_{CT}[T_M]$ (g) | *CMR* | *SSF* | *ACMR* |
| *Space RC SMF Systems Evaluated at $D_{min}$ - RB and FP Bearings* | | | | | | | |
| C3-1 | RB | 0.09 | 0.45 | 0.38 | 4.01 | 1.19 | 4.77 |
| C3-2 | FP | 0.11 | 0.43 | 0.52 | 4.86 | 1.20 | 5.83 |

Beyond approximately 30 inches of moat wall clearance (for SDC $D_{max}$ ground motions) there may be some benefit to increasing the gap size. This benefit is especially apparent for the space frame system, which has sufficient overstrength to avoid significant nonlinear behavior even when the forces in the isolator are large. These results indicate that the code criteria for base isolated systems are adequate, and may be conservative in the case of moat wall clearance criteria for structures that have sufficient overstrength.

Since the simulation model does not account for torsional effects, it is possible that the real displacements in the isolation system will be greater than those observed in the analysis model. This increase in displacements would effectively reduce the moat wall clearance. However, it is expected that the possible increase in displacement associated with torsion is smaller than the variation in moat wall clearances considered, so that the results in Figure 10-14 are reasonable.

The effect of variability in isolator properties permitted by the provisions in ASCE/SEI 7-05 does not have a significant effect on the collapse margin computed, as shown in Table 10-5b. When upper-bound (GEN-UB) and lower-bound (GEN-LB) isolator properties are used, the *ACMR*s recorded are very close to the results for the nominal properties (GEN).

Tables 10-5a and 10-5b report collapse margins evaluated for SDC $D_{max}$ seismic criteria. For comparison, Table 10-5c reports collapse margin ratios computed for SDC $D_{min}$, seismic criteria, and systems with elastomeric (RB) and friction pendulum (FPS) bearings, respectively. As observed in Chapter 9, the collapse margins tend to increase as the seismic criteria decreases such that the *ACMR*s in Table 10-5c are quite large. Therefore, the high seismic criteria ($D_{max}$) govern the acceptability of this system.

**Collapse Results for Non-Code-Compliant Archetypes**

Tables 10-6a and 10-6b and Figures 10-15 and 10-16 show the collapse results for the non-code-compliant base isolation archetypes. As described earlier, these non-code-compliant archetypes are systems that violate the specific code provisions, in order to examine the validity of the design requirements. Specifically, this study probes the effects of superstructure strength (i.e., superstructures designed for a higher or lower base shear than required according to ASCE/SEI 7-05) and superstructure ductility (i.e., superstructures designed as ordinary moment frames, without the ductile detailing requirements for special moment frame systems). The effect of relaxing the moat clearance wall requirements was discussed previously (Table 10-5a and Figure 10-14). All the results in this section are for SDC $D_{max}$ seismic criteria.

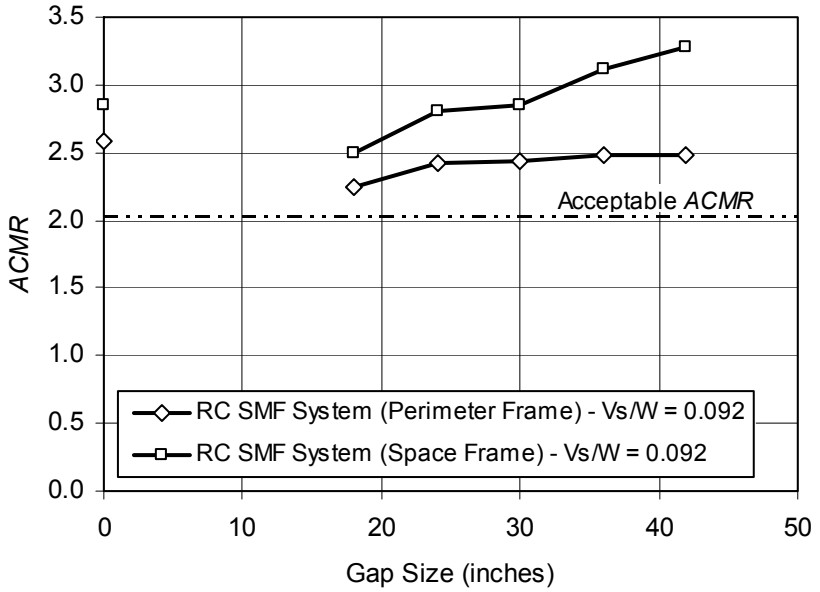


Figure 10-14 Values of Adjusted Collapse Margin Ratio (*ACMR*) for Code-Compliant isolated archetypes with various moat wall gap sizes and fixed-base archetypes (effectively 0-inch gap size), designed and evaluated for SDC $D_{max}$ seismic criteria.

**Table 10-6a Collapse Results for Non-Code-Compliant Archetypes: Ductile Superstructures with Normalized Design Shears ($V_s/W$) not equal to Code Required Value ($V_s/W = 0.092$)**

| Arch. No. | Gap Size (in.) | $S_{MT}[T_M]$ (g) | NDA (IDA) Results | | Collapse Margin Evaluation | | |
|---|---|---|---|---|---|---|---|
| | | | $\beta_{RTR}$ | $\hat{S}_{CT}[T_M]$ (g) | *CMR* | *SSF* | *ACMR* |
| *RC SMF Space Frame Systems Evaluated at $D_{max}$ - $V_s/W$ = 0.164, $V_{max}/W$ = 0.46* | | | | | | | |
| NC1-1 | 18 | 0.26 | 0.43 | 0.54 | 2.08 | 1.24 | 2.58 |
| NC1-2 | 24 | 0.26 | 0.47 | 0.59 | 2.28 | 1.24 | 2.83 |
| NC1-3 | 30 | 0.26 | 0.46 | 0.60 | 2.32 | 1.24 | 2.87 |
| NC1-4 | 42 | 0.26 | 0.47 | 0.69 | 2.64 | 1.24 | 3.27 |
| *RC SMF Space Frame Systems Evaluated at $D_{max}$ - $V_s/W$ = 0.046, $V_{max}/W$ = 0.24* | | | | | | | |
| NC2-1 | 18 | 0.26 | 0.47 | 0.42 | 1.62 | 1.33 | 2.16 |
| NC2-2 | 24 | 0.26 | 0.46 | 0.50 | 1.93 | 1.33 | 2.57 |
| NC2-3 | 30 | 0.26 | 0.48 | 0.53 | 2.03 | 1.33 | 2.71 |
| NC2-4 | 42 | 0.26 | 0.51 | 0.62 | 2.40 | 1.33 | 3.19 |

**Table 10-6b Collapse Results for Non-Code-Compliant Archetypes: Non-Conforming (Non-Ductile) Superstructures of Various Normalized Design Shears ($V_s/W$)**

| Arch. No. | Gap Size (in.) | $S_{MT}[T_M]$ (g) | NDA (IDA) Results | | Collapse Margin Evaluation | | |
|---|---|---|---|---|---|---|---|
| | | | $\beta_{RTR}$ | $\hat{S}_{CT}[T_M]$ (g) | *CMR* | *SSF* | *ACMR* |
| *RC OMF Space Frame Systems Evaluated at $D_{max}$ - $V_s/W$ = 0.246, $V_{max}/W$ = 0.47* | | | | | | | |
| NC3-1 | 30 | 0.26 | 0.43 | 0.35 | 1.36 | 1.19 | 1.62 |
| NC3-2 | 42 | 0.26 | 0.47 | 0.45 | 1.73 | 1.19 | 2.06 |
| *RC OMF Space Frame Systems Evaluated at $D_{max}$ - $V_s/W$ = 0.164, $V_{max}/W$ = 0.30* | | | | | | | |
| NC4-1 | 30 | 0.26 | 0.46 | 0.28 | 1.08 | 1.20 | 1.30 |
| NC4-2 | 42 | 0.26 | 0.48 | 0.42 | 1.62 | 1.20 | 1.94 |
| *RC OMF Space Frame Systems Evaluated at $D_{max}$ - $V_s/W$ = 0.092, $V_{max}/W$ = 0.17* | | | | | | | |
| NC5-1 | 30 | 0.26 | 0.48 | 0.27 | 1.02 | 1.24 | 1.27 |
| NC5-2 | 42 | 0.26 | 0.46 | 0.33 | 1.27 | 1.24 | 1.57 |

The effect of superstructure strength is demonstrated in Table 10-6a. For a SMF space frame with a design base shear of $V_s/W = 0.164$ and gap size of 30 inches, the computed *ACMR* is 2.87. When the design base shear is reduced to $V_s/W = 0.092$ the computed *ACMR* is 2.85 (code-conforming archetype, results are shown in Table 10-5a). For an even smaller design base shear ($V_s/W$) = 0.046, the computed *ACMR* is 2.71. These results suggest that a large difference in the design base shear (varying between 0.046 and 0.164 times the weight of the structure) has only a modest effect on the collapse results.

The reason the design base shear does not have a bigger effect on the collapse margin ratio is that the maximum strength of these structures is not linearly related to the design base shear (as illustrated in Figure 10-13). The design rules for special moment frame systems require capacity design and strong-column-weak-beam requirements such that the actual strength is much larger than the design strength, particularly for space frame systems which have significant gravity loads that are incorporated in the design. As a result, the structure designed with $V_s/W = 0.046$ has a true strength $V_{max}/W = 0.24$, accounting for its high collapse capacity. The observations indicate that the maximum strength of the structure ($V_{max}/W$) is a much better indicator of collapse performance of isolated structures than the base shear used for design of the superstructure ($V_s/W$).

Figure 10-16 shows the collapse capacity of the non-code-compliant RC SMF archetypes as a function of the strength of the structure ($V_{max}/W$). These structures have a peak MCE response of approximately 0.25g, on average.

Systems that have a greater strength than 0.25g have approximately the same *ACMR* (i.e.,. the curve flattens out such that increasing strength doesn't benefit the collapse safety). For lower strength values, the systems with less strength have progressively lower values of *ACMR*. Due to their ductility, RC SMF systems with superstructure strength significantly less than the MCE demand meet the Methodology's acceptance criteria.

The base isolated archetypes in Table 10-6b are all RC ordinary moment frame (OMF) systems, thereby violating the code requirements for superstructure ductility (i.e., SDC D structures). As in Chapter 9.3, the RC OMF structures are evaluated both for sidesway failure modes (directly simulated in the analysis) and non-simulated failure modes (loss of gravity load carrying capacity in columns due to column shear failure). Additional discussion of incorporation of non-simulated failure modes in the Methodology is available in Sections 9.3 and 10.2.

For RC OMF structures the acceptable *ACMR* is 2.30, due to the larger uncertainty associated with modeling archetypes of these systems. Comparing the reported *ACMR*s in Table 10-6b to the required *ACMR* of 2.30, none of the RC OMF systems are found to have acceptable collapse performance. This result indicates that the code-required ductile detailing requirements are generally necessary for maintaining adequate safety of isolated structures (during MCE ground motions). The collapse results for RC OMFs are also illustrated in Figures 10-15 and 10-16. The question remains whether a larger moat wall clearance and/or stronger structure would increase the collapse capacity of the RC OMF systems sufficiently to effect acceptable collapse performance.

As noted previously, *ACMR*s in Table 10-6b include the contributions of both simulated and non-simulated failure modes. On average, for these structures the non-simulated failure modes – or the potential for a column to lose gravity load carrying capacity following shear failure that is not modeled – reduced the collapse margin by approximately 25%. If the brittle shear failure mode could be prevented in these structures, the strongest OMFs (NC3) could potentially be acceptable with large moat wall clearances (see Figure 10-16). Note also that the non-simulated failure mode procedure is intentionally somewhat conservative, and considers loss of vertical carrying capacity in one column as equivalent to collapse. For a more detailed study of non-ductile systems on base isolation it may be necessary to include shear failure and post-shear failure degradation directly in the models.

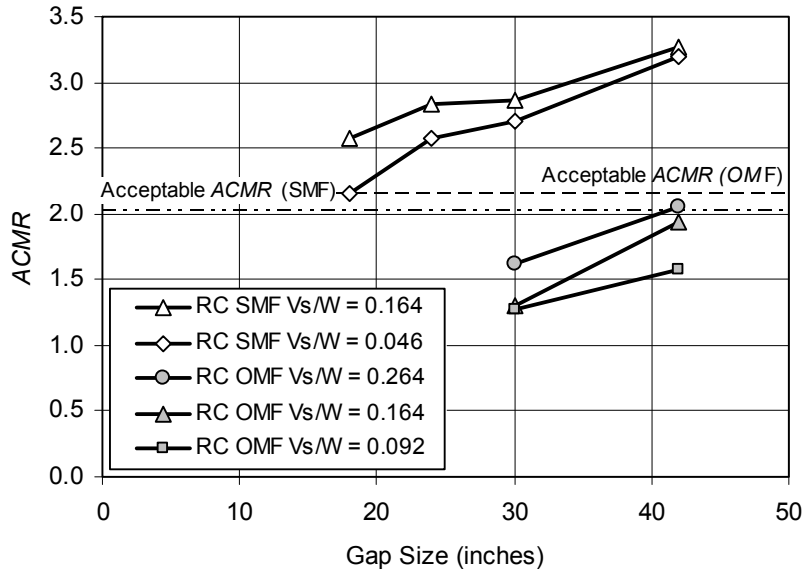


Figure 10-15 Values of Adjusted Collapse Margin Ratio (*ACMR*) for Non-Code-Compliant isolated archetypes with various moat wall gap sizes, evaluated for SDC $D_{max}$ seismic criteria

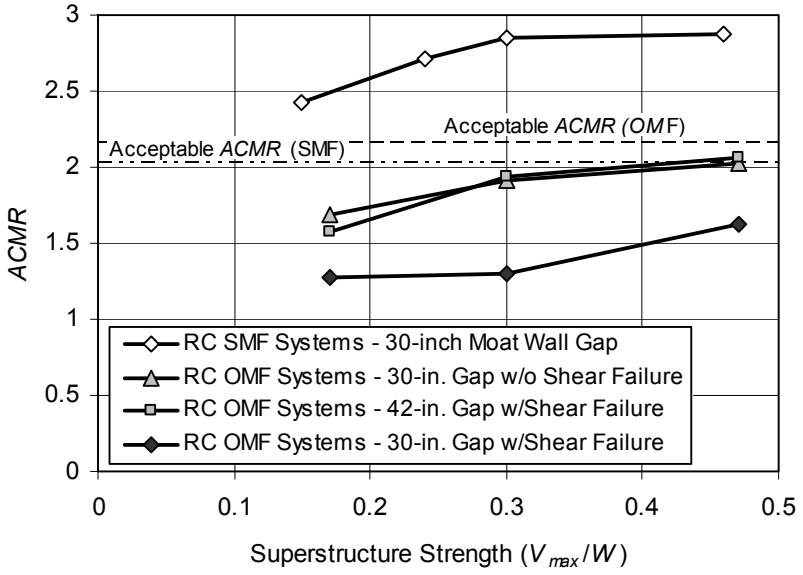


Figure 10-16 Values of Adjusted Collapse Margin Ratio (*ACMR*) for isolated archetypes with different super-structure strengths evaluated for SDC $D_{max}$ seismic criteria.

**Summary of Collapse Results**

This study demonstrates that when evaluated according to the Methodology base isolated systems provide comparable levels of safety against collapse to

conventional, fixed-base structures. When compared to conventional structures, the major benefit of base isolating structures is in reduced damage and losses in smaller earthquakes, but these effects have not been quantified in this study.

In evaluating non-code compliant archetypes for base isolated systems, the effect of code provisions moat wall clearance, superstructure strength, and superstructure ductility (on concrete frame superstructures) were considered. In the case of moat wall clearance, it is observed that superstructures with sufficient strength and ductility are relatively insensitive to the moat wall clearance. For small moat wall clearances the structure behaves more like a fixed-base structure.

The study of superstructure strength suggests (unsurprisingly) that the behavior of base isolated systems is more sensitive to the real strength of the structure, rather than the design base shear. For systems with high inherent overstrength, such as the special space frame designs, very low design base shears can be used. Other systems that have less overstrength may behave differently when isolated. Comparison of the performance of isolated special moment frames and isolated ordinary moment frames indicates that the code ductility requirements for special moment frames significantly reduce the collapse risk.

### *10.3.7 Discussion - Analysis Properties and Methods Unique to Isolated Structures*

**Definition of Fundamental Period**

In applying the methodology to base isolated structures $T = T_M$ was used as the fundamental period of the structure, i.e., the record set is scaled at $T_M$ and the collapse margin ratio is computed by comparison to the MCE at $T_M$ ($S_{MT}(T_M)$). Two other period definitions are possible. The first definition would base $T$ on the fundamental period of the superstructure (i.e., on a fixed base). The second definition, $T = T_D$, would use the effective period of the isolated structure at the design displacement (rather than the MCE displacement). (A third option would be to use the period defined by the effective stiffness shown in Figure 10-9, which is calculated to be slightly smaller than $T_M$ or $T_D$. This option is not used for consistency with code-based equations for computing period of base isolated systems.)

Collapse results are very close for $T_D$ and $T_M$ since there is only a small difference in these two period definitions. If the period of the superstructure (on a fixed base) were used instead of $T_M$ the reported *CMR*s would be higher. This discrepancy results from differences in energy content at long

periods between the median spectrum of the Far-Field record set and the code spectrum. As period increases, the median spectrum of the Far-Field record set decreases faster than the arbitrary, 1/T, shape of the code spectrum. Since the 1/T shape of the code spectrum is assumed (and isolated structures are typically designed for site-specific ground motions), the effective period, $T_M$, is the most appropriate choice of period. Use of the fundamental period of the superstructure (on a fixed base) to evaluate collapse margin would be highly non-conservative.

**Discussion of Composite Uncertainty**

In the evaluation of base isolation systems, as described above, it was necessary to make judgments on each of the component sources of uncertainty in order to determine the total uncertainty. Record-to-record variability, design requirement-related variability, test data-related variability and model-related variability each contribute to the uncertainty in the predicted collapse fragility.

In Chapter 7, it is assumed that the record-to-record variability is given by $\beta_{RTR} = 0.40$. This value is typical for many structural systems, but varies slightly depending on the type of structure and the period of interest. It is also a function of the ground motion scaling procedure (which is fixed in this Methodology). The results shown in Tables 10-5 and 10-6 indicate that the record-to-record variability for these structures lies in the range $0.45 < \beta_{RTR} < 0.50$.

Other issues related to the uncertainty include the assessment of the model uncertainty and the test-data related uncertainty. For both types of uncertainty there is significantly smaller uncertainty related to the isolator behavior than to the superstructure behavior. This difference is especially important in the case of the test data, since the isolation designs are based on design-specific tests. To obtain an approximate idea of the uncertainty associated with isolator modeling, Table 10-5b can be revisited, which shows that variability in modeling of the isolator between the upper bound, nominal and lower bound models result in very small differences in the *ACMR*. Since both the superstructure and isolator uncertainties contribute to the collapse uncertainty, model and test data uncertainty are rated according to the superstructure behavior. It should be noted that this may be conservative in some cases, as the isolator filters out some of the higher mode effects etc. that contribute to the collapse variability in fixed-base structures.

In evaluation of base isolation systems, the same methods are used to compute the total uncertainty as in earlier examples, following the requirements of Chapter 7. This may underestimate the record-to-record

contribution slightly, but is remedied by conservative estimates of the contribution of modeling and test data uncertainties to the total uncertainty of collapse.

**Spectral Shape Effects**

Despite the significant differences between isolated systems and conventional fixed-base structures, the same procedure for determining the spectral shape factor (*SSF*) is used, as described in Chapter 7 and Appendix B. This method relies on a pushover analysis to determine the building ductility capacity ($\mu_C$), as shown in Figure 10-9. The primary difference, as mentioned previously, is the pushover load pattern, i.e., a uniform load pattern should be used for the isolated structure. In addition, it was decided to use the pushover computed without the moat wall springs (as the sudden increase in stiffness associated with the moat wall is inconsistent with the assumptions used in developing the relationship between μ and *SSF* in Appendix B). Once the pushover results are obtained, the computation of $\mu_C$ is exactly the same as in the examples of Chapter 9.

The computed ductility capacity is smaller for isolated systems due to the relative stiffness of the isolator (i.e., for fixed-base SMFs (SDC D), $\mu_c$ = 9.2 to 11.4, whereas isolated SMFs (SDC D), $\mu_c$ = 1.7 – 4.2). However, the decrease in ductility capacity is offset by an increase in period by considering $T = T_M$ when determining the *SSF*. As shown in Table 10-7, the *SSF* factors are within the same range, or in some cases slightly smaller for the isolated system (as compared to the fixed-base).

**Table 10-7 Typical ranges of spectral shape factors (*SSF*s) for various archetype systems.**

| 4-Story Archetype | Seismic Criteria | *SSF* |
|---|---|---|
| Fixed Base RC SMF | SDC $D_{max}$ | 1.42 |
| Fixed Base RC OMF | SDC $B_{max}$ | 1.10 – 1.15 |
| Isolated RC SMF | SDC $D_{max}$ | 1.24 – 1.46 |
| Isolated RC SMF | SDC $D_{min}$ | 1.20 |
| Isolated RC OMF | SDC $D_{max}$ | 1.19 – 1.24 |

Since the spectral shape factors in Appendix B were developed based on fixed-base conventional structures, this study was also used to verify the general applicability of the *SSF* to a wider range of systems. In order to verify the applicability of the computation of *SSF* as a function of building ductility ($\mu_c$), values of the *SSF* were first computed according to the requirements of Appendix. B. These values are reported as results in Tables 10-5 and 10-6. Secondly, the *SSF* were computed using linear regression

analysis between the collapse capacity and epsilon of each ground motion record (as described in Appendix B and shown in Figure B-2), illustrating what the *SSF* should be. The predicted *SSF* (based on ductility) and the observed *SSF* (directly from analysis results) were very close in most cases. For the code-compliant systems evaluated at $D_{max}$, on average the predicted *SSF* overestimates the observed *SSF* by about 1%. For non-code-compliant systems evaluated at $D_{max}$ the predicted *SSF* underestimates the *SSF* by approximately 3% on average. One caveat is that although the *SSF* are correct on average, there are some trends, especially in the non-code-compliant systems that are not fully captured by the definitions of ductility and *SSF* in Appendix B. However, the results are close enough to justify the use of the Methodology for developing *SSF*s in this study.

# Chapter 11

# Conclusions and Recommendations

This recommended Methodology provides a rational basis for establishing global seismic performance factors (SPF's), including the response modification coefficient ($R$ factor), the system overstrength factor ($\Omega_0$), and the deflection amplification factor ($C_d$) of new seismic-force-resisting systems proposed for inclusion in model building codes. The Methodology also provides a more reliable basis for re-evaluation of seismic performance factors of seismic-force-resisting systems currently available in model building codes and resource documents.

This chapter describes assumptions and limitations of the Methodology, summarizes observations and conclusions resulting from its development, discusses an adaptation of the Methodology to collapse performance evaluation for an individual building, and provides recommendations for further study.

## 11.1 Assumptions and Limitations

The Methodology is intended to apply broadly to all buildings, recognizing that this objective may not be fully achieved for certain seismic environments and building configurations. Likewise, the Methodology has incorporated certain simplifying assumptions deemed appropriate for reliable evaluation of seismic performance. Key assumptions and potential limitations of the Methodology are summarized in the following sections.

### *11.1.1 Far-Field Record Set Ground Motions*

The Methodology specifies the same set of ground motions (i.e., Far-Field record set) for collapse performance evaluation of all systems. Records of the Far-Field record set are unambiguously defined (including scaling) to avoid any subjectivity in the ground motions used for nonlinear dynamic analyses. The Far-Field record set is a robust sample of strong motion records from large magnitude events. Even so, these records have inherent limitations for certain buildings.

**Buildings at Sites near Active Faults**

Two sets of ground motion data, the Far-Field record set (records at sites at least 10 km from fault rupture) and the Near-Field record set (records at sites within 10 km of fault rupture) were developed. An internal study, documented in Appendix A, found that the collapse margin ratio (*CMR*) was somewhat smaller for a system designed for "near-fault" (SDC E) seismic criteria and evaluated using the Near-Field record set, than for same system designed for SDC D seismic criteria and evaluated using the Far-Field record set. This implies that somewhat smaller values of the response modification coefficient, *R*, would be appropriate for design of buildings near active faults.

Various alternatives were considered, including the development of a separate set seismic performance factors for design of buildings near active faults. For simplicity, as well as consistency with ASCE/SEI 7-05, a single set of seismic performance factors based on collapse assessments using the Far-Field record set was chosen. In so doing, the Methodology implicitly accepts somewhat greater life safety risk for buildings located close to active faults. This is consistent with the approach in ASCE/SEI 7-05, which implicitly accepts somewhat greater life safety risk for buildings near active faults by limiting MCE ground motions to deterministic values of seismic hazard.

Although the Methodology uses the Far-Field record set to establish seismic performance factors for a new seismic-force-resisting systems, the Near-Field record set would be more appropriate for verifying life safety performance of an individual building located near an active fault.

**Buildings at Sites in the Central and Eastern United States or Subject to Deep Subduction Earthquakes**

The Far-Field record set is a robust sample of all strong motion records from large magnitude events recorded at sites greater than 10 km from fault a rupture. No attempt was made to limit records based on tectonic setting or fault mechanism during the record selection process. The Far-Field record set is dominated by shallow crustal earthquakes, representative of areas in the Western United States. It does not include strong motions records from deep subduction earthquakes, or from Central and Eastern United States earthquakes, since such records do not exist.

Duration of strong shaking is an important parameter in collapse analyses of degrading systems, and strong motion records were purposely selected from large magnitude events to adequately capture shaking duration. Very large magnitude earthquakes associated with deep subduction zone events would

be expected to have longer durations of strong shaking, on average. Central and Eastern United States events could have different shaking characteristics also affecting the collapse margin ratio and related values of seismic performance factors. In spite of limitations in available deep subduction zone, or Central and Eastern United States earthquake records, actual earthquake records, rather than artificial or theoretical ground motions, were selected as the basis for collapse assessment.

**Buildings with Very Long Periods**

The usefulness of earthquake records at very long periods is limited by the ability of strong motion instruments to accurately record long-period vibration. Records from older instruments may only be accurate to one or two seconds, while records from the newer instruments are typically accurate to at least 10 seconds. The Far-Field and Near-Field record sets include only those records deemed accurate to a period of at least 4 seconds by the agency responsible for processing the record. Most records in these sets are accurate to a period of at least 10 seconds.

The Methodology conservatively limits the elastic period of index archetype configurations to a period not greater than 4 seconds to ensure valid evaluations of collapse performance. Records from the Far-Field and Near-Field record sets should be used with caution to evaluate collapse performance of buildings with elastic periods greater than 4 seconds (e.g., very tall buildings), since the spectral content of some records may not be valid, and the associated value of the spectral shape factor, *SSF*, may be overstated by the Methodology.

### *11.1.2 Influence of Secondary Systems on Collapse Performance*

The Methodology evaluates collapse performance of the seismic-force-resisting system, ignoring the influence of secondary systems, such as gravity systems and nonstructural components, which are not included in the designation of the seismic-force-resisting system. Such systems can either improve or diminish the collapse performance of a system of interest.

**Buildings with Potentially Improved Performance**

For many buildings, elements of the gravity or nonstructural systems can significantly improve collapse performance by providing additional resistance to lateral forces. This is particularly true when the secondary system has a larger lateral capacity than that of that of the primary system (ATC, 2007b).

Incorporation of elements of the gravity or nonstructural systems in index archetype configurations was considered. It was ultimately decided to limit participating elements to those defined as part of the seismic-force-resisting system. It was not considered appropriate to take the beneficial effects of elements and components that would not be subject to earthquake design provisions. As an alternative, it would be permissible to include elements of the gravity or nonstructural systems in the assessment, if they were also included in the definition of the seismic-force-resisting system, and subject to the criteria contained within the system design requirements.

**Buildings with Potentially Reduced Performance**

Partial collapse of buildings has occurred when elements of the gravity or nonstructural systems are not able to sustain lateral deformations of the seismic-force-resisting system. Options for explicitly modeling and evaluating gravity system performance were considered. Ultimately it was considered to be problematic, and not pertinent to evaluation of seismic performance factors for a seismic-force-resisting system that must be qualified for use with many different secondary systems. Rather, displacement compatibility requirements of ASCE/SEI 7-05 are relied upon to protect secondary systems from collapse failure.

It should be noted that current displacement compatibility requirements of Section 12.12.4 of ASCE/SEI 7-05 may not be adequate to protect against premature failure of a gravity system. They only apply to SDC D (and SDC E and F) structures, and are based on design story drift, which is substantially less than the peak inelastic story drift of ductile seismic-force-resisting systems at the point of incipient collapse.

### *11.1.3 Buildings with Significant Irregularities*

Significant irregularities, including torsion (horizontal structural irregularity Types 1a and 1b, Table 12.3-1, ASCE/SEI 7-05) and soft/weak story (vertical structural irregularity Types 1a and 1b, Table 12.3-2, ASCE/SEI 7-05), are known contributors to building collapse. Options for explicit modeling of irregularity were considered, but internal studies showed this to be unnecessary for evaluating collapse margins and related seismic performance factors for a generic seismic-force-resisting system. Limits on the use of equivalent lateral force (ELF) analysis given in Table 12.6-1 of ASCE/SEI 7-05 and related design conservatisms of the ELF procedure (e.g., accidental torsion, P-Delta effects, etc.) were considered adequate to either limit the effects of significant irregularities, or require more detailed, dynamic analysis.

It should be noted that limits on the use of the ELF procedure are more restrictive for SDC D (and SDC E and F) structures, and certain design requirements (e.g., amplification of accidental torsion) do not apply to SDC B structures, so that there may be some additional life safety risk due to irregularity inherent to systems designed for either SDC B or C criteria.

### *11.1.4 Redundancy of the Seismic-Force-Resisting System*

Section 12.3.4.2 of ASCE/SEI 7-05 requires the seismic-force-resisting system of structures assigned to SDC D, E and F to be designed for seismic loads increased by the redundancy factor, $\rho$, where $\rho = 1.3$ unless the configuration meets certain "redundancy" requirements. Options for explicit modeling of non-redundant systems were considered, but internal studies showed this to be unnecessary for evaluating collapse margins and related seismic performance factors for a generic seismic-force-resisting system. The Methodology assumes $\rho = 1.0$ for design of structural system archetypes, since larger values of $\rho$ would be unconservative for collapse evaluation of archetypes that generally meet redundancy requirements of Table 12.3-3 of ASCE/SEI 7-05.

## 11.2 Observations and Conclusions

In the development of this Methodology, selected seismic-force-resisting systems were evaluated to illustrate the application of the Methodology and verify its methods. Results of these studies provide insight into the collapse performance of buildings and appropriate values of seismic performance factors. Observations and conclusions in terms of generic findings applicable to all systems, and specific findings for certain types of seismic-force-resisting systems are described below. These findings should be considered generally representative, but not necessarily indicative of all possible trends, given limitations in the number and type of systems evaluated.

### *11.2.1 Generic Findings*

The following generic findings and conclusions apply to seismic-force-resisting systems in general.

**Systems Approach**

Collapse performance (and associated seismic performance factors) must be evaluated in terms of the behavior of the overall seismic-force-resisting system, and not the behavior of individual components or elements of the system. Collapse failure modes are highly dependent on the configuration and interaction of elements within a seismic-force-resisting system. Seismic

performance factors should be considered as applying to an entire seismic-force-resisting system, and not elements comprising it.

**Precision of Seismic Performance Factors**

In general, there is no practical difference in the collapse performance of systems designed with fractional differences in the response modification coefficient, *R*. For example, collapse performance of structures designed for *R* = 6 and *R* = 6.5 is essentially the same, all else being equal. There is a discernible, but modest difference in collapse performance for systems designed for moderately different values of *R*, for example *R* = 6 and *R* = 8. There is, however, a significant difference in collapse performance for systems designed using different multiples of *R* , as in *R* = 3 versus *R* = 6. Current values of *R* provided in Table 12.2-1 (e.g., 3, 3-1/4 and 3-1/2) reflect a degree of precision that is not supported by results of example collapse evaluations.

**Spectral Content of Ground Motions**

Consideration of spectral content (spectral shape) of ground motions can be very important to the evaluation of collapse performance of ductile structures. Epsilon-neutral earthquake records that are scaled to represent very rare ground motions (ground motions corresponding to large positive values of epsilon) can significantly overestimate demand on ductile structures. The Methodology incorporates a spectral shape factor (*SSF*) that adjusts calculated response to account for the spectral content of rare earthquake ground motions and avoid overestimation of nonlinear response.

**Short-Period Buildings**

Consistent with prior research, values of collapse margin ratio are consistently smaller for short-period buildings, regardless of the type of seismic-force-resisting system. Without adequate design strength short-period buildings do not meet collapse performance objectives of the Methodology.

These findings suggest a possible need for period-dependent seismic performance factors (e.g., a short-period value and a 1-second value of the response modification coefficient, *R*, for each system). At present, the Methodology determines a single value of each seismic performance factor, independent of period, and consistent with the design requirements of ASCE/SEI 7-05. It could, however, be modified to determine period-dependent values of each factor.

**Governing Seismic Design Category**

Values of collapse margin ratio for a seismic-force-resisting system designed and evaluated for seismic criteria of Seismic Design Category (SDC) D are generally smaller than corresponding values of collapse margin ratio for the same seismic-force-resisting system designed and evaluated for the seismic criteria of SDC C, all else being equal.

This trend is attributed to the increasing role of gravity loads in the strength of seismic-force-resisting elements as the level of seismic design decreases. The size and strength of seismic-force-resisting elements supporting both seismic and gravity loads is not necessarily proportional to a decrease in seismic design loads, since gravity loads do not decrease. The role of gravity loads in the strength of the seismic-force-resisting system is directly related to system overstrength, $\Omega$, which also tends to increase as the level of seismic design decreases.

These findings suggest that the response modification coefficient, $R$, will generally be governed by the Seismic Design Category with the strongest ground motions for which the system is proposed for use (i.e., SDC D for seismic-force-resisting systems that are permitted for use in all SDCs). In general, $R$ based on SDC D evaluations are conservative for design of the same seismic-force-resisting system designed for SDC C or SDC B seismic criteria.

These findings also suggest a possible need for seismic load-dependent seismic performance factors. For example, a system designed for SDC C seismic criteria could be assigned a larger value of $R$ than would be required for the same system designed for SDC D seismic criteria. At present, the Methodology determines a single value of each seismic performance factor, independent of seismic design criteria, and consistent with the design requirements of ASCE/SEI 7-05. It could, however, be modified to determine SDC-specific values of each factor.

**Overstrength**

Consistent with prior research, values of collapse margin ratio are strongly related to calculated values of overstrength, regardless of the type of seismic-force-resisting system. For larger values of overstrength, larger values of collapse margin ratio are observed.

Calculated values of overstrength for different index archetype models vary widely, depending on configuration and seismic design criteria (SDC). Results suggest that current values of system overstrength, $\Omega_O$, given in Table 12.2-1 of ASCE/SEI 7-05 are not representative of actual seismic-

force-resisting system overstrength. Values in the table generally vary between 2 and 3 for all systems except cantilevered structures, while calculated values of $\Omega$ varied from as low as 1.5 to over 6 for structural system archetypes evaluated in the development of the Methodology.

**Distribution of Inelastic Response**

Consistent with prior research, values of collapse margin ratio are strongly related to the distribution of inelastic response over the height of a structure, regardless of the type of seismic-force-resisting system. Values of collapse margin ratio are significantly larger for systems with more evenly distributed inelastic response over height.

### *11.2.2 Specific Findings*

The following key findings and conclusions apply specifically to reinforced-concrete moment frame systems, wood light-frame systems, and base-isolated systems that were evaluated as part of the development of the Methodology.

**Example Application - Reinforced-Concrete Special Moment Frame Systems**

Evaluation of reinforced concrete (RC) special moment frame (SMF) systems found that, in general, designs based on current ASCE/SEI 7-05 requirements ($R$ = 8) meet the collapse performance objectives of this Methodology. However, trends in collapse margin ratio results suggested a potential collapse deficiency for taller buildings that did not meet minimum base shear requirements consistent with requirements in the predecessor document, ASCE 7-02. This information was made available to the ASCE 7 Seismic Committee, and a special code change proposal was passed in 2007 (Supplement No. 2), amending the minimum base shear requirements of ASCE/SEI 7-05 to correct for this potential deficiency.

The root cause of this potential deficiency in collapse performance of RC SMF systems is the localization of large lateral deformations in the lower stories, and the associated detrimental $P$-$\Delta$ effects on post-yield behavior. While imposing a minimum value of design base shear eliminated the potential deficiency for these systems, other approaches could have been used, including the introduction of height limits (which would not be practical), enhancement of $P$-$\Delta$ and strong-column- weak-beam design criteria (which would require additional study), or the development of period-dependent response modification coefficients, $R$ (which would effectively increase the design base shear for taller buildings).

**Example Application - Reinforced-Concrete Ordinary Moment Frame Systems**

Example evaluation of reinforced concrete (RC) ordinary moment frame (OMF) systems found that, in general, designs based on current ASCE/SEI 7-05 requirements (e.g., $R = 3$) meet the collapse performance objectives of this Methodology, considering that these systems are only permitted for use in SDC B structures.

**Example Application - Wood Light-Frame Systems**

Example evaluations of wood light-frame systems found that, in general, designs based on current ASCE/SEI 7-05 requirements (e.g., $R = 6$) need additional strength from architectural finishes, such as gypsum wall board sheathing, to be included in the seismic-force-resisting system in order to meet the collapse performance objectives of this Methodology.

While somewhat controversial, this finding simply confirms that gypsum wall board, and other finishes common to single family and multi-family residences, are important to the seismic performance of this class of structure. It suggests that these components should be made a formal part of the seismic-force-resisting system so that design requirements for wood light-frame buildings will result in sufficient total strength to meet intended performance objectives.

**Supporting Study - Seismically-Isolated Structures**

A special study of seismically-isolated buildings focused on the performance of isolated special and ordinary reinforced concrete frame systems. This study found that code-conforming isolated structures with ductile superstructures (e.g., special moment frame systems) generally collapse performance objectives, but that isolated structures with non-ductile superstructures (e.g., ordinary moment frame systems) may not. However, it also found that with higher strengths, superstructures of isolated systems did not need to have the full ductility capacity required of conventional buildings to achieve acceptable collapse performance. This is an important finding for the introduction of more economically detailed superstructures of isolated buildings, although more comprehensive studies would be required to develop appropriate code requirements.

Pushover evaluations of isolated structures found poor correlation between the true (maximum) strength of the superstructure and the design strength. This suggests that nonlinear static (pushover) analyses would be more appropriate for verifying adequate overstrength of the superstructure than

selecting superstructure strength based on the approximate values of $R_I$, and would also provide a more reliable and economical basis for design.

## 11.3 Collapse Evaluation of Individual Buildings

Although developed as a tool to establish seismic performance factors for generic seismic-force-resisting systems, the Methodology could be readily adapted for collapse assessment of an individual building system. As such, it could be used to demonstrate adequate collapse performance of the structural system of a building designed using performance-based design methods, permitted by Section 11.1.4 of ASCE/SEI 7-05. Specific methods for collapse evaluation of an individual building system are described in Appendix F.

### *11.3.1 Feasibility*

It is anticipated that buildings designed using performance-based methods will likely be large or important structures. Projects using performance-based design methods typically utilize detailed models for linear and nonlinear analyses of the building, and peer review is commonly required. Such projects are already set up to utilize many of the components of the Methodology.

### *11.3.2 Approach*

The Methodology is based on the concept of collapse level ground motions, defined as the level of ground motions that cause median collapse (i.e., one-half of the records in the set cause collapse). For a building to meet the collapse performance objectives of this Methodology, the median collapse capacity must be an acceptable amount above the MCE ground motion demand level (i.e., the adjusted collapse margin ratio, *ACMR*, must exceed acceptable values).

By starting with an acceptable collapse probability (for MCE ground motions) and working backwards through the Methodology, values of the spectral shape factor, *SSF*, and collapse margin ratio, *CMR*, can be evaluated to determine the level of ground motions corresponding to median collapse. The Methodology can be "reverse engineered" to determine the level of ground motions for which not more than one-half of the records should cause collapse. By scaling the record set to this level, trial designs for a subject building can be evaluated. If the analytical model of the trial design survives one-half or more of the records without collapse, then the building has a collapse probability that is equal to (or less than) the acceptable collapse

probability (for MCE ground motions), and meets collapse performance objective of the Methodology.

## 11.4 Recommendations for Further Study

The following recommendations are provided for possible future studies that would help to: (1) further improve or refine the Methodology; or (2) utilize the Methodology to investigate and develop potential improvements to the seismic provisions of ASCE/SEI 7-05.

### *11.4.1 Studies Related to Improving and Refining the Methodology*

**Comprehensive Evaluation of Existing Systems**

The primary objective of this study would be to "beta test" the Methodology to further verify that this procedure will reliably and reasonably quantify building seismic performance for the various building systems that are, or will eventually become adopted by current building codes and standards organizations.

The Methodology could also be used to set minimum acceptable design criteria for standard code-approved systems and to provide guidance in the selection of appropriate design criteria for other systems when linear design methods are applied. It is possible that the Methodology could then be used to modify or eliminate those systems or requirements that cannot reliably meet, or do not relate, to these objectives.

**Component Qualification**

The Methodology thus far has been developed to comprehensively evaluate entire building systems, including variations in system configuration. This study would be intended to modify and simplify the procedure so that it can be used on individual building components.

The need for a simplified component methodology has been identified by construction materials industries and codes and standards organizations for the purpose of reliably and accurately quantifying seismic performance of various building components that currently are, or will eventually become available for use as seismic-force-resisting elements within building systems.

**Simplified Methods**

Collapse simulation is a detailed, data-intensive process, which has a high degree of uncertainty. In order to comprehensively evaluate entire building systems, and all permissible variations in system configuration, the Methodology is necessarily complex. This study would investigate and test

possible short cuts in the process to simplify the overall application of the Methodology for use when more comprehensive evaluations are not necessarily warranted.

**Modeling of Short-Period Structures**

The Methodology does not currently provide any specific guidance for modeling foundation flexibility and considering possible beneficial effects of soil-structure-interaction on the collapse performance of short-period structures. This study would investigate these effects and, if justified, develop guidance for explicitly modeling of foundation flexibility and adjustment factors (similar to *SSF*) that would adjust collapse margin ratios as function of period, for evaluation of structural system archetypes assumed to be fixed on a rigid base.

### *11.4.2 Studies Related to Advancing Seismic Design Practice and Building Code Requirements (ASCE/SEI 7-05)*

**Period-Dependent and Seismic Load- Dependent R factors**

The equivalent lateral force (ELF) procedure of ASCE/SEI 7-05 defines base shear in terms of a single value of *R* for a given seismic-force-resisting system, independent of the period of the structure or the level of seismic design criteria. Studies show that designs based on a single value of *R* do not necessarily have consistent collapse performance, and that such inconsistencies could be reduced or eliminated by specifying period-dependent or seismic load-dependent values of *R*.

Use of period-dependent and load-dependent values of *R* would require substantial revision to the equivalent lateral force method and related requirements in seismic design codes and standards, but could provide a basis for more efficient and economical design. The Methodology could be used to investigate period and seismic load dependency of *R*, and the feasibility of incorporating such factors. Potential benefits would be greater in regions of lower seismicity, where seismic load-dependent values of *R* are likely to be more liberal than those now specified for the same system in regions of high seismicity.

**Consideration of Gravity and Nonstructural Systems and Components**

The Methodology could be used to investigate the importance of the gravity system and certain nonstructural components to collapse performance, and investigate the feasibility of enhancing current seismic design requirements to more appropriately incorporate these systems in the seismic design process. This would include accounting for both the possible beneficial and

detrimental effects of these systems on collapse performance. Comparisons of collapse results for archetypical models both with and without selected elements could be made to quantify the results.

**Structural Irregularities and Redundancy**

The Methodology could be used to investigate the importance of structural system regularity and redundancy to collapse performance, and investigate possible changes to current seismic design requirements with regard to these characteristics. Comparisons of collapse results for archetypical models both with and without features of regularity and redundancy could be made to quantify the effects.

**Structures with Isolation and Damping Systems**

Due to limited experience in strong earthquakes, code development committees have necessarily and appropriately imposed certain conservative restrictions on design requirements for seismically isolated and damped structures. The Methodology could be used to evaluate the importance of current design requirements for isolated systems, and investigate the feasibility of removing unnecessary conservatism. Comparisons of collapse results of archetypical models with non-ductile superstructures of varying strength levels could be made to quantify required strength for meeting collapse performance objectives. Removal of unnecessary conservatism would reduce system cost and support greater use of these types of protective systems.

# Appendix A
# Ground Motion Record Sets

This appendix describes the selection of ground motion record sets for collapse assessment of building structures using nonlinear dynamic analysis (NDA) methods. It summarizes the characteristics of the Far-Field and Near-Field record sets and defines the scaling methods appropriate for collapse evaluation of building archetypes based on incremental dynamic analysis.

Both the Far-Field and Near-Fault record sets have average epsilon values that are lower than expected for MCE motions, and therefore can substantially underestimate calculated collapse margin ratios without appropriate adjustment for spectral shape effects. Adjustment of results from nonlinear dynamic analysis using these record sets is described in Appendix B.

## A.1 Introduction

Ground motion record sets include a set of ground motions recorded at sites located greater than or equal to 10 km from fault rupture, referred to as the "Far-Field" record set, and a set of ground motions recorded at sites less than 10 km from fault rupture, referred to as the "Near-Field" record set. The Near-Field record set includes two subsets, including ground motions with strong pulses, referred to as the "NF-Pulse" record subset, and ground motions without such pulses, referred to as the "NF-No Pulse" record subset.

## A.2 Objectives

The Methodology requires a set of records that can be used for NDA of buildings, and evaluation of the probability of collapse for maximum considered earthquake (MCE) ground motions. These records meet a number of conflicting objectives, described below.

- **Code (*ASCE/SEI 7-05*) Consistent** – The records should be consistent (to the extent possible) with the ground motion requirements of Section 16.1.3.2 of ASCE/SEI 7-05 (ASCE, 2006a) for three-dimensional analysis of structures. In particular, "ground motions shall consist of pairs of appropriate horizontal ground motion acceleration components that shall be selected and scaled from individual recorded events."

- **Very Strong Ground Motions** – The records should represent very strong ground motions corresponding to the MCE motion. In high seismic regions where buildings are at greatest risk, few recorded ground motions are intense enough, and often significant upward scaling of the records is required.
- **Large Number of Records** – The number of records in the set should be "statistically" sufficient such that the results of collapse evaluations adequately describe both the median value and record-to-record (RTR) variability of collapse capacity.
- **Structure Type Independent** – The records should be broadly applicable to collapse evaluation of a variety of structural systems (i.e., systems that have different dynamic response properties, performance characteristics, etc.). Accordingly, records should not depend on period, or other building-specific properties of the structure.
- **Site Hazard Independent** – The records should be broadly applicable to collapse evaluation of structures located at different sites (i.e., sites with different ground motion hazard functions, site and source conditions, etc.). Accordingly, records should not depend on hazard de-aggregation, or other site- or hazard-dependent properties.

No single set of records can fully meet all of the above objectives due, in part, to inherent limitations in available data. Large magnitude events are rare, and few existing earthquake ground motion records are strong enough to collapse large fractions of modern, code-compliant buildings. In the United States, strong-motion records date to the 1933 Long Beach earthquake, with only a few records obtained from each event until the 1971 San Fernando earthquake.

Even with many instruments, strong motion instrumentation networks (e.g., Taiwan and California) provide coverage for only a small fraction of all regions of high seismicity. Considering the size of the earth and period of geologic time, the available sample of strong motion records from large-magnitude earthquakes is still quite limited (and potentially biased by records from more recent, relatively well-recorded events).

## A.3 Approach

The Methodology requires a set of ground motion records for collapse assessment of archetypical models that are appropriate for Incremental Dynamic Analysis (Vamvatsikos and Cornell, 2002), as adapted herein. Incremental Dynamic Analysis (IDA) makes use of multiple response history analyses for a given ground motion record of increasing intensity until

collapse occurs (or the model otherwise reaches a collapse limit state). This process is repeated for a set of ground motion records of sufficient number to determine median collapse and record-to-record variability.

The Methodology follows the IDA concept of increasing ground motion intensity to collapse, but applies each sequential increase in intensity, collectively, to the entire set of ground motion records. Similar to IDA, the Methodology characterizes intensity in terms of response spectral acceleration at the fundamental period, $T$, of the system of interest, except that intensity is defined collectively by the median spectral acceleration of the record set, $S_T$, rather than by different intensities for each record. Record set intensity, $S_T$, is the parameter used to define record set intensity when the record set is scaled to a particular level of ground motions (e.g., MCE spectral acceleration). The median value of collapse spectral acceleration, $\hat{S}_{CT}$, is the value of $S_T$ when the record set is scaled such that one-half of the records affect collapse.

To ensure broad representation of different recorded earthquakes, sets of ground motions contain records selected from all large-magnitude events in the PEER-NGA database (PEER, 2006). The PEER-NGA database is described in Section A.6. A sufficient number of the strongest ground motion records are selected from each event to permit statistical evaluation of record-to-record variability.

Record selection does not distinguish ground motion records based on either site condition or source mechanism. However, distance to fault rupture is used to develop separate Far-Field and Near-Field record sets (for examination of potential differences in collapse fragility due to near-source directivity and pulse effects).

## A.4 Spectral Shape Consideration

Spectral shape (i.e., frequency content of ground motions) can significantly influence the calculation of collapse fragility and the collapse margin ratio of "ductile" structures. Baker and Cornell (2006) have shown that rare ground motions in the Western United States, such as those corresponding to the MCE, have a distinctive spectral shape that, for a given fundamental-period spectral acceleration, causes the record to be less damaging than other records of less intensity.

In essence, the shape of the spectrum of rare ground motions drops off more rapidly at periods both greater and less than the fundamental period of interest (i.e., has less energy), as compared to spectra of other (less rare) records. The amount by which spectral shape can influence the collapse ratio

is a function of the "rareness" of the ground motions. For ductile structures located in coastal California, accounting for this spectral shape effect can cause a 40% to 60% increase in the collapse margin ratio (i.e. median collapse capacity).

The ground motion record sets do not (could not) directly incorporate the effect of spectral shape. Direct incorporation of spectral shape would necessarily require records to be selected based on the fundamental period of the structure, resulting in a different set of records for each structure of differing period. Rather, collapse margin ratios calculated using the ground motion record sets are adjusted for spectral shape effects based on structure deformation capacity and seismic design category, described in Section 7.4, using factors developed in Appendix B.

## A.5 MCE and DE Demand (*ASCE/SEI 7-05*)

The seismic provisions of ASCE/SEI 7-05 specify ground motions and design requirements in terms of the structure's Seismic Design Category (SDC), which is a function of the level of design earthquake (DE) ground motions and the Occupancy Category of the structure. The Methodology is based on life safety and assumes all structures to be either Occupancy Category I or II (i.e., structures that do not have special functionality requirements). Seismic Design Categories for Occupancy I and II structures vary from SDC A in regions of very low seismicity (which is of least interest) to SDC E in regions of highest seismicity near active faults.

The seismic provisions of ASCE/SEI 7-05 define MCE demand in terms of mapped values of short-period spectral acceleration, $S_S$, and 1-second spectral acceleration, $S_1$, site coefficients, $F_a$ and $F_v$, and a standard response spectrum shape. For seismic design of the structural system, ASCE/SEI 7-05 defines the DE demand as two-thirds of the MCE demand. Archetypical systems are designed for DE ground motions and evaluated for collapse using the corresponding set of MCE ground motions.

Mapped values of spectral acceleration vary greatly by seismic region. The Methodology defines MCE and DE ground motions by the range of spectral accelerations associated with SDC's B, C and D, respectively. For each SDC, Maximum and Minimum ground motions are based on the respective upper-bound and lower-bound values of DE spectral acceleration, as given in Table 11.6-1 of ASCE/SEI 7-05, for short-period response, and in Table 11.6-2 of ASCE/SEI 7-05, for 1-second response. MCE spectral accelerations are derived from DE spectral accelerations for site coefficients

corresponding to Site Class D (stiff soil) following the requirements of Section 11.4 of ASCE/SEI 7-05.

Tables A-1A and A-1B list values of spectral acceleration, site coefficients and design parameters for Maximum and Minimum ground motions of SDC B, C and D, respectively. Figure A-1 shows MCE response spectra for these ground motions.

**Table A-1A Summary of Mapped Values of Short-Period Spectral Acceleration, Site Coefficients and Design Parameters Used for Collapse Evaluation of Seismic Design Category D, C and B Structure Archetypes, Respectively**

| Seismic Design Category | | Maximum Considered Earthquake | | | Design |
|---|---|---|---|---|---|
| Maximum | Minimum | $S_S$ (g) | $F_a$ | $S_{MS}$ (g) | $S_{DS}$ (g) |
| D | | 1.5 | 1.0 | 1.5 | 1.0 |
| C | D | 0.55 | 1.36 | 0.75 | 0.50 |
| B | C | 0.33 | 1.53 | 0.50 | 0.33 |
| | B | 0.156 | 1.6 | 0.25 | 0.167 |

**Table A-1B Summary of Mapped Values of 1-Second Spectral Acceleration, Site Coefficients and Design Parameters Used for Collapse Evaluation of Seismic Design Category D, C and B Structure Archetypes, Respectively**

| Seismic Design Category | | Maximum Considered Earthquake | | | Design |
|---|---|---|---|---|---|
| Maximum | Minimum | $S_1$ (g) | $F_v$ | $S_{M1}$ (g) | $S_{D1}$ (g) |
| D | | 0.60 | 1.50 | 0.90 | 0.60 |
| C | D | 0.132 | 2.28 | 0.30 | 0.20 |
| B | C | 0.083 | 2.4 | 0.20 | 0.133 |
| | B | 0.042 | 2.4 | 0.10 | 0.067 |

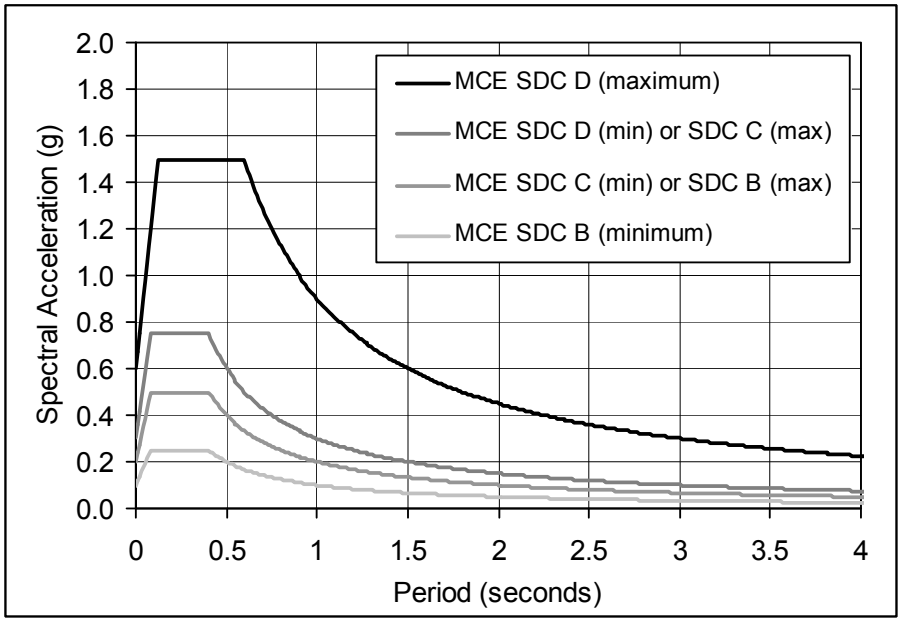


Figure A-1 Plots of MCE response spectral accelerations used for collapse evaluation of Seismic Design Category D, C and B structure archetypes, respectively.

Note. Maximum ground motions for SDC D ($S_s$ = 1.5 g and $S_1$ = 0.60 g) are based on the effective boundary between deterministic (near-source) MCE ground motions and probabilistic MCE ground motions, as defined in Section 21.2 of ASCE/SEI 7-05.

The seismic response coefficient, $C_s$, used for design of the structure archetypes, is based on the fundamental period, $T$, computed using equation A-1. $T$ is the code-defined period, and not the period computed using eigenvalue analysis of the structural model.

$$T = C_u T_a = C_u C_t h_n^x \geq 0.25 \; seconds \qquad \text{(A-1)}$$

where $h_n$ is the height, in feet, of the building above the base to the highest level of the structure, and values of the coefficient, $C_u$, are given in Table 12.8-1 and values of period parameters, $C_t$ and $x$, are given in Table 12.8-2 of ASCE/SEI 7-05.

Period parameters, $C_t$ and $x$ are a function of structure type, distinguishing between steel moment-resisting frames, concrete moment-resisting frames, eccentrically braced steel frames and all other (stiff) structural systems. Example values of the fundamental period, $T$, and corresponding MCE spectral acceleration, $S_{MT}$, are given in Table A-2 for concrete moment resisting frame structures of various heights, ranging from 1-story to 20

stories. Table A-2 lists example values of the fundamental period and MCE spectral acceleration corresponding to Maximum and Minimum seismic criteria of Seismic Design Categories B, C and D, respectively.

**Table A-2 Example Values of the Fundamental Period, *T*, and Corresponding MCE Spectral Acceleration, $S_{MT}$, for Concrete Moment-Resisting Frame Structures of Various Heights**

| System Properties | | Seismic Design Category (SDC) Max and Min Seismic Criteria | | | | | | | |
|---|---|---|---|---|---|---|---|---|---|
| | | SDC Dmax | | SDC Cmax | | SDC Bmax | | | |
| | | | | SDC Dmin | | SDC Cmin | | SDC Bmin | |
| No. of Stories | Height (feet) | *T* (sec) | $S_{MT}$ (g) | *T* (sec) | $S_{MT}$ (g) | *T* (sec) | $S_{MT}$ (g) | *T* (sec) | $S_{MT}$ (g) |
| 1 | 15 | 0.26 | 1.50 | 0.27 | 0.75 | 0.30 | 0.50 | 0.31 | 0.25 |
| 2 | 28 | 0.45 | 1.50 | 0.48 | 0.62 | 0.52 | 0.38 | 0.55 | 0.183 |
| 4 | 54 | 0.81 | 1.11 | 0.87 | 0.34 | 0.95 | 0.21 | 0.99 | 0.101 |
| 8 | 106 | 1.49 | 0.60 | 1.60 | 0.188 | 1.74 | 0.115 | 1.81 | 0.055 |
| 12 | 158 | 2.13 | 0.42 | 2.29 | 0.131 | 2.49 | 0.080 | 2.59 | 0.039 |
| 20 | 262 | 3.36 | 0.27 | 3.60 | 0.083 | 3.92 | 0.051 | 4.08 | 0.024 |

Section A.8 discusses scaling of record sets and provides factors for scaling the Far Field record set to match MCE spectral acceleration, $S_{MT}$, for Seismic Design Categories B, C and D, respectively.

## A.6 PEER-NGA Database

The PEER-NGA database is an extension of the earlier PEER Strong Motion Database that was first made publicly available in 1999. The PEER-NGA database is composed of over 3,550 ground motion recordings that represent over 160 seismic events (including aftershock events) ranging in magnitude from M4.2 to M7.9.

Each ground motion recording includes two horizontal components of acceleration; the vertical acceleration component is also available for many records. In addition, the rotated fault-normal and fault-parallel motions components are also available. This database contains records from a wide range of domestic and international sources including the United States Geological Survey, the California Division of Mines and Geology, the Central Weather Bureau, the Earthquake Research Department of Turkey, and many others.

This database was chosen for use in this study for several reasons, including the large number of ground motion records, and the availability of fault-normal and fault-parallel components of ground motion.

## A.7 Record Selection Criteria

This section describes record selection criteria developed to meet Methodology objectives. Each criterion is listed, followed by a brief discussion of the intent of the rule.

- **Source Magnitude – M ≥ 6.5.** Large-magnitude events pose the greatest risk of building collapse due to inherently longer durations of strong shaking and larger amounts of energy released. Ground motions of smaller magnitude (M < 6.5) events can cause building damage (typically of a nonstructural nature), but are not likely to collapse new structures. Even when small magnitude events generate strong ground motions, the duration of strong shaking is relatively short and the affected area is relatively small. In contrast, large-magnitude events can generate strong, long duration, ground motions over a large region, affecting a much larger population of buildings.
- **Source Type – Strike-slip and Reverse (Thrust) Sources.** Record sets include ground motions from earthquakes with either strike-slip or reverse (thrust) sources. These sources are typical of shallow crustal earthquakes in California and other Western United States locations. Few strong-motion records are available from other source mechanisms.
- **Site Conditions – Soft Rock and Stiff Soil Sites.** Record sets include ground motions recorded on either soft rock (Site Class C) or stiff soil (Site Class D) sites. Records on soft soil (Site Class E) or sites susceptible to ground failure (Site Class F) are not used. Relatively few strong-motion records are available for Site Class B (rock) sites.
- **Site-Source Distance – Far-Field records, Greater than 10 km (Near-Field records, Less than or equal to 10 km).** The 10 km source-to-site distance boundary between Near-Field and Far-Field records is arbitrary, but generally consistent with the "near fault" region of MCE design values maps in ASCE/SEI 7-05. Several different measures of this distance are available. For this project, the source-to-site distance was taken as the average of Campbell and Joyner-Boore fault distances provided in the PEER-NGA database.
- **Number of Records per Event – Not more than Two for a Record Set.** Strong-motion instruments are not evenly distributed across seismically active regions. Some large-magnitude events have generated

many records, while others have produced only a few, due to the number of instruments in place at the time of the earthquake. To avoid potential event-based bias in record sets, not more than two records are taken from any one earthquake (for a record set). The two-record limit was applied separately to the Near-Field "Pulse" and "No Pulse" record sets, respectively. When more than two records of an event pass the other selection criteria, the two records with highest peak ground velocity are selected.

- **Strongest Ground Motion Records –** Peak ground acceleration (PGA) greater than 0.2 g and peak ground velocity (PGV) greater than 15 cm/sec. The limits on PGA and PGV are arbitrary, but generally represent the threshold of structural damage (for new buildings) and capture a large enough sample of the strongest ground motions (recorded to date) to permit calculation of record-to-record variability.
- **Strong-Motion Instrument Capability – Valid Frequency Content to at Least 4-Seconds.** Some strong-motion instruments, particularly older models, have inherent limitations on their ability to record long-period vibration accurately. Most records have a valid frequency content of at least 8 seconds, but some records do not, and records not valid to at least 4 seconds are excluded from the record sets. The record sets are considered valid for collapse evaluation of tall buildings with elastic fundamental periods up to about 4 seconds.
- **Strong-Motion Instrument Location – Free-Field Location (or Ground Floor of a Small Building).** Strong-motion instruments are sometimes located in buildings (e.g., ground floor or basement) that, if large, can influence recorded motion due to soil-structure-foundation interaction.

## A.8 Scaling Method

Scaling of ground motion records is an unfortunate, but necessary, element of nonlinear dynamic analysis, since few, if any, available unscaled records are strong enough to collapse modern buildings. The scaling process of the Methodology involves two elements:

1. Normalization of Records. Ground motion records are normalized by peak ground velocity (PGV) to remove unwarranted record-to-record variability. Normalization is an inherent feature of record sets described in this appendix. Users of the Methodology need only scale the record set as required for collapse evaluation.

2. Scaling of Record Sets. For collapse evaluation, the set of (normalized) records is collectively increased (or decreased) in strength (e.g., algebraic scaling of each record by the same factor) as required to determine median collapse (i.e., the record set is scaled such that 50 percent of the records cause collapse of archetype analysis model of interest).

**Normalization of Records:** Individual records (of a given set) are "normalized" by their respective peak ground velocities. In essence, some records are factored upwards (and some factored downwards), while maintaining the same overall ground motion strength of the record set. Normalization by peak ground velocity is a simple way to remove unwarranted variability between records due to inherent differences in event magnitude, distance to source, source type and site conditions, while still maintaining the inherent aleatory (i.e., record-to-record) variability necessary for accurately predicting collapse fragility.

The normalization is done with respect to the value of peak ground velocity computed in the PEER-NGA database ($PGV_{PEER}$), which is the geometric mean of PGV of the two horizontal components considering different record orientations. The geometric mean (or geomean) is the square root of the product of the two horizontal components and is a common parameter used to characterize ground motions.

The following formulas define the normalization factor, $NM_i$, and calculation of normalized horizontal components of the $i^{th}$ record, respectively:

$$NM_i = \text{Median}(PGV_{PEER,i})/PGV_{PEER,i} \tag{A-2}$$

$$\begin{aligned} NTH_{1,i} &= NM_i \times TH_{1,i} \\ NTH_{2,i} &= NM_i \times TH_{2,i} \end{aligned} \tag{A-3}$$

where:

$NM_i$ = Normalization factor of both horizontal components of the $i^{th}$ record (of the set of interest)

$PGV_{PEER,i}$ = Peak ground velocity of the $i^{th}$ record (PEER database)

$Median\ (PGV_{PEER,i})$ = Median of $PGV_{PEER,i}$ values of records in the set

$NTH_{1,i}$ = Normalized $i^{th}$ record, horizontal component 1

$NTH_{2,i}$ = Normalized $i^{th}$ record, horizontal component 2

$TH_{1,i}$ = Record $i$, horizontal component 1 (PEER database)

$TH_{2,i}$ = Record $i$, horizontal component 2 (PEER database).

Records and their corresponding values of $PGV_{PEER}$ are taken directly from the PEER-NGA database. For the Near-Field records, the components rotated to the fault normal (FN) and fault parallel (FP) directions are utilized. Horizontal components of Far-Field records are not rotated based on the orientation with respect to the fault (i.e., as-recorded orientation is used). Horizontal components of each record are normalized by the same factor ($NM_i$) to maintain the relative, as-recorded, strength of the two components (which can be important for analysis of three-dimensional archetype models).

Table A-3 provides median values of 5%-damped spectral acceleration, $\hat{S}_{NRT}$, of normalized Far-Field and Near-Field record sets, respectively. The Far-Field record set is described in Section A.9 and the Near-Field record set is described in Section A.10, and Tables A-4D and A-6D summarize normalization factors for each record of the Far-Field and Near-Field ground motion sets, respectively.

**Scaling of Record Sets.** For collapse evaluation, the Methodology requires the set of normalized ground motion records to be collectively scaled upward (or downward) to the point that causes 50 percent of the ground motions to collapse the archetype analysis model being evaluated. This approach is used to determine the median collapse capacity, $\hat{S}_{CT}$, of the model. Once this has been established, the Methodology requires that the collapse margin ratio, *CMR*, be computed between median collapse capacity, $\hat{S}_{CT}$, and MCE demand, $S_{MT}$.

In the same manner, record sets can be scaled to a specific level of ground motions (e.g., MCE spectral acceleration). Record normalization and record set scaling to match a particular level of ground motions parallels the ground motion scaling requirements of Section 16.1.3.2 of ASCE/SEI 7-05, with the notable exception that the median value of the scaled record set need only match the MCE demand at the fundamental period, *T*, rather than over the range of periods required by ASCE/SEI 7-05.

Table A-3 provides scaling factors for anchoring the normalized Far-Field record set to the MCE demand level of interest. Scaling factors (for anchoring the normalized Far-Field record set to MCE demand) depend on the fundamental period of the building (*T*), which is shown in the left column of the table. Figure A-2 illustrates the median spectrum of the normalized Far-Field record set anchored to various levels of MCE demand at a period of 1 second.

**Table A-3 Median 5%-Damped Spectral Acceleration of Normalized Far-Field and Near-Field Record Sets and Scaling Factors for Anchoring the Normalized Far-Field Record Set to MCE Spectral Demand[1].**

| Period $T = C_u T_a$ (seconds) | Median Value of Normalized Record Set, $S_{NRT}$ (g) | | Scaling Factors for Anchroing Far-Field Record Set to MCE Spectral Demand | | | |
|---|---|---|---|---|---|---|
| | Near-Field Set | Far-Field Set | Dmax | Cmax | Bmax | |
| | | | | Dmin | Cmin | Bmin |
| 0.25 | 0.936 | 0.779 | 1.93 | 0.96 | 0.64 | 0.32 |
| 0.3 | 1.020 | 0.775 | 1.94 | 0.97 | 0.65 | 0.32 |
| 0.35 | 0.939 | 0.761 | 1.97 | 0.99 | 0.66 | 0.33 |
| 0.4 | 0.901 | 0.748 | 2.00 | 1.00 | 0.67 | 0.33 |
| 0.45 | 0.886 | 0.749 | 2.00 | 0.89 | 0.59 | 0.30 |
| 0.5 | 0.855 | 0.736 | 2.04 | 0.82 | 0.54 | 0.27 |
| 0.6 | 0.833 | 0.602 | 2.49 | 0.83 | 0.55 | 0.28 |
| 0.7 | 0.805 | 0.537 | 2.40 | 0.80 | 0.53 | 0.27 |
| 0.8 | 0.739 | 0.449 | 2.50 | 0.83 | 0.56 | 0.28 |
| 0.9 | 0.633 | 0.399 | 2.50 | 0.83 | 0.56 | 0.28 |
| 1.0 | 0.571 | 0.348 | 2.59 | 0.86 | 0.58 | 0.29 |
| 1.2 | 0.476 | 0.301 | 2.49 | 0.83 | 0.55 | 0.28 |
| 1.4 | 0.404 | 0.256 | 2.51 | 0.84 | 0.56 | 0.28 |
| 1.6 | 0.356 | 0.208 | 2.70 | 0.90 | 0.60 | 0.30 |
| 1.8 | 0.319 | 0.168 | 2.98 | 0.99 | 0.66 | 0.33 |
| 2.0 | 0.284 | 0.148 | 3.05 | 1.02 | 0.68 | 0.34 |
| 2.2 | 0.258 | 0.133 | 3.08 | 1.03 | 0.68 | 0.34 |
| 2.4 | 0.230 | 0.118 | 3.18 | 1.06 | 0.71 | 0.35 |
| 2.6 | 0.210 | 0.106 | 3.28 | 1.09 | 0.73 | 0.36 |
| 2.8 | 0.190 | 0.091 | 3.53 | 1.18 | 0.79 | 0.39 |
| 3.0 | 0.172 | 0.080 | 3.75 | 1.25 | 0.83 | 0.42 |
| 3.5 | 0.132 | 0.063 | 4.10 | 1.37 | 0.91 | 0.46 |
| 4.0 | 0.104 | 0.052 | 4.29 | 1.43 | 0.95 | 0.48 |
| 4.5 | 0.086 | 0.046 | 4.34 | 1.45 | 0.96 | 0.48 |
| 5.0 | 0.072 | 0.041 | 4.43 | 1.48 | 0.98 | 0.49 |

1. Spectral acceleration values and scaling factors may be based on linear interpolation for periods not listed in the table.

In Figure A-2, the median spectrum of the normalized Far-Field record set is factored by 2.59 to match the Maximum MCE spectral acceleration of SDC D (Dmax) at a period of 1 second, and factored by 0.86 to match the

Minimum MCE spectral acceleration of SDC D (Dmin) at a period of 1 second. The figure shows that the median spectrum of the Far-Field record set tends to match MCE spectral acceleration at periods near the "anchor" period, but can substantially deviate from MCE spectra at other periods. Such deviations are unavoidable due to the approximate shape of code-defined spectra.

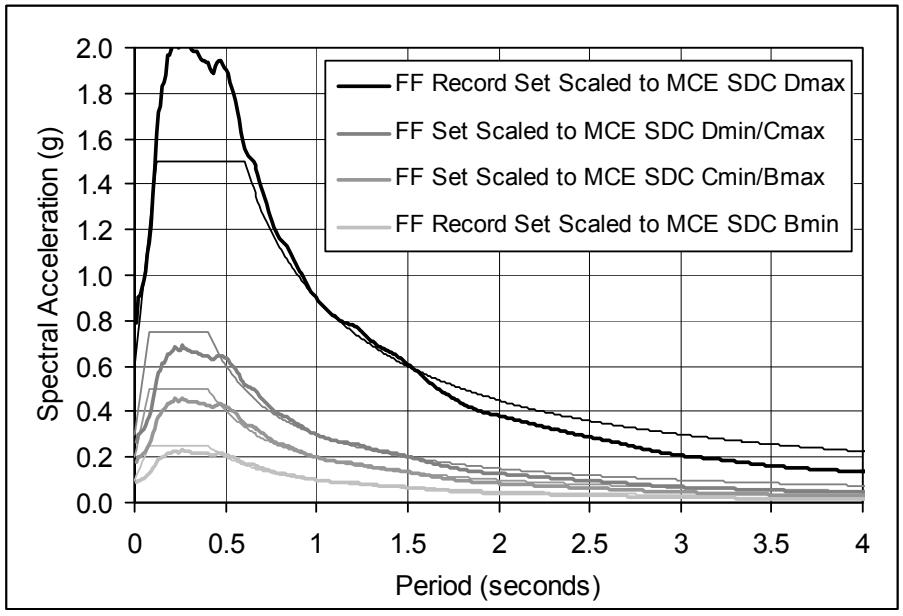


Figure A-2 Example anchoring of median spectrum of the Far-Field record set to MCE spectral acceleration at 1 second for Maximum and Minimum seismic criteria of Seismic Design Categories B, C and D ,respectively.

## A.9 Far-Field Record Set

The Far-Field record set includes twenty-two records (44 individual components) selected from the PEER-NGA database using the criteria from Section A.7 of this appendix.

For each record, Table A-4A summarizes the magnitude, year, and name of the event, as well as the name and owner of the station. The twenty-two records are taken from 14 events that occurred between 1971 and 1999. Of the 14 events, eight were United States (California) earthquakes and six were from five different foreign countries. Event magnitudes range from M6.5 to M7.6 with an average magnitude of M7.0 for the Far-Field record set.

**Table A-4A Summary of Earthquake Event and Recording Station Data for the Far-Field Record Set**

| ID No. | Earthquake | | | Recording Station | |
|---|---|---|---|---|---|
| | M | Year | Name | Name | Owner |
| 1 | 6.7 | 1994 | Northridge | Beverly Hills - Mulhol | USC |
| 2 | 6.7 | 1994 | Northridge | Canyon Country-WLC | USC |
| 3 | 7.1 | 1999 | Duzce, Turkey | Bolu | ERD |
| 4 | 7.1 | 1999 | Hector Mine | Hector | SCSN |
| 5 | 6.5 | 1979 | Imperial Valley | Delta | UNAMUCSD |
| 6 | 6.5 | 1979 | Imperial Valley | El Centro Array #11 | USGS |
| 7 | 6.9 | 1995 | Kobe, Japan | Nishi-Akashi | CUE |
| 8 | 6.9 | 1995 | Kobe, Japan | Shin-Osaka | CUE |
| 9 | 7.5 | 1999 | Kocaeli, Turkey | Duzce | ERD |
| 10 | 7.5 | 1999 | Kocaeli, Turkey | Arcelik | KOERI |
| 11 | 7.3 | 1992 | Landers | Yermo Fire Station | CDMG |
| 12 | 7.3 | 1992 | Landers | Coolwater | SCE |
| 13 | 6.9 | 1989 | Loma Prieta | Capitola | CDMG |
| 14 | 6.9 | 1989 | Loma Prieta | Gilroy Array #3 | CDMG |
| 15 | 7.4 | 1990 | Manjil, Iran | Abbar | BHRC |
| 16 | 6.5 | 1987 | Superstition Hills | El Centro Imp. Co. | CDMG |
| 17 | 6.5 | 1987 | Superstition Hills | Poe Road (temp) | USGS |
| 18 | 7.0 | 1992 | Cape Mendocino | Rio Dell Overpass | CDMG |
| 19 | 7.6 | 1999 | Chi-Chi, Taiwan | CHY101 | CWB |
| 20 | 7.6 | 1999 | Chi-Chi, Taiwan | TCU045 | CWB |
| 21 | 6.6 | 1971 | San Fernando | LA - Hollywood Stor | CDMG |
| 22 | 6.5 | 1976 | Friuli, Italy | Tolmezzo | -- |

For each record, Table A-4B summarizes site and source characteristics, epicentral distances, and various other measures of site-source distance. Site characteristics include shear wave velocity (e.g., in the upper 30 meters of soil) and the corresponding *NEHRP* Site Class. Sixteen sites are classified as Site Class D (stiff soil sites) and the remaining six are classified as Site Class C (very stiff soil sites). Fifteen records are from events of predominantly strike-slip faulting and the remaining seven records are from events of predominantly thrust (or reverse) faulting.

Site-source distances are given for the closest distance to fault rupture, Campbell R distance, and Joyner-Boore horizontal distance to the surface projection of the rupture. Based on the average of Campbell and Boore-Joyner fault distances, the minimum site-source distance is 11.1 km, the maximum distance is 26.4 km and the average distance is 16.4 km for the Far-Field record set.

**Table A-4B Summary of Site and Source Data for the Far-Field Record Set**

| ID No. | Site Data | | Source (Fault Type) | Site-Source Distance (km) | | | |
|---|---|---|---|---|---|---|---|
| | NEHRP Class | Vs_30 (m/sec) | | Epicentral | Closest to Plane | Campbell | Joyner-Boore |
| 1 | D | 356 | Thrust | 13.3 | 17.2 | 17.2 | 9.4 |
| 2 | D | 309 | Thrust | 26.5 | 12.4 | 12.4 | 11.4 |
| 3 | D | 326 | Strike-slip | 41.3 | 12 | 12.4 | 12 |
| 4 | C | 685 | Strike-slip | 26.5 | 11.7 | 12 | 10.4 |
| 5 | D | 275 | Strike-slip | 33.7 | 22 | 22.5 | 22 |
| 6 | D | 196 | Strike-slip | 29.4 | 12.5 | 13.5 | 12.5 |
| 7 | C | 609 | Strike-slip | 8.7 | 7.1 | 25.2 | 7.1 |
| 8 | D | 256 | Strike-slip | 46 | 19.2 | 28.5 | 19.1 |
| 9 | D | 276 | Strike-slip | 98.2 | 15.4 | 15.4 | 13.6 |
| 10 | C | 523 | Strike-slip | 53.7 | 13.5 | 13.5 | 10.6 |
| 11 | D | 354 | Strike-slip | 86 | 23.6 | 23.8 | 23.6 |
| 12 | D | 271 | Strike-slip | 82.1 | 19.7 | 20 | 19.7 |
| 13 | D | 289 | Strike-slip | 9.8 | 15.2 | 35.5 | 8.7 |
| 14 | D | 350 | Strike-slip | 31.4 | 12.8 | 12.8 | 12.2 |
| 15 | C | 724 | Strike-slip | 40.4 | 12.6 | 13 | 12.6 |
| 16 | D | 192 | Strike-slip | 35.8 | 18.2 | 18.5 | 18.2 |
| 17 | D | 208 | Strike-slip | 11.2 | 11.2 | 11.7 | 11.2 |
| 18 | D | 312 | Thrust | 22.7 | 14.3 | 14.3 | 7.9 |
| 19 | D | 259 | Thrust | 32 | 10 | 15.5 | 10 |
| 20 | C | 705 | Thrust | 77.5 | 26 | 26.8 | 26 |
| 21 | D | 316 | Thrust | 39.5 | 22.8 | 25.9 | 22.8 |
| 22 | C | 425 | Thrust | 20.2 | 15.8 | 15.8 | 15 |

For each record, Table A-4C summarizes key record information from the PEER-NGA database. This record information includes the record sequence number and file names of the two horizontal components, as well as the lowest frequency (longest period) for which frequency content is considered fully reliable.

Maximum values of as-recorded peak ground acceleration, $PGA_{max}$, and peak ground velocity, $PGV_{max}$, are also given for each record. The term "maximum" implies that the larger value of the two components is reported. Peak ground acceleration values vary from 0.21g to 0.82g with an average $PGA_{max}$ of 0.43g. Peak ground velocity values vary from 19 cm/second to 115 cm/second with an average $PGV_{max}$ of 46 cm/second.

**Table A-4C Summary of PEER-NGA Database Information and Parameters of Recorded Ground Motions for the Far-Field Record Set**

| ID No. | PEER-NGA Record Information | | | | Recorded Motions | |
|---|---|---|---|---|---|---|
| | Record Seq. No. | Lowest Freq (Hz.) | File Names - Horizontal Records | | $PGA_{max}$ (g) | $PGV_{max}$ (cm/s.) |
| | | | Component 1 | Component 2 | | |
| 1 | 953 | 0.25 | NORTHR/MUL009 | NORTHR/MUL279 | 0.52 | 63 |
| 2 | 960 | 0.13 | NORTHR/LOS000 | NORTHR/LOS270 | 0.48 | 45 |
| 3 | 1602 | 0.06 | DUZCE/BOL000 | DUZCE/BOL090 | 0.82 | 62 |
| 4 | 1787 | 0.04 | HECTOR/HEC000 | HECTOR/HEC090 | 0.34 | 42 |
| 5 | 169 | 0.06 | IMPVALL/H-DLT262 | IMPVALL/H-DLT352 | 0.35 | 33 |
| 6 | 174 | 0.25 | IMPVALL/H-E11140 | IMPVALL/H-E11230 | 0.38 | 42 |
| 7 | 1111 | 0.13 | KOBE/NIS000 | KOBE/NIS090 | 0.51 | 37 |
| 8 | 1116 | 0.13 | KOBE/SHI000 | KOBE/SHI090 | 0.24 | 38 |
| 9 | 1158 | 0.24 | KOCAELI/DZC180 | KOCAELI/DZC270 | 0.36 | 59 |
| 10 | 1148 | 0.09 | KOCAELI/ARC000 | KOCAELI/ARC090 | 0.22 | 40 |
| 11 | 900 | 0.07 | LANDERS/YER270 | LANDERS/YER360 | 0.24 | 52 |
| 12 | 848 | 0.13 | LANDERS/CLW-LN | LANDERS/CLW-TR | 0.42 | 42 |
| 13 | 752 | 0.13 | LOMAP/CAP000 | LOMAP/CAP090 | 0.53 | 35 |
| 14 | 767 | 0.13 | LOMAP/G03000 | LOMAP/G03090 | 0.56 | 45 |
| 15 | 1633 | 0.13 | MANJIL/ABBAR--L | MANJIL/ABBAR--T | 0.51 | 54 |
| 16 | 721 | 0.13 | SUPERST/B-ICC000 | SUPERST/B-ICC090 | 0.36 | 46 |
| 17 | 725 | 0.25 | SUPERST/B-POE270 | SUPERST/B-POE360 | 0.45 | 36 |
| 18 | 829 | 0.07 | CAPEMEND/RIO270 | CAPEMEND/RIO360 | 0.55 | 44 |
| 19 | 1244 | 0.05 | CHICHI/CHY101-E | CHICHI/CHY101-N | 0.44 | 115 |
| 20 | 1485 | 0.05 | CHICHI/TCU045-E | CHICHI/TCU045-N | 0.51 | 39 |
| 21 | 68 | 0.25 | SFERN/PEL090 | SFERN/PEL180 | 0.21 | 19 |
| 22 | 125 | 0.13 | FRIULI/A-TMZ000 | FRIULI/A-TMZ270 | 0.35 | 31 |

For each record, Table A-4D summarizes the 1-second spectral acceleration (both horizontal components), peak ground velocity reported in the PEER database, $PGV_{PEER}$ (i.e., single value of peak ground velocity based on the geometric mean of rotated components), normalization factors ($NM_i$), and values of $PGA_{max}$ and $PGV_{max}$ after normalization by $PGV_{PEER}$.

Normalization factors vary from 0.41 to 2.10. After normalization, peak ground acceleration values vary from 0.18g to 0.58g with an average $PGA_{max}$ of 0.40g. Peak ground velocity values vary from 36 cm/second to 54 cm/second with an average $PGV_{max}$ of 42 cm/second. Table A-5 shows that normalization of the records (by $PGV_{PEER}$) has reduced the dispersion in $PGV_{max}$ to a level consistent with that of $PGA_{max}$ without appreciably affecting average values of $PGA_{max}$ or $PGV_{max}$ for the record set.

**Table A-4D Summary of Factors Used to Normalize Recorded Ground Motions, and Parameters of Normalized Ground Motions for the Far-Field Record Set**

| ID No. | As-Recorded Parameters | | | Normaliz. Factor | Normalized Motions | |
|---|---|---|---|---|---|---|
| | 1-Sec. Spec. Acc. (g) | | $PGV_{PEER}$ (cm/s.) | | $PGA_{max}$ (g) | $PGV_{max}$ (cm/s.) |
| | Comp. 1 | Comp. 2 | | | | |
| 1 | 1.02 | 0.94 | 57.2 | 0.65 | 0.34 | 41 |
| 2 | 0.38 | 0.63 | 44.8 | 0.83 | 0.40 | 38 |
| 3 | 0.72 | 1.16 | 59.2 | 0.63 | 0.52 | 39 |
| 4 | 0.35 | 0.37 | 34.1 | 1.09 | 0.37 | 46 |
| 5 | 0.26 | 0.48 | 28.4 | 1.31 | 0.46 | 43 |
| 6 | 0.24 | 0.23 | 36.7 | 1.01 | 0.39 | 43 |
| 7 | 0.31 | 0.29 | 36.0 | 1.03 | 0.53 | 39 |
| 8 | 0.33 | 0.23 | 33.9 | 1.10 | 0.26 | 42 |
| 9 | 0.43 | 0.61 | 54.1 | 0.69 | 0.25 | 41 |
| 10 | 0.11 | 0.11 | 27.4 | 1.36 | 0.30 | 54 |
| 11 | 0.50 | 0.33 | 37.7 | 0.99 | 0.24 | 51 |
| 12 | 0.20 | 0.36 | 32.4 | 1.15 | 0.48 | 49 |
| 13 | 0.46 | 0.28 | 34.2 | 1.09 | 0.58 | 38 |
| 14 | 0.27 | 0.38 | 42.3 | 0.88 | 0.49 | 39 |
| 15 | 0.35 | 0.54 | 47.3 | 0.79 | 0.40 | 43 |
| 16 | 0.31 | 0.25 | 42.8 | 0.87 | 0.31 | 40 |
| 17 | 0.33 | 0.34 | 31.7 | 1.17 | 0.53 | 42 |
| 18 | 0.54 | 0.39 | 45.4 | 0.82 | 0.45 | 36 |
| 19 | 0.49 | 0.95 | 90.7 | 0.41 | 0.18 | 47 |
| 20 | 0.30 | 0.43 | 38.8 | 0.96 | 0.49 | 38 |
| 21 | 0.25 | 0.15 | 17.8 | 2.10 | 0.44 | 40 |
| 22 | 0.25 | 0.30 | 25.9 | 1.44 | 0.50 | 44 |

**Table A-5** **Far-Field Record Set (as-Recorded and After Normalization): Comparison of Maximum, Minimum and Average Values of Peak Ground Acceleration ($PGA_{max}$) and Peak Ground Velocity ($PGV_{max}$), Respectively**

| Parameter Value | PGA (g) | | PGV (cm/sec.) | |
|---|---|---|---|---|
| | As-Recorded | Normalized | As-Recorded | Normalized |
| Maximum | 0.82 | 0.58 | 115 | 54 |
| Minimum | 0.21 | 0.18 | 19 | 36 |
| Max/Min Ratio | 3.9 | 3.2 | 6.1 | 1.5 |
| Average | 0.43 | 0.43 | 46 | 42 |

Figures A-3 (log format) shows response spectra of individual records of the normalized Far-Field record set, as well as the median and one and two standard deviation spectra of the set. Figure A-4 (linear format) shows median and one-standard deviation spectra, as well as a plot of the standard deviation (natural log of spectral acceleration) of the normalized Far-Field record set.

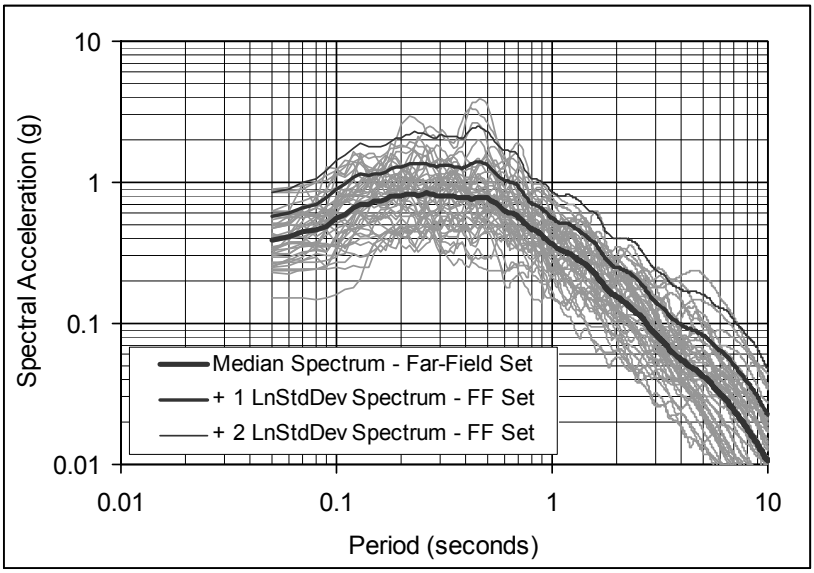


Figure A-3 Plots of response spectra of the forty-four individual components of the normalized Far-Field record set, and median, one and two standard deviation response spectra of the total record set.

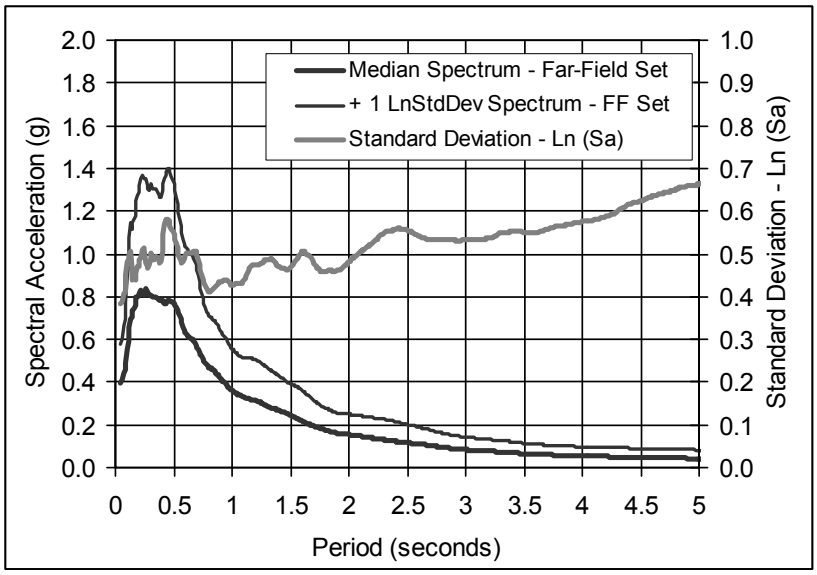


Figure A-4 Plots of median and one standard deviation response spectra of the normalized Far-Field record set, and plot of the standard deviation (natural log) of response spectral acceleration.

The median spectrum of the normalized Far-Field record set has frequency content consistent with that of a large magnitude (M7) event recorded at 15 km from fault rupture. The median spectral acceleration at short periods is about 0.8g and median spectral acceleration at 1-second is about 0.35g. The domain of "constant acceleration" transitions to the domain of "constant velocity" at about 0.5 second, consistent with soft rock and stiff soil site response. Record-to-record variability (standard deviation of the logarithm of spectral acceleration) ranges from about 0.5 at short periods to about 0.6 at long periods, consistent with the values of dispersion from common ground motion (attenuation) relations (e.g., see Figure 8, Campbell and Borzorgnia, 2003).

Recent research has shown that spectral shape is an important aspect of collapse capacity prediction (Baker and Cornell, 2006 and 2005) and that this is related to a parameter called epsilon. Epsilon is defined as the number of standard deviations between the observed spectral value and the median prediction from an attenuation function (so epsilon depends on both the period and the attenuation function used). Figure A-5 is a plot of the median value of epsilon calculated for the forty-four components of the Far-Field record set. These values are based on the attenuation relationship developed by Abrahamson and Silva (1997).

Median values of epsilon are generally small and near zero at all periods beyond 1 second, indicating that the Far-Field record set is approximately "epsilon neutral." Accordingly, collapse margin ratios (*CMR*'s) based on

IDA using these records do not account for the effects of spectral shape, discussed in Section A.4, and are later increased to account for these effects, using the factors described in Section 7.4 and developed in Appendix B.

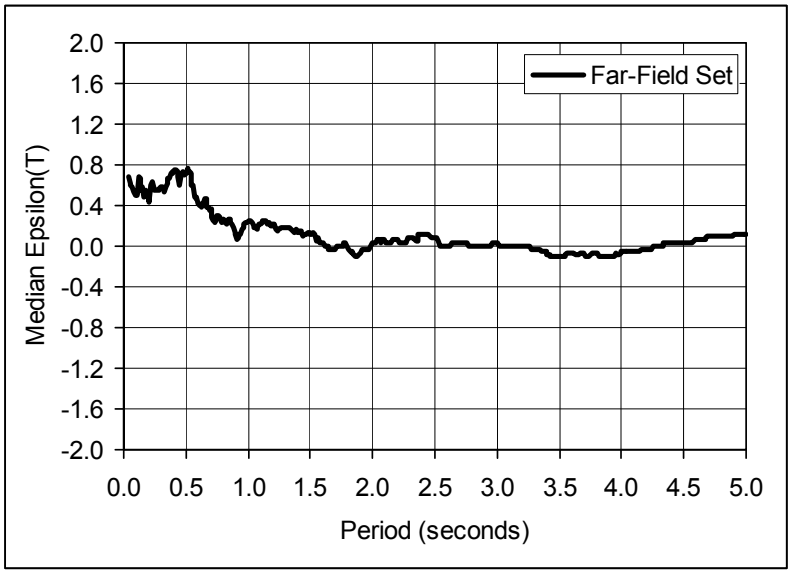


Figure A-5 Plot of median value of epsilon for the Far-Field record set.

## A.10 Near-Field Record Set

The Near-Field record set includes twenty-eight records (56 individual components) selected from the PEER-NGA database using the criteria from Section A.7 of this appendix. Fourteen records have pulses (Pulse subset) and fourteen records do not have pulses (No-Pulse subset), as judged by wavelet analysis classification of the records (Baker, 2007).

For each record, Table A-6A summarizes the magnitude, year and name of earthquake events and the name and owner of the station. The twenty-eight records are taken from 14 events that occurred between 1976 and 2002. Of the 14 events, seven were United States earthquakes (six in California) and seven were from five different foreign countries. Event magnitudes range from M6.5 to M7.9 with an average magnitude of M7.0.

For each record, Table A-6B summarizes site and source characteristics, epicentral distances, and various measures of site-source distance. Site characteristics include shear wave velocity (in the upper 30 meters of soil) and the corresponding NEHRP Site Class. Eleven sites are classified as Site Class D (stiff soil sites), fifteen are classified as Site Class C (very stiff soil sites), and the remaining two are classified as Site Class B (rock sites). Fourteen records are from events of predominantly strike-slip faulting and the remaining fourteen records are from events of predominantly thrust (or

reverse) faulting. Based on the average of Campbell and Boore-Joyner fault distances, the minimum site-source distance is 1.7 km, the maximum distance is 8.8 km, and the average distance is 4.2 km.

For each record, Table A-6C summarizes key record information and "as-recorded" values of peak ground acceleration and peak ground velocity from the PEER-NGA database. PEER-NGA record information includes the record sequence number, the file names of the two horizontal components, and the lowest frequency (longest period) for which frequency content is considered fully reliable.

Maximum values of as-recorded peak ground acceleration, $PGA_{max}$, and peak ground velocity, $PGV_{max}$, are given for each record. The term "maximum" implies the larger peak ground velocity of the two components is reported. Peak ground acceleration values range from 0.22g to 1.43g with an average $PGA_{max}$ of 0.60g. Peak ground velocity values range from 30 cm/second to 167 cm/second with an average $PGV_{max}$ of 84 cm/second.

For each record, Table A-6D summarizes the 1-second spectral acceleration (both horizontal components), peak ground velocity reported in the PEER database, $PGV_{PEER}$ (i.e., single value of peak ground velocity based on the geometric mean of rotated components), normalization factors ($NM_i$), and values of $PGA_{max}$ and $PGV_{max}$ after normalization by $PGV_{PEER}$. In recognition that the two ground motion subsets have different properties, the normalizations are done separately for the Pulse subset and the No-Pulse subset.

**Table A-6A Summary of Earthquake Event and Recording Station Data for the Near-Field Record Set**

| ID No. | Earthquake | | | Recording Station | |
|---|---|---|---|---|---|
| | M | Year | Name | Name | Owner |
| Pulse Records Subset | | | | | |
| 1 | 6.5 | 1979 | Imperial Valley-06 | El Centro Array #6 | CDMG |
| 2 | 6.5 | 1979 | Imperial Valley-06 | El Centro Array #7 | USGS |
| 3 | 6.9 | 1980 | Irpinia, Italy-01 | Sturno | ENEL |
| 4 | 6.5 | 1987 | Superstition Hills-02 | Parachute Test Site | USGS |
| 5 | 6.9 | 1989 | Loma Prieta | Saratoga - Aloha | CDMG |
| 6 | 6.7 | 1992 | Erzican, Turkey | Erzincan | -- |
| 7 | 7.0 | 1992 | Cape Mendocino | Petrolia | CDMG |
| 8 | 7.3 | 1992 | Landers | Lucerne | SCE |
| 9 | 6.7 | 1994 | Northridge-01 | Rinaldi Receiving Sta | DWP |
| 10 | 6.7 | 1994 | Northridge-01 | Sylmar - Olive View | CDMG |
| 11 | 7.5 | 1999 | Kocaeli, Turkey | Izmit | ERD |
| 12 | 7.6 | 1999 | Chi-Chi, Taiwan | TCU065 | CWB |
| 13 | 7.6 | 1999 | Chi-Chi, Taiwan | TCU102 | CWB |
| 14 | 7.1 | 1999 | Duzce, Turkey | Duzce | ERD |
| No Pulse Records Subset | | | | | |
| 15 | 6.8 | 6.8 | Gazli, USSR | Karakyr | -- |
| 16 | 6.5 | 1979 | Imperial Valley-06 | Bonds Corner | USGS |
| 17 | 6.5 | 1979 | Imperial Valley-06 | Chihuahua | UNAMUCSD |
| 18 | 6.8 | 1985 | Nahanni, Canada | Site 1 | -- |
| 19 | 6.8 | 1985 | Nahanni, Canada | Site 2 | -- |
| 20 | 6.9 | 1989 | Loma Prieta | BRAN | UCSC |
| 21 | 6.9 | 1989 | Loma Prieta | Corralitos | CDMG |
| 22 | 7.0 | 1992 | Cape Mendocino | Cape Mendocino | CDMG |
| 23 | 6.7 | 1994 | Northridge-01 | LA - Sepulveda VA | USGS/VA |
| 24 | 6.7 | 1994 | Northridge-01 | Northridge - Saticoy | USC |
| 25 | 7.5 | 1999 | Kocaeli, Turkey | Yarimca | KOERI |
| 26 | 7.6 | 1999 | Chi-Chi, Taiwan | TCU067 | CWB |
| 27 | 7.6 | 1999 | Chi-Chi, Taiwan | TCU084 | CWB |
| 28 | 7.9 | 2002 | Denali, Alaska | TAPS Pump Sta. #10 | CWB |

**Table A-6B Summary of Site and Source Data for the Near-Field Record Set**

| ID No. | Site Data | | Source (Fault Type) | Site-Source Distance (km) | | | |
|---|---|---|---|---|---|---|---|
| | NEHRP Class | Vs_30 (m/sec) | | Epicentral | Closest to Plane | Campbell | Joyner-Boore |
| Pulse Records Subset | | | | | | | |
| 1 | D | 203 | Strike-slip | 27.5 | 1.4 | 3.5 | 0.0 |
| 2 | D | 211 | Strike-slip | 27.6 | 0.6 | 3.6 | 0.6 |
| 3 | B | 1000 | Normal | 30.4 | 10.8 | 10.8 | 6.8 |
| 4 | D | 349 | Strike-slip | 16.0 | 1.0 | 3.5 | 1.0 |
| 5 | C | 371 | Strike-slip | 27.2 | 8.5 | 8.5 | 7.6 |
| 6 | D | 275 | Strike-slip | 9.0 | 4.4 | 4.4 | 0.0 |
| 7 | C | 713 | Thrust | 4.5 | 8.2 | 8.2 | 0.0 |
| 8 | C | 685 | Strike-slip | 44.0 | 2.2 | 3.7 | 2.2 |
| 9 | D | 282 | Thrust | 10.9 | 6.5 | 6.5 | 0.0 |
| 10 | C | 441 | Thrust | 16.8 | 5.3 | 5.3 | 1.7 |
| 11 | B | 811 | Strike-slip | 5.3 | 7.2 | 7.4 | 3.6 |
| 12 | D | 306 | Thrust | 26.7 | 0.6 | 6.7 | 0.6 |
| 13 | C | 714 | Thrust | 45.6 | 1.5 | 7.7 | 1.5 |
| 14 | D | 276 | Strike-slip | 1.6 | 6.6 | 6.6 | 0.0 |
| No Pulse Records Subset | | | | | | | |
| 15 | C | 660 | Thrust | 12.8 | 5.5 | 5.5 | 3.9 |
| 16 | D | 223 | Strike-slip | 6.2 | 2.7 | 4.0 | 0.5 |
| 17 | D | 275 | Strike-slip | 18.9 | 7.3 | 8.4 | 7.3 |
| 18 | C | 660 | Thrust | 6.8 | 9.6 | 9.6 | 2.5 |
| 19 | C | 660 | Thrust | 6.5 | 4.9 | 4.9 | 0.0 |
| 20 | C | 376 | Strike-slip | 9.0 | 10.7 | 10.7 | 3.9 |
| 21 | C | 462 | Strike-slip | 7.2 | 3.9 | 3.9 | 0.2 |
| 22 | C | 514 | Thrust | 10.4 | 7.0 | 7.0 | 0.0 |
| 23 | C | 380 | Thrust | 8.5 | 8.4 | 8.4 | 0.0 |
| 24 | D | 281 | Thrust | 3.4 | 12.1 | 12.1 | 0.0 |
| 25 | D | 297 | Strike-slip | 19.3 | 4.8 | 5.3 | 1.4 |
| 26 | C | 434 | Thrust | 28.7 | 0.6 | 6.5 | 0.6 |
| 27 | C | 553 | Thrust | 8.9 | 11.2 | 11.2 | 0.0 |
| 28 | C | 553 | Strike-slip | 7.0 | 8.9 | 8.9 | 0.0 |

**Table A-6C Summary of PEER-NGA Database Information and Parameters of Recorded Ground Motions for the Near-Field Record Set**

| ID No. | PEER-NGA Record Information | | | | Recorded Motions | |
|---|---|---|---|---|---|---|
| | Record Seq. No. | Lowest Freq (Hz.) | File Names - Horizontal Records | | $PGA_{max}$ (g) | $PGV_{max}$ (cm/s.) |
| | | | FN Component | FP Component | | |
| Pulse Records Subset | | | | | | |
| 1 | 181 | 0.13 | IMPVALL/H-E06_233 | IMPVALL/H-E06_323 | 0.44 | 111.9 |
| 2 | 182 | 0.13 | IMPVALL/H-E07_233 | IMPVALL/H-E07_323 | 0.46 | 108.9 |
| 3 | 292 | 0.16 | ITALY/A-STU_223 | ITALY/A-STU_313 | 0.31 | 45.5 |
| 4 | 723 | 0.15 | SUPERST/B-PTS_037 | SUPERST/B-PTS_127 | 0.42 | 106.8 |
| 5 | 802 | 0.13 | LOMAP/STG_038 | LOMAP/STG_128 | 0.38 | 55.6 |
| 6 | 821 | 0.13 | ERZIKAN/ERZ_032 | ERZIKAN/ERZ_122 | 0.49 | 95.5 |
| 7 | 828 | 0.07 | CAPEMEND/PET_260 | CAPEMEND/PET_350 | 0.63 | 82.1 |
| 8 | 879 | 0.10 | LANDERS/LCN_239 | LANDERS/LCN_329 | 0.79 | 140.3 |
| 9 | 1063 | 0.11 | NORTHR/RRS_032 | NORTHR/RRS_122 | 0.87 | 167.3 |
| 10 | 1086 | 0.12 | NORTHR/SYL_032 | NORTHR/SYL_122 | 0.73 | 122.8 |
| 11 | 1165 | 0.13 | KOCAELI/IZT_180 | KOCAELI/IZT_270 | 0.22 | 29.8 |
| 12 | 1503 | 0.08 | CHICHI/TCU065_272 | CHICHI/TCU065_002 | 0.82 | 127.7 |
| 13 | 1529 | 0.06 | CHICHI/TCU102_278 | CHICHI/TCU102_008 | 0.29 | 106.6 |
| 14 | 1605 | 0.10 | DUZCE/DZC_172 | DUZCE/DZC_262 | 0.52 | 79.3 |
| No Pulse Records Subset | | | | | | |
| 15 | 126 | 0.06 | GAZLI/GAZ_177 | GAZLI/GAZ_267 | 0.71 | 71.2 |
| 16 | 160 | 0.13 | IMPVALL/H-BCR_233 | IMPVALL/H-BCR_323 | 0.76 | 44.3 |
| 17 | 165 | 0.06 | IMPVALL/H-CHI_233 | IMPVALL/H-CHI_323 | 0.28 | 30.5 |
| 18 | 495 | 0.06 | NAHANNI/S1_070 | NAHANNI/S1_160 | 1.18 | 43.9 |
| 19 | 496 | 0.13 | NAHANNI/S2_070 | NAHANNI/S2_160 | 0.45 | 34.7 |
| 20 | 741 | 0.13 | LOMAP/BRN_038 | LOMAP/BRN_128 | 0.64 | 55.9 |
| 21 | 753 | 0.25 | LOMAP/CLS_038 | LOMAP/CLS_128 | 0.51 | 45.5 |
| 22 | 825 | 0.07 | CAPEMEND/CPM_260 | CAPEMEND/CPM_350 | 1.43 | 119.5 |
| 23 | 1004 | 0.12 | NORTHR/0637_032 | NORTHR/0637_122 | 0.73 | 70.1 |
| 24 | 1048 | 0.13 | NORTHR/STC_032 | NORTHR/STC_122 | 0.42 | 53.2 |
| 25 | 1176 | 0.09 | KOCAELI/YPT_180 | KOCAELI/YPT_270 | 0.31 | 73.0 |
| 26 | 1504 | 0.04 | CHICHI/TCU067_285 | CHICHI/TCU067_015 | 0.56 | 91.8 |
| 27 | 1517 | 0.25 | CHICHI/TCU084_271 | CHICHI/TCU084_001 | 1.16 | 115.1 |
| 28 | 2114 | 0.03 | DENALI/ps10_199 | DENALI/ps10_289 | 0.33 | 126.4 |

**Table A-6D Summary of Factors Used to Normalize Recorded Ground Motions, and Parameters of Normalized Ground Motions for the Near-Field record Set**

| ID No. | As-Recorded Parameters | | | Normaliz. Factor | Normalized Motions | |
|---|---|---|---|---|---|---|
| | 1-Sec.Spec. Acc. (g) | | $PGV_{PEER}$ (cm/s.) | | $PGA_{max}$ (g) | $PGV_{max}$ (cm/s.) |
| | FN Comp. | FP Comp. | | | | |
| Pulse Records Subset | | | | | | |
| 1 | 0.43 | 0.60 | 83.9 | 0.90 | 0.40 | 100.1 |
| 2 | 0.66 | 0.64 | 78.3 | 0.96 | 0.44 | 104.4 |
| 3 | 0.25 | 0.41 | 43.7 | 1.72 | 0.53 | 78.2 |
| 4 | 0.97 | 0.51 | 71.9 | 1.04 | 0.44 | 111.6 |
| 5 | 0.47 | 0.32 | 46.1 | 1.63 | 0.62 | 90.6 |
| 6 | 0.98 | 0.37 | 68.8 | 1.09 | 0.53 | 104.2 |
| 7 | 0.92 | 0.70 | 69.6 | 1.08 | 0.68 | 88.6 |
| 8 | 0.43 | 0.34 | 97.2 | 0.77 | 0.62 | 108.4 |
| 9 | 1.96 | 0.47 | 109.3 | 0.69 | 0.59 | 114.9 |
| 10 | 0.89 | 0.65 | 94.4 | 0.80 | 0.58 | 97.7 |
| 11 | 0.29 | 0.28 | 26.9 | 2.79 | 0.62 | 83.2 |
| 12 | 1.33 | 1.10 | 101.6 | 0.74 | 0.60 | 94.4 |
| 13 | 0.60 | 0.58 | 87.5 | 0.86 | 0.25 | 91.5 |
| 14 | 0.54 | 0.73 | 69.6 | 1.08 | 0.56 | 85.6 |
| No Pulse Records Subset | | | | | | |
| 15 | 0.81 | 0.42 | 65.0 | 0.86 | 0.61 | 61.4 |
| 16 | 0.44 | 0.44 | 49.8 | 1.13 | 0.86 | 49.8 |
| 17 | 0.41 | 0.37 | 28.2 | 1.99 | 0.56 | 60.8 |
| 18 | 0.53 | 0.29 | 44.1 | 1.27 | 1.50 | 55.9 |
| 19 | 0.16 | 0.29 | 28.7 | 1.95 | 0.87 | 67.8 |
| 20 | 0.55 | 0.45 | 49.0 | 1.15 | 0.73 | 64.0 |
| 21 | 0.53 | 0.50 | 47.9 | 1.17 | 0.60 | 53.3 |
| 22 | 0.42 | 0.73 | 84.4 | 0.66 | 0.95 | 79.4 |
| 23 | 0.62 | 1.00 | 72.6 | 0.77 | 0.56 | 54.2 |
| 24 | 0.81 | 0.40 | 47.7 | 1.18 | 0.50 | 62.6 |
| 25 | 0.38 | 0.35 | 62.4 | 0.90 | 0.28 | 65.6 |
| 26 | 0.75 | 0.75 | 72.3 | 0.78 | 0.44 | 71.3 |
| 27 | 2.54 | 0.86 | 90.3 | 0.62 | 0.72 | 71.5 |
| 28 | 0.69 | 0.82 | 98.5 | 0.57 | 0.19 | 72.0 |

Normalization factors vary from 0.57 to 2.79. After normalization, peak ground acceleration values range from 0.19g to 1.50g with an average $PGA_{max}$ of 0.60g. Peak ground velocity values range from 50 cm/second to 115 cm/second with an average $PGV_{max}$ of 80 cm/second. Table A-7 shows that normalization of the records (by $PGV_{PEER}$) has substantially reduced the

dispersion in $PGV_{max}$ without greatly affecting average values of $PGA_{max}$ or $PGV_{max}$, or the dispersion in $PGA_{max}$.

**Table A-7 Near-Field Record Set (as-Recorded and After Normalization): Comparison of Maximum, Minimum and Average Values of Peak Ground Acceleration ($PGA_{max}$) and Peak Ground Velocity ($PGV_{max}$), Respectively**

| Parameter Value | PGA (g) | | PGV (cm/sec.) | |
|---|---|---|---|---|
| | As-Recorded | Normalized | As-Recorded | Normalized |
| Maximum | 1.43 | 1.50 | 167 | 115 |
| Minimum | 0.22 | 0.19 | 30 | 50 |
| Max/Min Ratio | 6.5 | 7.9 | 5.6 | 2.3 |
| Average | 0.60 | 0.60 | 84 | 80 |

Figures A-6 (log format) shows response spectra of individual records of the normalized Near-Field record set, as well as the median and one and two standard deviation spectra of the set. Figure A-7 (linear format) shows median and one-standard deviation spectra, as well as a plot of the standard deviation (natural log of spectral acceleration) of the normalized Near-Field record set.

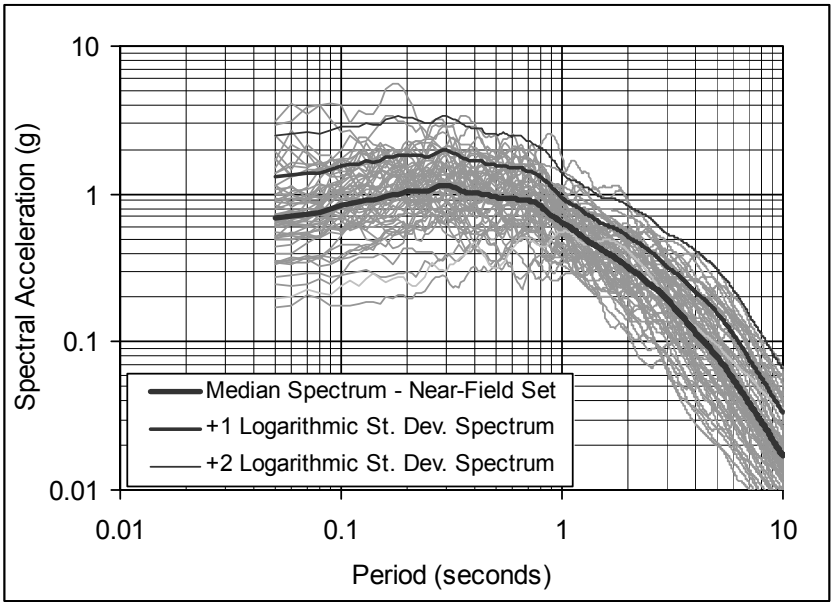


Figure A-6 Plots of response spectra of the fifty-six individual components of the normalized Near-Field record set, and median, one and two standard deviation response spectra of the total record.

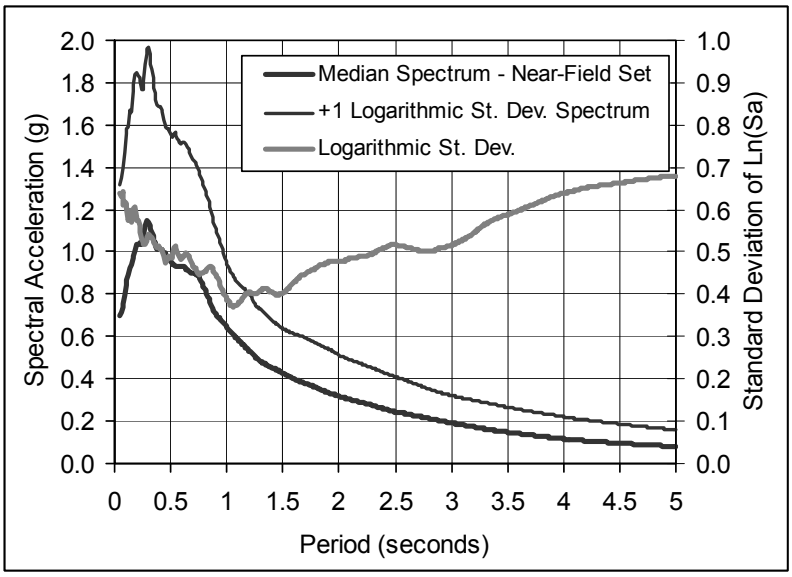


Figure A-7 Plots of median and one standard deviation response spectra of the normalized Near-Field record set, and plot of the standard deviation (natural log) of response spectral acceleration.

The median spectrum of the normalized Near-Field record set has frequency content consistent with a large magnitude (M7) event recorded relatively close (5 km) to the fault rupture. The median spectral acceleration at short periods is about 1.0g and median spectral acceleration at 1-second is about 0.6g. Record-to-record variability (standard deviation of the logarithm of spectral acceleration) ranges from about 0.4-0.5 at short periods to about 0.6 at long periods, generally consistent (except at very short periods) with the values of dispersion from common ground motion (attenuation) relations (e.g., see Figure 8, Campbell and Borzorgnia, 2003).

Figure A-8 is a plot of the median value of epsilon calculated for the fifty-six components of the Near-Field record set. For comparison, Figure A-8 also shows the median value of epsilon calculated for the Far-Field record (from Figure A-5). These values are based on the attenuation relationship developed by Abrahamson and Silva (1997). Median values of epsilon are generally small and near zero at all periods, with mildly positive epsilon values occurring at periods of 2.5 to 4.5 seconds, indicating that the Near-Field record set is approximately "epsilon neutral." Accordingly, collapse margin ratios (*CMR*'s) based on IDA using these records do not account for the effects of spectral shape, discussed in Section A.4, and are later increased to account for these effects, using the factors of Section 7.4 and Appendix B.

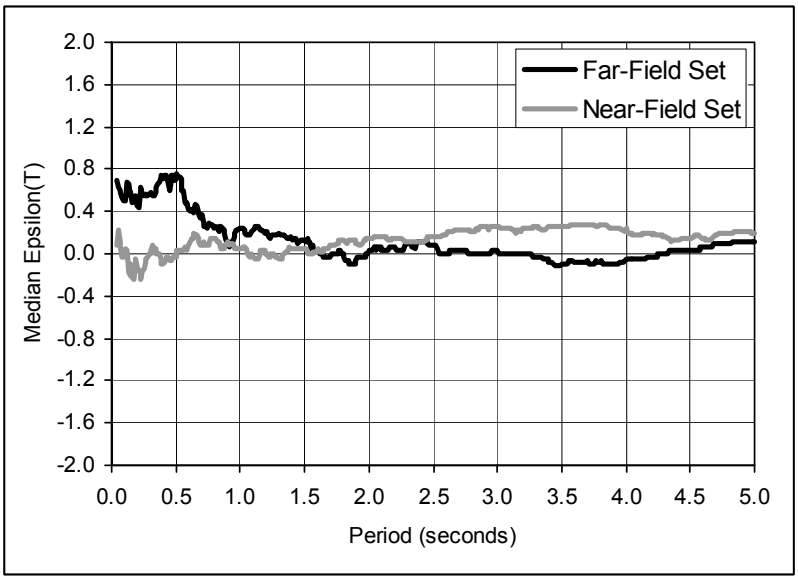


Figure A-8 Plot of median value of epsilon for the Near-Field record set (and plot of median value of epsilon for the Far-Field record set for comparison).

## A.11 Comparison of Far-Field and Near-Field Record Sets

This section compares median response spectra of the Far-Field and Near-Field record sets, and collapse margin ratios (*CMR*'s) calculated using these record sets. Comparisons of collapse margin ratios are made to determine if margins are, in general, substantially less for SDC E structures subjected to near-fault seismic demands than for SDC D structures subjected to SDC D (Dmax) seismic demands. These comparisons necessarily consider that higher seismic loads are required for design of SDC E structures (than for SDC D structures).

The three record sets used in this section to evaluate collapse margin are: (1) Far-Field record set (full set of 44 records), (2) Near-Field record set (full set of 56 records), and (3) Near-Field subset of pulse records in the fault normal (FN) direction (14 records of Near-Field record that are oriented in the fault normal direction and which have pulses). All records are normalized and scaled as described in Section A.8. These sets permit assessment of the effect of differences in frequency content and response characteristics of records on collapse margin. For example, are collapse margins similar for Far-Field and Near-Field record sets (when both sets are anchored to the same level of SDC E seismic criteria)? Similarly, are collapse margins substantially lower for Near-Field FN-Pulse records than for the full Near-Field record set?

Figure A-9 shows unscaled median response spectra for Near-Field and Far-Field record sets, respectively, and the ratio of these spectra. The ratio of median spectra varies from about 1.2 at short periods to about 1.6 at a period of 1-second (and over 2.0 at periods beyond 2 seconds) consistent with mapped values of ground motion required by ASCE/SEI 7-05, and other codes, for structural design near active sources. For example, the near-source coefficients of the 1997 *Uniform Building Code* (ICBO, 1997), summarized in Table A-8, increase seismic design loads by 1.2 (acceleration domain) and 1.6 (velocity domain) for structures located 5 km of an active fault capable of generating large magnitude earthquakes. Corresponding increases in MCE seismic criteria are used for evaluation of collapse margin for SDC E seismic demands.

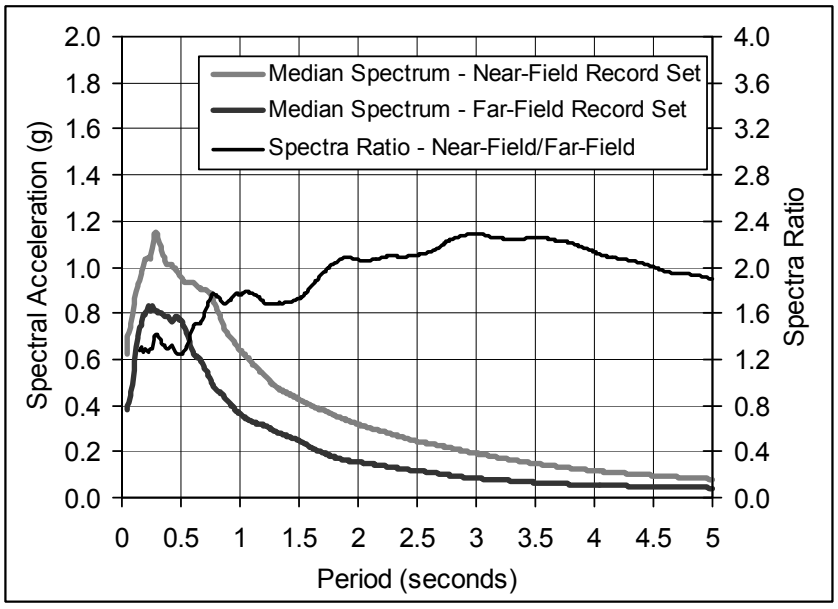


Figure A-9 Plots of median response spectra of normalized Near-Field and Far-Field record sets, respectively, and the ratio of these spectra.

**Table A-8 Near-Source Coefficients of the *1997 Uniform Building Code* (from Tables 16-S and 16-T, ICBO, 1997)**

| Spectral Domain | Closest Distance to Fault | | | |
|---|---|---|---|---|
| | ≤ 2 km | 5 km | 10 km | ≥15 km |
| Acceleration | 1.5 | 1.2 | 1.0 | 1.0 |
| Velocity | 2.0 | 1.6 | 1.2 | 1.0 |

Figure A-10 compares unscaled median response spectra of the Far-Field record set, the full Near-Field record set, and the fault normal records of the

Near-Field Pulse subset. At short periods, the three response spectra are similar, but they diverge significantly at long periods. As expected, at long periods, the median response spectrum of fault normal records of the Near-Field Pulse subset shows substantially greater seismic demand than both the Near-Field and Far-Field record sets.

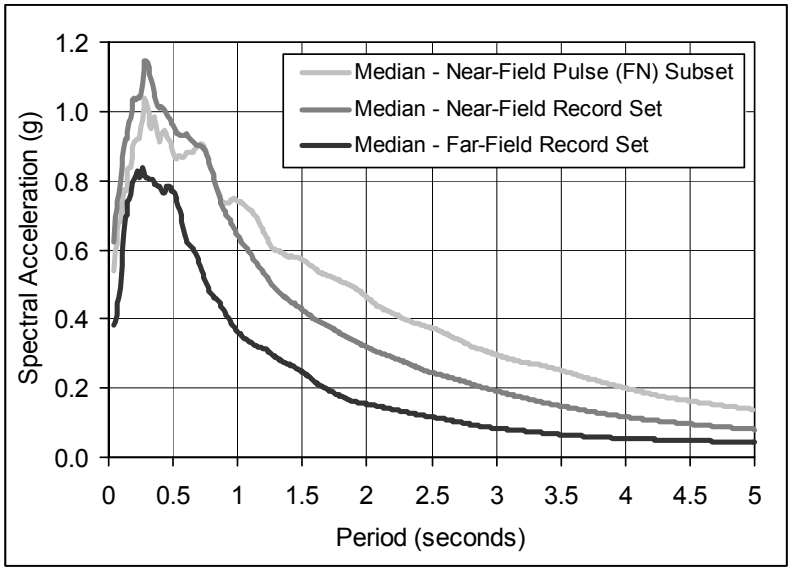


Figure A-10 Plots of median response spectra of the normalized Near-Field record set, the Far-Field record set, and fault normal records of the Near-Field Pulse subset, respectively.

Potential differences in collapse margin ratio due to differences in the frequency content of the three record sets are investigated using archetypes of reinforced-concrete (RC) special moment-frame (SMF) structures (i.e., RC SMF archetypes of Section 9.2, perimeter frame and 30-foot bay configuration). Three archetype heights are considered: 1-story, 4-story and 20-story heights. In the case of the 20-story archetype, two designs are prepared, one design without lower-bound limits on design base shear (i.e., design ignores Formula (12.8-6) of ASCE/SEI 7-05), and one design with lower-bound base shear limits, including also the base shear limit of Eq. 9.5.5.2.1-3 of ASCE 7-02 (ASCE, 2003).

Each RC SMF archetype is designed in accordance with ASCE/SEI 7-05 criteria for both SDC $D_{max}$ and SDC E design requirements (i.e. one design is prepared for SDC $D_{max}$ and another for SDC E), respectively, with certain exceptions for 20-story archetypes. Note that the SDC E demands were not previously defined in Table A-1, since SDC E is not used in the basic

assessment Methodology of this document; SDC E is only used for this comparison, so the SDC E demands are given in Table A-9.

Table A-9 summarizes fundamental periods and seismic design coefficients for each the eight archetypes. As shown, the seismic coefficients of archetypes designed for SDC E requirements are 20% to 60% greater than those of archetypes designed for SDC $D_{max}$ requirements.

**Table A-9 Summary of Key Reinforced-Concrete Special Moment Frame Archetype Properties and Seismic Coefficients Used to Evaluate Collapse Margin Ratio (*CMR*)**

| Building Archetype | | | Seismic Coefficient, $C_s$ | | |
|---|---|---|---|---|---|
| Height/Label | T (sec.) | $C_s$ Limits | SDC Dmax | SDC E | Ratio |
| 1-Story | 0.26 | NA | 0.125 | 0.15 | 1.2 |
| 4-Story | 0.81 | NA | 0.092 | 0.149 | 1.6 |
| 20-Story - 02 | 3.36 | ASCE 7-02[1] | 0.044[1] | 0.053[2] | 1.2 |
| 20-Story - NL | 3.36 | None[3] | 0.022 | 0.036 | 1.6 |

1. Archetype design includes lower-bound limit of ASCE 7-02, Eq. 9.5.5.2.1-3.
2. Archetype design slightly less than $C_s = 0.06$ limit of *ASCE 7-05*, Formula (12.8-6).
3. Archetype design Ignores lower-bound limit of *ASCE 7-05*, Formula (12.8-6).

Tables A-10A and A-10B summarize collapse margin ratios (*CMR*'s) for the eight archetypes of Table A-9. In both tables, *CMR*'s of the four archetypes designed and evaluated for SDC $D_{max}$ (far-field) sites are compared with *CMR*'s of the same four archetypes designed and evaluated for SDC E (near-field) sites.

Table A-10A compares two *CMR* values computed for SDC E sites, against the baseline *CMR* values (for SDC $D_{max}$ design assessed using the far-field ground motion set). The SDC E *CMR* values are computed both (a) using the far-field ground motion set, and (b) using the near-field ground motion set. Both sets are anchored to SDC E demands (from Table A-9) according to section A.8. Note that the near-field record set should be used when assessing performance at a SDC E (near-field) site; the far-field set is only used for comparison and to help explain the observed differences between the computed *CMR* values for SDC E and SDC $D_{max}$ sites.

**Table A-10A Summary of Selected Collapse Margin Ratios (*CMR*'s) for Reinforced-Concrete Special Moment Frame Archetypes – Comparison of *CMR*'s for Far-Field and Near-Field Record Sets**

| Building Archetype | Far-Field Baseline (SDC Dmax) | Near-Field Designs Evaluated for SDC E Seismic Demand (MCE) | | | |
|---|---|---|---|---|---|
| | | Near-Field Record Set | | Far-Field Record Set | |
| Height | CMR | CMR | CMR/Baseline | CMR | CMR/Baseline |
| 1-Story | 1.26 | 0.86 | 68% | 1.03 | 82% |
| 4-Story | 1.98 | 1.32 | 67% | 1.55 | 78% |
| 20-Story - 02 | 1.62 | 1.34 | 83% | 1.39 | 86% |
| 20-Story - NL | 0.82 | 1.01 | 123% | 0.91 | 111% |

Table A-10A shows the *CMR* values for SDC E sites, computed using both the far-field and near-field record sets. When the near-field record set is used for the SDC E evaluation, the *CMR* is an average of 30% lower as compared to SDC $D_{max}$ (with the exception of the 20-Story-NL archetype, which will be discussed later).

This 30% difference is caused by two aspects: (a) the higher seismic demand of SDC E (it has been shown in Chapter 9 that *CMR* values are typically lower for buildings designed and assessed for higher seismic demands), and (b) the use of the near-field record set instead of the far-field set. To clearly separate these two effects, columns two and five show the *CMR* values for SDC $D_{max}$ and SDC E, respectively, both evaluated using the far-field record set. This shows that the *CMR* values are an average of 20% lower for SDC E, simply due to SDC E having higher seismic demand. This shows that the use of near-field records, rather than far-field records, only leads to an average 10% reduction in the *CMR*.

Table A-10B shows how low the *CMR* could become if one used only the subset of near-field motions which are fault-normal and have pulses (this is not recommended for performance evaluation); for comparison, this table also replicates the results from the full near-field set. This table shows that the resulting CMR values are an average of 45% lower than the baseline SDC $D_{max}$ case, and 15% lower than the values computed when the full near-field set is utilized.

**Table A-10B Summary of Selected Collapse Margin Ratios (*CMR*'s) for Reinforced-Concrete Special Moment Frame Archetypes - Comparison of *CMR*'s for the Near Field (NF) Record Set and the NF Pulse FN Subset**

| Building Archetype | Far-Field Baseline (SDC Dmax) | Near-Field Designs Evaluated for SDC E Seismic Demand (MCE) | | | |
|---|---|---|---|---|---|
| | | Near-Field Record Set | | NF - Pulse FN Subset | |
| Height | CMR | CMR | CMR/Baseline | CMR | CMR/Baseline |
| 1-Story | 1.26 | 0.86 | 68% | 0.67 | 53% |
| 4-Story | 1.98 | 1.32 | 67% | 0.99 | 50% |
| 20-Story - 02 | 1.62 | 1.34 | 83% | 0.92 | 57% |
| 20-Story - NL | 0.82 | 1.01 | 123% | 0.70 | 85% |

The 20-Story-NL archetype is the only building that does not follow the trends described in the preceding discussion. One possible reason for this is that the minimum base shear limit was not imposed in this design, which caused the design strengths to become very low ($C_s$ = 0.022g to 0.036g), and the collapse capacity of extremely weak structures becomes more sensitive to changes in design strength. Another possible contributing factor is that the fundamental period, $T_1$, is longer for this design, and the spectral shapes change slightly for periods above 3.5 seconds (see Figure A-9).

In summary, as compared to far-field motions, when a structure is subjected to the full set of near-field records, the *CMR* is typically 10% lower. However, when a structure is subjected to the subset of FN pulse-type records, the *CMR* is decreased by about 25%. This shows that the increase in the seismic response coefficient, $C_s$, required for design of structures located near faults does not appear sufficient to result in performance comparable to that of the same system (i.e., same *R* factor) located further away from fault rupture.

Another finding shown in Tables A-10A and A-10B is that without lower-bound limits on design base shear, collapse margins for the 20-Story-NL archetype are very low; but with lower-bound limits, collapse margins for the 20-Story-02 archetype are approximately the same as the 4-Story archetype. While the margins for the 20-Story-NL archetype are very low, it should be noted that a 60% increase in SDC E design strength affects comparable or better performance than the baseline (SDC D) archetype. In fact, a 60% increase in design base shear is able to cause about the same collapse margin for the 20-Story-NL (SDC E) archetype, when evaluated with fault normal components of the Near-Field pulse records, as that of the 20-Story-NL archetype (SDC D) evaluated with Far-Field records (Table A-10B).

# Appendix B
# Adjustment of Collapse Capacity Considering Effects of Spectral Shape

This appendix describes the background and development of simplified spectral shape factors that depend on fundamental period, $T$, and ductility capacity, $\mu_C$, and are used to adjust collapse capacity for the effects of frequency content (spectral shape) of the ground motion record set.

## B.1 Introduction

A challenge associated with analytical prediction of structural collapse is the selection of ground motions for use in dynamic analysis. A characteristic of ground motions that can affect collapse capacity is the spectral shape. For rare ground motions in California, such as maximum considered earthquake (MCE) ground motions, the spectral shape is much different than the shape of a structural design spectrum (ASCE 2005) or the shape of a uniform hazard spectrum (Baker 2005; Baker and Cornell 2006).

Figure B-1 shows the acceleration spectrum of a Loma Prieta ground motion[1] (PEER 2006). This motion has a rare MCE intensity at a period of 1.0 second, which is Sa(T = 1.0 sec) = 0.9g for this example. This spectrum is labeled as "2% in 50 year Sa" which is the same as the MCE for this site. This figure also shows the intensity predicted by the Boore et al. (1997) attenuation prediction, consistent with the event and site associated with this ground motion. These predicted spectra include the median spectrum and the plus/minus one and two standard deviation spectra, assuming that Sa values are lognormally distributed.

In Figure B-1, this extreme (rare) MCE motion has an unusual spectral shape with a "peak" from 0.6 to 1.8 seconds that is much different from the shape of a uniform hazard spectrum. This peak occurs around the period for which

[1] This motion is from the Saratoga station and is owned by the California Department of Mines and Geology. For this illustration, this spectrum was scaled by a factor of +1.4, in order to make the Sa(1s) demand the same as the MCE demand. For the purposes of this example, please consider this spectrum to be *unscaled*, since later values (e.g. ε) should be computed using unscaled spectra.

the motion is said to have an MCE intensity, and at this period the observed $Sa(T_1)$ is much higher (0.9g) than the mean expected $Sa(T_1)$ from the attenuation function (0.3g). This peaked shape makes intuitive sense because it seems unlikely that a ground motion with a much larger than expected spectral acceleration at one period would have similarly large spectral accelerations at all other periods.

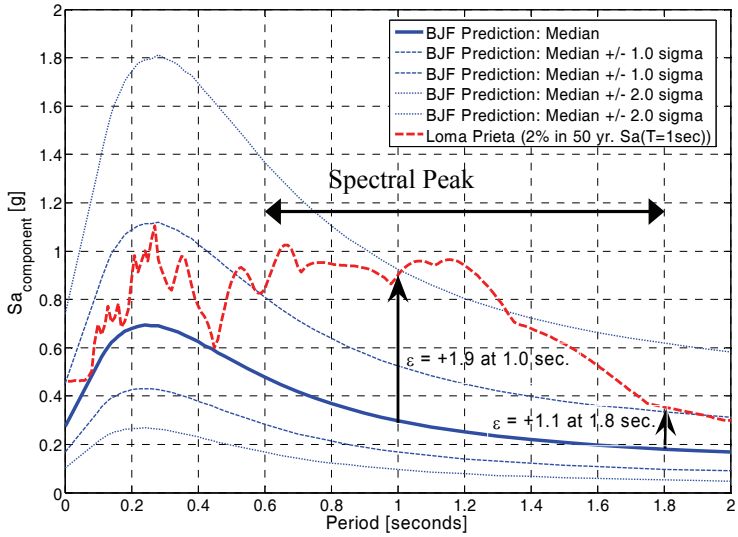


Figure B-1 Comparison of an observed spectrum with spectra predicted by Boore, Joyner, and Fumal (1997); after Haselton and Baker (2006).

Epsilon, ε, is defined as the number of logarithmic standard deviations between the observed spectral value and the median prediction from an attenuation function. At a period of 1.0 second, the spectral value is 1.9 logarithmic standard deviations above the predicted mean spectral value, so this record is said to have "ε = 1.9 at 1.0 second." Similarly, this record has ε = 1.1 at 1.8 seconds. Thus, the ε value is a function of the ground motion record, the period of interest, and the attenuation function used for prediction.

Trends shown in Figure B-1 are general to sites in coastal California where ε values ranging from 1.0 to 1.75 are typically expected for the MCE (or 2% in 50 year) ground motion level. These positive ε values come from the fact that the return period of the ground motion (i.e. 2475 years for a 2% in 50 year motion) is much longer than the return period of the event that causes the ground motion (i.e. 150-500 years for typical events in California). Record selection for structural analyses at such sites should reflect the expected ε for the site and the ground motion hazard level of interest.

It should be noted that this expected ε is both hazard-level and site dependent. For example, for 50% in 5 year ground motions in coastal California, ε values ranging from 0 to -2 are expected (Haselton 2006). In the eastern United States, ε values ranging from 0.25 to 1.0 are expected for a 2% in 50 year motion. Negative ε values for a 50% in 5 year motion stems from the fact that the return period of the ground motion (i.e. 10 years) is much shorter than the typical return period of the event that causes the ground motion (e.g. 150 to 500 years). The Eastern United States has low positive ε values because seismic events are less frequent than in California, but the return periods are still typically shorter than the return period of a 2% in 50 year motion (i.e. 2475 years).

Collapse capacity is defined as the $Sa(T_1)$ value that causes dynamic sidesway collapse (termed $S_{CT1}$). Research has shown that collapse capacity is higher for motions with a peaked spectral shape relative to motions without a peaked spectral shape. This is especially true when the peak of the spectrum is near the fundamental period of the building ($T_1$), and ground motions are scaled based on $Sa(T_1)$ (Haselton and Baker 2006, Baker 2006, Baker 2005, Goulet et al. 2006, Zareian 2006). Spectral accelerations at periods other than $T_1$ are often important to the collapse response of a building. Period elongation as building responds inelastically makes $T > T_1$ important to collapse response, and higher mode effects make $T < T_1$ important to collapse response. Positive ε peaked spectra typically have lower spectral demands at periods away from $T_1$

Past studies have shown that if $\varepsilon = 0$ ground motions are used when $\varepsilon = 1.5$ to 2.0 ground motions are appropriate, the median collapse capacity is typically under-predicted by a factor of 1.3 to 1.8. In cases where rare motions with high positive ε values drive the performance assessment, such as with modern buildings, properly accounting for this expected +ε is critical. Large under-predictions of median collapse capacity cause more significant over-predictions of conditional collapse probabilities and mean annual rates of collapse. This is particularly true for modern buildings where collapse probabilities are typically driven by the lower tail of the collapse capacity distribution.

The most direct approach to account for spectral shape is to select ground motions that have the appropriate $\varepsilon(T_1)$ expected for the site and hazard level of interest. This approach is difficult when assessing the collapse capacities of many buildings with differing $T_1$, because it would require a unique ground motion set for each building. To address this issue, a simplified method allowing the use of a general set of ground motion records (selected independent of ε values) was developed (Haselton et al., 2007), in which

collapse capacity estimates are corrected to account for spectral shape, as quantified by the $\varepsilon(T_1)$ value expected for the site and hazard level of interest.

## B.2 Previous Research on Simplified Methods to Account for Spectral Shape (Epsilon)

Several recent studies have focused on how spectral shape ($\varepsilon$) affects collapse capacity and pre-collapse structural responses (Baker 2006, Baker 2005, Goulet et al. 2006, Haselton and Baker 2006, Zareian 2006). To develop a simplified correction method, the collapse capacity (in terms of $S_{CT1}$) of 65 modern reinforced concrete (RC) special moment frame (SMF) buildings was predicted. For the collapse assessment of each building, 80 ground motions were utilized, with the goal of finding a relationship between the collapse capacity ($S_{CT1}$) and $\varepsilon(T_1)$.

Figure B-2 shows the findings for a single 8-story reinforce concrete perimeter frame building which has a fundamental period of $T_1 = 1.71$ seconds. This shows the results of linear regression analysis that is used to define the relationship: $LN[S_{CT1}] = \beta_0 + \beta_1\varepsilon$. The value of $\beta_0$ indicates the average collapse capacity when $\varepsilon = 0$, and the value of $\beta_1$ indicates how sensitive the collapse capacity ($S_{CT1}$) is to changes in the $\varepsilon$ value. To achieve the goal of a simplified correction method, the $\beta_1$ value is a required ingredient. For this specific 8-story building, $\beta_1 = 0.311$. For the full set of modern code-conforming RC SMF buildings, Haselton et al. found an average value of $\beta_1 = 0.28$, and found that this value is exceptionally consistent for modern RC SMF buildings with various designs (perimeter frame, space frame, various bay widths, etc.) and various heights (1-story to 20-stories).

The relationship between $\beta_1$ and inelastic building deformation capacity was also investigated. For buildings with larger inelastic deformation capacity, the effective period elongates more before structural collapse. This causes spectral values at $T > T_1$ to have larger impact on collapse response, and subsequently causes the spectral shape of the ground motion to become more important (thus increasing $\beta_1$).

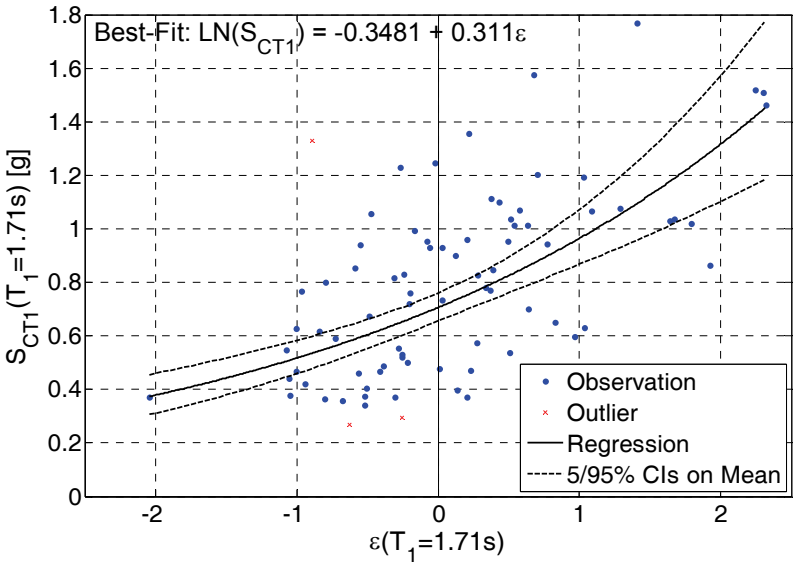


Figure B-2 Relationship between collapse spectral acceleration ($S_{CT1}$) and $\varepsilon(T_1)$ for a single 8-story building; after Haselton et al. (2007). This includes linear regression analysis results which relate $LN[S_{CT1}(T_1)]$ to $\varepsilon(T_1)$.

To investigate the impact of inelastic building deformation capacity, a set of 26 1967-era RC frame buildings was investigated in the same manner as the previous set of RC SMF buildings. This revealed an average value of $\beta_1$ = 0.18, which is 35% lower than that of the RC SMF buildings; this confirms that the ground motion spectral shape is less important for buildings with lower deformation capacity. To further add to the comparison, a set of 20 RC Ordinary Moment Frame (OMF) buildings was also considered, which showed an average value of $\beta_1$ = 0.19, being consistent with the finding for the 1967-era RC frame buildings.

## B.3 Simplified Method to Adjust Collapse Capacity for Effects of Spectral Shape (Epsilon)

This simplified method corrects the collapse capacity distribution without computing the $\varepsilon(T_1)$ values of the ground motion records, and without performing a regression analysis. It involves using the Far-Field record set (Appendix A) for structural collapse analyses, and then applying an adjustment factor to the median collapse capacity ($\hat{S}_{CT}$).

The simplified correction factor depends on the following:

1. Differences between:
   a. the $\varepsilon(T_1)$ values of the ground motions used in the structural analyses (i.e. the Far-Field record set), and

b. the $\varepsilon(T_1)$ value expected for the site and ground motion hazard level of interest.

2. How drastically the ground motion ε values affect the building collapse capacity; quantified by $\beta_1$, as described in section B.2. The ground motion ε values will have a greater effect on buildings with larger inelastic deformation capacity, which will have more extensive period elongation prior to collapse.

### *B.3.1 Epsilon Values for the Ground Motions in the Far-Field Set*

To adjust collapse capacity predictions for spectral shape, the epsilon, ε(T), values for the ground motion set used for collapse simulation are needed. Figure B-3 shows the mean ε(T) values for the Far-Field record set, computed using the Abrahamson and Silva attenuation function (1997). The mean ε(T) values computed using the Boore et al. (1997) attenuation function are similar but not shown. For the Far-Field record set, mean ε(T) are approximately +0.6 for periods less than 0.5 seconds, and are nearly 0.0 for periods greater than 1.5 seconds.

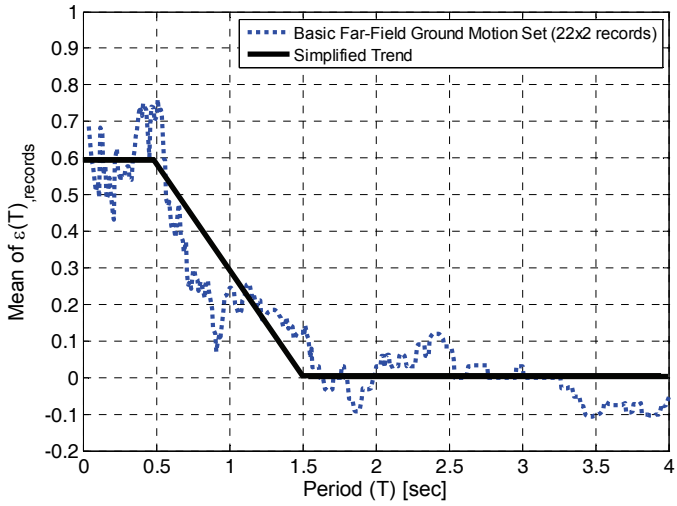


Figure B-3 Mean ε values for the Basic Far-Field Ground Motion Set [$\bar{\varepsilon}(T)_{,records}$].

The simplified trend from Figure B-3 can be express using equation B-1:

$$\bar{\varepsilon}(T)_{,records} = (0.6)(1.5 - T) \qquad \text{(B-1)}$$

where $0.0 \le \bar{\varepsilon}(T)_{,records} \le 0.6$.

Note that for consistency with the Methodology, the period used for $\overline{\varepsilon}(\mathrm{T})_{,\mathrm{records}}$ should be the code-defined fundamental period (T), and not the fundamental period computed from eigenvalue analysis ($T_1$).

### *B.3.2 Target Epsilon Values*

The expected epsilon, $\overline{\varepsilon}_0$, value (also called "proper ε" or "target ε") depends on both the site and hazard level of interest. A proper target ε is needed in the process of adjusting the median collapse capacity to account for spectral shape.

To quantify the target ε for various seismic design categories around the United States, data from the United States Geological Survey (USGS) is utilized. The USGS conducted the seismic hazard analysis for the United States and used dissagregation to determine the mean ε ($\overline{\varepsilon}_0$) values for various periods and hazard levels of interest (Harmsen, Frankel, and Petersen, 2002; Harmsen 2001). Luco, Harmsen, and Frankel of the USGS provided electronic $\overline{\varepsilon}_0$ data, by zip code, for use in this study. These data included $\overline{\varepsilon}_0$ values at four ground motion hazard levels.

Figure B-4 shows a map of expected $\overline{\varepsilon}_0(1\mathrm{s})$ for a 2% in 50 year motion in the Western United States. Values of $\overline{\varepsilon}_0(1\mathrm{s})$ = 0.50 to 1.25 are typical in areas other than the seismic regions of California. The values are higher in most of California, since the earthquake events have shorter return periods, with typical values being $\overline{\varepsilon}_0$ (1s) = 1.25 to 1.75, and some values ranging upward to 3.0.

Figure B-5a is the same as Figure B-4, but for the Eastern United States. It shows typical values of $\overline{\varepsilon}_0(1\mathrm{s})$ = 0.75 to 1.0, with some values reaching up to 1.25. Expected $\overline{\varepsilon}_0(1\mathrm{s})$ values fall below 0.75 for the New Madrid Fault Zone, portions of the eastern coast, most of Florida, southern Texas, and areas in the north-west portion of the map.

To see the effects of period, Figure B-5b shows the $\overline{\varepsilon}_0(0.2\mathrm{s})$ instead of $\overline{\varepsilon}_0(1\mathrm{s})$. This shows that typical $\overline{\varepsilon}_0(0.2\mathrm{s})$ are slightly lower and more variable, having a typical range of 0.25 to 1.0. This is in contrast to the typical range of 0.75 to 1.0 for $\overline{\varepsilon}_0(1\mathrm{s})$.

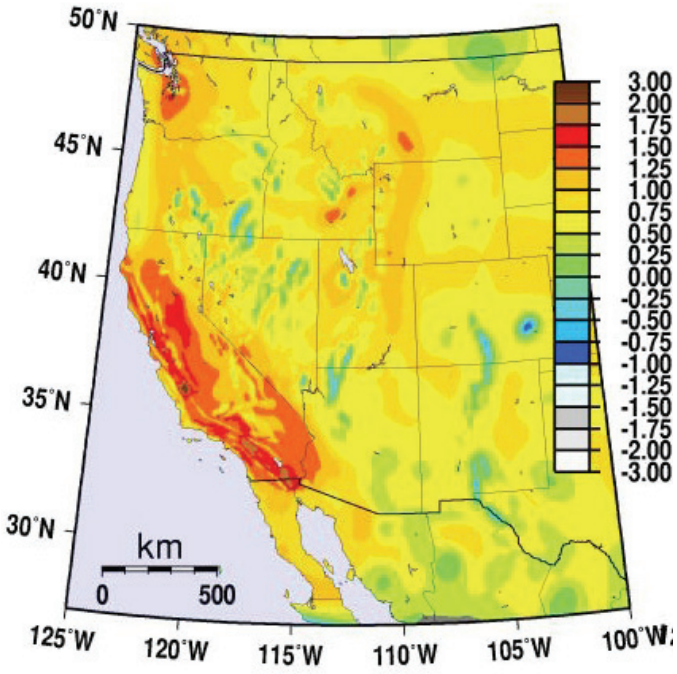


Figure B-4 Predicted $\overline{\varepsilon}_0$ values from dissagregation of ground motion hazard, for the Western United States. The values are for a 1.0 second period and the 2% exceedance in 50 year motion. This figure comes directly from the United States Geological Survey Open-File Report (Harmsen et al. 2002).

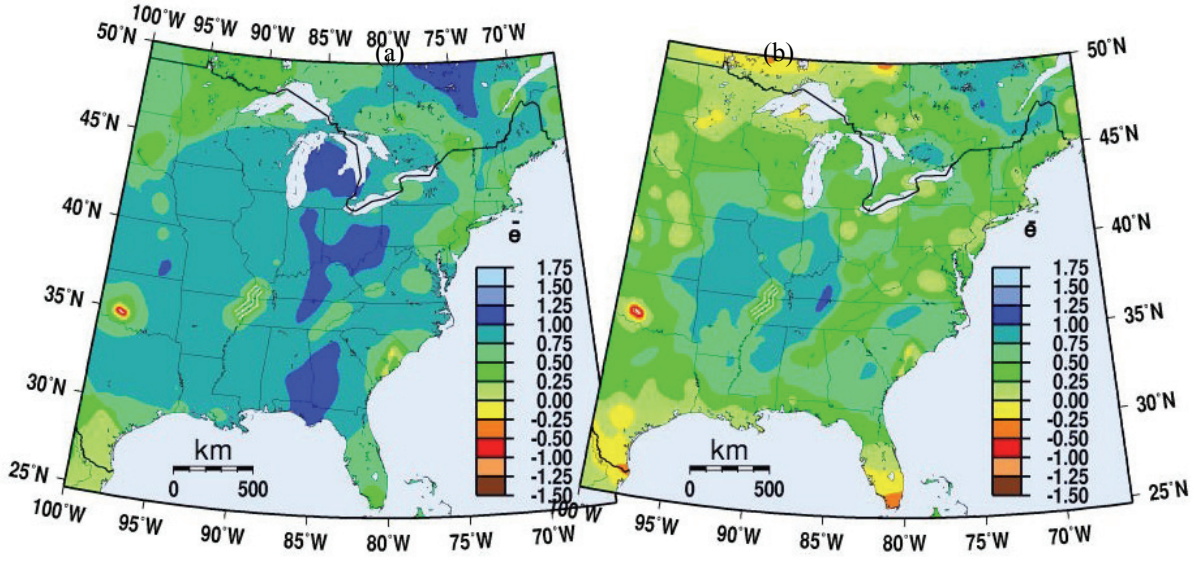


Figure B-5 Mean predicted $\overline{\varepsilon}_0$ values from dissagregation of ground motion hazard, for the Eastern United States. The values are for (a) 1.0 second and (b) 0.2 second periods and the 2% exceedance in 50 year motion. This figure comes directly from the United States Geological Survey Open-File Report (Harmsen et al. 2002).

To better quantify the $\overline{\varepsilon}_0$ values presented in the previous figures, Table B-1 and Table B-2 show the average $\overline{\varepsilon}_0$ and spectral acceleration values for Seismic Design Categories (SDC) B, C, and D. These data are given for four levels of ground motion: the motion with 10% exceedance in 50 years, 2% in 50 years, 1% in 50 years, and 0.5% in 50 years. These tables also show the number of zip code data points included in each SDC.

**Table B-1 Tabulated $\overline{\varepsilon}_0$ Values for Various Seismic Design Categories**

| Seismic Design Category | Average ε Values | | | | | | | | Number of Zip Code Data Points |
|---|---|---|---|---|---|---|---|---|---|
| | $\varepsilon_0$(0.2s) | | | | $\varepsilon_0$(1.0s) | | | | |
| | $\varepsilon_{10/50}$ | $\varepsilon_{2/50}$ | $\varepsilon_{1/50}$ | $\varepsilon_{0.5/50}$ | $\varepsilon_{10/50}$ | $\varepsilon_{2/50}$ | $\varepsilon_{1/50}$ | $\varepsilon_{0.5/50}$ | |
| SDC B | 0.14 | 0.42 | 0.49 | 0.55 | 0.31 | 0.80 | 0.94 | 1.04 | 20,142 |
| SDC C | 0.11 | 0.51 | 0.63 | 0.75 | 0.23 | 0.74 | 0.88 | 1.00 | 7,456 |
| SDC D | 0.25 | 0.88 | 1.09 | 1.27 | 0.33 | 0.99 | 1.21 | 1.39 | 6,461 |
| SDC D, 0.35 < S1 < 0.599g | 0.32 | 0.97 | 1.21 | 1.41 | 0.39 | 1.01 | 1.24 | 1.45 | 1,305 |

**Table B-2 Tabulated Spectral Demands for Various Seismic Design Categories**

| Seismic Design Category | Average Sa Values | | | | | | | | Number of Zip Code Data Points |
|---|---|---|---|---|---|---|---|---|---|
| | Sa(0.2s) [g] | | | | Sa(1.0s) [g] | | | | |
| | $Sa_{10/50}$ | $Sa_{2/50}$ | $Sa_{1/50}$ | $Sa_{0.5/50}$ | $Sa_{10/50}$ | $Sa_{2/50}$ | $Sa_{1/50}$ | $Sa_{0.5/50}$ | |
| SDC B | 0.06 | 0.18 | 0.26 | 0.39 | 0.02 | 0.06 | 0.08 | 0.11 | 20,142 |
| SDC C | 0.11 | 0.31 | 0.46 | 0.66 | 0.04 | 0.10 | 0.14 | 0.19 | 7,456 |
| SDC D | 0.50 | 1.05 | 1.35 | 1.68 | 0.18 | 0.38 | 0.49 | 0.62 | 6,461 |
| SDC D, 0.35 < S1 < 0.599g | 0.61 | 1.31 | 1.69 | 2.09 | 0.21 | 0.46 | 0.61 | 0.77 | 1,305 |

SDC D is treated differently from the other categories, since it is the category with highest spectral demand and often controls the collapse performance assessment. Studies have shown that buildings designed for SDC D have the lowest collapse margin ratio, and control the collapse performance assessment. Therefore, sites in SDC D with higher values of $S_1$ (i.e. $0.35 < S_1 < 0.599$) are expected to control the performance assessment for the SDC D sites, and are accordingly used to define the target ε.

It should be noted that the $\overline{\varepsilon}_0$ values in Table B-1 are a bit lower than some may expect for SDC D sites in seismic zones of California. This comes from the values in Table B-1 being *averages* for all SDC D sites in the United

States. The SDC D sites are located in seismic regions of California, as well as in the Eastern United States. Seismic sources in these two regions have very different return periods, which causes $\overline{\varepsilon}_0$ values to be different, and the values in California to be larger. Average 2% in 50 year and 0.5% in 50 year $\overline{\varepsilon}_0$(1.0s) values are listed for selected California cities. These values are averages over all SDC D zip codes in a given city, and are comparable to 0.99 and 1.39 values from Table B-1 (which are for the full United States). Since these values are averages over the city, the values at each specific site in the city may be higher or lower than these values.

- 1.5 and 1.9 in San Francisco (average over 16 zip codes)
- 1.7 and 2.1 in Oakland (average over 10 zip codes)
- 1.6 and 2.0 in Berkeley (average over 3 zip codes)
- 1.6 and 2.1 in San Jose (average over 29 zip codes)
- 1.3 and 1.7 in Los Angeles (average over 58 zip codes)
- 2.0 and 2.2 in Riverside (average over 8 zip codes)

Table B-1 presented $\overline{\varepsilon}_0$(0.2s) and $\overline{\varepsilon}_0$(1.0s) values. The $\overline{\varepsilon}_0$(1.0s) values are used to develop the target ε values, since most building structures have periods closer to 1.0 second, or greater than 1.0 second. Buildings with periods near 0.2 seconds are relatively rare.

To complete the target ε values for each SDC, the proper ground motion hazard level must be established. Since the spectral shape (ε) adjustment will be used to modify the *median* collapse capacity, the appropriate hazard level should be near this median. Table 7-3 shows that for a structure to pass a 10% conditional collapse probability acceptance criterion, the median collapse capacity must be greater than twice the MCE (which in most cases is twice the 2% in 50 year motion). Therefore, a ground motion hazard level should be used that has spectral acceleration demand that is twice (or more) of 2% in 50 year demand. Table B-1 shows that the 0.5% in 50 year demand meets this criterion, and is still conservative for SDC D, so the 0.5% in 50 year $\overline{\varepsilon}_0$(1.0s) is used as the target ε. Based on this, the target ε value for SDC B/C is 1.0, and the target ε value for SDC D is 1.5.

SDC E must be treated differently, because the 2% in 50 year motion and the MCE can differ widely in near-fault regions. At sites close to a fault, MCE motion occurs more frequently than the 2% in 50 year motion. This is the result of the methodology used to construct the 1994 NEHRP maps, as explained in Appendix B of FEMA 369 (FEMA 2001). In the near-field, the

MCE is set to be one logarithmic standard deviation greater than the median predicted motion, i.e., $\varepsilon = 1.0$. To approximately account for the fact that the median collapse capacity is larger than the MCE motion, a target $\varepsilon = 1.2$ is used for SDC E.

### *B.3.3 Impact of Spectral Shape on Median Collapse Capacity*

For buildings with larger inelastic deformation capacity, the effective period elongates more significantly before structural collapse, causing the spectral values at $T > T_1$ to have more drastic impacts on structural response. This subsequently causes the spectral shape ($\varepsilon$) of the ground motions to become more important. The $\beta_1$ value (defined in section B.2) is used to quantify how drastically the spectral shape ($\varepsilon$) affects the collapse capacity, with $\beta_1$ being larger for buildings with larger deformation capacity.

**Quantification of Building Inelastic Deformation Capacity**

To quantify the building inelastic deformation capacity building ductility capacity ($\mu_c$) is defined in Equation B-2:

$$\mu_c = \Delta_{ult} / \Delta_y \qquad \text{(B-2)}$$

where ($\Delta_{ult}$) is the ultimate displacement, and ($\Delta_y$) is the effective yield displacement.

It is important to note that the above equation includes a normalization by the effective yield displacement of the building. This normalization makes it important that the initial stiffness of each structural member be modeled appropriately. In calibrating Equation B-3 (below), the effective element-level initial stiffness was defined as the secant stiffness from the origin through the point at 40% of the yield strength of the element. Overestimating the initial stiffness results in an unconservatively large estimate of $\mu_c$ and the resulting spectral shape correction factor.

**Values of $\beta_1$ for Buildings with Various Inelastic Deformation Capacities**

The proposed relationship between $\beta_1$ and $\mu_c$ is shown in Equation B-3:

$$\hat{\beta}_1 = (0.17)\left(\mu^*_c - 1\right)^{0.33} \qquad \text{(B-3)}$$

where $\mu^*_c = \mu_c$ if $\mu_c \le 8$ and $\mu_c = 8$ otherwise.

## B.4 Final Simplified Factors to Adjust Median Collapse Capacity for the Effects of Spectral Shape

Following the rationale above, simplified spectral shape factors, *SSF*, can be computed using Equation B-4.

$$SSF = \exp\left[\beta_1\left(\overline{\varepsilon}_o(T) - \overline{\varepsilon}(T)_{,records}\right)\right] \quad \text{(B-4)}$$

where $\beta_1$ depends on building inelastic deformation capacity; $\overline{\varepsilon}_0$ depends on SDC and is equal to 1.0 for SDC B/C, 1.5 for SDC D (section B.3.2), and 1.2 for SDC E; and $\varepsilon(T)_{,records}$ is for the Far-Field record set.

Table B-3 through Table B-5 present values of spectral shape factor, *SSF*, for various levels of building deformation capacity and various building periods, using Equation B-4. Table B-3 presents values for SDC B/C, Table B-4 presents values for SDC D, and Table B-5 presents values for SDC E.

To compute the adjusted collapse margin ratio, multiply tabulated *SSF* values by the collapse margin ratio that was predicted using the Far-Field record set, as shown in Equation B-5:

$$ACMR = SSF * CMR \quad \text{(B-5)}$$

**Table B-3 Spectral Shape Factors for SDC B/C/$D_{min}$**

| Spectral Shape Factor (SSF) - Seismic Design Category B/C/Dmin | | | | | | | | |
|---|---|---|---|---|---|---|---|---|
| T (sec) | Building Ductility Capacity, $\mu_C$ | | | | | | | |
| | 1.0 | 1.1 | 1.5 | 2 | 3 | 4 | 6 | >=8 |
| <= 0.5 | 1.00 | 1.03 | 1.06 | 1.07 | 1.09 | 1.10 | 1.12 | 1.14 |
| 0.6 | 1.00 | 1.04 | 1.06 | 1.08 | 1.10 | 1.12 | 1.14 | 1.16 |
| 0.7 | 1.00 | 1.04 | 1.07 | 1.09 | 1.12 | 1.14 | 1.16 | 1.18 |
| 0.8 | 1.00 | 1.05 | 1.08 | 1.10 | 1.13 | 1.15 | 1.18 | 1.21 |
| 0.9 | 1.00 | 1.05 | 1.09 | 1.11 | 1.15 | 1.17 | 1.20 | 1.23 |
| 1.0 | 1.00 | 1.06 | 1.10 | 1.13 | 1.16 | 1.19 | 1.22 | 1.25 |
| 1.1 | 1.00 | 1.06 | 1.11 | 1.14 | 1.18 | 1.20 | 1.25 | 1.28 |
| 1.2 | 1.00 | 1.07 | 1.12 | 1.15 | 1.19 | 1.22 | 1.27 | 1.30 |
| 1.3 | 1.00 | 1.07 | 1.13 | 1.16 | 1.21 | 1.24 | 1.29 | 1.33 |
| 1.4 | 1.00 | 1.08 | 1.14 | 1.17 | 1.22 | 1.26 | 1.31 | 1.35 |
| >= 1.5 | 1.00 | 1.08 | 1.14 | 1.19 | 1.24 | 1.28 | 1.34 | 1.38 |

**Table B-4 Spectral Shape Factors for SDC $D_{max}$**

| Spectral Shape Factor (SSF) - Seismic Design Category Dmax | | | | | | | | |
|---|---|---|---|---|---|---|---|---|
| T (sec) | Building Ductility Capacity, $\mu_C$ | | | | | | | |
| | 1.0 | 1.1 | 1.5 | 2 | 3 | 4 | 6 | >=8 |
| <= 0.5 | 1.00 | 1.07 | 1.13 | 1.17 | 1.21 | 1.25 | 1.30 | 1.34 |
| 0.6 | 1.00 | 1.08 | 1.14 | 1.18 | 1.23 | 1.26 | 1.32 | 1.36 |
| 0.7 | 1.00 | 1.08 | 1.15 | 1.19 | 1.24 | 1.28 | 1.34 | 1.39 |
| 0.8 | 1.00 | 1.09 | 1.16 | 1.20 | 1.26 | 1.30 | 1.37 | 1.42 |
| 0.9 | 1.00 | 1.09 | 1.17 | 1.21 | 1.28 | 1.32 | 1.39 | 1.45 |
| 1.0 | 1.00 | 1.10 | 1.18 | 1.23 | 1.29 | 1.34 | 1.41 | 1.47 |
| 1.1 | 1.00 | 1.11 | 1.19 | 1.24 | 1.31 | 1.36 | 1.44 | 1.50 |
| 1.2 | 1.00 | 1.11 | 1.20 | 1.25 | 1.33 | 1.38 | 1.46 | 1.53 |
| 1.3 | 1.00 | 1.12 | 1.21 | 1.26 | 1.34 | 1.40 | 1.49 | 1.56 |
| 1.4 | 1.00 | 1.12 | 1.22 | 1.28 | 1.36 | 1.42 | 1.52 | 1.59 |
| >= 1.5 | 1.00 | 1.13 | 1.22 | 1.29 | 1.38 | 1.44 | 1.54 | 1.62 |

**Table B-5 Spectral Shape Factors for SDC E**

| Spectral Shape Factor (SSF) - Seismic Design Category E | | | | | | | | |
|---|---|---|---|---|---|---|---|---|
| T (sec) | Building Ductility Capacity, $\mu_C$ | | | | | | | |
| | 1.0 | 1.1 | 1.5 | 2 | 3 | 4 | 6 | >=8 |
| <= 0.5 | 1.00 | 1.05 | 1.08 | 1.11 | 1.14 | 1.16 | 1.19 | 1.21 |
| 0.6 | 1.00 | 1.05 | 1.09 | 1.12 | 1.15 | 1.17 | 1.21 | 1.24 |
| 0.7 | 1.00 | 1.06 | 1.10 | 1.13 | 1.17 | 1.19 | 1.23 | 1.26 |
| 0.8 | 1.00 | 1.06 | 1.11 | 1.14 | 1.18 | 1.21 | 1.25 | 1.29 |
| 0.9 | 1.00 | 1.07 | 1.12 | 1.15 | 1.20 | 1.23 | 1.27 | 1.31 |
| 1.0 | 1.00 | 1.07 | 1.13 | 1.17 | 1.21 | 1.25 | 1.30 | 1.34 |
| 1.1 | 1.00 | 1.08 | 1.14 | 1.18 | 1.23 | 1.26 | 1.32 | 1.36 |
| 1.2 | 1.00 | 1.08 | 1.15 | 1.19 | 1.24 | 1.28 | 1.34 | 1.39 |
| 1.3 | 1.00 | 1.09 | 1.16 | 1.20 | 1.26 | 1.30 | 1.37 | 1.42 |
| 1.4 | 1.00 | 1.09 | 1.17 | 1.21 | 1.28 | 1.32 | 1.39 | 1.45 |
| >= 1.5 | 1.00 | 1.10 | 1.18 | 1.23 | 1.29 | 1.34 | 1.41 | 1.47 |

## B.5 Application to Site Specific Performance Assessment

Simplified spectral shape adjustment factors can be modified for site-specific and building-specific collapse performance assessment. To compute the *SSF* for a site-specific collapse performance assessment, use Equation B-4 with the following values:

- $\beta_1$ should be computed using equation B-3.
- $\overline{\varepsilon}_0(T)$ should not be based on section B.3.2. Instead, $\overline{\varepsilon}_0(T)$ should be based directly on the dissagregation of the probabilistic seismic hazard analysis for the site of interest.

- $\varepsilon(T)_{,records}$ will differ depending on the ground motion set utilized in the performance assessment. If the site is within 10 km of an active fault capable of producing an M > 6.5 event, then the Near-Field ground motion record set should be used (Appendix A); otherwise, the Far-Field record set should be used. If the Far-Field record set is used, then the $\varepsilon(T)_{,records}$ should be taken from Figure B-3 and equation B-1. If the Near-Field record set is used, then the $\varepsilon(T)_{,records}$ should be taken to equal $\varepsilon(T)_{,records.NF}$ from Figure B-6 and Equation B-6.

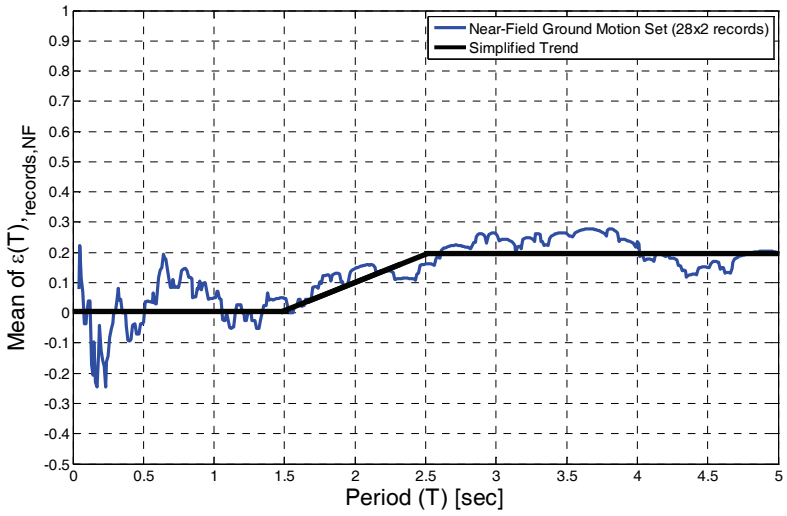


Figure B-6 Mean ε values for the Near-Field Ground Motion Set [$\bar{\varepsilon}(\mathrm{T})_{,\mathrm{records,NF}}$].

The near-field set is nearly ε-neutral at all periods, but a slight simplified trend from Figure B-6 can be express using equation B-6:

$$\bar{\varepsilon}(\mathrm{T})_{,\mathrm{records,NF}} = (0.2)(T - 1.5) \qquad \text{(B-6)}$$

where $0.0 \le \bar{\varepsilon}(\mathrm{T})_{,\mathrm{records,NF}} \le 0.2$.

# Appendix C
# Development of Index Archetype Configurations

This appendix illustrates how configuration issues are considered in the development of index archetype configurations for reinforced concrete moment frame systems and wood light-frame shear wall systems.

Development of structural system archetypes considers both structural configuration issues and seismic behavioral effects described in Chapter 4. Consideration of structural configuration issues is discussed in this appendix. Examination of seismic behavioral effects is described in Appendix D. Index archetype configurations are eventually used to develop index archetype designs, which are then used to develop index archetype models. Development and calibration of nonlinear index archetype models is described in Appendix E.

## C.1 Development of Index Archetype Configurations for a Reinforced Concrete Moment Frame System

In this section, index archetype configurations are developed for a reinforced concrete moment frame system conforming to design requirements contained in ASCE/SEI 7-05, *Minimum Design Loads for Buildings and Other Structures*, and ACI 318-05, *Building Code Requirements for Structural Concrete*. When the process is applied to a proposed new seismic-force-resisting system, index archetype configurations will be based on existing code requirements, as appropriate, and new design requirements developed specifically for the proposed system.

### *C.1.1 Establishing the Archetype Design Space*

To establish the archetype design space, design parameters that significantly affect seismic performance are first identified, and then the bounds on each design parameter are established. The overall range of permissible configurations, structural design parameters, and other features that define the application limits for a seismic-force-resisting system are specified in the system design requirements, and in existing code requirements, as applicable.

Parameters that were identified as having a critical impact on the seismic performance of reinforced concrete moment frame systems, along with related physical properties and associated design variables, are listed in Table C-1. This organizational approach is useful for deciding which of the many design variables should be the focus of further investigation in index archetype configurations.

**Table C-1 Important Parameters, Related Physical Properties, and Design Variables for Reinforced Concrete Moment Frame Systems**

| Parameters Important to Seismic Collapse Performance | Related Physical Properties | Design Variables |
|---|---|---|
| Column and beam plastic rotation capacity | Axial load ratio | Building height, bay width, ratio of tributary areas for gravity and lateral loads |
| | Column aspect ratio | Building height, bay width, story heights, allowable reinforcement ratio |
| | Confinement ratio | Confinement ratio used in design |
| | Stirrup spacing | Stirrup spacing used in design |
| | Longitudinal bar diameter | Longitudinal bar diameter used in design |
| | Reinforcement ratios | Reinforcement ratio allowed in design |
| | Concrete strength | Concrete strength used in design |
| Element Strengths | All element strengths | Conservatism of engineer, dead and live loads used in design |
| | Beam strengths | Slab width (steel) assumed effective |
| | Column strengths | Ratio of factored to expected axial loads, level of conservatism in applying strong-column weak-beam provision |
| Number of stories in collapse mechanism | Strength/stiffness irregularities | Presence of strength or stiffness irregularity, ratio of first to upper story heights, how column heights are stepped down over height |
| Lateral stiffness of frame | Member sizes in frame | Member/joint/footing stiffness used in design |
| Gravity system strength/stiffness | Gravity system | Not considered in this assessment |

Key design variables are those that are likely to have a significant effect on the seismic performance of the proposed system. Key design variables identified for reinforced concrete moment frame systems, along with their applicable ranges, are listed in Table C-2. Figure C-1 illustrates one example of how index archetype configurations might change for a design variable associated with the ratio of tributary areas for gravity and lateral loads. In the case of moment frame systems, this variable is primarily affected by whether the building is designed as a space frame or a perimeter frame system. Table C-1 identifies a range of 0.1 to 1.0 for this design variable, which is schematically shown in the figure.

The design variables and ranges identified in Table C-2 provide the basis for identifying a finite number of design variations for use in developing index archetype configurations.

**Table C-2 Key Design Variables and Ranges for Reinforced Concrete Moment Frame Systems**

| Design Variables | Range Considered in Archetype Design Space |
|---|---|
| **Structural System:** | |
| Special Reinforced Concrete Moment Frame (as per ASCE/SEI 7-05, ACI 318-05) | All designs meet code requirements |
| Seismic framing system | Perimeter and space frames |
| **Configuration:** | |
| Building Height | 1 to 20 stories |
| Bay Width | 20 to 30 feet |
| First and upper story heights | 15/ 13 feet |
| **Element Design:** | |
| Confinement ratio and stirrup spacing | Conforming to ACI 318-05 |
| Concrete compressive strength | 5 to 7 ksi |
| Longitudinal bar diameter | #8 and #9 are commonly used |
| Strength/stiffness irregularities | As permitted by existing code |
| **Loading:** | |
| Ratio of tributary areas for gravity and lateral loads | 0.1 (perimeter frame) to 1.0 (space frame) |
| Design floor loads | 175 psf |
| Lower and upper bounds on design floor load | 150 to 200 psf |
| Design floor live load | Constant: 50 psf |

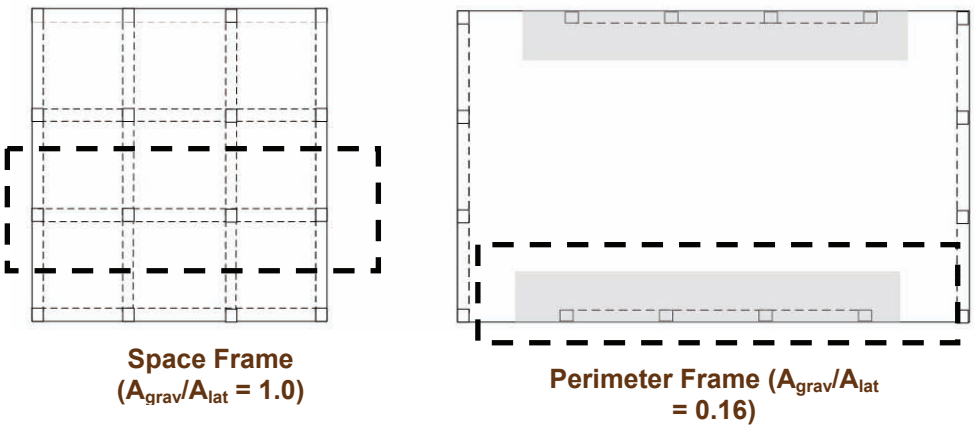


Figure C-1 Different index archetype configurations for varying ratios of tributary areas for gravity and lateral loads.

### *C.1.2 Identifying Index Archetype Configurations and Populating Performance Groups*

Identification of a set of index archetype configurations requires consideration of eventual performance group binning and nonlinear analysis modeling. As a minimum, performance groups should consider the maximum and minimum design ground motion intensities for the governing Seismic Design Category, as well as variations in gravity load intensity. This results in the need for index archetype configurations to populate the following four performance groups:

- Maximum Seismic (for governing SDC), High Gravity
- Minimum Seismic (for governing SDC), High Gravity
- Maximum Seismic (for governing SDC), Low Gravity
- Minimum Seismic (for governing SDC), Low Gravity

Each Performance Group must be robustly populated by buildings that have representative configurations and heights across the entire archetype design space.

Index archetype configurations must be conceived in such a way that index archetype models will capture important system behavior. For moment frames in general, three framing bays are considered to be the minimum number feasible for capturing variations in behavior related to interior and exterior columns and beam-column joints, strong-column weak-beam design provisions, and induced column axial loads due to overturning effects. As a result, the three-bay, variable story-height configuration shown in Figure C-2 was selected as the simplest model still capable of capturing important collapse performance behaviors for reinforced concrete moment frame systems.

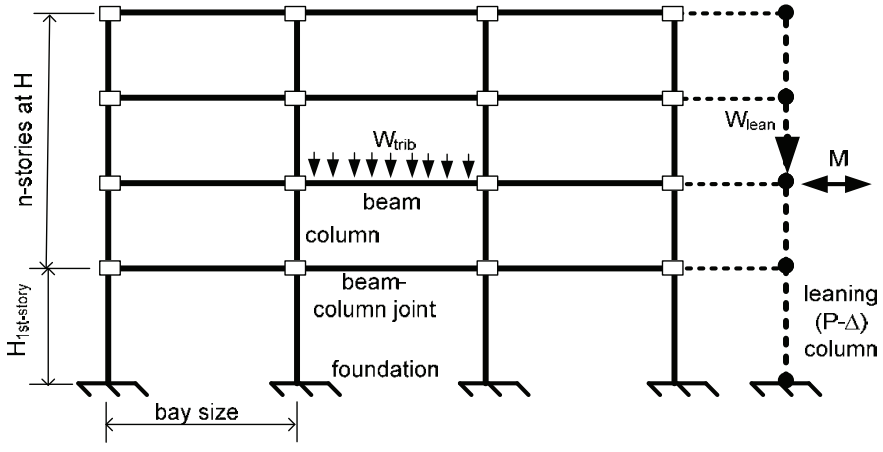


Figure C-2 Index archetype model for reinforced concrete moment frame systems.

To develop a set of index archetype configurations, the range of parameters that will be commonly utilized in design and construction must be understood. As identified in Table C-2, building heights between one and twenty stories are expected, with the thought that most buildings above 20-stories would include a core wall in addition to moment frames. Considering typical office occupancies, story heights are expected to be relatively consistent, taken as 15-feet for the first story and 13 feet for the upper stories. Plan dimensions of 120 feet by 120 feet and 120 feet by 180 feet, along with bay widths ranging between 20 feet and 30 feet, are also expected to be typical for such buildings.

Figure C-3 illustrates a set of 12 index archetype configurations representing the range of expected heights and bay widths that would be used to populate each of the four performance groups.

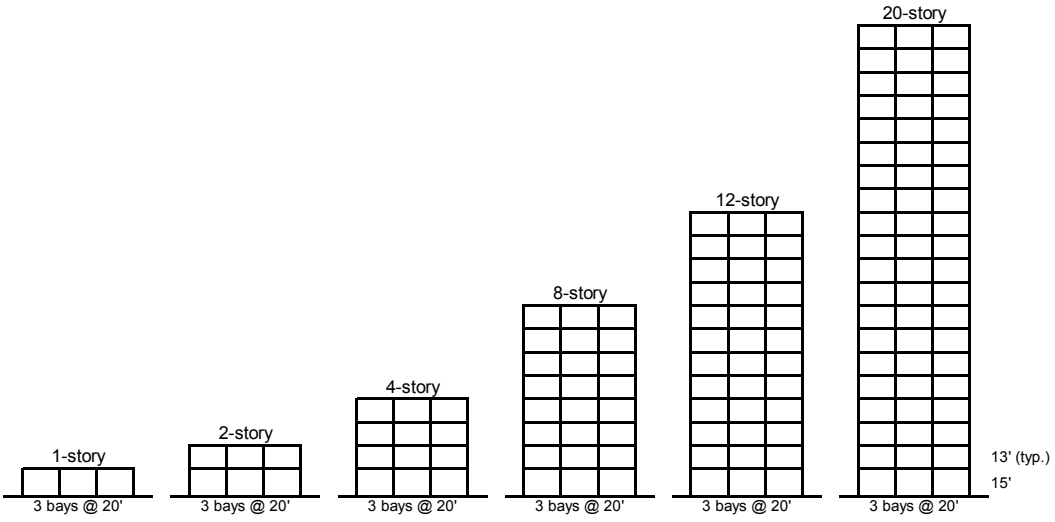


(a) Twenty foot bay width

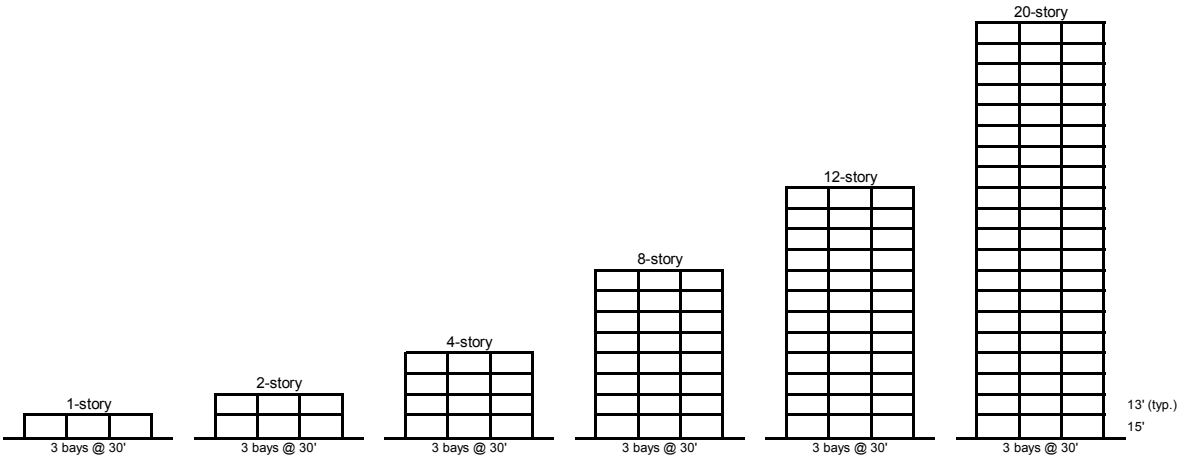


(b) Thirty foot bay width

Figure C-3 Set of 12 index archetype configurations for a reinforced concrete moment frame system.

Maximum and Minimum seismic loads are defined by the range of possible design loads for Seismic Design Category D ($D_{max}$ and $D_{min}$ for SDC D). High and low gravity load intensities are represented by the space frame or perimeter frame configurations.

Based on the information summarized in Table C-1 and Table C-2, and consideration of performance group binning and nonlinear analysis modeling, a matrix of index archetype configurations, such as the one described in Table C-3, can be developed. In this example, index archetype configurations include six building heights from one to twenty stories, two bay widths (20 and 30 feet), both perimeter and space frames, and two design lateral load intensities ($D_{max}$ and $D_{min}$).

**Table C-3 Matrix of Index Archetype Configurations for a Reinforced Concrete Moment Frame System**

| Design Number | Number of Stories | Bay Width (ft) | Gravity Loads | Seismic Design Category |
|---|---|---|---|---|
| 1 | 1 | 20 | Perimeter | $D_{max}$ |
| 2 | | 20 | Space | $D_{max}$ |
| 3 | 2 | 20 | Perimeter | $D_{max}$ |
| 4 | | 20 | Space | $D_{max}$ |
| 5 | 4 | 20 | Perimeter | $D_{max}$ |
| 6 | | 20 | Space | $D_{max}$ |
| 7 | | 30 | Perimeter | $D_{max}$ |
| 8 | | 30 | Space | $D_{max}$ |
| 9 | 8 | 20 | Perimeter | $D_{max}$ |
| 10 | | 20 | Space | $D_{max}$ |
| 11 | | 20 | Perimeter | $D_{min}$ |
| 11* | | 20 | Perimeter | $D_{min}$ |
| 12 | 12 | 20 | Perimeter | $D_{max}$ |
| 13 | | 20 | Space | $D_{max}$ |
| 14 | | 20 | Perimeter | $D_{min}$ |
| 12* | | 20 | Perimeter | $D_{max}$ |
| 13* | | 20 | Space | $D_{max}$ |
| 14* | | 20 | Perimeter | $D_{min}$ |
| 15 | 20 | 20 | Perimeter | $D_{max}$ |
| 16 | | 20 | Space | $D_{max}$ |
| 17 | | 20 | Perimeter | $D_{min}$ |
| 18 | | 20 | Space | $D_{min}$ |
| 15* | | 20 | Perimeter | $D_{max}$ |
| 16* | | 20 | Space | $D_{max}$ |
| 17* | | 20 | Perimeter | $D_{min}$ |
| 18* | | 20 | Space | $D_{min}$ |
| * Redesigned according to ASCE 7-02 with minimum base shear | | | | |

### *C.1.3 Preparing Index Archetype Designs and Index Archetype Models*

Each of the index archetype configurations in Table C-3 are used to prepare index archetype designs, which are then used to prepare index archetype models. In this example, index archetype designs for reinforced concrete moment frames were prepared in accordance with the requirements of ASCE/SEI 7-05 and ACI 318-05. Complete adherence to design requirements is essential for adequately evaluating the performance of a class of buildings designed using the proposed system. Designs should address minimum design requirements, should utilize nominal material properties, and should not be overly conservative. Assumptions used in the development of index archetype designs for reinforced concrete moment frames are listed in Table C-4.

While index archetype designs are prepared using nominal material properties and other standard assumptions, index archetype models should be defined based on the expected behavior of the building. For modeling and assessment of the mean performance of reinforced concrete moment frame systems, this included the use of expected material properties, element stiffness assumptions based on test data, tributary slab contributions for beam strength and stiffness, and expected gravity loads.

**Table C-4 Index Archetype Design Assumptions for a Reinforced Concrete Moment Frame System**

| Design Parameter | Design Assumption |
|---|---|
| **Assumed Stiffnesses:** | |
| Member stiffness assumed in design: Beams | $0.5EI_g$ (FEMA 356) |
| Member stiffness assumed in design: Columns | $0.7EI_g$ for all axial load levels (based on practitioner recommendation) |
| Slab consideration | Slab not included in stiffness/strength design of beams |
| Footing rotational stiffness assumed in design: 2-4 story | Effective stiffness of grade beam |
| Footing rotational stiffness assumed in design: 8-20 story | Basement assumed; exterior columns fixed at basement wall, interior columns consider stiffness of first floor beam and basement column |
| Joint stiffness assumed in design | Elastic joint stiffness |
| **Expected Design Conservatisms:** | |
| Conservatism applied in element flexural and shear (capacity) strength design | 1.15 of required strength |
| Conservatism applied in joint strength design | 1.0 of required strength |
| Conservatism applied in strong-column weak-beam design | Use expected ratio of 1.3 instead of 1.2 |

## C.2 Development of Index Archetype Configurations for a Wood Light-Frame Shear Wall System

In this section, index archetype configurations are developed for a wood light-frame shear wall system conforming to design requirements contained in ASCE/SEI 7-05, *Minimum Design Loads for Buildings and Other Structures*. The system consists of wood light-frame bearing wall structures braced with wood structural panel shear walls.

### *C.2.1 Establishing the Archetype Design Space*

The following design variables were considered in the development of index archetype configurations for this system: (1) number of stories; (2) maximum and minimum seismic hazard for the governing Seismic Design Category (SDC D in this case); (3) building occupancy and use; and (4) shear wall aspect ratio.

Wood light-frame buildings of one two three stories are common across most of the United States. Wood light-frame multi-family residential buildings of four to five stories represent a growing trend along the West Coast. The number of stories considered in the archetype design space ranges from one to five.

Minimum and maximum values of design spectral response acceleration, $S_{DS}$, used in this example are 0.375g and 1.00g, respectively. The minimum value of 0.375g is lower than 0.50g specified for SDC D in ASCE/SEI 7-05, but is used in this illustrative example to make use of available designs. An $S_{DS}$ of 1.00g represents the maximum for SDC D for regular structures with short fundamental periods. Design for wind loads is not considered.

The range of building occupancies considered includes residential and commercial occupancies, the latter including educational and institutional uses. The primary difference between residential and commercial buildings is the spacing between shear wall lines, which affects the tributary seismic mass. Residential buildings generally have more walls and closer spacing. A typical spacing of 25 feet between shear wall lines and a tributary width of 12.5 feet for seismic mass was used for residential occupancies. Commercial buildings are more likely to be open configurations with widely spaced shear walls at the perimeter. A typical spacing of 80 feet between shear wall lines and a tributary width of 40 feet for seismic mass was used for commercial occupancies.

Residential occupancies were further split into one- and two-family detached dwellings and multi-family dwellings. One- and two-family detached dwellings were assumed to be one- and two-stories tall, with typical wood-

frame floor weights (without topping slabs). Multi-family dwellings were assumed to be three- to five-stories tall, with floor weights including gypcrete topping slabs.

Shear wall aspect ratios included high aspect ratio shear walls (height/width ratios of 2.7 to 3.3) and low aspect ratio shear walls (height/width ratios of 1.5 or less). In accordance with ASCE/SEI 7-05, a capacity reduction was considered for high aspect ratio shear walls, resulting in the need for configurations with more dense nailing patterns.

### *C.2.2 Identifying Index Archetype Configurations and Populating Performance Groups*

In order to completely address the identified set of design variables, a set of 40 index archetype configurations would be required (5 heights x 2 seismic hazard levels x 2 uses x 2 wall aspect ratios). This was reduced to a set of 20 index archetype configurations based on the predominant use of high aspect ratio shear walls in residential buildings and low aspect ratio shear walls in commercial buildings. An additional four configurations were eliminated because the specific combinations of parameters do not currently exist in the building stock of wood light-frame construction. The resulting set of 16 index archetype configurations for wood light-frame shear wall systems are described in Table C-5.

### *C.2.3 Preparing Index Archetype Designs and Index Archetype Models*

Each of the index archetype configurations in Table C-5 are used to prepare index archetype designs, which are then used to prepare index archetype models. In this example, index archetype designs were prepared in accordance with the requirements of ASCE/SEI 7-05, considering only the contribution of wood structural panel sheathing, and ignoring the possible beneficial effects of gypsum wallboard that is likely to be present.

Designs were initially performed using a response modification coefficient, $R$, equal to 6. Index archetype designs, including number of piers, sheathing, and fasteners for $R$=6 are provided in Table C-6.

**Table C-5 Index Archetype Configurations for Wood Light-Frame Shear Wall Systems**

| Model | Stories | Seismic Hazard ($S_{DS}$) | Tributary Width for Seismic Mass (ft) | Floor Unit Weight for Seismic Mass (psf) | Shear Wall Aspect Ratio | Description |
|---|---|---|---|---|---|---|
| 1 | 1 | 1 | 40' | NA | Low | Commercial |
| 2 | 1 | 1 | 12.5' | NA | High | 1&2 Family |
| 3 | 1 | 0.375 | 40' | NA | High | Commercial |
| 4 | 1 | 0.375 | 12.5' | NA | High | 1&2 Family |
| 5 | 2 | 1 | 40' | 30 | Low | Commercial |
| 6 | 2 | 1 | 12.5' | 10 | High | 1&2 Family |
| 7 | 2 | 0.375 | 40' | 30 | High | Commercial |
| 8 | 2 | 0.375 | 12.5' | 10 | High | 1&2 Family |
| 9 | 3 | 1 | 40' | 30 | Low | Commercial |
| 10 | 3 | 1 | 12.5' | 30 | High | Multi-Family |
| 11 | 3 | 0.375 | 40' | 30 | Low | Commercial |
| 12 | 3 | 0.375 | 12.5' | 30 | High | Multi-Family |
| 13 | 4 | 1 | 12.5′ | 30 | High | Multi-Family |
| 14 | 4 | 0.375 | 12.5' | 30 | High | Multi-Family |
| 15 | 5 | 1 | 12.5′ | 30 | High | Multi-Family |
| 16 | 5 | 0.375 | 12.5' | 30 | High | Multi-Family |

**Table C-6 Index Archetype Designs for Wood Light-Frame Shear Wall Systems ($R$=6)**

| Model | Story | No. of Piers | Pier Length (ft) | Sheathing | Shear Wall Nailing |
|---|---|---|---|---|---|
| 1 | 1 | 2 | 9.0 | 7/16 OSB | 8d at 6" |
| 2 | 1 | 4 | 3.0 | 7/16 OSB | 8d at 6" |
| 3 | 1 | 4 | 3.0 | 7/16 OSB | 8d at 6" |
| 4 | 1 | 2 | 3.0 | 7/16 OSB | 8d at 6" |
| 5 | 2 | 3 | 8.0 | 7/16 OSB | 8d at 4" |
| | 1 | 3 | 8.0 | 7/16 OSB | 8d at 2" |
| 6 | 2 | 5 | 3.0 | 7/16 OSB | 8d at 6" |
| | 1 | 5 | 3.0 | 7/16 OSB | 8d at 3" |
| 7 | 2 | 5 | 3.0 | 7/16 OSB | 8d at 4" |
| | 1 | 5 | 3.0 | 7/16 OSB | 8d at 2" |
| 8 | 2 | 2 | 3.0 | 7/16 OSB | 8d at 6" |
| | 1 | 2 | 3.0 | 7/16 OSB | 8d at 4" |
| 9 | 3 | 3 | 10.0 | 7/16 OSB | 8d at 6" |
| | 2 | 3 | 10.0 | 7/16 OSB | 8d at 2" |
| | 1 | 3 | 10.0 | 19/32 PLWD | 10d at 2" |
| 10 | 3 | 6 | 3.0 | 7/16 OSB | 8d at 6" |
| | 2 | 6 | 3.0 | 7/16 OSB | 8d at 2" |
| | 1 | 6 | 3.0 | 19/32 PLWD | 10d at 2" |
| 11 | 3 | 2 | 7.0 | 7/16 OSB | 8d at 6" |
| | 2 | 2 | 7.0 | 7/16 OSB | 8d at 3" |
| | 1 | 2 | 7.0 | 7/16 OSB | 8d at 2" |
| 12 | 3 | 3 | 3.0 | 7/16 OSB | 8d at 6" |
| | 2 | 3 | 3.0 | 7/16 OSB | 8d at 3" |
| | 1 | 3 | 3.0 | 7/16 OSB | 8d at 2" |
| 13 | 4 | 6 | 3.3 | 7/16 OSB | 8d at 6" |
| | 3 | 6 | 3.3 | 7/16 OSB | 8d at 2" |
| | 2 | 6 | 3.3 | 19/32 PLWD | 10 at 2" |
| | 1 | 6 | 3.3 | 19/32 PLWD | 10 at 2" |

**Table C-6 Index Archetype Designs for Wood Light-Frame Shear Wall Systems ($R$=6) Continued**

| Model | Story | No. of Piers | Pier Length (ft) | Sheathing | Shear Wall Nailing |
|---|---|---|---|---|---|
| 14 | 4 | 4 | 3.0 | 7/16 OSB | 8d at 6" |
| | 3 | 4 | 3.0 | 7/16 OSB | 8d at 4" |
| | 2 | 4 | 3.0 | 7/16 OSB | 8d at 3" |
| | 1 | 4 | 3.0 | 7/16 OSB | 8d at 2" |
| 15 | 5 | 6 | 3.7 | 7/16 OSB | 8d at 6" |
| | 4 | 6 | 3.7 | 7/16 OSB | 8d at 3" |
| | 3 | 6 | 3.7 | 7/16 OSB | 8d at 2" |
| | 2 | 6 | 3.7 | 19/32 PLWD | 10d at 2" |
| | 1 | 6 | 3.7 | 19/32 PLWD | 10d at 2" |
| 16 | 5 | 4 | 3.3 | 7/16 OSB | 8d at 6" |
| | 4 | 4 | 3.3 | 7/16 OSB | 8d at 4" |
| | 3 | 4 | 3.3 | 7/16 OSB | 8d at 3" |
| | 2 | 4 | 3.3 | 7/16 OSB | 8d at 2" |
| | 1 | 4 | 3.3 | 7/16 OSB | 8d at 2" |

Index archetype designs that did not meet the acceptance criteria using $R$=6 were redesigned using reduced values of $R$=4 and $R$=2. Index archetype designs, including number of piers, sheathing, and fasteners for $R$=4 and $R$=2 designs are provided in Table C-7 and Table C-8, respectively.

**Table C-7 Index Archetype Designs for Wood Light-Frame Shear Wall Systems ($R$=4)**

| Model | Story | No. of Piers | Pier Length (ft) | Sheathing | Shear Wall Nailing |
|---|---|---|---|---|---|
| 1 | 1 | 2 | 10.0 | 7/16 OSB | 8d at 4" |
| 5 | 2 | 3 | 8.0 | 7/16 OSB | 8d at 3" |
| | 1 | 3 | 8.0 | 19/32 PLWD | 10d at 2" |
| 9 | 3 | 1 | 40.0 | 7/16 OSB | 8d at 4" |
| | 2 | 1 | 40.0 | 19/32 PLWD | 10d at 2" |
| | 1 | 1 | 40.0 | 19/32 PLWD | 10d at 2" |

**Table C-8 Index Archetype Designs for Wood Light-Frame Shear Wall Systems ($R=2$)**

| Model | Story | No. of Piers | Pier Length (ft) | Sheathing | Shear Wall Nailing |
|---|---|---|---|---|---|
| 1 | 1 | 3 | 8.0 | 7/16 OSB | 8d at 2" |
| 5 | 2 | 6 | 8.0 | 7/16 OSB | 8d at 3" |
| | 1 | 6 | 8.0 | 19/32 PLWD | 10d at 2" |
| 9 | 3 | 1 | 40.0 | 7/16 OSB | 8d at 6" |
| | 2 | 1 | 80.0 | 19/32 PLWD | 10d at 2" |
| | 1 | 1 | 80.0 | 19/32 PLWD | 10d at 2" |

### *C.2.4 Other Considerations for Wood Light-Frame Shear Wall Systems*

The following considerations were not addressed in this example, but are provided for the purpose of further illustrating the development of index archetype configurations.

A mix of shear wall aspect ratios could very likely occur within a given wood light-frame system. Careful thought should be given as to whether performance groups consisting of all high, all low, or mixed aspect ratio walls will be most representative or most critical. This could change with the system being considered.

It is becoming common practice to mix alternative bracing elements with conventional shear wall bracing in this type of construction. These elements could be designed to carry a small or large portion of the seismic story shear forces. Consideration should be given as to whether the seismic story shear carried by alternative bracing elements needs to be added as another variable in the index archetype configurations.

For wood light-frame systems in particular, finish materials are known to have a very significant impact on the overall collapse behavior of the system. The effects of finish materials should be considered in the context of the system being proposed. It may be appropriate to include a range of finish materials as another variable in the index archetype configurations.

# Appendix D
# Consideration of Behavioral Effects

This appendix illustrates how behavioral effects are considered in the development of index archetype configurations for reinforced concrete moment frame systems conforming to design requirements contained in ASCE/SEI 7-05, *Minimum Design Loads for Buildings and Other Structures*, and ACI 318-05, *Building Code Requirements for Structural Concrete*.

Development of structural system archetypes considers both structural configuration issues and seismic behavioral effects described in Chapter 4. Consideration of structural configuration issues is discussed in Appendix C. Index archetype configurations are eventually used to develop index archetype designs, which are then used to develop index archetype models. Development and calibration of nonlinear index archetype models is described in Appendix E.

## D.1 Identification of Structural Failure Modes

Consideration of seismic behavioral effects includes identifying critical limit states, dominant deterioration modes, and collapse mechanisms that are possible, and assessing the likelihood that they will occur. How a component or system behaves under seismic loading is often influenced by configuration decisions, so behavioral effects and configuration issues should be considered concurrently in the development of index archetype configurations. This process is illustrated in Figure D-1.

Once all possible failure modes have been identified for a given system, the list is narrowed to a subset of likely collapse mechanisms by ruling out failure modes that are unlikely to occur based on system design and detailing requirements, experimental data, engineering judgment, analytical models, or observations from past earthquakes. Remaining failure modes will be assessed though explicit simulation of failure modes through nonlinear analyses, or through evaluation of non-simulated failure modes using alternative limit state checks on demand quantities from nonlinear analyses. Index archetype configurations must address failure modes that will be explicitly simulated in nonlinear analysis models in Chapter 5.

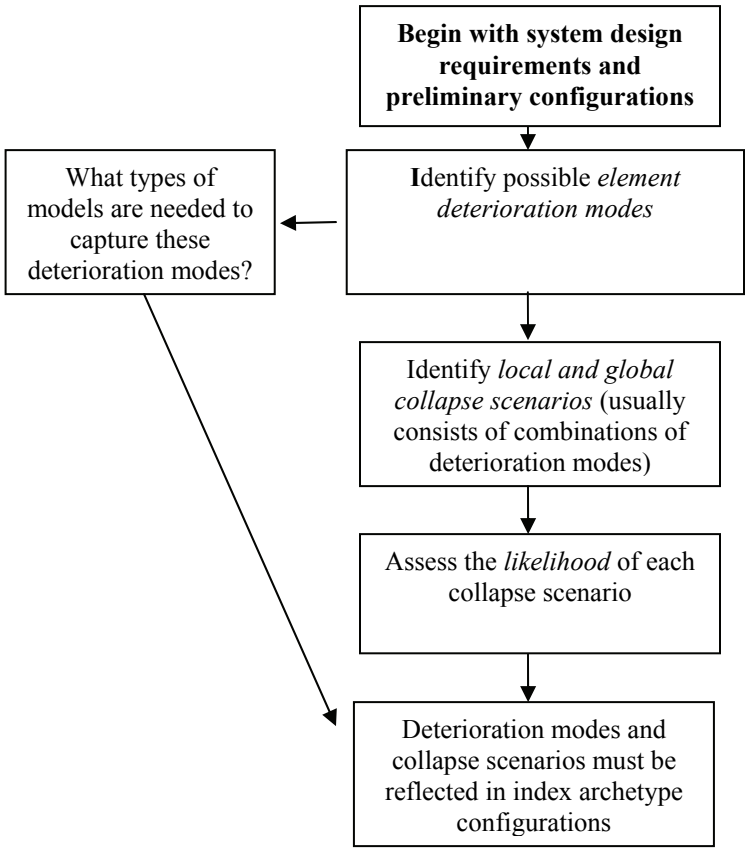


Figure D-1 Consideration of behavioral effects in developing index archetype configurations.

## D.2 System Definition

Possible element deterioration and failure modes are influenced by the material properties, mechanical properties, and design requirements of the proposed seismic-force-resisting system.

Concrete moment frame systems in this example are assumed to meet design requirements for concrete moment frames specified in ASCE/SEI 7-05 and ACI 318-05. For "special" moment frames, these standards provide rigorous and specific design and detailing provisions intended to prevent certain failure modes from occurring, and to promote ductile failure modes in selected members. Special reinforced concrete moment frame requirements include, for example, an upper limit on longitudinal steel reinforcement ratio, seismic hoop detailing, confinement reinforcing in columns and beam-column joints, exclusion of lap splices from hinge regions, strong-column-weak-beam provisions, and other capacity design requirements.

For a proposed seismic-force-resisting system, design and detailing requirements must be well-defined and specific before element deterioration modes and system collapse scenarios can be identified.

## D.3 Element Deterioration Modes

In this example, failure modes have been identified for reinforced concrete moment frame components based on a review of experimental tests, available published information, and observations from past earthquakes. Potential deterioration modes for reinforced concrete moment frame components are listed and shown in Figure D-2. They are classified into five groups (A to F) depending on the type of structural element and the physical behavior associated with deterioration, as shown in Figure D-3. For each mode, currently available nonlinear element models are rated for their ability to simulate the deterioration behavior.

| Deterioration Mode | Element | Behavior | Simulation Model Availability* | Fragility Model Availability | Description |
|---|---|---|---|---|---|
| A | Beam-column | Flexural | 4 | NR | Concrete<br>Concrete spalling<br>Reinforcing bar yielding<br>Concrete core<br>Reinforcing bar buckling (Incl. Stirrup fracture)<br>Reinforcing bar fracture |
| B | Beam-column | Axial compression | 2 | 4 | Concrete crushing, longitudinal bar yielding<br>Stirrup-rupture, longitudinal bar buckling |
| C | Beam-column | Shear<br>Shear +Axial | 1 | 4 | Concrete Shear<br>Transverse tie pull-out of rupture<br>Concrete<br>Loss of aggregate interlock<br>Possible loss of axial load-carrying capacity in columns |
| D | Joint | Shear | 3 | 2 | Panel shear failure |
| E | Reinforcing bar | Pull-out or Bond-slip | 2 | 2 | Reinforcing bar bond-slip or anchorage failure at joint<br>Reinforcing bar lap-splice failure<br>Reinforcing bar pull-out (in beams or at footing) |
| F | Slab Connection | Shear | 2 | 3 | Punching shear or large shear eccentricity at slab column connection, in shear wall structures possible loss of connection between slab and wall<br>Possible vertical collapse of slab |

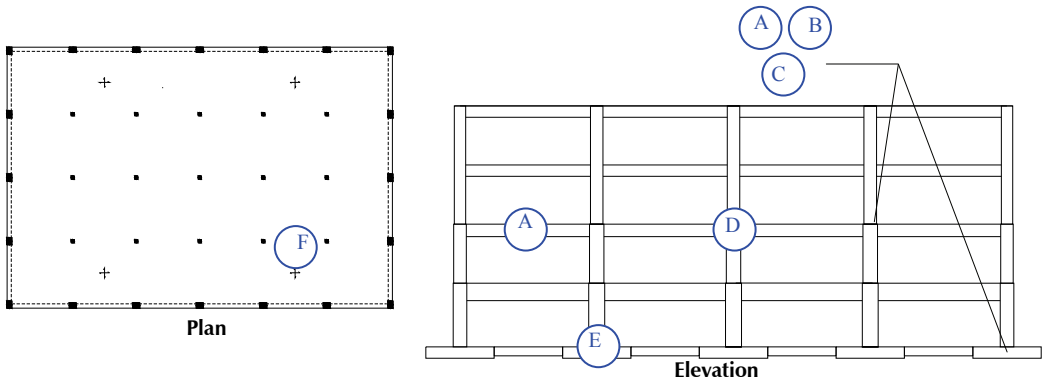


Figure D-2 Reinforced concrete frame plan and elevation views, showing location of possible deterioration modes.

In this example, foundation failure modes have not been included because they are judged not critical for this system. Foundation failure modes should

be considered if they are judged to have a potentially significant effect on the collapse performance of a proposed system.

**A Flexural hinging of beam-column elements, Managua Earthquake, 1972**

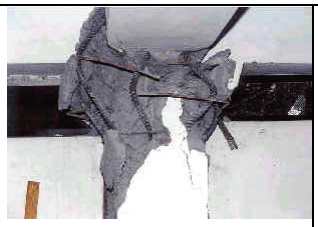

**B Column compressive failure, Chi-Chi Earthquake, 1999**

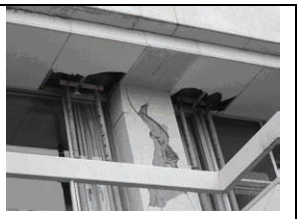

**C Beam-column shear failure, Miyagi earthquake, 2003**

**D Joint shear failure, Chi Chi earthquake, 1999**

**E Pull-out and bond-slip of rebar at connections, Chi Chi earthquake, 1999**

**F Slab-column connection punching shear, Northridge earthquake, 1995**

Figure D-3 Classification of possible deterioration modes for reinforced concrete moment frame components.[1]

[1] Photo sources: (A) nisee.berkeley.edu/thumbnail/6257_3021_0662/ IMG0071.jpg (B) www.structures.ucsd.edu/Taiwaneq/buildi25.jpg (C) www.disaster.archi.tohoku.ac.jp/ eng/topicse/ 030726htm/5-28.jpg (D) www.structures. ucsd.edu/ Taiwaneq/ buildi21.jpg (E) www.structures.ucsd.edu/Taiwaneq/buildil9.jpg (F) www.nbmg.unr.edu/nesc/bobcox/ndx2.php

### *D.3.1 Flexural Hinging of Beam and Columns*

Deterioration Mode 'A' consists of flexural hinging in beams and columns and associated concrete spalling, concrete core crushing, stirrup fracture, and reinforcing bar yielding, buckling and fracture. Reinforcing bar yielding, concrete core crushing, and the associated strength and stiffness degradation, can be simulated fairly accurately. In contrast, modeling of buckling and fracture of longitudinal reinforcement, or stirrup fracture is less accurate. These behaviors are important contributors to the deterioration of strength and stiffness in reinforced concrete frame elements at large deformations near collapse.

Fiber-type models capture the spread of plasticity along the length of the element and the constituent concrete models can be calibrated to adequately model the behavior associated with concrete deterioration from cracking to crushing (Haselton et al, 2007). However, currently available steel material models are not able to replicate the behavior of rebar as it buckles and fractures. Due to this limitation, current fiber models were judged inadequate for simulating collapse. While lumped plasticity models do not have the precision of fiber models, they can be calibrated to capture the deterioration associated with rebar buckling and stirrup fracture leading to loss of confinement (Haselton 2006; Ibarra 2003).

### *D.3.2 Shear Failure of Beam and Columns*

Deterioration Mode 'C' corresponds to shear failure of beam-columns, characterized by shear cracking in concrete and yielding and/or pull-out of transverse stirrups. This mode of deterioration is particularly dangerous for columns with significant axial load. Shear deterioration and increased displacement demands can lead to subsequent vertical collapse of the column (Elwood 2005), and possibly progressive collapse of a structure.

Modeling the cyclic response of a reinforced concrete element experiencing shear deterioration is complex due to interactions between shear, moment, and axial force, as well as the overall brittle nature of the deterioration mode. Elwood (2004) and others have simulated deterioration in the lateral strength and stiffness of a column by adding a shear spring. To date, models for vertical collapse of columns following shear failure have been challenged by a lack of experimental data for columns experiencing vertical collapse.

Due to the brittle nature of this failure mode, special and intermediate moment frames in seismically active areas are required to utilize capacity design principles that ensure flexural hinging prior to shear failure (ACI

2005). Capacity design requirements, however, do not apply to ordinary concrete moment frames. Due to limitations in the ability to directly simulate shear failure, this mode is treated as a non-simulated collapse mode in evaluating ordinary moment frame systems.

### *D.3.3 Joint Panel Shear Behavior*

Deterioration Mode 'D' is associated with deterioration in shear strength and stiffness of the joint panel region. In reinforced concrete frame models, shear panels are modeled with an inelastic rotational spring inserted at the joint (Lowes et al. 2004, Altoontash 2004). This joint modeling capability is available in OpenSees (Altoontash 2004) and in most structural analysis software (ATC 1996, pp. 9-11).

Several researchers have used a detailed approach that employs the modified compression field theory (Vecchio 1986, Stevens 1991) to develop a monotonic backbone that relates the panel shear force to the shear deformation angle (Altoontash 2004, Lowes 2004). Modified compression field theory has been shown to work well for conforming joints, but is not as reliable for non-conforming joints with less confinement (Lowes, 2005, personal communication). Modeling of joint shear behavior is especially important for joints that are not protected by capacity design requirements (e.g., ordinary concrete moment frame systems).

### *D.3.4 Bond-Slip of Reinforcing Bars*

Deterioration Mode 'E' corresponds to slip of the reinforcing bar relative to the surrounding concrete, including anchorage pull-out, bond slip, and splice failure. The extent of slip, and the possible occurrence of bar pull-out, depends on the embedded length, bar diameter, concrete strength, and the number and magnitude of load cycles.

Slip without pull-out occurs when the embedment or splice length is sufficient to prevent the cut end of the rebar from moving relative to the surrounding concrete, even under cyclic loading. The effects of slip without pull-out include: (1) decreased pre-yield stiffness, (2) decreased post-yield stiffness, and (3) increased element plastic deformation capacity. These effects are included in the calibration of the plastic hinges for reinforced concrete moment frame models.

Slip with pull-out occurs when the rebar slips relative to the concrete over the full length of embedment. This occurs when the embedment or lap splice lengths are relatively short, as is typical of ordinary concrete moment frames. Slip with pull-out can lead to severe reduction in strength and stiffness, as

well as a significant reduction in plastic rotation capacity. Models for pull-out are moderately well developed and range from continuum finite element models (which attempt to model the interface between the rebar and concrete) to simple rotational spring models.

### *D.3.5 Punching Shear in Slab-Column Connections*

Deterioration Mode 'F' corresponds to punching shear in slab-column connections or in wall-slab connections. Following punching shear failure, a slab may experience local collapse depending on the gravity load intensity and continuity of reinforcement in the area of the slab-column connection (Aslani 2005).

Punching shear deterioration can be modeled with a standard nonlinear lumped plasticity spring. The resulting vertical collapse is difficult to directly simulate, so this failure mode is treated as a non-simulated collapse mode (Aslani and Miranda 2005a, Aslani 2005).

## D.4 Local and Global Collapse Scenarios

Collapse occurs when seismic loading causes element deterioration modes to combine in a way that forms a sidesway collapse mechanism or a vertical (local) collapse mechanism. For reinforced concrete frame systems, possible collapse scenarios and contributing element deterioration modes are identified and organized as shown in Figure D-4. These scenarios were established using engineering judgment based on examination of collapses in previous earthquakes, experimental test data, and analytical studies.

## D.5 Likelihood of Collapse Scenarios

Figure D-4 includes the range of possible collapse scenarios for reinforced concrete frame structures. From this list, the scenarios which are most likely to occur for each type of moment frame (ordinary, intermediate, and special) are identified.

Changes in detailing requirements for different reinforced concrete frame systems govern which collapse modes are likely to occur for that system. Design requirements for special concrete moment frames (ACI 2005) are designed to promote ductile collapse modes, and to prevent the formation of brittle collapse modes. These requirements serve to limit the likelihood of several possible collapse modes.

**Sidesway Collapse Scenarios**

| Scenario | Element Deterioration Mode | | | | | | Description |
|---|---|---|---|---|---|---|---|
| | A | B | C | D | E | F | |
| FS1 | ■ | | | | | | Beam and column flexural hinging, forming sidesway mechanism |
| FS2 | ■ | | | | | | Column hinging, forming soft-story mechanism; a combination soft-story and |
| FS3 | ■ | | ■ | | | | Beam or column flexural-shear failure, forming sidesway mechanism |
| FS4 | ■ | | | ■ | | | Joint-shear failure, possibly with beam and/or column hinging |
| FS5 | ■ | | | | ■ | | Reinforcing bar pull-out or splice failure in columns or beams, leading to sidesway mechanism |

**Vertical Collapse Scenarios**

| Scenario | Element Deterioration Mode | | | | | | Description |
|---|---|---|---|---|---|---|---|
| | A | B | C | D | E | F | |
| FV1 | | | ■ | | | | Column shear failure, leading to column axial collapse |
| FV2 | ■ | | ■ | | | | Column flexure-shear failure, leading to column axial collapse |
| FV3 | | | | | | ■ | Punching shear failure, leading to slab collapse |
| FV4 | | | | | | | Failure of floor diaphragm, leading to column instability |
| FV5 | | ■ | | | | | Crushing of column, leading to column axial collapse; possibly from overturning effects |

Figure D-4 Collapse scenarios for reinforced concrete moment frame components.

In comparison, ordinary moment frames are vulnerable to a wider range of possible collapse modes, due to less stringent design requirements. Several researchers (Aycardi et al. 1994; Kunnath et al. 1995a, Filiatrault et al. 1998) have noted the tendency for soft story or column-hinging mechanisms to form in ordinary concrete moment frames. In addition, ordinary concrete moment frames might experience lap-splice failure, pull-out of reinforcing bars at beam-column joints, and column shear failures. The behavior of intermediate moment frames is anticipated to be somewhere between special and ordinary moment frames.

The likelihood of each collapse scenario for special, intermediate, and ordinary moment frames is shown in Figure D-5. Depending on the proposed system, and associated design requirements, there may be one or several collapse modes that are likely to occur.

| Systems | Sidesway Collapse | | | | | Vertical Collapse | | | | | |
|---|---|---|---|---|---|---|---|---|---|---|---|
| | FS1 | FS2 | FS3 | FS4 | FS5 | FV1 | FV2 | FV3 | FV4 | FV5 | FV6 |
| SMF | H | M | L | L | L | L | L | L | L | L-M | L-M |
| IMF | H | M-H | L | M | M | L | L | L | M | L-M | L-M |
| OMF | H | H | H | H | H | M | H | M | M | M-H | M-H |

SMF: Special reinforced concrete moment frame
IMF: Intermediate reinforced concrete moment frame
OMF: Ordinary reinforced concrete moment frame
H: High
M: Medium
L: Low

Figure D-5 Likelihood of collapse scenarios by frame type.

## D.6 Collapse Simulation

For reinforced concrete moment frame systems, possible collapse modes are considered in the context of the three-bay variable-height archetype frame model described in Appendix C. Index archetype configurations must account for all collapse scenarios that have been identified as likely to occur, and will be explicitly simulated in the nonlinear index archetype models. Critical limit states or failure modes that cannot be explicitly simulated in index archetype models are evaluated using the procedure for non-simulated collapse modes.

# Appendix E

# Nonlinear Modeling of Reinforced Concrete Moment Frame Systems

## E.1 Purpose

This appendix describes the development of nonlinear index archetype models used for collapse assessment of reinforced concrete (RC) special moment frame (SMF) and reinforced concrete ordinary moment frame (OMF) example structures presented in Chapter 9. It includes an overview of critical modeling decisions and a description of the calibration procedures used for beam-column element models.

Although the information is specific to reinforced concrete moment frame systems, the example is illustrative of the issues and considerations typical of nonlinear collapse simulation for any structural system type. Similar procedures were used to create nonlinear models for the wood light-frame system presented in Chapter 9, and the steel special moment frame system presented in Chapter 10.

## E.2 Structural Modeling Overview

Structural models must be capable of simulating the accrual of structural damage and the resulting sidesway collapse when a structure is subjected to severe ground shaking. Identification of key deterioration and collapse modes is an important precursor to the choice of the nonlinear analysis model. Consideration of structural configuration issues for reinforced concrete moment frames is discussed in Appendix C. Consideration of behavioral effects is described in Appendix D. The seismic-force-resisting system is represented by a two-dimensional, three-bay index archetype configuration. The destabilizing $P$-$\Delta$ effects are modeled using a leaning column. At the element level, frames are modeled with the following features illustrated in Figure E-1: beam-column elements with concentrated inelastic rotational hinges at each end and finite size beam-column joints that employ five concentrated inelastic springs to model joint panel shear distortion and bond slip at each face of the joint. The collapse behavior is simulated using the OpenSees software (PEER 2006).

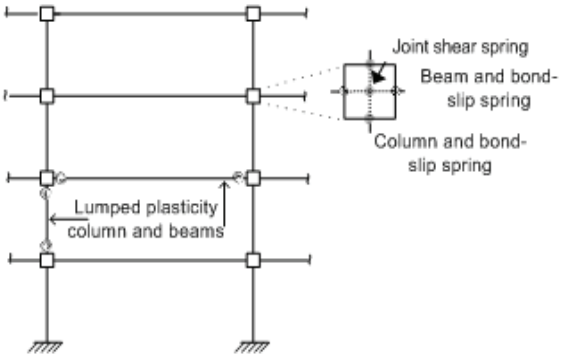


Figure E-1 Schematic diagram, illustrating key elements of nonlinear frame model.

Although not shown in Figure E-1, the effect of foundation flexibility on the archetype models is incorporated using elastic, semi-rigid rotational springs at the base of the column. For shorter frame structures (fewer than 4 stories), the stiffness of the rotational springs is determined from assumed grade beam and soil stiffness. For taller buildings, the structure is assumed to have a basement, exterior columns are assumed to be fixed (connected to the basement wall), and the properties of the rotational spring attached to interior columns are computed based on the basement column and beam stiffnesses.

## E.3 Beam-Column Element Model

Since the damage is likely to concentrate in the beams and columns of the RC moment frame structures, accurate modeling of the inelastic effects in beam and column elements is an essential component of collapse modeling of these structures. As shown in Figure E-1, the beam-column elements of the lateral resisting frame are modeled with lumped plasticity elements in the plastic hinge locations. Lumped plasticity elements are frequently used in structural analysis models, and their use here follows the precedent established in ASCE/SEI 41-06 (ASCE 2006) and other guideline documents. When calibrated properly, they are capable of capturing degradation of strength and stiffness that is essential to collapse modeling. Their properties can also be easily modified in sensitivity analysis to determine the effects of uncertainties in material modeling.

Researchers have also used a variety of other methods to simulate cyclic response of RC beam-columns, including creating fiber models which can capture cracking behavior and the spread of plasticity throughout the element (see eg. Filippou, 1999) The decision to use a lumped-plasticity approach here was based on simplicity, and an inherent limitation in the fiber element formulation which makes simulation of the strain softening associated with rebar buckling difficult. It should be noted, however, that the choice of

element model should be carefully evaluated for any given structural system, and with careful consideration of available simulation technologies.

In this section, the properties of the lumped plasticity elements used to model the example RC SMF structures are illustrated, including descriptions of both the element model used and the process through which the key modeling parameters were calibrated. The calibration process described here demonstrates the level of detail and sophistication that it is possible in studies of this type. Depending on the structural system and type of analytical model, a greater or lesser degree of detail may be required.

### *E.3.1 Element and Hysteretic Model*

Lumped plasticity element models for the RC SMF structures utilize a material model developed by Ibarra, Medina, and Krawinkler (2005, 2003), and implemented in OpenSees. This model is chosen because it is capable of capturing the important modes of deterioration that precipitate sidesway collapse of RC frames, but one could imagine using another material model and/or software platform that also met these requirements.

Figure E-2 shows the tri-linear monotonic backbone curve and associated hysteretic rules of the model, which permit versatile modeling of cyclic behavior. For simulating structural collapse, the most important aspect of this model is the post-peak response, which enables modeling the strain softening behavior associated with concrete crushing, rebar buckling and fracture, and/or bond failure. The model also captures four basic modes of cyclic deterioration: (1) strength deterioration of the inelastic strain hardening branch; (2) strength deterioration of the post-peak strain softening branch; (3) accelerated reloading stiffness deterioration; and (4) unloading stiffness deterioration. Cyclic deterioration is based on an energy index that includes normalized energy dissipation capacity ($\lambda$) and an exponent term to describe how the rate of cyclic deterioration changes with accumulation of damage (c).

This element model requires the specification of seven parameters to control the monotonic and cyclic behavior of the model: $M_y$, $\theta_y$, $M_c/M_y$, $\theta_{cap,pl}$, $\theta_{pc}$, $\lambda$, and $c$. The post-yield and post-capping stiffnesses are quantified by $M_c/M_y$ and $\theta_{pc}$; $K_s$ and $K_c$ can be easily computed as $K_s = K_e\left(\theta_y/\theta_{cap,pl}\right)\left(\left(M_c - M_y\right)/M_y\right)$ and $K_c = -K_e\left(\theta_y/\theta_{pc}\right)\left(M_c/M_y\right)$. These symbols are defined in the notation list and Figure E-2.

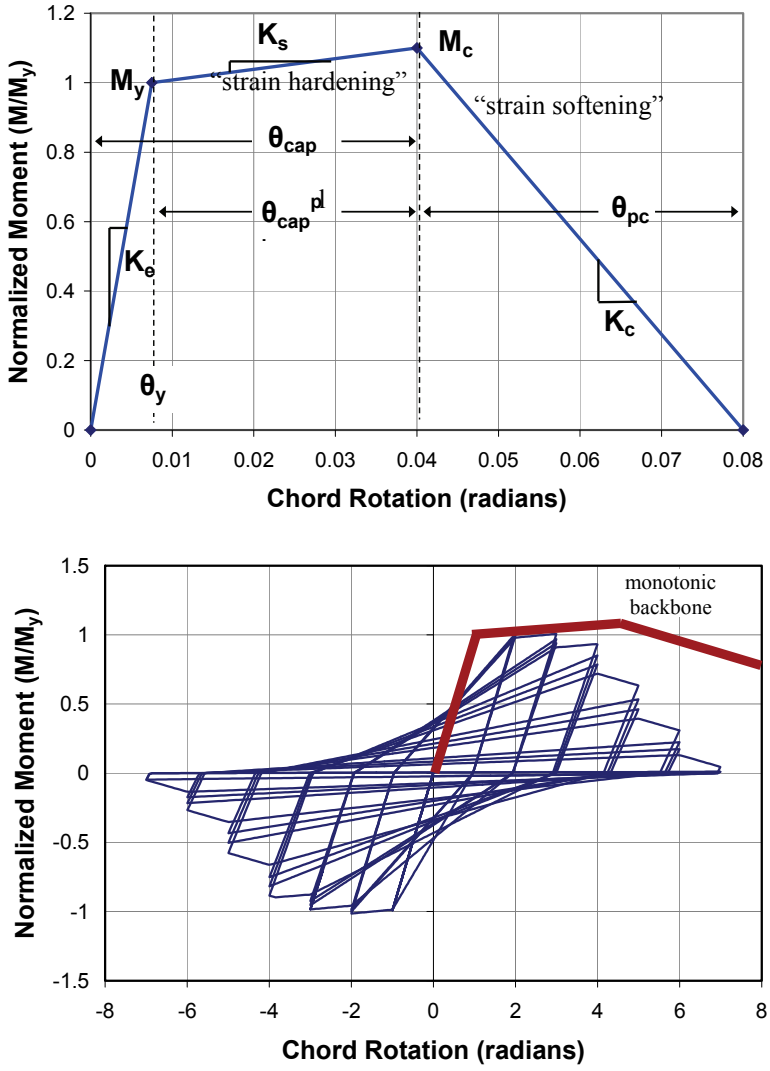


Figure E-2 Monotonic and cyclic behavior of component model used to model beam-column elements.

In order to determine the appropriate values of each of these parameters, the model was carefully calibrated to 255 experimental tests of reinforced concrete columns. These calibrations were then used to develop empirical equations relating the design parameters of a beam-column to the modeling parameters needed for input in the lumped plasticity model. All calibrations are based on mean values, unlike, for example, the conservative values given in the FEMA 356/ASCE 41 documents. This type of calibration procedure can be used in conjunction with any type of material model, provided that there is sufficient test data available.

### *E.3.2 Calibration of Parameters for the RC Beam-Column Element Model*

**Experimental Database**

Parameters of the material model are calibrated with data from the PEER Structural Performance Database (PEER 2006a, Berry et al. 2004), assembled by Berry and Eberhard. This database includes the results of cyclic and monotonic tests of 306 rectangular columns and 177 circular columns. For each column test, the database reports the force-displacement time history, the column geometry and reinforcement information, the failure mode, and other relevant information. All data is converted to that of an equivalent cantilever, regardless of experimental setup.

From this database, rectangular columns failing in a flexural mode (220 tests) or in a combined flexure-shear mode (35 tests) were selected, for a total of 255 tests. These tests cover the typical range of column design parameters: $0.0 < v < 0.7$, $0.0 < P/P_b < 2.0$, $1.5 < L_s/H < 6.0$, $20 < f'_c\ (MPa) < 120$, $340 < f_y\ (MPa) < 520$, $0.015 < \rho < 0.043$, $0.1 < s/d < 0.6$, $0.002 < \rho_{sh} < 0.02$. These symbols are defined in the notation list.

**Calibration Procedure**

In order to calibrate the element model parameters, we modeled each column test in the database as a cantilever column in OpenSees, idealized using an elastic element and a zero-length Ibarra model plastic hinge at the column base. The properties of the plastic hinge are the subject of this calibration effort. This report provides only a brief description of the calibration process. The interested reader is referred to Haselton et al. (2007) for more details.

The calibration of the beam-column element model to the data from each experimental test was done systematically and, referring to Figure E-3, each test was calibrated according to the following standardized procedure. First, the yield shear force (1) was estimated visually from the experimental results. Then, the "yield" displacement (2) was calibrated as the point of a significant observed change in lateral stiffness, i.e. where rebar yielding or significant concrete crushing occurs. Calibration of this point often required judgment, since concrete response is nonlinear well before rebar yielding. In addition, displacement at 40% of the yield force (3) was calibrated to provide an estimate of initial stiffness. In step (4), the post-yield hardening stiffness was visually calibrated.

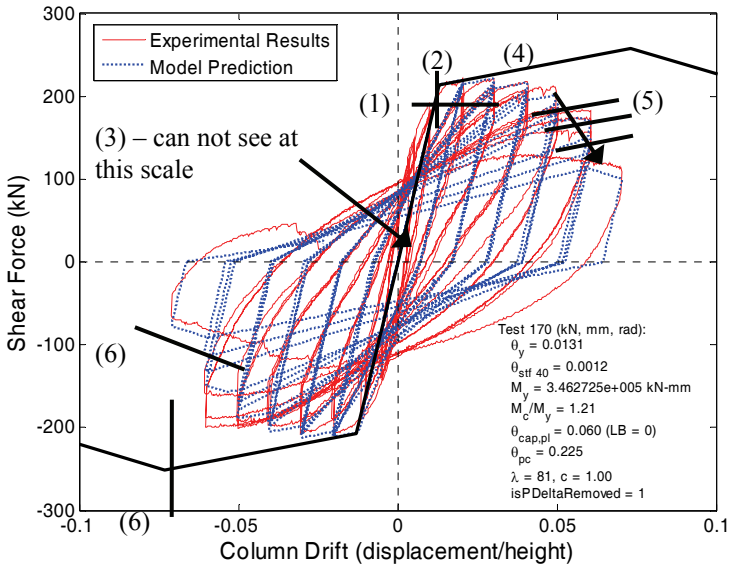


Figure E-3 Example of calibration procedure; calibration of RC beam-column element to experimental test by Saatcioglu and Grira, specimen BG-6.

The next step (5) was to calibrate the normalized cyclic energy dissipation capacity, $\lambda$. The element model allows cyclic deterioration coefficients $\lambda$ and $c$ to be calibrated independently for each of the four cyclic deterioration modes. However, based on a pilot study of 20 columns, $c = 1.0$ was found to be acceptable for columns failing in flexure and flexure-shear modes. The deterioration rates, $\lambda$, were set to be equal for the basic strength and post-capping strength deterioration modes, following recommendations by Ibarra (2003). Based on observations of the hysteretic response of the RC columns, no accelerated stiffness deterioration was used. Unloading stiffness deterioration was neglected to avoid an error in the OpenSees implementation of the element model; in future, unloading stiffness deterioration should be employed, as it leads to better modeling of cyclic response. These simplifications reduce the calibration of cyclic energy dissipation capacity to one parameter ($\lambda$). When calibrating $\lambda$, the aim was to match the average deterioration for the full displacement history, but with a slightly higher emphasis on matching the deterioration rate of the later, more damaging, cycles.

The final step of the calibration process (6) involved quantification of the capping point and the post-capping deformation capacity. It has been shown (eg. Haselton et a. 2007) that incorrect calibration of strength deterioration can have a significant impact on structural response prediction, and the calibration procedure carefully distinguished between in-cycle and (cyclic) strength deterioration. The capping point and post-capping stiffness were only calibrated when a negative post-peak stiffness was clearly observed in

the data, such that strength loss occurs within a single cycle (often called "in-cycle strength deterioration"). Often the test specimen did not undergo sufficient deformations for a capping point to be observed. In such cases where the data do not reveal the capping point, a lower bound value of the capping point was calibrated.

It should be noted that the hinge model is based on the definition of a monotonic backbone and cyclic deterioration rules. This calibration relied primarily on cyclic tests with many cycles to calibrate both the monotonic backbone parameters and the cyclic deterioration rules. As a result, the monotonic backbone and the cyclic deterioration rules are interdependent, and the approximation of the monotonic backbone depends on cyclic deterioration rules assumed and, to some extent, the displacement pattern used in experimental tests. This approximation of the monotonic backbone from cyclic data is not ideal, but is necessary because of sufficient data is not available to calibrate the monotonic and cyclic behavior separately.

A full table of calibrated model parameters for each of the 255 experimental tests used can be found in the extended report on this study (Haselton et al. 2007).

**Interpretation of Calibration Results and Regression Analysis**

Calibrated model parameters from the 255 column tests are used to create empirical equations that predict model parameters based on the column design parameters. The functional form used in regression analysis was carefully determined based on trends in the data and isolated effects of individual variables, previous research and existing equations, and judgment based on mechanics and expected behavior. As is often done, the regression analysis was performed using the natural logarithm of the model parameter, and the logarithmic standard deviation quantifies the uncertainty. The parent report on this study provides more details on how the data was dissected to create empirical regression equations to predict each model parameter (Haselton et al. 2007).

As noted previously, those test specimens in which post-capping behavior was not observed were calibrated with a lower-bound value for deformation capacity. In the regression analysis, this lower-bound calibration data was given special consideration. . In order to take advantage of the lower bound data, without unnecessarily biasing the results, the deformation capacity equations presented here are based on all of the data, and the prediction uncertainties are reported based on only the data with an observed capping point in order to avoid reporting the artificially high uncertainty associated with the lower bound data. Note that this approach is still conservative for

elements with high deformation capacity because the lower-bound data underestimates the actual deformation capacity.

**Proposed Equations**

Predictive equations were developed for each of the parameters of the element model for reinforced concrete columns. Each equation includes all statistically significant parameters, unless otherwise noted. The extended report and paper on this study also include more simplified equations (Haselton et al. 2007).

**Effective Initial Stiffness ($EI_y/EI_g$ and $EI_{stf}/EI_g$)**

Due to nonlinearities in RC behavior associated with cracking, the definition of the stiffness of a RC element depends on the load and deformation level. In this work, two values of effective stiffness are defined: (a) the secant stiffness to the yield point of the component (termed $EI_y$ or $K_e$), and (b) the secant stiffness to 40% of the yield force of the component (termed $EI_{stf}$). $EI_{stf}$ is used in the creation of the structural models in Example 9.2, based on a study by Haselton et al. (2007). The component stiffness includes all modes of deformation, including flexure, shear, and bond-slip.

The equation for secant stiffness to yield depends on both axial load ratio and shear span ratio of the column, and is given as follows:

$$\frac{EI_y}{EI_g} = -0.07 + 0.59\left[\frac{P}{A_g f_c^{'}}\right] + 0.07\left[\frac{L_s}{H}\right] \qquad \text{(E-1)}$$

where $0.2 \le \frac{EI_y}{EI_g} \le 0.6$

This equation represents the mean value of effective stiffness to yield. The prediction uncertainty, assuming the residuals are lognormally distributed, is given by the logarithmic standard deviation: $\sigma_{LN} = 0.28$ . $R^2$, a measure of the extent to which the proposed equation explains the data, is 0.80. For this and all equations to follow, these values are reported below in Table G-1. The upper and lower limits on the stiffness were imposed because there is limited data for columns with very low axial loads and, at high levels of axial load, the positive trend diminishes and the scatter in the data is large. The limits were chosen based on a visual inspection of the data.

The effective initial stiffness, defined as the secant stiffness to 40% of the yield force of an RC column, can be predicted as follows:

$$\frac{EI_{stf}}{EI_g} = -0.02 + 0.98\left[\frac{P}{A_g f_c'}\right] + 0.09\left[\frac{L_s}{H}\right] \qquad \text{(E-2)}$$

where $0.35 \le \frac{EI_{stf}}{EI_g} \le 0.8$

For a typical column, Equation (E-2) predicts the initial stiffness will be approximately 1.7 times stiffer than the secant stiffness to yield (Equation (E-1)).

The effective stiffness of reinforced concrete columns has been the subject of much research; for comparison, selected studies are presented here. FEMA 356 guidelines (FEMA 2000a) permit the use of standard simplified values based on the level of axial load for linear analysis: $0.5E_cI_g$ when $P/\left(A_g f'_c\right) < 0.3$, and $0.7E_cI_g$ when $P/\left(A_g f'_c\right) > 0.5$. More recently, Elwood and Eberhard (2006) proposed an equation for effective stiffness that includes all components of deformation (flexure, shear, and bond-slip), where the effective stiffness is defined as the secant stiffness to the yield point of the component. Their equation proposes $0.2E_cI_g$ when $P/\left(A_g f'_c\right) < 0.2$, $0.7E_cI_g$ when $P/\left(A_g f'_c\right) > 0.5$, with a linear transition between these two extremes.

The equations proposed here for $EI_y$ are similar to those recently proposed by Elwood and Eberhard (2006), but also includes an $L_s/H$ term. Due to this additional term, the proposed Equation (E-1) has a lower prediction uncertainty of $\sigma_{LN} = 0.28$, as compared to the coefficient of variation of 0.35 reported by Elwood et al. The stiffness predictions in FEMA 356 (FEMA 2000) are much higher than the values of $EI_y$ predicted in this study, and slightly larger than the predicted values of $EI_{stf}$. Elwood and Eberhard (2006) found that most of this difference can be explained if it is assumed that the FEMA 356 values only include flexural deformation, and do not account for the bond-slip deformations, which can account for a significant proportion of an element's flexibility.

**Flexural Strength ($M_y$)**

Panagiotakos and Fardis (2001) have published equations to predict flexural strength. Their equation works well, so for this study their method is used to predict $M_y$. When comparing the calibrated values to flexural strength for the 255 columns to predictions by Panagiotakos and Fardis (2001) for these columns, the median ratio of $M_y / M_{y,\text{Fardis}}$ is 0.97, and the coefficient of variation is 0.36.

**Plastic rotation capacity ($\theta_{cap,pl}$)**

The following equation is proposed for predicting plastic rotation capacity, including all parameters that are statistically significant:

$$\theta_{cap,pl} = 0.12\left(1+0.55a_{sl}\right)\left(0.16\right)^{v}\left(0.02+40\rho_{sh}\right)^{0.43} \left(0.54\right)^{0.01c_{units}f_c'}\left(0.66\right)^{0.1s_n}\left(2.27\right)^{10.0\rho} \quad \text{(E-3)}$$

Possible correlations between $\rho_{sh}$ and $s_n$ were verified to be small to eliminate concerns regarding collinearity in regression. This equation is based on all data, including the lower bound data for plastic rotation capacity, as discussed previously. The shear span ratio ($L_s/H$) is notably absent from the predictive equations for rotation capacity. The stepwise regression process consistently showed the shear-span ratio to be statistically insignificant. These findings differ from those of Panagiotakos and Fardis (2001).

The experimental data used in this study is limited to tests of columns with symmetrical arrangements of reinforcement and, as a result, Equation (E-3) applies only to columns with symmetric reinforcement. To eliminate the symmetric reinforcement limitation from the rotation capacity equation, it is proposed to multiply the rotation capacity obtained from these equations by the term proposed by Fardis et al. (2003), which accounts for the ratio between the areas of compressive and tensile steel.

It is also useful as verification to compare the predicted rotation capacity to the ultimate rotation capacity predicted by Fardis et al., based on their study of 700+ reinforced concrete elements, including beams, columns and walls (Fardis and Biskinis 2003, Panagiotakos and Fardis 2001). The Fardis et al. equation consistently predicts higher values, which is expected since Equation (E-3) predicts the capping point and the Fardis equation is based on the ultimate (20% strength loss) point. To make a more consistent comparison, the Fardis et al. predictions of the ultimate rotation (at 20% strength loss) are combined with the calibrated values of post-capping slope ($\theta_{pc}$) to back-calculate a prediction of $\theta_{cap,pl}$ from the Fardis et al. equation. This comparison shows that the proposed equation here predicts lower deformation capacity, with a mean ratio of 0.94 and a median ratio of 0.69. Based on this comparison, Equation (E-3) likely still includes some conservatism. This conservatism exists even though even though the predicted deformation capacities are already much higher than what is typically used; for example, values in FEMA 273/356 are typically less than one-half of those shown in Table E-2.

**Post-capping Rotation Capacity ($\theta_{pc}$)**

Previous research on predicting post-capping rotation capacity has been limited, despite its important impact on predicting collapse capacity. The key parameters considered in the development of an equation for post-capping response are those that are known to most impact deformation capacity: axial load ratio (ν), transverse steel ratio ($\rho_{sh}$), rebar buckling coefficient ($s_n$), stirrup spacing, and longitudinal steel ratio. The equation is based on only those tests where a post-capping slope was observed. The proposed equation for post-capping rotation capacity is as follows:

$$\theta_{pc} = (0.76)(0.031)^{\nu}(0.02 + 40\rho_{sh})^{1.02} \leq 0.10 \qquad \text{(E-4)}$$

The upper bound imposed on Equation (E-4) is due to lack of reliable data for elements with shallow post-capping slopes. The upper limit of 0.10 may be conservative for well-confined, conforming elements, but the existing test data does not justify using a larger value.

**Post-Yield Hardening Stiffness**

Regression analysis shows that axial load ratio and concrete strength statistically impact the prediction of hardening stiffness ($M_c/M_y$). Even so, inclusion of both of the parameters scarcely improved the regression analysis, so a constant value of $M_c/M_y$ is recommended. Equation (E-5) led to an acceptably low prediction uncertainty of $\sigma_{LN} = 0.10$.

$$M_c/M_y = 1.13 \qquad \text{(E-5)}$$

**Cyclic Energy Dissipation Capacity**

Based on the observed trends in the data, the following equation is proposed for the mean energy dissipation capacity, including all statistically significant predictors:

$$\lambda = (131.0)(0.18)^{\nu}(0.26)^{s/d}(0.57)^{V_p/V_n}(61.4)^{\rho_{sh,eff}} \qquad \text{(E-6)}$$

As discussed previously this value is calibrated for both types of strength deterioration and should be used with c = 1.0.

**Discussion of Proposed Equations**

The proposed equations can be evaluated to determine (a) how well they reflect the mean tendencies in the data, and (b) whether they provide suitably small prediction errors. Table E-1 reports the median ratio of predicted to observed values (from model calibrations) for each proposed equation. The regression analyses (eg. Equations (E-1) – (E-6)) assumed the prediction

uncertainty is lognormally distributed, so this median ratio should be close to 1.0; this ratio varies between 1.00 and 1.06 for the proposed equations, showing that the predictive equations have little bias.

**Table E-1 Prediction Uncertainties and Bias in Proposed Equations**

| Equation | Median (predicted/observed) | $\sigma_{ln}$ | $R^2$ |
|---|---|---|---|
| Effective Stiffness to Yield (E.1) | 1.03 | 0.28 | 0.80 |
| Effective Stiffness to 40% Yield (E.2) | 1.02 | 0.33 | 0.59 |
| Plastic Rotation Capacity (E.3) | 1.02 | 0.54 | 0.60 |
| Post-Capping Rotation Capacity (E.4) | 1.00 | 0.72 | 0.51 |
| Post-Yield Hardening Stiffness (E.5) | 1.01 | 0.10 | n/a |
| Cyclic Energy Dissipation Capacity (E.6) | 1.06 | 0.47 | 0.51 |

Table E-1 also shows that the prediction uncertainty is large for many of the important parameters. For example, the prediction uncertainty for plastic deformation capacity is $\sigma_{LN} = 0.54$. Previous research has shown that these large uncertainties in element deformation capacity cause similarly large uncertainties in collapse capacity (Ibarra 2003, Goulet et al. 2006, Haselton et al. 2007). These large uncertainties are associated with the wide variability in the physical phenomena we are trying to predict, and limitations in the available test data. With the availability of more test data in the future we may be able to reduce these uncertainties.

Due to its particularly large effect on collapse assessment, it is useful to also examine the prediction bias for selected subsets of the data for $\theta_{cap,pl}$ as given in equation (E-3). For non-conforming elements (ie. those with $\rho_{sh} < 0.003$) the prediction is unbiased, with a median ratio of predicted to observed values of 1.02. The plastic rotation capacity equation tends to overpredict the plastic rotation capacity by approximately 12% for conforming elements ($\rho_{sh} > 0.006$), and underpredicts the plastic rotation capacity by approximately 10% for elements with extremely high axial load (ie. axial load ratios above 0.65). Considering the large uncertainty in the prediction of plastic rotation capacity and the small number of datapoints in some of the subsets, these computed biases seem reasonable. With more data, the prediction error and biases could be further reduced.

To illustrate the impact of column design variables on the model parameters predicted by Equation (E-1) through (E-6), modeling parameters obtained for an 8-story RC perimeter frame structure are shown in Table E-2. When the proposed equations are used, a typical column at the base should be modeled with an effective stiffness to yield of 35% of $EI_g$, a post-yield hardening ratio of 1.13, a plastic rotation capacity of 0.085, a post-capping rotation capacity of 0.10 and $\lambda$ equal to 154.

**Table E-2 Predicted Model Parameters for 8-Story Special Perimeter Frame**

| design parameter | value | $EI_{stf}/EI_g$ | $M_c/M_y$ | $\theta_{cap,pl}$ | $\theta_{pc}$ | $\lambda$ |
|---|---|---|---|---|---|---|
| *8-story special perimeter frame, interior column, 1st story* | v = 0.06, $L_s/h$ = 2.7, $\rho_{sh}$ = 0.0121, s/d = 0.14,f'$_c$ = 35 MPa, $\alpha_{sl}$ = 1, $s_n$ = 7.5, ρ = 0.018 | 0.35 | 1.13 | 0.085 | 0.100 | 154 |
| *v* | 0.0 | 0.35 | 1.13 | 0.095 | 0.100 | 170 |
| | 0.3 | 0.52 | | 0.055 | 0.100 | 104 |
| $\rho_{sh}$ | 0.002 | 0.35 | 1.13 | 0.042 | 0.059 | 154 |
| | 0.010 | | | 0.078 | 0.100 | |
| | 0.020 | | | 0.105 | 0.100 | |
| $L_s/h$ | 2 | 0.35 | 1.13 | 0.085 | 0.100 | 154 |
| | 6 | 0.58 | | | | |
| *s/d* | 0.1 | 0.35 | 1.13 | 0.085 | 0.100 | 163 |
| | 0.4 | | | | | 106 |
| | 0.6 | | | | | 80 |
| ρ | 0.01 | 0.35 | 1.13 | 0.080 | 0.100 | 154 |
| | 0.03 | | | 0.094 | | |

Table E-2 also illustrates how changes in each design parameter impact predicted model parameters. For example, suppose various design parameters were changed such that the column under consideration in the first row of Table E-2 has a different axial load ratio, amount of transverse reinforcement, or column reinforcement ratio; these changes would change the parameters used to model that column. Within the range of column parameters considered in Table E-2, the predicted plastic rotation capacity varies from 0.042 to 0.105 radians. Axial load ratio ($v$) and the lateral confinement ratio ($\rho_{sh}$) have the largest effect on the predicted value of $\theta_{cap,pl}$, while concrete strength ($f'_c$), rebar buckling coefficient ($s_n$), and longitudinal reinforcement ratio (ρ) have less dominant effects ($f'_c$ and $s_n$ are not shown here). Table E-2 also shows the effects of the design parameters on initial stiffness, hardening stiffness ratio, post-capping stiffness and cyclic deterioration parameters.

**Summary and Limitations**

The calibration process provided a comprehensive set of equations capable of predicting the parameters of a lumped plasticity element model for a RC beam-column, with the empirical predictive equations having the ability to capture the effects of design aspects such as detailing, level of axial load, etc. These equations are proposed for use with the element model developed by Ibarra et al. (2003, 2005), and can be used to model cyclic and in-cycle strength and stiffness degradation to capture element behavior up to the point

of structural collapse. Even so, these equations are general and can be used with slight modifications with most lumped plasticity models currently used in research.

The predictive empirical equations proposed here provide a critical link between column design parameters and element modeling parameters, facilitating the creation of nonlinear structural models of reinforced concrete frame elements. The empirical predictive equations predict the mean value of each parameters, so the prediction uncertainty associated with each equation is also quantified and reported. This provides an indication of the uncertainty in the prediction of model parameters, and can be used in sensitivity analyses and propagation of structural modeling uncertainties.

As with any study, there are limitations in terms of the applicability of these equations, which are discussed briefly here.

The equations developed here are based on a comprehensive database assembled by Berry et al. (Berry et al. 2004, PEER 2006a). Even so, the range of column parameters included in the database is limited, and the derived equations may not be applicable outside the range of column parameters considered.

The equations are also limited more generally by the number of test specimens available that have an observed capping point. There are only a small number of experimental tests with clearly observable negative post-capping stiffness. For model calibration and understanding of element behavior, it is important that future testing continue to deformation levels large enough to clearly show the negative post-capping stiffness. In addition, there is virtually no data that shows post-peak cyclic deterioration behavior. With additional data, it may be possible to further remove some of the conservatism still in the proposed equations and reduce the prediction uncertainties. A further limitation is associated with the testing protocols; virtually all of the available test data is based on a cyclic loading protocol with many cycles and 2-3 cycles per deformation level. This type of loading may not be representative of the type of earthquake loading that typically causes structural collapse, which would generally only contain a few large displacement cycles before collapse occurs. Tests conducted under a variety of loading histories will lead to a better understanding of how load history affects cyclic behavior, and provide a basis for better development/ calibration of the element model cyclic rules.

In addition to the above mentioned issues, it is also important to remember that the empirical equations developed in this work are all based on

laboratory test data where the test specimen was constructed in a controlled environment, and thus indicative of a high quality of construction. Actual buildings are constructed in a less controlled environment, so we expect the elements of actual buildings to have a lower level of performance than that predicted using the equations presented here. This work does not attempt to quantify this difference in performance coming from construction quality, but this may be a useful topic to consider for some structural systems.

## E.4 Joint Modeling

Nonlinear models of RC structures employ a two-dimensional joint model developed and implemented by Lowes and Altoontash (Lowes 2004). This model accounts for the finite joint size, and includes rotational springs and systems of constraints for direct modeling of the shear panel and bond-slip behavior. Figure E-4 shows a schematic diagram of this model.

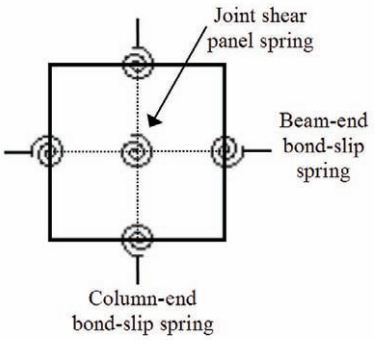


Figure E-4 Schematic diagram of joint model.

In order to determine the appropriate parameters to model the joints of the RC SMF structures we use a different approach than the detailed calibration study presented earlier to determine the parameters for beam-column elements. In this case, the joint model and parameters are based on a careful review of previous research.

### *E.4.1 Shear Panel Spring*

Current building code provisions require that the joint shear capacity be based on capacity design principles, so if properly implemented, the joint shear demand should never exceed the capacity. A review of available research finds that the joint shear capacity designs provisions are conservative, and should be able to prohibit joint shear failure in all properly designed SMF structures. For example, Brown and Lowes (2006) reviewed results of 45 experimental tests of conforming joints, finding that not one of these conforming joints exhibited damage requiring joint replacement. As a result of observations like these, the joint shear modeling is not judged to be

a critical part of the overall behavior of the frame; damage in the joint shear panel will increase the flexibility of the frame, but the joint shear panel is not a dominant damage/failure mode (see also Appendix D).

For the case study SMF structures, then, the joint models are developed to accurately reflect system stiffness. For simplicity, we model the joint as an elastic element with the cracked stiffness based on simple mechanics (Umemura 1969). The OMF structures are modeled to account for the deterioration that may occur in the joints of those structures. For readers interested in a more detailed approach, the modified compression field theory (MCFT) (Vecchio 1986, Stevens 1991, Altoontash 2004, Lowes 2004, Lowes 2003) is often used to develop panel shear models.

### *E.4.2 Bond-Slip Spring Model*

The effect of bond-slip in joints and column footings is to decrease the pre-yield and post-yield stiffnesses and increase the plastic rotation capacity or RC elements. In this study, bond-slip deformations are directly included in the plastic hinge calibration and so do not need to be separately determined here.

By lumping the effects of bond-slip in the plastic hinge model, it is inherently assumed that the bond-slip component of deformation is linear from zero load to the yield load. This is a simplification, and a quadrilinear model could instead be used to capture the nonlinear bond-slip behavior prior to rebar yielding.

# Appendix F

# Collapse Evaluation of Individual Buildings

## F.1 Introduction

Although developed as a tool to establish seismic performance factors for generic seismic-force-resisting systems, the Methodology could be readily adapted for collapse assessment of an individual building system. As such, it could be used to demonstrate adequate collapse performance of the structural system of a building designed using performance-based design methods, permitted by Section 11.1.4 of ASCE/SEI 7-05. This appendix describes one such adaptation of the Methodology for use in collapse evaluation of an individual building system.

## F.2 Feasibility

It is anticipated that buildings designed using performance-based methods will likely be large or important structures. Projects using performance-based design methods typically utilize detailed models for analyses of the building, and peer review is commonly required. Such projects are already set up to utilize many of the components of the Methodology.

In contrast to index archetype models, project models might have more elements (based on the actual configuration and geometry of the specific building), but might not incorporate same level of sophistication in modeling nonlinear behavior. Collapse evaluation could be performed using two-dimensional or three-dimensional models of the building. Project models could be used, but detailed simulation of nonlinear behavior on a very large number of elements may not be feasible, and might require some level of idealization of the actual configuration and geometry of the building.

## F.3 Approach

The Methodology is based on the concept of collapse level ground motions, defined as the level of ground motions that cause median collapse (i.e., one-half of the records in the set cause collapse). For a building to meet the collapse performance objectives of this Methodology, the median collapse capacity must be an acceptable amount above the MCE ground motion

demand level (i.e., the adjusted collapse margin ratio, *ACMR*, must exceed acceptable values).

By starting with an acceptable collapse probability (for MCE ground motions) and working backwards through the Methodology, values of the spectral shape factor, *SSF*, and collapse margin ratio, *CMR*, can be evaluated to determine the level of ground motions corresponding to median collapse. The Methodology can be "reverse engineered" to determine the level of ground motions for which not more than one-half of the records should cause collapse. By scaling the record set to this level, trial designs for a subject building can be evaluated. If the analytical model of the trial design survives one-half or more of the records without collapse, then the building has a collapse probability that is equal to (or less than) the acceptable collapse probability (for MCE ground motions), and meets collapse performance objective of the Methodology.

## F.4 Collapse Evaluation of Individual Building Systems

The process for collapse evaluation of an individual building system is summarized in the following steps.

### *F.4.1 Step One: Develop Nonlinear Model(s)*

Development of a representative model (or models) of the building must incorporate the nonlinear behavioral characteristics of building-specific components.

- **Two-Dimensional Versus Three-Dimensional Models.** It is likely that the project has developed a three-dimensional (3-D) model of the building (for design), which could be used for collapse evaluation. Two-dimensional (2-D) models could be used, but such models would need to address response in both horizontal directions (e.g., two 2-D models) and account for torsion and potential coupling of bi-directional response.
- **Gravity System.** Elements of the gravity system can be incorporated into the building-specific model. Whether or not they are modeled, potential collapse modes of the gravity system must be included in the collapse assessment process. This is required because displacement compatibility requirements of ASCE/SEI 7-05 do not prohibit gravity system collapse from becoming the controlling failure mode, and they only address compatibility of displacements at the MCE ground motion level, not at collapse level ground motions. P-Delta effects must consider the full weight of the building.

Inclusion of gravity system collapse modes differs from the general application of the Methodology, which does not account for gravity system collapse. Accounting for collapse modes of the gravity system is typically accomplished by using limit state criteria for non-simulated collapse modes. Practically speaking, there is little experimental data on which to base limit state criteria for some gravity system collapse modes. In these cases, the peer review team will need to assist in determining appropriate criteria for use in the collapse assessment.

- **Nonlinear Elements.** Model(s) should incorporate nonlinear properties for all elements of seismic force-resisting system (and gravity system) that cannot be shown to remain fully elastic in a near-collapse condition.

### *F.4.2 Step Two: Define Limit States and Acceptance Criteria*

- **Limit States.** It is unlikely that project nonlinear models will be capable of adequately simulating sidesway collapse, which would require sophisticated modeling of element degradation and strain softening that is not typical of most design efforts. Collapse will most likely be defined by non-simulated collapse limit states for key elements of the seismic-force-resisting system and gravity system components.
- **Acceptable Collapse Probability.** The maximum acceptable probability of collapse should be determined. An acceptable collapse probability of 10% is consistent with the collapse performance objectives of this Methodology.

### *F.4.3 Step Three: Determine Total System Uncertainty and Acceptable Collapse Margin Ratio*

- **Total System Uncertainty ($\beta_{TOT}$).** The value of total system collapse uncertainty, $\beta_{TOT}$, is determined in accordance with Chapter 7, based on quality of the design requirements, quality of the test data used to develop nonlinear properties, and quality of the nonlinear model.

  The quality of design requirements would be expected to be "Superior" for buildings generally conforming to materials and detailing requirements of ASCE/SEI 7-05. The quality of modeling and test data would be expected to range from "Good" to "Fair" depending on the extent to which the models and supporting test data accurately capture degrading behavior of nonlinear elements.

- **Acceptable Value of Adjusted Collapse Margin Ratio (e.g., *ACMR10%*).** The acceptable value of the adjusted collapse margin ratio should be determined. Based on an acceptable collapse probability of

10%, *ACMR10%* is consistent with the collapse performance objectives of this Methodology.

### *F.4.4 Step Four: Perform Nonlinear Static Analysis (NSA)*

- **Nonlinear Static Analysis.** A nonlinear static (pushover) analysis is performed to check nonlinear behavior of the model to verify that all elements assumed to be essentially elastic have not yielded at the point that a collapse mechanism develops in the structure. Pushover analyses should be completed in both horizontal directions.
- **Structure Ductility Capacity ($\mu_C$).** The ductility capacity, $\mu_C$, is determined from pushover analysis results, for both horizontal directions, in accordance with Chapter 6.
- **Spectral Shape Factor (*SSF*).** The spectral shape factor, *SSF*, for both horizontal directions, is determined based on the ductility capacity, $\mu_C$, and fundamental period, *T*, in the direction of interest, in accordance with Chapter 7.

### *F.4.5 Step Five: Select Record Set and Scale Records*

- **Record Set Selection.** If the building is located within 10 km of an active fault, then the Near-Field record set should be selected for collapse evaluation, otherwise the Far-Field record set should be used.
- **Record Set Scaling.** Both components of each record in the record set should be scaled up to the required collapse level intensity at which one-half or more of the records must not cause collapse.

  To scale the records to this level, all normalized records are multiplied by the same scale factor, *SF*. The scaling factor, *SF*, should be evaluated in both horizontal directions and the average value used to scale both components of each record.

$$SF = \frac{ACMR10\%}{C_{3D}\, SSF}\left(\frac{S_{MT}}{S_{NRT}}\right) \qquad \text{(G-1)}$$

  where:

  *SF* = record (and component) scale factor in the direction of interest, required for collapse evaluation of an individual building system.

  *ACMR10%* = acceptable value of the adjusted collapse margin ratio from Chapter 7, corresponding to an acceptable collapse probability of 10%.

$SSF$ = spectral shape factor in the direction of interest, as defined in Chapter 7.

$C_{3D}$ = three-dimensional analysis coefficient, taken as 1.2 for three-dimensional analysis, and 1.0 for two-dimensional analysis.

$S_{MT}$ = MCE, 5% damped, spectral response acceleration at the fundamental period, $T$, of the building in the direction of interest, as defined in Section 11.4.3 of ASCE/SEI 7-05, including Site Class.

$S_{NRT}$ = median value of normalized record set, 5% damped, spectral response acceleration at the fundamental period, $T$, of the building in the direction of interest

$T$ = the fundamental period of the building in the direction of interest, based on the limits of Section 12.8.2 of ASCE/SEI 7-05, computed in accordance with Equation (A-1) in Appendix A.

### *F.4.6 Step Six: Perform Nonlinear Dynamic Analysis (NDA) and Evaluate Performance*

- **Nonlinear Dynamic Analysis.** A nonlinear dynamic analysis of the model(s) is performed separately for each scaled record of the record set. The response is classified either as either "collapse" or "non-collapse" based on sidesway collapse of the analytical model or through the use of non-simulated collapse component acceptance criteria. Ground motion record pairs should be applied to two-dimensional and three-dimensional models in accordance with Chapter 6.
- **Collapse Evaluation.** If less than one-half of the records cause collapse, then the trial design meets the collapse performance objective, and the building has an acceptably low probability of collapse for MCE ground motions. If one-half or more of the records cause collapse, then the design does not meet the collapse performance objective, and re-design and re-evaluation is required.

# Symbols

$A$ = force normalized by effective seismic weight, $W$, corresponding to arbitrary post-yield displacement, $D$, of the isolation system in the horizontal direction under consideration, used to define bi-linear spring properties of isolators

$A_g$ = gross cross-sectional area of an element

$a_{sl}$ = indicator variable (0 or 1) to signify possibility of longitudinal rebar slip past the column end, where $a_{sl} = 1$ if slip is possible (Panagiotakos, 2001)

$A_y$ = force normalized by effective seismic weight, $W$, corresponding to idealized yield displacement, $D_y$, of the isolation system in the horizontal direction under consideration, used to define bi-linear spring properties of isolators

*ACMR* = adjusted collapse margin ratio

*ACMR10%* = acceptable value of the adjusted collapse margin ratio (*ACMR*), on average, for the performance group of interest

*ACMR20%* = acceptable value of the adjusted collapse margin ratio (*ACMR*) for an individual archetype of the performance group of interest

$b$ = element width

$B_{1E}$ = numerical coefficient as set forth in Table 18.6-1 of ASCE/SEI 7-05 for the effective equal to $\beta_I + \beta_{VI}$ and period equal to $T$

$c$ = cyclic deterioration calibration term (exponent); describes the change in the *rate* of cyclic deterioration as the energy dissipation capacity is exhausted

$C_{3D}$ = 3-dimensional analysis coefficient, 1.2 for 3-dimensional analysis (and 1.0 for 2-dimensional analysis)

$C_d$ = deflection amplification factor (current values given in Table 12.2-1 of ASCE/SEI 7-05)

$C_s$ = seismic response coefficient as determined in Section 12.8.1.1 of ASCE/SEI 7-05)

$C_t$ = approximate period coefficient as determined in Table 12.8-2 of ASCE/SEI 7-05)

$C_u$ = upper-limit period coefficient as determined in Table 12.8-2 of ASCE/SEI 7-05)

$c_{units}$ = a units conversion variable that equals 1.0 when f'$_c$ is in MPa units and 6.9 for ksi units

CI = confidence interval

$CMR$ = collapse margin ratio

$d$ = column depth

$D$ = arbitrary post-yield displacement, in inches, of the isolation system in the horizontal direction under consideration used to define bi-linear spring properties of isolators

$D_M$ = maximum displacement, in inches, at the center of rigidity of the isolation system in the direction under consideration, as prescribed by Eq. 17.5-3 of ASCE/SEI 7-05

$D_{TM}$ = total maximum displacement, in inches, of the isolation system in the direction under consideration considering both translational and torsional displacement, as prescribed by Eq. 17.5-6 of ASCE/SEI 7-05

$D_y$ = idealized yield displacement, in inches, of the isolation system in the horizontal direction under consideration used to define bi-linear spring properties of isolators

$EI_g$ = gross cross-sectional moment of inertia

$EI_{stf}$ = effective cross-sectional moment of inertia such that the secant stiffness is defined to 40% of the yield moment/force of the component

$EI_y$ = effective cross-sectional moment of inertia that provides a secant stiffness through the yield point

EXP = exponential

$F_a$ = short-period site coefficient (at 0.2-second period) as given in Section 11.4.3 of ASCE/SEI 7-05

$F_v$ = long-period site coefficient (at 1.0-second period) as given in Section 11.4.3 of ASCE/SEI 7-05

$f'_c$ = compressive strength of unconfined concrete, based on standard cylinder test

$f_y$ = yield stress of longitudinal reinforcement (Appendix E).

$h$ = element height

$h_n$ = height in feet above the base to the highest level of the structure (ASCE/SEI 7-05)

$I$ = the importance factor in Section 11.5.1 of ASCE/SEI 7-05

$K$ = residual strength present in material model, defined as a ratio of $M_y$

$K_c$ = post-capping stiffness, i.e., stiffness beyond $\theta_{cap,pl}$

$K_e$ = secant stiffness to the yield point

$k_{eff}$ = effective stiffness of the isolation system, in kips/in., at displacement, $D$, in the horizontal direction under consideration

$k_{Mmin}$= minimum effective stiffness, in kips/in., of the isolation system at the maximum displacement in the horizontal direction under consideration, as prescribed by Eq. 17.8-6 of ASCE/SEI 7-05

$K_s$ = hardening stiffness, i.e., stiffness between $\theta_y$ and $\theta_{cap,pl}$

$L_s$ = shear span, distance between column end and point of inflection

LN = natural logarithm

$M_c$ = moment capacity at the capping point; used for prediction of hardening stiffness

$M_y$ = yield moment for Ibarra material model (this is the nominal moment capacity of the column)

$M_{y(Fardis)}$ = yield moment as calculated based on Fardis' predictive equations (Pangiotakos et al. 2001)

$NMi$ = normalization factor of the $i^{th}$ record of the set of interest

$NTH_{1,I}$ = normalized $i^{th}$ record, horizontal component 1

$NTH_{2,I}$ = normalized $i^{th}$ record, horizontal component 2

$P$ = perimeter frame system

$P$ = axial load

$P_b$ = axial load at the balanced condition

$PGV_{PEER}$ = peak ground velocity of the $i^{th}$ record, PEER database

$R$ = response modification coefficient (current values given in Table 12.2-1 of ASCE/SEI 7-05)

$R_{eff}$ = effective R factor which accounts for the additional strength caused by the minimum base shear requirement

$R_I$ = numerical coefficient related to the type of seismic force-resisting system above the isolation system (i.e., three-eights of the $R$ value

given in Table 12.2.-1 of ASCE/SEI 7-05, not to exceed 2.0, need not be taken as less than 1.0)

RC = reinforced concrete

$s$ = spacing of transverse reinforcement in the column hinge region

$S$ = space frame system

$S_1$ = mapped MCE, 5 percent damped, spectral response acceleration parameter at a period of 1 second as defined in Section 11.4.1 of ASCE/SEI 7-05

$S_{CT}$ = random variable representing collapse level earthquake, 5 percent damped, spectral response acceleration at the fundamental period, $T$, of the building (Site Class D)

$S_{CT(SC)}$= collapse level earthquake, 5 percent damped, spectral response acceleration at the fundamental period, $T$, of the building (Site Class D) obtained from simulated collapse failure modes.

$S_{CT(NSC)}$=collapse level earthquake, 5 percent damped, spectral response acceleration at the fundamental period, $T$, of the building (Site Class D) obtained from non-simulated collapse failure modes.

$\hat{S}_{CT}$ = median value of collapse level earthquake, 5 percent damped, spectral response acceleration at the fundamental period, $T$, of the building (Site Class D)

$S_{CT1}$ = collapse level earthquake, 5 percent damped, spectral response acceleration at the fundamental period, $T_1$, of the building, Site Class D

$S_{DS}$ = design, 5 percent damped, spectral response acceleration parameter at short periods as defined in Section 11.4.4 of ASCE/SEI 7-05

$S_{D1}$ = design, 5 percent damped, spectral response acceleration parameter at a period of 1 second as defined in Section 11.4.4 of ASCE/SEI 7-05

$S_{max}$ = maximum lateral force of the fully-yielded seismic force-resisting system normalized by the effective seismic weight of the building, $W$

$S_{MS}$ = the MCE, 5 percent damped, spectral response acceleration parameter at short periods adjusted for site class effects as defined in Section 11.4.3 of ASCE/SEI 7-05

$S_{MT}$ = MCE, 5 percent damped, spectral response acceleration at the fundamental period, $T$, of the building, as defined in Section 11.4.3 of ASCE/SEI 7-05 for Site Class D

$S_{MI}$ = the MCE, 5 percent damped, spectral response acceleration parameter at a period of 1 second adjusted for site class effects as defined in Section 11.4.3 of ASCE/SEI 7-05

$s_n$ = rebar buckling coefficient, $(s/d_{b.})(f_y/100)^{0.5}$, (where $f_y$ is in MPa) (similar to a term proposed by Dhakal and Maekawa (2002))

$S_{NRT}$ = median value of normalized record set, 5 percent damped, spectral response acceleration at the fundamental period, *T*, of the building

$S_S$ = mapped MCE, 5 percent damped, spectral response acceleration parameter at short periods as defined in Section 11.4.1 of ASCE/SEI 7-05

$S_T$ = median value of normalized record set, 5 percent damped, spectral response acceleration at the fundamental period, *T*, for record set scaled to an arbitrary intensity. This parameter is also the anchor point for individual ground motion records of the record set at this intensity

*Sa* = spectra acceleration, g

Sa(T) = the spectral acceleration at the period, T

*SCWB*= ratio of flexure strengths of column and beams framing into a joint, computed as per ACI 318-05 (ACI 2005)

$SD_{CT}$ = median value of collapse level earthquake, 5 percent damped, spectral response displacement at the fundamental period, *T*, of the building corresponding to spectral response acceleration, $\hat{S}_{CT}$

$SD_{MT}$ = MCE, 5 percent damped, spectral response displacement at the fundamental period, *T*, of the building, corresponding to spectral response acceleration, $S_{MT}$

*SF* = record (and component) scale factor required for collapse evaluation of an individual building

SMF = special moment frame concrete building, as per ACI 318-05 (ACI 2005)

*SSF* = spectral shape factor

*T* = the fundamental period of the building based on the limits of Section 12.8.2 of the ASCE/SEI 7-05 and the approximate fundamental period, $T_a$

$T_1$ = the fundamental period of the building, as determined using eigenvalue analysis using the structural model (seconds)

$T_a$ = the approximate fundamental period of the building as determined in Section 12.8.2.1 of ASCE/SEI 7-05

$T_{eff}$ = effective period of isolation system, in seconds, at displacement, $D$, in the horizontal direction under consideration.

$T_M$ = effective period, in seconds, of the seismically isolated structure at the maximum displacement in the direction under consideration, as prescribed by Eq. 17.5-4 of ASCE/SEI 7-05

$TH_{1,I}$ = record $i$, horizontal component 1, PEER database

$TH_{2,I}$ = record $i$, horizontal component 2, PEER database

$V$ = total design lateral force or shear at base (ASCE/SEI 7-05)

$V_c$ = shear capacity of concrete, as per ACI 318-05

$V_E$ = lateral force that would be developed in the seismic force-resisting system if the system remained entirely elastic for design earthquake ground motions (FEMA, 2004b)

$V_{max}$ = maximum lateral force of the fully-yielded seismic force-resisting system (same as $V_Y$ parameter, FEMA, 2004b)

$V_{mpr}$ = capacity shear demand, caused by fully plastic moments at each end of the element, and including 25% overstrength, as per ACI 318-05 (ACI 2005)

$V_n$ = nominal shear capacity including contributions from concrete and steel, as per the ACI 318-05

$V_s$ = total lateral seismic design force or shear on elements above the isolation system, as prescribed by Eq. 17.5-8 of ASCE/SEI 7-05

$V_u$ = shear demand

$W$ = effective seismic weight of the structure above the isolation interface, as defined in Section 17.5.3.4 of ASCE/SEI 7-05

$W$ = effective seismic weight of the building as defined in Section 12.7.2 of ASCE/SEI 7-05

$x$ = parameter of Equation (12.8-7) given in Table 12.8-2 of ASCE/SEI 7-05

$\beta_0$ = regression coefficient from the equation $LN[S_{CT1}] = \beta_0 + \beta_1\varepsilon$

$\beta_1$ = regression coefficient from the equation $LN[S_{CT1}] = \beta_0 + \beta_1\varepsilon$

$\beta_{DR}$ = design requirements-related collapse uncertainty

$\beta_{eff}$ = effective damping of the isolation system, percent of critical damping, at displacement, $D$, in the horizontal direction under consideration.

$\beta_F$ = uncertainty associated with ductile fracture of steel reduced beam sections, logarithmic standard deviation

$\beta_I$ = component of effective damping of the structure due to the inherent dissipation of energy by elements of the structure, at or just below the effective yield displacement of the seismic force-resisting system, Section 18.6.2.1 of ASCE/SEI 7-05

$\beta_M$ = effective damping, percent of critical, of the isolation system at the maximum displacement in the direction under consideration, as prescribed by Eq. 17.8-8 of ASCE/SEI 7-05

$\beta_{MDL}$ = modeling-related collapse uncertainty

$\beta_{RTR}$ = record-to-record collapse uncertainty

$\beta_{TD}$ = test data-related collapse uncertainty

$\beta_{TOT}$ = total system collapse uncertainty

$\beta_{VI}$ = component of effective damping of the fundamental mode of vibration of the structure in the direction of interest due to viscous dissipation of energy by the damping system, at or just below the effective yield displacement of the seismic force-resisting system, Section 16.6.2.3 of ASCE/SEI 7-05

$\delta$ = roof drift of the seismic force-resisting system for design earthquake ground motions (FEMA, 2004b)

$\delta_E$ = roof drift of the seismic force-resisting system if the system remained entirely elastic for design earthquake ground motions (FEMA, 2004b)

$\Delta_{ult}$ = roof displacement (in inches) used to approximate the ultimate displacement capacity of the seismic force-resisting system, as derived from pushover analysis

$\Delta_y$ = roof displacement (in inches) used to approximate full yield of the seismic force-resisting system, as derived from pushover analysis

$\varepsilon(T)$ = the epsilon value of a ground motion, evaluated at period, T

$\varepsilon(T)_{,records}$ = the mean epsilon value of the Far-Field ground motion set, evaluated at period, T

$\overline{\varepsilon}_0(T)$ = the expected ε value for the site and hazard-level of interest

$\varphi$ = strength reduction factor

$\lambda$ = normalized energy dissipation capacity; this is a normalized value defined by the total energy dissipation capacity of $E_t = \lambda M_y \theta_y$ (Ibarra et al. 2005)

$\lambda_{DR}$ = random variable representing design requirements-related collapse uncertainty

$\lambda_{MDL}$ = random variable representing modeling-related collapse uncertainty

$\lambda_{RTR}$ = random variable representing record-to-record collapse uncertainty

$\lambda_{TD}$ = random variable representing test data-related collapse uncertainty

$\mu_C$ = calculated ductility capacity of an index archetype analysis model

$\nu$ = axial load ratio ($P/A_g f'_c$)

$\theta_{cap}$ = total chord rotation at capping, sum of elastic and plastic deformations (radians)

$\theta_{cap,pl}$ (or $\theta_p$), = plastic chord rotation from yield to cap (radians)

$\theta_p$ = plastic hinge rotation (radians)

$\theta_{pc}$ = post-capping plastic rotation capacity, from the cap to point of zero strength (radians)

$\hat{\theta}_p$ = median value of plastic hinge rotation at which ductile fracture in steel RBS is initiated (radians)

$\theta_y$ = chord rotation at yielding, taken as the sum of flexural, shear and bond-slip components; yielding is defined as the point of significant stiffness change, i.e., steel yielding or concrete crushing (radians)

$\rho$ (or $\rho_{tot}$) = ratio of total area of longitudinal reinforcement (for columns) or ratio of tensile longitudinal reinforcement (for beams)

$\rho'$ = ratio compressive longitudinal reinforcement (for beams)

$\rho_{sh}$ = area ratio of transverse reinforcement in column hinge region

$\rho_{sh,eff}$ = effective ratio of transverse reinforcement in column hinge region ($\rho_{sh} f_{y,w} / f'_c$)

$\Omega$ = calculated overstrength of an index archetype analysis model

$\Omega_O$ = overstrength factor appropriate for use in the load combinations of Section 12.4 of ASCE/SEI 7-05 (current values of $\Omega_O$ are given in Table 12.2-1 of ASCE/SEI 7-05)

# Glossary

## Definitions

**Archetype:** A prototypical representation of a seismic-force-resisting system.

**Archetype Design Space:** The **overall** range of permissible configurations, structural design parameters, and other features that define the application limits for a seismic-force-resisting system.

**Base**: The level at which the horizontal seismic ground motions are considered to be imparted to the structure (*ASCE 7-05*).

**Base Shear**: Total design lateral force or shear at the base (*ASCE 7-05*).

**Building**: Any structure whose intended use includes shelter of human occupants (*ASCE 7-05*).

**Collapse Level Earthquake Ground Motions**: The level of earthquake ground motions that cause collapse of the seismic force-resisting system of interest.

**Component**: A part or element of an architectural, electrical, mechanical or structural system (*ASCE 7-05*).

**Damping Device**: A flexible structural element of the damping system that dissipates energy due to relative motion of each ned of the device (*ASCE 7-05*).

**Damping System**: The collection of structural elements that includes all individual damping devices, all structural elements or bracing required to transfer forces from damping devices to the base of the structure, and the structural elements required to transfer forces from damping devices to the seismic force-resisting system (*ASCE 7-05*).

**Design Earthquake Ground Motions**: The earthquake ground motions that are two-thirds of the corresponding MCE ground motions (*ASCE 7-05*).

**Design Requirements-Related Uncertainty**: Collapse uncertainty associated with the design requirements (of the system of interest), based on qualitative evaluation of the completeness/appropriateness of the design requirements.

**Displacement Restraint System:** A collection of structural elements that limits lateral displacement of seismically isolated structures due to the maximum considered earthquake (Chapter 17, *ASCE 7-05*).

**Effective Damping:** The value of equivalent viscous damping corresponding to energy dissipated during cyclic response of the isolation system (Chapter 17, *ASCE 7-05*).

**Effective Stiffness:** The value of the lateral force in the isolation system, or element thereof, divided by the corresponding lateral displacement (Chapter 17, *ASCE 7-05*).

**Importance Factor**: A factor assigned to each structure according to its Occupancy Category as prescribed in Section 11.5.1 of *ASCE 7-05*.

**Incremental Dynamic Analysis**: Series of nonlinear time-history analyses of a structural analysis model under an input ground motion whose intensity (acceleration amplitude) is incrementally scaled up until collapse is detected in the analysis.

**Index Archetype Configuration:** A prototypical representation of a seismic-force-resisting system configuration that embodies key features and behaviors related to collapse performance when subjected to earthquake ground motions.

**Index Archetype Design:** An index archetype configuration that has been proportioned and detailed using design requirements for the seismic-force-resisting system of interest.

**Index Archetype Model:** An idealized mathematical representation of an index archetype design used to simulate collapse using nonlinear static and dynamic analyses.

**Isolation Interface:** The boundary between the upper portion of the structure, which is isolated, and the lower portion of the structure, which moves rigidly with the ground (Chapter 17, *ASCE 7-05*).

**Isolation System:** The collection of structural elements that includes all individual isolator units, all structural elements that transfer force between elements of the isolation system, and all connections to other structural elements. The isolation system also includes the wind--restraint system, energy-dissipation devices, and/or the displacement restraint system if such systems and devices are used to meet the design requirements of Chapter 17 ( *ASCE 7-05*).

**Isolator Unit:** A horizontally flexible and vertically stiff structural element of the isolation system that permits large lateral deformations under

design seismic loads. An isolator unit is permitted to be used either as part of, or in addition to, the weight-supporting system of the structure (Chapter 17, *ASCE 7-05*).

**Maximum Considered Earthquake (MCE) Ground Motions**: The most severe earthquake effects considered by *ASCE 7-05*, as defined by Section 11.4 of *ASCE 7-05*.

**Modeling Uncertainty**: Collapse uncertainty due to modeling-related uncertainty of archetype analysis models.

**Nonbuilding Structure**: A structure, other than a building, constructed of a type included in Chapter 15 of *ASCE 7-05*.

**Non-Simulated Collapse:** Structural collapse caused by collapse modes that are not represented in the analytical model. Non-simulated collapse occurs when a component limit state is exceeded, as defined by component fragility functions.

**Occupancy**: The purpose for which a building or other structure, or part thereof, is used or intended to be used (*ASCE 7-05*).

**Occupancy Category**: A classification assigned to a structure based on occupancy as defined in Table 1-1 of *ASCE 7-05*.

**Performance Group:** A subset of the archetype design space containing a group of index archetype configurations that share a set of common features or behavioral characteristics, binned for statistical evaluation of collapse performance.

**Record-to-Record Uncertainty**: Collapse uncertainty due to ground motion uncertainty, based on the RTR variability of archetype analysis models using the ATC-63 records.

**Record-to-Record Variability**: Variation in the response of a structure under multiple input ground motions that are scaled to a consistent ground motion intensity.

**Seismic Design Category**: A classification assigned to a structure based on Occupancy Category and the severity of design earthquake ground motions at the site as defined in Section 11.4 of *ASCE 7-05*.

**Seismic Force-Resisting System**: That part of the structural system that has been considered in the design to provide the required resistance to seismic forces prescribed in *ASCE 7-05*.

**Sidesway Collapse:** Structural collapse associated with loss of lateral strength and stiffness due to material and geometric nonlinearities.

Sidesway collapse occurs when the interstory drift of one or more stories increases without bounds.

**Simulated Collapse:** Structural collapse caused by collapse modes that are represented in the analytical model.

**Site Class**: A classification assigned to a site based on the types of soils present and their engineering properties as defined in Chapter 20 of *ASCE 7-05*.

**Structure**: That which is built or constructed and limited to buildings and nonbuilding structures as defined in *ASCE 7-05*.

**Test Data-Related Uncertainty**: Collapse uncertainty associated with the test data (for the system of interest), based on qualitative evaluation of the robustness/comprehensiveness of test data used to support development of nonlinear archetype analysis models.

**Total Maximum Displacement:** The maximum considered earthquake lateral displacement, including additional displacement due to actual and accidental torsion, required for verification of the stability of the isolation system or elements thereof, design of structure separations, and vertical load testing of isolator unit prototypes (Chapter 17, *ASCE 7-05*).

**Vertical Collapse:** Structural collapse due to the loss of vertical carrying capacity of a critical component. This may precipitate either local or progressive collapse.

# References


Aycardi, L. E., Mander, J., and Reinhorn, A., 1994, "Seismic Resistance of Reinforced Concrete Frame Structures Designed Only for Gravity Loads: Experimental Performance of Subassemblages." *ACI Structural Journal*.

Abrahamson N.A. and Silva W.J., 1997, *Empirical Response Spectral Attenuation Relations For Shallow Crustal Earthquake*, Seismological Research Letters, 68 (1), 94-126.

Altoontash, A., 2004, *Simulation and Damage Models for Performance Assessment of Reinforced Concrete Beam-Column Joints*, Doctoral Dissertation, Stanford University.

ACI, 2005, *Building Code Requirements for Structural Concrete (ACI 318-05) and Commentary, (ACI 318R-05)*, American Concrete Institute, Farmington Hills, MI.

ACI, 2002, *Building Code Requirements for Structural Concrete (ACI 318-02) and Commentary (ACI 318R-02)*, American Concrete Institute, Farmington Hills, MI.

ACI, 2001, *Acceptance Criteria for Moment Frames Based on Structural Testing* (ACI T1.1-01) and *Commentary* (ACI T1.1R-01), Innovation Task Group 1 and Collaborators. 2001. ACI, Farmington Hills, MI.

AF&PA, 2005, *National Design Specification for Wood Construction (AF&PA NDS-05)*, American Forest and Paper Association, Washington, D.C.

AISC, 2005, *Seismic Provisions for Structural Steel Buildings*, ANSI/AISC 341-05, American Institute for Steel Construction, Chicago, Illinois.

ASCE, 2006a, *Minimum Design Loads for Buildings and Other Structures,* ASCE Standard ASCE/SEI 7-05, Including Supplement No. 1, American Society of Civil Engineers, Reston, Virginia.

ASCE, 2006b, *Seismic Rehabilitation of Existing Buildings*, ASCE Standard ASCE/SEI 41-06, American Society of Civil Engineers, Reston, Virginia.

ASCE, 2005, *Minimum Design Loads for Buildings and Other Structures* (*ASCE 7-05*), American Society of Civil Engineers, Reston, Virginia.

ASCE, 2003, (ASCE). 2003, *Minimum Design Loads for Buildings and Other Structures*. ASCE Standard ASCE/SEI 7-02, American Society of Civil Engineers, Washington, D. C.).

ASCE, 2002, *Minimum Design Loads for Buildings and Other Structures* (*ASCE 7-02*), American Society of Civil Engineers, Reston, VA.

ASTM, 2003, *ASTM ES 2126-02a Standard Test Method for Cyclic (Reversed) Load Test for Shear Resistance of Walls for Buildings*, American Society for Testing and Materials.

ATC, 2008, *Interim Guidelines on Modeling and Acceptance Criteria for Seismic Design and Analysis of Tall Buildings, 90% Draft*, Report No. ATC-72-1 Applied Technology Council, Redwood City, California..

ATC, 2007a, *Guidelines for Seismic Performance Assessment of Buildings - 35% Draft*, Report No. ATC-58, prepared by the Applied Technology Council for the Federal Emergency Management Agency, Washington, D.C.

ATC, 2007b, *The Effects of Degradation of Stiffness and Strength on the Seismic Stability of Structural Systems - 70% Draft*, Report No. ATC-62, prepared by the Applied Technology Council for the Federal Emergency Management Agency, Washington, D.C.

ATC, 1992, *Guidelines for Cyclic Seismic Testing of Components of Steel Structures for Buildings*, Report No. ATC-24, Applied Technology Council, Redwood City, California.

ATC, 1978, *Tentative Provisions for the Development of Seismic Regulations for Buildings (ATC 3-06)*, Applied Technology Council, also NSF Publication 78-8 and NBS Special Publication 510, Washington, D.C.

Aslani, H., 2005, *Probabilitistic earthquake loss estimation and loss disaggregation in buildings*, Doctoral Dissertation, Stanford University.

Aslani, H. and Miranda, E., 2005, "Fragility Assessment of Slab-Column Connections in Existing Non-Ductile Reinforced Concrete Buildings," *Journal of Earthquake Engineering* 9(6).

Baker J.W., 2007, Quantitative classification of near-fault ground motions using wavelet analysis, *Bulletin of the Seismological Society of America* (in review).

Baker J.W. and C.A. Cornell, 2006, "Spectral shape, epsilon and record selection", *Earthquake Engineering. & Structural Dynamics*, 34 (10), 1193-1217.

Baker, J.W., 2005, *Vector-Valued Ground Motion Intensity Measures for Probabilistic Seismic Demand Analysis*, Ph.D. Dissertation, Department of Civil and Environmental Engineering, Stanford University.

Benjamin, J.R. and Cornell, C.A, 1970, *Probability, statistics, and decision for civil engineers*, McGraw-Hill, New York, 684 pp.

Berry, M., Parrish, M., and Eberhard, M., 2004, *PEER Structural Performance Database User's Manual*, Pacific Engineering Research Center, University of California, Berkeley, California, 38 pp. Available at http://nisee.berkeley.edu/spd/ and http://maximus.ce.washington.edu/~peera1/

Boore D.M., Joyner W.B., and Fumal T.E., 1997, *Equations for estimating horizontal response spectra and peak accelerations from western North America earthquakes: A summary of recent work*, Seismological Research Letters, 68 (1), 128-153.

Brown, P. C., and Lowes, L. N., 2006, "Fragility Functions for Modern Reinforced Concrete Beam-Column Joints."

Campbell, K. W. and Y. Borzorgnia. 2003, "Updated Near-Source Ground-Motion (Attenuation) relations for the Horizontal and Vertical Components of Peak Ground Acceleration and Acceleration response Spectra." *Bulletin of the Seismological Society of America*, Vol. 93, No. 1, pp. 314-331.

Clark, P., Frank, K., Krawinkler, H., and Shaw, R., 1997, *Protocol for Fabrication, Inspection, Testing, and Documentation of Beam-Column Connection Tests and Other Experimental Specimens*, SAC Steel Project Background Document, Report No. SAC/BD-97/02.

COLA, 2001, "Report of a Testing Program of Light-Framed Walls with Wood Sheathed Panels," Final Report to the City of Los Angeles Department of Building and Safety, Structural Engineering Association of Southern California, COLA-UCI Light Frame Test Committee, Department of Civil Engineering, University of California, Irvine, CA. 93 p.

Dhakal, R.P. and Maekawa, K., 2002 "Modeling of Postyielding Buckling of Reinforcement," *Journal of Structural Engineering*, Vol. 128, No. 9, September 2002, pp. 1139-1147.

Ekiert, C. and Hong, J, 2006, "Framing-to-Sheathing Connection Tests in Support of NEESWood Project," *Network of Earthquake Engineering Simulation*, Host Institution: State University of New York at University at Buffalo, Buffalo, NY. 20 p.

Elghadamsi, F.E. and B. Mohraz, 1987, "Inelastic Earthquake Spectra," *Earthquake Engineering and Structural Dynamics*, Vol. 15, pp. 91-104.

Ellingwood, B., Galambos, T.V., MacGregor, J.G., and Cornell, C.A., 1980, *Development of a Probability-Based Load Criterion for American National Standard A58*, National Bureau of Standards, Washington, DC, 222 pp.

Elwood, K., 2004, "Modeling failures in existing reinforced concrete columns." *Canadian Journal of Civil Engineering*, 31.

Elwood, K. J., and Eberhard, M. O., 2006, "Effective Stiffness of Reinforced Concrete Columns." *PEER Research Digest* (2006-1), 1- 5.

Elwood, K., and Moehle, J., 2005, "Axial Capacity Model for Shear-Damaged Columns." *ACI Structural Journal*, 102(4).

Engelhardt, M., Winneberger, T., Zekany, A. J., Potyraj, T. J., 1998, "Experimental investigation of dogbone moment connections", *Engineering Journal of Steel Construction* Vol. (4) 1998 pp 128-139.

Fardis, M. N., and Biskini, D. E., 2003, "Deformation Capacity of RC Members, as Controlled by Flexure or Shear." *Otani Symposium*, 511- 530.

FEMA, 2007, *Interim Protocols for Determining Seismic Performance Characteristics of Structural and Nonstructural Components Through Laboratory Testing*, FEMA 461 Draft document, Federal Emergency Management Agency.

FEMA, 2005, Improvement of Nonlinear Static Seismic Analysis Procedures, FEMA 440, Federal Emergency Management Agency.

FEMA, 2004a, *NEHRP Recommended Provisions for Seismic Regulations for New Buildings and Other Structures*, FEMA 450-1/2003 Edition, Part 1: Provisions, Federal Emergency Management Agency, Washington, D.C.

FEMA, 2004b, *NEHRP Recommended Provisions for Seismic Regulations for New Buildings and Other Structures*, FEMA 450-2/2003 Edition, Part 2: Commentary, Federal Emergency Management Agency, Washington, D.C.

FEMA, 2001, *FEMA 369: NEHRP Recommended Provisions for Seismic Regulations for New Buildings and Other Structures*, Federal Emergency Management Agency, Washington, D.C.

FEMA, 2000, *Prestandard and Commentary for Seismic Rehabilitation of Buildings,* FEMA 356, Prepared by the American Society of Civil Engineers for the Federal Emergency Management Agency, Washington, D.C.

Filiatrault, A., Wanitkorkul, A. and Constantinou, M.C., 2008, *Development and Appraisal of a Numerical Cyclic Loading Protocol for Quantifying Building System Performance*, Technical Report MCEER-08-0013, MCEER, University at Buffalo, State University of New York, Buffalo, New York.

Filiatrault, A., Lachapelle, E., and Lamontagne, P., 1998, "Seismic Performance of Ductile and Nominally Ductile Reinforced Concrete Moment Resisting Frames I. Experimental Study." *Canadian Journal of Civil Engineering,* 25.

Filippou, F. C., 1999, "Analysis Platform and Member Models for Performance-Based Earthquake Engineering," *U.S.-Japan Workshop on Performance-Based Earthquake Engineering Methodology for Reinforced Concrete Building Structures*, PEER Report 1999/10, Pacific Engineering Research Center, University of California, Berkeley, California, pp. 95-106.

Folz, B., and Filiatrault, A., 2001, “Cyclic Analysis of Wood Shear Walls”, *ASCE Journal of Structural Engineering*, 127(4), 433-441,

Folz, B., and Filiatrault, A., 2004a, “Seismic Analysis of Woodframe Structures I: Model Formulation”, *ASCE Journal of Structural Engineering*, Vol. 130, No. 8, 1353-1360.

Folz, B., and Filiatrault, A., 2004b, “Seismic Analysis of Woodframe Structures II: Model Implementation and Verification”, *ASCE Journal of Structural Engineering*, Vol. 130, No. 8, 1361-1370.

Fonseca, F., Rose, S. and Campbell, S., 2002, *Nail, Wood Screw, and Staple Fastener Connections*, CUREE Report No. W-16, Consortium of Universities for Earthquake Engineering Research, Richmond, CA.

Gatto, K., and Uang, C.M., 2002, Cyclic Response of Woodframe Shearwalls: Loading Protocol and Rate of Loading Effects, CUREE Publication No. W-13.

Goulet, C., C.B. Haselton, J. Mitrani-Reiser, J. Beck, G.G. Deierlein, K.A. Porter, and J. Stewart, 2006a, "Evaluation of the Seismic Performance of a Code-Conforming Reinforced-Concrete Frame Building - from seismic hazard to collapse Safety and Economic Losses", *Earthquake Spectra*, (in press).

Goulet, C., Haselton, C., Mitrani-Reiser, J., Stewart, J., Taciroglu, E., and Deierlein, G., 2006, *Evaluation of Seismic Performance of a Code-Conforming Reinforced-Concrete Frame Buildings- Part I. Ground Motion Selection and Structural Collapse Simulation*. 8NCEE.

Harmsen, S.C., 2001, "Mean and Modal ε in the Deaggregation of Probabilistic Ground Motion", *Bulletin of the Seismological Society of America*, 91, 6, pp. 1537-1552, December 2001.

Haselton, C.B., 2006, *Assessing Seismic Collapse Safety of Modern Reinforced Concrete Moment Frame Buildings*, Ph.D. Dissertation, Department of Civil and Environmental Engineering, Stanford University.

Haselton, C.B. and J.W. Baker, 2006, "Ground motion intensity measures for collapse capacity prediction: Choice of optimal spectral period and effect of spectral shape", *8th National Conference on Earthquake Engineering*, San Francisco, California, April 18-22, 2006.

Haselton, C. B. and G. G. Deierlein, 2007, *Assessing Seismic Collapse Safety of Modern Reinforced Concrete Frame Buildings*, Blume Center Technical Report No. 156.

Haselton, C., Liel, A., Taylor Lange, S., and Deierlein, G. G., 2007, *Beam-Column Element Model Calibrated for Predicting Flexural Response Leading to Global Collapse of RC Frame Buildings* (In Preparation). Pacific Earthquake Engineering Research Center 2007/xx, University of California, Berkeley.

Haselton, C.B., J.W. Baker, A.B. Liel, C.A. Kircher, and G.G. Deierlein (2007). "Accounting for Expected Spectral Shape (Epsilon) in Collapse Performance Assessment," *Earthquake Spectra* (in preparation).

Ibarra, L., 2003, *Global Collapse of Frame Structures under Seismic Excitations*, Blume Center TR 152, Stanford University, Stanford, California.

Ibarra, L., and Krawinkler, H., 2005a, "Effect of Uncertainty in System Deterioration Parameters on the Variance of Collapse Capacity,"

*Proceedings, ICOSSAR'05*, Rome, Italy, June 20-24, pp. 3583-3590 Millpress, Rotterdam, ISBN 90 5966 040 4

Ibarra, L.F., and Krawinkler, H., 2005b, "Global Collapse of Frame Structures Under Seismic Excitations," PEER Report 2005/06, Sept. 2005, and *John A. Blume Earthquake Engineering Center Report No. TR 152,* Department of Civil Engineering, Stanford University.

Ibarra, L.F., Medina, R.A., and Krawinkler, H., 2005, "Hysteretic Models that Incorporate Strength and Stiffness Deterioration," *International Journal for Earthquake Engineering and Structural Dynamics,* Vol. 34, No.12, pp. 1489-1511.

Ibarra, L., Medina, R., and Krawinkler, H., 2002, "Collapse Assessment of Deteriorating SDOF Systems," *Proceedings of the 12th European Conference on Earthquake Engineering*, London, Sept. 2002, Elsevier Science Ltd, paper # 665.

ICBO-ES, 2002 *Acceptance Criteria for Prefabricated Wood Shear Panels*, AC130-0102-0902, International Conference of Building Officials, Whittier, California.

ICBO, 2000, *Acceptance Criteria for Laboratory Accreditation (AC89)*, International Conference of Building Officials, Whittier, California.

ICBO, 1997, *Uniform Building Code*. 1997 Edition. (International Conference of Building Officials, Whittier, California).

Isoda, H., Folz, B., and Filiatrault, A., 2001, *Seismic Modeling of Index Woodframe Buildings*, Report No. W-12, Consortium of Universities for Research in Earthquake Engineering, Richmond, CA, 144 p.

Isoda, H., Furuya, O., Tatsuya, M., Hirano, S. and Minowa, C., 2007, "Collapse Behavior of Wood House Designed by Minimum Requirement In Law." *Journal of Japan Association for Earthquake Engineering*. (Under Review).

Kircher, C. A., (2006). "Seismically Isolated Structures," Chapter 11, *NEHRP Recommended Provisions:: Design Examples*. FEMA 451. Prepared by the Building Seismic Safety Council for the Federal Emergency Management Agency (FEMA) of the Department of Homeland Security (FEMA: Washington, D.C.).

Krawinkler, H., 1996, "Cyclic Loading Histories for Seismic Experimentation on Structural Components," *Earthquake Spectra*, The Professional Journal of the Earthquake Engineering Research Institute, Vol. 12, Number 1, pp. 1-12.

Krawinkler, H., 1978, “Shear design of steel frame joints,” *Engineering Journal*, AISC, Vol. 15, No. 3.

Krawinkler, H., Bertero, V. V., and Popov, E. P., 1971, “Inelastic behavior of steel beam-to-column sub-assemblages,” *Report No. UCB/EERC-71/07*, Earthquake Engineering Research Center (EERC), University of California at Berkeley.

Krawinkler, H., Parisi, F., Ibarra, L., Ayoub, A., and Medina, R., 2000, “Development of a Testing Protocol for Woodframe Structures” *CUREE Publication No. W-02*.

Krawinkler, H. and F. Zareian, 2007, “Prediction of Global Collapse – How Realistic and Practical is It, and What Can We Learn From It?,” *Tall Buildings Journal*, December 2007.

Kunnath, S. K., Hoffmann, G., Reinhorn, A. M., and Mander, J. B., 1995, "Gravity-Load-Designed Reinforced Concrete Buildings -- Part I: Seismic Evaluation of Existing Construction," *ACI Structural Journal*, 92(3).

Lai, S.P., and J.M. Biggs, 1980, “Inelastic Response Spectra for Aseismic Buildings,” *Journal of the Structural Division*, ASCE, Vol. 106, No. ST6, pp. 1295-1310.

Liel, A.B., 2006, Personal communication about recent research findings on how spectral shape (epsilon) affects collapse capacity of brittle 1967-era reinforced concrete frame buildings.

Lignos, D.G., and Krawinkler, H., 2007, "A Database in Support of Modeling of Component Deterioration for Collapse Prediction of Steel Frame Structures", *ASCE Structures Congress*, Long Beach, California, May 18-20, 2007.

Lowes, L. N., and Altoontash, A., 2003, "Modeling of Reinforced-Concrete Beam-Column Joints Subjected to Cyclic Loading," *Journal of Structural Engineering*, 129(12).

Lowes, L. N., Mitra, N., and Altoontash, A., 2004, *A Beam-Column Joint Model for Simulating the Earthquake Response of Reinforced Concrete Frames*, PEER 2003/10, PEER.

Miranda, E. and V.V. Bertero, 1994, “Evaluation of Strength Reduction Factors for Earthquake-Resistant Design,” *Earthquake Spectra*, Vol. 10, No. 2, pp. 357-379.

Nassar, A.A. and H. Krawinkler, 1991, "Seismic Demands for SDOF and MDOF Systems," *Report No. 95*, The John A. Blume Earthquake Engineering Center, Stanford University, Stanford, California.

Newmark, N.M. and W.J. Hall, 1973, "Seismic Design Criteria for Nuclear Reactor Facilities," *Report No. 46*, *Building Practices for Disaster Mitigation*, National Bureau of Standards, U.S. Department of Commerce, pp. 209-236.

Opensees, 2006, *Open System for Earthquake Engineering Simulation*, Pacific Earthquake Engineering Research Center, University of California, Berkeley, http://opensees.berkeley.edu/

Pang, W.C. and Rosowsky, D.V. (2007). Personal Communications. NEESWood Project, Texas A&M University.

Pangiotakos, T. B., and Fardis, M. N., 2001, "Deformations of Reinforced Concrete Members at Yielding and Ultimate," *ACI Structural Journal*.

PEER, 2006, *PEER NGA Database*, Pacific Earthquake Engineering Research Center, University of California, Berkeley, California, http://peer.berkeley.edu/nga/

PEER, 2006a, *Pacific Earthquake Engineering Research Center: Structural Performance Database*, Pacific Earthquake Engineering Research Center, University of California, Berkeley, Available at http://nisee.berkeley.edu/spd/ and http://maximus.ce.washington.edu/~peera1/.

Ricles, J. M., Zhang, X., Lu, L. W., Fisher, J., 2004, *Development of seismic guidelines for deep-column steel moment connections*, ATLSS report No. 04-13.

Riddell, R., P. Hidalgo, and E. Cruz, 1989, "Response Modification Factors for Earthquake Resistant Design of Short Period Structures," *Earthquake Spectra*, Vol. 5, No. 3, pp. 571-590.

Sivaselvan M., and Reinhorn, A.M., 2000, "Hysteretic Models for Deteriorating Inelastic Structures", ASCE/Journal of Engineering Mechanics, Vol. 126(6), 633-640.

Stevens, N., Uzumeri, S., and Collins, M., 2001, "Reinforced Concrete Subjected to Reversed Cyclic Shear." *ACI Structural Journal*.

Takeda, T., H.H.M. Hwang, and M. Shinozuka, 1988, "Response Modification Factors for Multiple-Degree-of-Freedom Systems," *Proceedings of the 9th World Conference on Earthquake Engineering*, Tokyo-Kyoto, Japan, Vol. V, pp. 129-134.

Uang, C.M., Yu, K., and Gilton, C., 2000, *Cyclic Response of RBS Moment Connections: Loading Sequence and Lateral Bracing Effects*, Report No. Structural Steel Research Project (SSRP)-99/13.

Umemura, H., and Aoyama, H., 1969, "Empirical Evaluation of the Behavior of Structural Elements," *4th World Conference on Earthquake Engineering*, Chile.

Vamvatsikos, D. and C. Allin Cornell, 2002, "Incremental Dynamic Analysis," *Earthquake Engineering and Structural Dynamics*, Vol. 31, Issue 3, pp. 491-514.

Vecchio, F. J., and Collins, M. P., 1986. "Modified Compression-Field Theory for Reinforced Concrete Elements Subjected to Shear," *ACI Structural Journa*l.

Vidic, T., P. Fajfar, and M. Fischinger, 1992, "A Procedure for Determining Consistent Inelastic Design Spectra," *Proceedings of the Workshop on Nonlinear Seismic Analysis of RC Structures*, Bled, Slovenia, July 1992.

White, T.W. and Ventura, C., 2007, "Seismic Behavior of Residential Wood-Frame Construction in British-Columbia: Part I – Modeling and Validation," *Proceedings of the Ninth Canadian Conference on Earthquake Engineering*, Ottawa, Canada, 10 p.

Zareian, F, 2006, *Simplified Performance-Based Earthquake Engineering*, Ph.D. Dissertation, Dept. of Civil and Environmental Engineering, Stanford University, Stanford California, June.

# Project Participants

### Task Order Contract Management

Christopher Rojahn (Project Executive Director)
Applied Technology Council
201 Redwood Shores Parkway, Suite 240
Redwood City, California 94065

Jon A. Heintz (Project Quality Control Monitor)
Applied Technology Council
201 Redwood Shores Parkway, Suite 240
Redwood City, California 94065

William T. Holmes (Project Technical Monitor)
Rutherford & Chekene
55 Second Street, Suite 600
San Francisco, California 94105

### FEMA Project Officer

Michael Mahoney
Federal Emergency Management Agency
500 C Street, SW, Room 416
Washington, DC 20472

### FEMA Technical Monitor

Robert D. Hanson
Federal Emergency Management Agency
2926 Saklan Indian Drive
Walnut Creek, California 94595

### Project Management Committee

Charles Kircher (Chair)
Kircher & Associates, Consulting Engineers
1121 San Antonio Road, Suite D-202
Palo Alto, California 94303

Michael Constantinou
University at Buffalo
Dept. of Civil, Structural & Environmental Engineering
132 Ketter Hall
Buffalo, New York 14260

Gregory Deierlein
Stanford University
Dept. of Civil & Environmental Engineering
240 Terman Engineering Center
Stanford, California 94305

James R. Harris
J. R. Harris & Company
1776 Lincoln Street, Suite 1100
Denver, Colorado 80203

John Hooper
Magnesson Klemencic Associates
1301 Fifth Avenue, Suite 3200
Seattle, Washington 98101

Allan R. Porush
URS Corporation
915 Wilshire Blvd., Suite 700
Los Angeles, California 90017

Christopher Rojahn (ex-officio)
William Holmes (ex-officio)
Jon A. Heintz (ex- officio)

### Working Group on Nonlinear Static Analysis

Michael Constantinou, Group Leader
University at Buffalo
Dept. of Civil, Structural & Environmental Engineering
132 Ketter Hall
Buffalo, New York 14260

Assawin Wanitkorkul
The University at Buffalo Foundation
Suite 211, The UB Commons
520 Lee Entrance
Amherst, New York 14228

### Working Group on Nonlinear Dynamic Analysis

Gregory Deierlein, Group Leader
Stanford University
Dept. of Civil & Environmental Engineering
Blume Earthquake Engineering Center
Stanford, California 94305

Curt Haselton
California State University, Chico
475 East 10th Avenue
Chico, California 95926

Abbie Liel
Stanford University
2 Comstock Circle #101
Stanford, California 94305

Jason Chou
University of California, Davis
11713 New Albion Drive
Gold River, California 95670

Stephen Cranford
Stanford University
119 Quillen Court, Apt. 417
Stanford, California 94305

Brian Dean
Stanford University
159 Melville Ave.
Palo Alto, California 94301

Kevin Haas
Stanford University
218 Ayrshire Farm Lane #108
Stanford, California 94305

Jiro Takagi
Stanford University
322 College Ave., #C
Palo Alto California 94306

### Working Group on Wood-frame Construction

Andre Filiatrault, Group Leader
University at Buffalo
Dept. of Civil, Struct & Environ Engrg
134 Ketter Hall
Buffalo, New York 14260

Jiannis Christovasilis
The University at Buffalo Foundation
Suite 211, The UB Commons
520 Lee Entrance
Amherst, New York 14228

Kelly Cobeen
Cobeen & Associates Structural Engineering
251 Lafayette Circle, Suite 230
Lafayette, California 94549

### Working Group on Autoclaved Aerated Concrete

Helmut Krawinkler, Group Leader
Stanford University
Dept. of Civil Engineering
380 Panama Mall
Stanford, California 94305

Farzin Zareian
University of California, Irvine
Dept. of Civil & Environmental Engineering
E/4141 Engineering Gateway
Irvine, California 9 2697

## Project Review Panel

Maryann T. Phipps (Chair)
Estructure
8331 Kent Court, Suite 100
El Cerrito, California 94530

Amr Elnashai
Mid-America Earthquake Center
University of Illinois at Urbana-Champaign
Department of Civil and Environmental
Engineering 1241 Newmark
Civil Engineering Lab
Urbana, Illinois 61801

S.K. Ghosh
S.K. Ghosh Associates Inc.
334 East Colfax Street, Unit E
Palatine, Illinois 60067

Ramon Gilsanz
Gilsanz Murray Steficek LLP
129 W. 27th Street, 5th Floor
New York, New York 10001

Ronald O. Hamburger
Simpson Gumpertz & Heger
The Landmark @ One Market, Suite 600
San Francisco, California 94105

Jack Hayes
National Institute of Standards and Technology
100 Bureau Drive, MS 8610
Gaithersburg, Maryland 20899

Richard E. Klingner
University of Texas at Austin
10100 Burnet Rd
Austin, Texas 78758

Philip Line
American Forest and Paper Association (AFPA)
1111 19th Street, NW, Suite 800
Washington, DC 20036

Bonnie E. Manley, P.E.
AISI Regional Director
4 Canvasback Way
Walpole, Maryland 02081

Andrei M. Reinhorn
University at Buffalo
Dept. of Civil, Structural & Envir. Engineering
231 Ketter Hall
Buffalo, New York 14260

Rafael Sabelli
DASSE Design, Inc.
33 New Montgomery Street, Suite 850
San Francisco, California 94105